STRUCTURAL BEHAVIOUR OF CONCRETE-FILLED ELLIPTICAL COLUMN TO I-BEAM CONNECTIONS

J. YANG

PHD

2017

Structural Behaviour of Concrete-filled Elliptical Column to I-beam Connections

Jie YANG

Submitted for the Degree of

Doctor of Philosophy

Faculty of Engineering and Informatics

University of Bradford

2017

Abstract

Jie Yang

Structural Behaviour of Concrete-filled Elliptical Column to I-beam Connections

Keywords: Concrete Filled Columns, Elliptical Hollow Section, Moment Capacity, Rotation Capacity, Joint Stiffness, Finite Element Model

Concrete-filled tubular (CFT) columns have been widely adopted in building structures owing to their superior structural performance, such as enhanced load bearing capacity, compared to hollow tubes. Circular, square and rectangular hollow sections are most commonly used in the past few decades. Elliptical hollow section (EHS) available recently is regarded as a new cross-section for the CFT columns due to its attractive appearance, optional orientation either on major axis or minor axis and improved structural efficiency.

The state of the research in terms of elliptical columns, tubular joints between EHSs and connections with CFT columns, etc., are reviewed in this thesis, showing a lack of investigations on EHSs, especially on beam to elliptical column connections which are essential in framed structures.

The structural behaviour of elliptical column to I-beam connections under bending is studied in this thesis to fill the research gap. Overall ten specimens with various joint assemblies were tested to failure to highlight the benefits of adopting concrete infill and stiffeners in the columns.

A three-dimensional finite element model developed by using ABAQUS software is presented and verified against obtained experimental results, which shows acceptable accuracy and reliability in predicting failure modes of the connections and their moment capacities. Parametric studies were performed to access the main parameters that affecting the bending behaviour of the connections. A simple hand calculation method in terms of ultimate moment capacity is proposed according to experiments conducted for connections with concrete-filled columns.

Declaration

I herby declare that this thesis entitled “Structural Behaviour of Concrete-filled Elliptical Column to I-beam Connections” is the result of my own work except where references have been made to the work related to others. This thesis has not been submitted anywhere for the application of another degree, diploma, or other qualification.

Jie Yang

Acknowledgements

First and foremost, I would like to express my sincere gratitude to my perfect supervisors Prof. Dennis Lam, Dr. Xianghe Dai, and Dr. Therese Sheehan, for the continuous support in completion of my Ph.D. thesis, for their patience, motivation, and immerse knowledge. Their guidance helped me in all the time of research and writing of this thesis.

My sincere thanks also goes to Mr. Stephen Robinson, Mr. Owen Baines, Ms Joanna Wood and other technicians/colleagues from the Heavy Structures Laboratory of University of Bradford and from Yantai University (China), for their technical support to my experiments with regards to this Ph.D. study, for their hard work and brilliant ideas.

I gratefully acknowledge the Bradford School of Engineering scholarship, without which, it may not be possible for me to start the challenging journey of the Ph.D. study in the UK.

I thank my fellow colleague Mr. Naveed Rehman for his precious help during the laboratory tests; thank the other colleagues in my research group for the inspiring discussions, for the time we are working together and all the fun we have had in the past few years.

Last but not the least, many thanks to my parents, my younger brother and my boyfriend for their selfless support and encouragement throughout my doctoral period and my life in general.

Table of Contents

List of Figures

List of Tables

Notations

a Half larger outer diameter of the EHS

b Half smaller outer diameter of the EHS

t Thickness

f_c Compressive cylinder strength of concrete

f_{cc} Maximum confined strength of concrete

f_{ck} Cylinder compressive strength of unconfined concrete

f_{cr} Critical stress

f_u Ultimate stress/strength

f_{uc} Cube compressive strength of unconfined concrete

f_y Yield stress

ε_{cc} Strain at the maximum confined strength of concrete

ξ Confinement factor of EHS to concrete

χ Reduction factor

λ Column local buckling slenderness

D_{eq} Equivalent maximum diameter of the EHS

A_g Gross cross-sectional area of hollow section

A_s Cross-sectional area of steel tube

A_c Cross-sectional area of concrete

A_n Critical net area of connection with an open slot

R_t Tension area mean stress correction factor

R_v Shear area mean stress correction factor

M_{pl} Plastic moment

M_{el} Elastic moment

Chapter 1

Introduction

This chapter presents an introductory background of this research. Profile, main advantages and applications of elliptical hollow section are presented. Motivation of research, aim and objectives as well as the outline of the thesis are given.

1.1 Background

Concrete-filled steel tubular (CFST) columns are widely adopted in the construction of frame structures due to their well-acknowledged advantages in structural performance such as high load-bearing capacity and ductility, superior seismic and fire resistance. A beam to column connection is a very important element in a frame structure because it transfers floor loads to the column, therefore, appropriate design of beam to column connections is crucial to ensure the structural stability and robustness, the economical, easy and fast construction of frame structures.

Fin plate (also termed “shear tabs” or “single shear plates”) connections are one of the most used beam to column connections because they are low cost and simple to erect and could overcome the difficulty and complexity of fitting connection components to curved column faces. A typical fin plate double-sided beam to column connection is constructed by simply welding the fin plates to the column outer face in the workshop and then bolting to the beam webs at each side on site.

Another connection type that is unique to hollow section connections is the through-plate connection. Because of its higher cost compared to simple fin plate connections, the through plate is seldom required when the fin plates are sufficient for structural design and thus little attention has been paid to this connection type. This thesis will cover the through plate connection for comparison when investigating the effect of joint type for beam to elliptical column connections. Due to the through plate’s specific position, it also acts as reinforcement to the tubular column.

Circular, square and rectangular sections are the traditionally used cross-sectional shapes for CFST columns. A new range of Elliptical Hollow Sections (EHSs) have become available recently in the manufacturing industry, which adds diversity to the sectional shape family.

1.2 EHS introduction

1.2.1 EHS profile

An ellipse (see Figure 1.1), which is a special example of an oval, can be described geometrically using the below equation 1.1:

$$\frac{x^2}{a^2}+\frac{y^2}{b^2}=1 \tag{1.1}$$

where *a* and *b* represent the half larger and smaller outer diameters of the EHS, respectively.

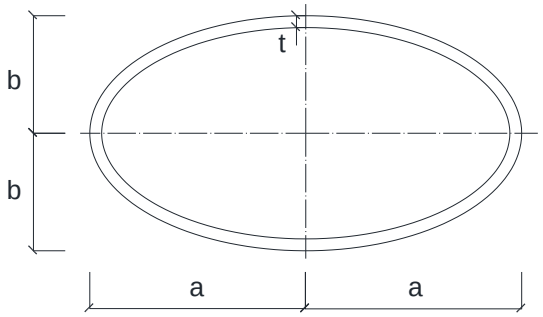

Figure 1.1 EHS profile

Currently, most EHSs are manufactured via a hot-finishing process with an aspect ratio of 2:1. European standard (BS EN 10210-2) [1] has presented the tolerances, dimensions and sectional properties of a limited range of hot-finished elliptical sections. EHS sectional sizes ranging from 120 × 60 × 3.2 mm up to 500 × 250 × 16 mm are currently being used in construction practices. The EHSs are commonly available in Grade S355J2H with a minimum yield strength of 355 MPa. With a more diverse range of aspect ratios being employed in the future, the EHS profile might fulfil the aesthetic design purpose in many construction practices.

1.2.2 Advantages of EHS

From a mechanical point of view, the following merits of the EHS are demonstrated:

- It has minimal residual stress, excellent welding capacity, and inherent toughness;
- It has better bending capacity compared with a circular hollow section (CHS) of the same area or weight due to having two different principal axes, one stronger and the other weaker [2];
- A stocky EHS has greater compressive capacity in comparison to its CHS counterpart because of, “the achievement of strain hardening in the stiffer regions of the section of low radii of curvature” [3];
- It is less susceptible to stress concentration problems than RHS and SHS; Moreover, its closed shape offers high torsional stiffness [4] and high resistance to lateral torsion [5].

1.2.3 Applications of EHS

With the advantages mentioned in the above section and potential structural efficiency, EHS has been utilised in columns, glass roofs, pedestrian bridges, and wind turbine masts, etc. [2]. Applications can be found in Zeeman Building at the University of Warwick, Society Bridge in Scotland, Barajas Airport in Madrid, Cork Airport in Ireland, glass façade of the AXA building in Paris [6], Heathrow Airport in London [7] ; and the main railway station at Bern in Switzerland [8].

1.3 Motivation of research

Motivation of this research arose from the awareness of the lack of design guidance for EHSs, which restricts the widespread application of this type of structural hollow sections. In recent years, EHSs have gained increasing attention from architects, however, proper design provisions for EHS members and connections are still not covered by the current design guidance and codes in structural design. In particular the structural behaviour of beam to EHS column connections remains indistinct to designers.

The ‘Green Book’ [9] by the Steel Construction Institute and British Constructional Steelwork Association, provides essential design guidance for simple joints to

Eurocode 3. It also gives detailed requirements, design checks, and procedures applicable for the design of beam to column connections with traditional cross-sectional shaped columns. In addition, although the CIDECT design guide No.9 [10] involves connections with circular or rectangular hollow sections, it has not been proved to be applicable for beam to EHS connections. Thus, research work presented in this thesis will aim to contribute to the development of design concepts and provisions of connection related to EHSs - simple fin plate/through plate connections, in particular.

1.4 Aim and objectives of research

The main aim of this research is to investigate the moment behaviour of elliptical column to I-beam connections and provide reliable information for design guidance of such connections. The main objectives are listed as follows:

- To contribute to the experimental data bank of the connections with elliptical columns by conducting a series of laboratory tests on elliptical column to I-beam connections with various joint assemblies;
- To justify the benefit of adopting concrete infill and stiffener plates in the EHS column on moment behaviour of the connections;
- To develop an acceptable nonlinear finite element model using ABAQUS software;
- To develop a simple hand calculation method to predict the moment capacities of various connection types and to evaluate the method using test data;

1.5 Outline of the thesis

In this thesis, Chapter 1 presents an introductory background of this research, including EHS's main advantages, applications and motivation of research. Aim and objectives of research as well as the outline of the thesis are presented.

Chapter 2 contains a detailed review on literature to date regarding experimental and numerical studies on EHS tubes, connections with EHSs, composite columns with elliptical tubes and connections with composite tubular columns, to present relevant research work and address the research gaps.

Chapter 3 describes the experimental programme including material tests of steel columns, steel plates (fin plates), steel bolts and concrete as well as a full-scale connection test setup and instrumentations of a series of laboratory tests.

Chapter 4 presents the results of ten elliptical column to beam connection tests, which include failure modes of the connections and moment vs. rotation curves. Material properties obtained from tensile testing are also provided. Comparisons of the connection test results between hollow and concrete-filled connections and among various joint types are presented as well.

Chapter 5 provides a finite element modelling method developed by using ABAQUS solver to replicate the experiments with its validation process against test data of both the concrete-filled connections and the corresponding hollow connections.

Chapter 6 presents a preliminary parametric study conducted by using the validated model on both hollow connections and concrete-filled connections, to address the effect of various geometrical parameters on the moment behaviour of the connections. Parameters considered include fin plate thickness, EHS tube wall thickness, joint types, bolt hole edge distance and bolt spacing. A simple hand calculation method in regards to the ultimate moment capacity of connections with concrete-filled columns within the scope of this research are provided. Good agreement between predicted results and the tested results is obtained.

Finally, Chapter 7 contains the major conclusions of the research presented in this thesis and gives some suggestions for future work.

The design drawings of the test specimens are included in Annex I at the end of this thesis. The articles published related to this thesis are provided in Annex II. Details are given as follows:

i. Jie Yang, Therese Sheehan, Xianghe Dai, & Dennis Lam. “Experimental study of beam to concrete-filled elliptical steel tubular column connections”, Thin-Walled Structures, 2015, Vol. 95, pp. 16-23.

ii. Jie Yang, Therese Sheehan, Xianghe Dai, & Dennis Lam. “Structural Behaviour of Beam to Concrete-filled Elliptical Steel Tubular Column Connections.”, Structures, 2016. (Article in Press)

Chapter 2

Literature Review

In this chapter, literatures to date on EHS tubes and connections, welded tubular joints, end connections, steel-concrete composite columns, beam to column connections, and fin plate connections are reviewed to present relevant research work and address the research gaps.

2.1 EHS tubes and connections

2.1.1 Elliptical hollow section tubes

Experimental and numerical studies have been conducted on elliptical hollow tubes with the loading cases covered from pure compression to eccentric compression and even combined compression plus uniaxial bending. Failure modes, ultimate strength, as well as local and global buckling behavior of the EHS columns were obtained, suggestions to design guidance for EHSs were proposed as well. Essentially, cross-section classification of EHS members which is of fundamental importance to structural metallic design has also been studied.

Based on the susceptibility to local buckling, classification of cross-sections can be described as follows:

Class 1: such cross-sections have the ability to reach and maintain their full plastic moment when subjected to bending;

Class 2: such cross-sections can also reach their full plastic moment when subjected to bending but they have lower deformation ability;

Class 3: local buckling will occur before cross-sections get full plastic moment and the bending capacity is limited by the yield moment;

Class 4: local buckling occurs before yielding and bending resistance is determined by the effective cross-section, which is determined by width-to-thickness or diameter-to-thickness ratios.

Figure 2.1 provided by Gardner and Chan [11] describes the above cross-sectional classification by using moment vs. rotation relationships, where M_{pl} and M_{el} denote plastic moment and elastic (yield) moment, respectively.

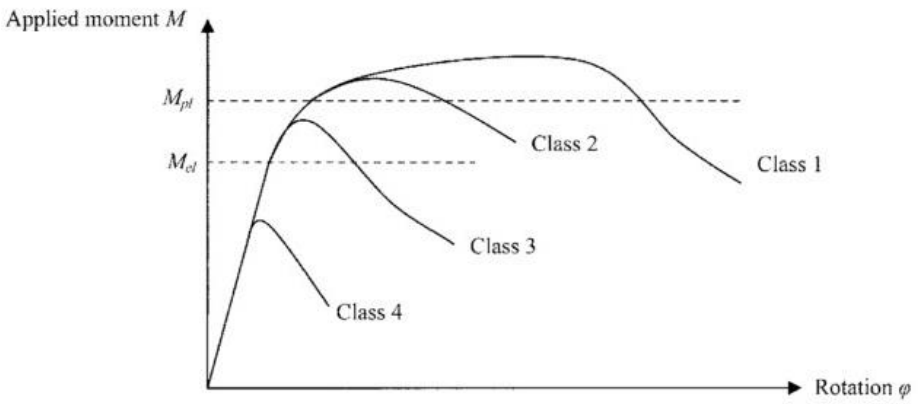

Figure 2.1 Four behavioral of cross-sections [11]

Axially pure compression is one of the basic loading cases for columns, and thus will be the loading conditions to the elliptical columns of the connections studied in this thesis. Compressive resistance of hot-rolled EHSs under axial compression has been investigated by Chan and Gardner [3] based on both experimental and numerical studies. Overall 25 stub column tests were carried out; all tested EHSs had an aspect ratio of 2 and their section sizes ranged from 150 × 75mm up to 500 × 250mm. Typical failure mode of the EHSs was found to be inwards local buckling which is illustrated in Figure 2.2.

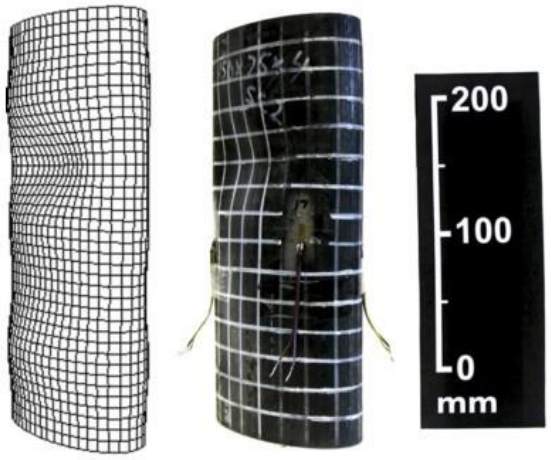

Figure 2.2 Typical failure mode of stub EHSs [3]

The observed stiffness, ultimate load, general load vs. end shortening relationship obtained from tests and the above failure mode were then used to validate the numerical models and satisfactory comparison has been found. A parametric study was then conducted using the verified FE models to investigate the EHSs of varying slenderness and aspect ratios. Based on the parametric analysis, conclusion can be made that a Class 3 slenderness limit of 90 in Eurocode 3 Part 1-1 [12] for CHSs can be safely adopted according to the cross-section slenderness parameter proposed by Gardner and Chan [13], shown in equation (2.1).

$$\frac{D_{eq}}{t\varepsilon^2} = 2\frac{(a^2/b)}{t\varepsilon^2} \tag{2.1}$$

where D_{eq} is the equivalent diameter of the EHS and $\varepsilon^2 = 235/f_y$ to allow for a range of yield strengths. The equivalent diameter is based on the assumption that local buckling initiates at the point that corresponds to the maximum radius of curvature ($r_{max}=a^2/b$).

The five thinnest EHSs among the twenty-five stub columns examined by Chan and Gardner were then selected to verify a numerical model developed by Silvestre and Gardner [14] to form the basis of a parametric study in investigating the yield-to-critical stress ratio (f_y/f_{cr}) on the ultimate strength and collapse of thin-walled EHS columns under compression. Based on the numerical results, a preliminary strength curve for the design of thin-walled EHS tubes based on the reduction factor χ shown in Equation (2.2) was proposed.

$$\chi = \begin{cases} 1 & \lambda \le 0.3 \\ 1.15 - 0.5\lambda & 0.3 < \lambda < 1.5 \\ \dfrac{0.9}{\lambda^2} & \lambda \ge 1.5 \end{cases} \tag{2.2}$$

where the column local buckling slenderness $\lambda = \sqrt{\dfrac{f_y}{f_{cr}}}$; the local critical stress f_{cr} can be calculated by Equation (2.3). Then with all the above equations, ultimate strength of a Class 4 EHS tube can be obtained by $f_u = \chi f_y$.

$$f_{cr} = \frac{E}{\sqrt{3(1-\nu^2)}} \frac{2t}{D_{eq}} \tag{2.3}$$

Elastic buckling of EHS tubes in compression were investigated by Ruiz-Teran and Gardner [15]. They concluded that the elastic buckling response of EHSs is intermediate between that of CHSs and flat plates, which depends on both aspect ratio *a*/*b* and relative thickness *t*/2*a* of the section. The transition can be seen from Figure 2.5.

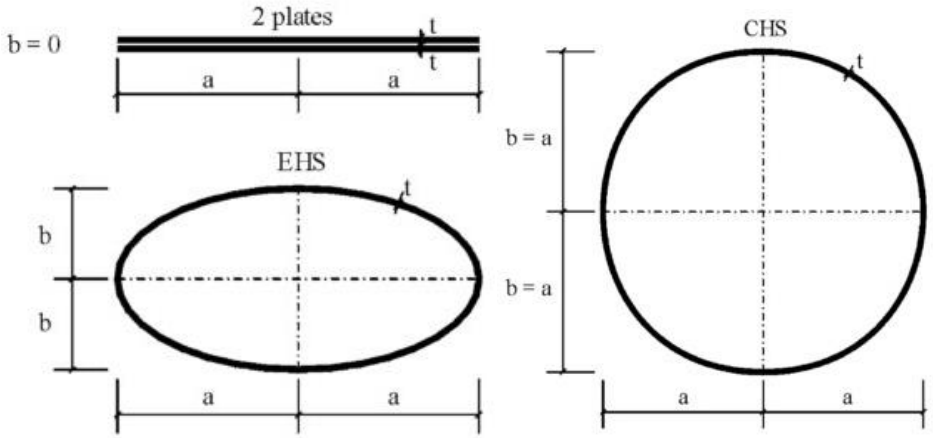

Figure 2.3 Transition between plate, EHS, and CHS [15]

When *a*=*b*, the EHS sectional shape will become a CHS while when *b*=0, two adjacent plates will be obtained. Therefore, the elastic buckling stress of the EHS should be bounded by that of a CHS and a plate. An improved slenderness of a compressed EHS more suitable for higher aspect ratios and tube thickness was defined as Equation (2.4) based on numerical and analytical studies, which covers a range of aspect ratio of EHSs (say $1 \le a/b \le 4$).

$$\frac{D_{eq}}{t\varepsilon^2} = 2a\left[1 + f\left(\frac{a}{b}\right) - 1\right]/t\varepsilon^2 \tag{2.4}$$

where $f = 1 - 2.3\left(\frac{t}{2a}\right)^{0.6}$.

Silvestre and Gardner [16] also investigated the transitional behaviour of EHSs from CHSs to plates through numerical study. Overall six different aspect ratios (1.1, 1.25, 1.5, 2, 3 and 5) were selected and all the EHSs had the same cross-sectional area. It was found that EHSs with lower aspect ratio failed in shell-type

buckling and had imperfection sensitivity while those with higher ratios were dominated by plate-type buckling and imperfection insensitivity. Moreover, by analyzing the normal stress distributions, it was expected that an ‘'effective width concept” widely used in strength analysis of flat plates could be adopted for the design of EHSs with moderate to high aspect ratios. The reason is that compressive stresses grown and accumulated near minimum radius of curvature area when aspect ratio was higher but the stress level around maximum radius of curvature was low.

Flexural buckling of EHS columns under compression has been investigated as well by Chan and Gardner in 2009 [17]. In total, 24 buckling tests about both the major and minor axes were conducted- 12 about the major axis and 12 about the minor axis. All EHS columns had a same aspect ratio of 2 but with several of slenderness from 0.19 to 1.58. Verifications of finite element models against tested full load-deflection histories and failure modes of EHSs were carried out and satisfactory replications were obtained. The parametric analysis was subsequently performed with 158 different models with a wider range of aspect ratios from 1.0 to 3.0 and different member slenderness (Figure 2.4 shows the comparison of column lengths). With both experimental and numerical results, the buckling curves adopted in Europe, North America, and Australia were all examined. And hence a conclusion is that the buckling curves in EN 1993-1-1 used for SHS, RHS, and CHS columns in are also suitable for EHSs, buckling about either major or minor axis.

Figure 2.4 Range of tested column lengths [17]

Complementary work to the above mentioned studies on cross-sectional classification was conducted in 2011 [18] by Gardner et al expanded to combined compression and uniaxial bending. Stub columns with different load eccentricities

were tested (four about major axis and four about the minor axis) and test data were then used to verify finite element models. For EHSs under compression and minor axis bending, it was found that the slenderness parameter $\frac{D_{eq}}{t\varepsilon^2} = 2\frac{(a^2/b)}{t\varepsilon^2}$ being for pure compression can also be used. The reason is that local buckling will also initiate at the point of maximum radius of curvature. While that point will change towards the centroidal axis as the compressive part of the loading increases for EHSs under compression and major axis bending. Therefore, another equation is suitable and is shown in Equation (2.5).

$$D_{e,ma} = D_{e,a} + (D_{e1} - D_{e,a})(2\psi - 1) \tag{2.5}$$

where D_{e1} proposed by Ruiz-Teran and Gardner [15] is calculated by Equation (2.4) and ψ (from 0.5 to 1.0) relates to a plastic stress distribution under combined loading; for pure compression, $D_{e,a} = 1.3a^2/b$; for pure bending, $D_{e,a} = 0.8a^2/b$ when a/b>1.357, $D_{e,a} = 2b^2/a$ when a/b≤1.357. Then the proposed slenderness limits were made to be $50\varepsilon^2$, $70\varepsilon^2$, $2520\varepsilon^2/(5\zeta + 23)$ for Class 1, Class 2 and Class 3, respectively, where ζ (from 1 to -1) relates to an elastic stress distribution under combined loading.

Experimental and numerical studies aiming to obtain buckling behaviour of EHSs under combined compression and uniaxial bending were performed by Law and Gardner [19] later, covering a wider range of slenderness. In total, 24 tests were conducted in which 6 were under pure compression, with 3 buckling about the major axis and 3 buckling about the minor axis. A further 18 were under eccentric compression, 9 with major axis bending and 9 with minor axis bending. Specimens subjected to major axis bending had slenderness ranged from 0.36 to 0.85 while those under minor axis bending covered the slenderness from 0.63 to 1.51. Subsequent parametric study based on verified models investigated the EHSs with aspect ratios from 2 to 4 and slenderness from 0.5 to 1.5. All the data from both experiments and modelling could form a database to access existing design rules for the corresponding CHSs to extend guides for EHS counterparts.

2.1.2 Welded tubular joints between EHSs

The first experiment on welded EHS tubular joint dates back to 2003, Bortolotti et al [6] and Pietrapertosa and Jaspart [20] tested the brace-to-chord N- and X-joints used in trusses in which a brace member was welded on the wide side of the EHS chord member. Obtained test data were then used to verify the finite element modelling method and thereafter a parametric study was carried out. They also reviewed the existing design rules for RHS and CHS connections to access the suitability for corresponding EHS connections.

Choo et al [21] conducted additional numerical analysis on welded EHS X-connections covering a wider range of variables; braces were welded on both sides of the EHS chord and the brace also oriented in both orthogonal directions of each chord orientation (joint types are shown in Figure 2.5). They concluded that among the above orientation method, axially loaded EHS connections can achieve higher capacities than equivalent CHS connections with the same brace and chord sectional areas.

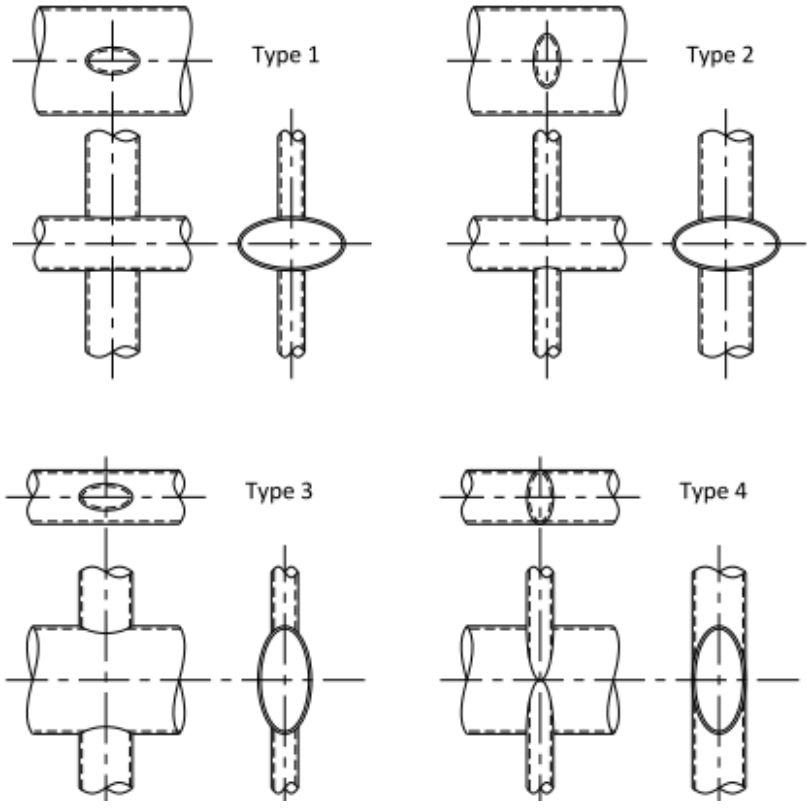

Figure 2.5 Welded EHS X-connections [21]

Further study on capacities and failure modes of welded EHS T- and X-connections was presented by Haque [22]. Twelve specimens were tested to investigate the effect of connection angle, orientation type, and loading conditions. Two methods adopted to predict connection ultimate load and failure modes named the equivalent RHS approach and the equivalent CHS approach were discussed. The former one was found to be more suitable in capturing the actual failure mode of EHS connection, though both methods were proved to be conservative. The locations of coupons for tensile tests were shown in Figure 2.6 which will be adopted for the material property testing conducted in this thesis.

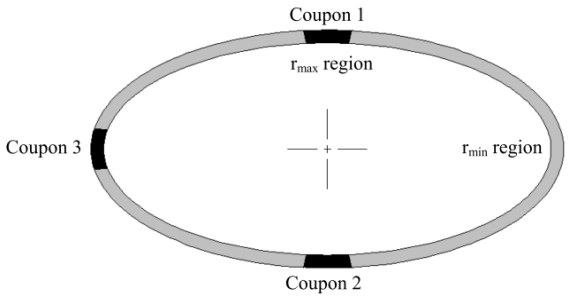

Figure 2.6 Tensile coupon locations [22]

Shen et al [23] derived an equation to estimate the static strength for EHS X-joints (Type 3 and 4 in Figure 2.5) with braces welded to the narrow sides of the chord based on both experimental and parametric studies. Moreover, a higher capacity under tensile was found compared to the compressive bearing capacity for Type 3 and Type 4 connections. For Type 1 and Type 2 connections whose braces were welded to the wide sides of the chord, their structural behaviour was found to be similar to that of the equivalent RHS joints as presented by Shen et al [24]. Additionally, two different failure modes observed were that chord sidewall failure for X-joints with equal diameters of brace and chord, and chord plasticization for those with a brace-to-chord ratio up to 0.8.

2.1.3 Gusset plate end-connections to EHSs

Behavior of gusset plate connections has been studied both experimentally and numerically. In general, a gusset plate connection is composed of a piece of steel plate and a structural member used in frames or trusses. Currently, two configurations of gusset plate connections have been investigated, (1) gusset plates welded to sides of EHS members and (2) gusset plates used in end-

connections, aiming to brace or support, for example, columns in frame structures and web members in roof trusses [7].

Experimental work has been carried out for the first configuration by Willibald et al [25], overall six specimens that varied in the orientation of the plate and EHS were tested to failure with the branch/through plate loaded in axial tension and the enhancement of strength of using through plate in each variation was obtained. Tested joint assemblies can be seen in Figure 2.7, where the branch/through plate was arranged in both longitudinal and transverse direction of the EHS steel tube; and was connected on both wide side and narrow side of EHS.

Some important conclusions obtained from the tests are that: final failure of these joints were found to be caused by punching shear resulting in tear out of branch/through plate; the yield strength of through plate connection is approximately twice or more as that of branch plate connection. In addition, comparisons of experimental results with CHS and RHS resistance formulae according to CIDECT revealed that neither of them can completely represent the performance of EHS counterparts but RHS formulae are closer and can be adopted as a conservative design guide for gusset plate connections to the ends of EHS members.

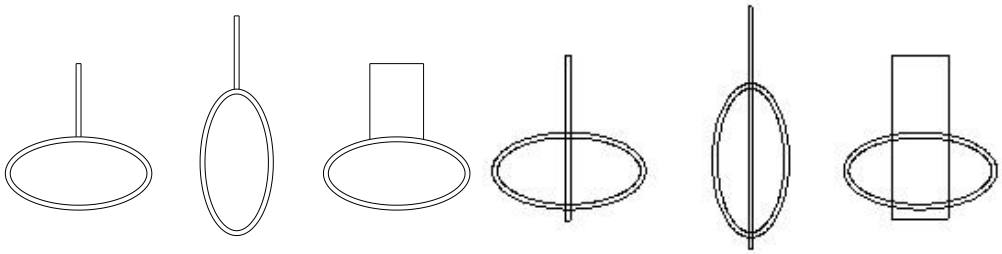

Figure 2.7 EHS and plate orientation of tested specimens [25]

For the second configuration, one way is to slot the guest plate into the EHS member end and, another way is to insert EHS into a slotted gusset plate. Five tension tests has been conducted by Willibald et al [26] covering the above two assemblies and both gusset plate orientations (plate parallel to major or minor axis of EHS) were taken into consideration. The details of five different specimens are shown in Figure 2.8, in which type E1 and E2 have different weld lengths and

type E3 and E4 have different weld lengths, however E1 and E3 have nearly the same weld length and E2 and E5 also have the same weld length.

By analyzing the experimental results, the following conclusions can be drawn: failure of all tensile specimens was caused by circumferential fracture of the EHS; the connection length has a major effect on ultimate load of such end-connections; fabrication method has a minor effect on ultimate load (by comparing E1 and E3) and specimen E5 with a smaller eccentricity had a slightly higher bearing load.

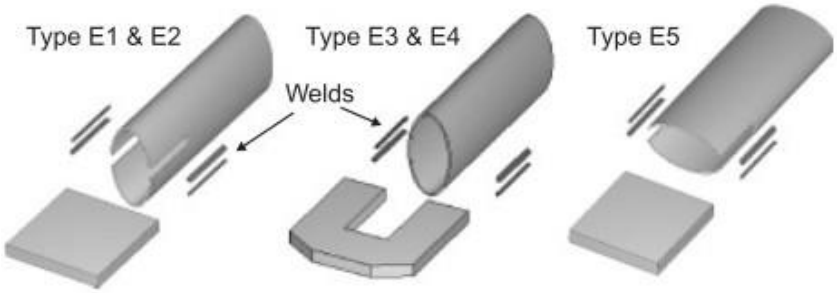

Figure 2.8 Exploded view of gusset plate end-connections with EHSs [26]

The five full-scale lab test results were then employed by Martinez-Saucedo et al [27] to verify FEMs and a parametric analysis was thereafter performed comprising 302 FEMs of gusset plate end-connections with EHSs. The parameters considered in the analysis included L_w/w ratio, D_{avg}/t ratio and types of joint assemblies (illustrated in Figure 2.8). The definition of variables can be seen from Figure 2.9, and D_{avg}, denotes the average of the larger and smaller diameter of the EHS.

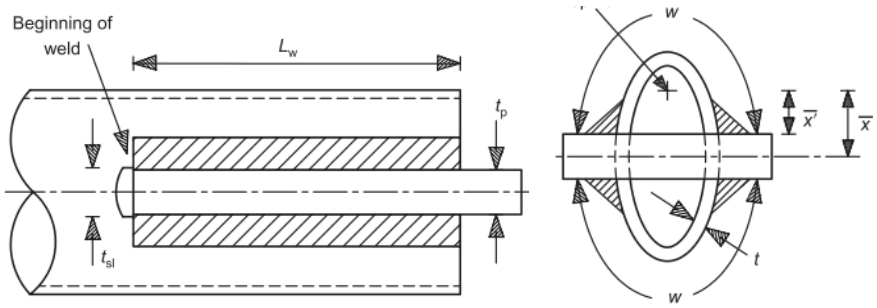

Figure 2.9 Important dimensions for slotted EHS end-connections [27]

Through the parametric analysis, a new design method divided by failure modes for slotted end-connections to EHSs in tension was suggested which is a significant improvement over the application of current international design provisions. The equations are shown in Table 2. 1, where the first one is for CF (circumferential tensile fracture) failure and the second one is for TO (tear-out) failure.

Table 2.1 Design method for slotted end-connections to EHS under static tension loading [27]

$L_w / w \geq 0.60$	$T_r = \phi \cdot A_n f_u \left[1 - \left[1 + \left(\frac{L_w}{w} \right)^{1.3} \right]^{-3.8} \right]$
$L_w / w < 0.60$	$T_r = \phi \cdot \left[R_t A_{nt} f_u + R_v A_{gv} \left(\frac{f_y + f_u}{2\sqrt{3}} \right) \right]$

where resistance factor $\phi = 0.9$ for CF and 0.85 for TO;

A_n =critical net area of connection with an open slot or $A_n = A_g$ when a slotted gusset plate is used (A_g denotes the gross cross-sectional area of hollow section); f_y =specified minimum yield stress, f_u =specified minimum tensile strength;

$R_t = 1.0$ and $R_v = 1.0$ for slotted EHS connections;

$R_t = 0.85$ and $R_v = 0.85$ for slotted gusset plate connections

(R_t and R_v represent tension and shear area mean stress correction factor, separately.)

2.2 CFST columns and connections

2.2.1 Composite columns with elliptical tubes

Firstly, the elastic local buckling of thin-walled EHSs containing elastic infill material subjected to axial compression was analyzed by Bradford and Roufegarinejad [28] using an energy-based technique. Then, experimental tests

on concrete-filled EHS columns were carried out by Yang et al [8], Zhao and Packer [29], Sheehan et al [30], Jamaluddin et al [31], and Uenaka [32]. Their research contents covered load-bearing capacity, elastic stiffness, ductility, confinement of steel tube to core concrete, and concrete shrinkage, etc. Steel tube wall thickness, concrete infill strength and various loading cases including loading compositely, loading on steel tube only and loading on core concrete only. Additionally, complementary numerical studies were performed by Dai and Lam [33], and Dai et al [34] to investigate axial compressive behavior of both the stub and slender concrete-filled EHS columns.

In total of 21 concrete-filled column specimens with three nominal EHS tube thickness (4mm, 5mm, 6mm) and three concrete grades (C30, C60, and C100) were subjected to axial compression and tested to failure by Yang et al [8]. In particular, the EHS tubes of 6 of 21 specimens were coated with grease prior to casting with concrete, to investigate the concrete shrinkage; another 6 of 21 specimens were loaded only on the concrete core to study the confinement provided by the EHS tubes.

Typical failure modes obtained from experiments are shown in Figure 2.10. For the hollow section column, both inward and outward local buckling may be observed as seen from Figure 2.10 (c) obtained by Chan and Gardner [3]. While though outward local buckling can be clearly seen from Figure 2.10 (a)-(b) for composite columns (from left to right, the dimensions are 150×75×4mm, 150×75×5mm, 150×75×6.3mm, 150×75×4mm), inward local buckling was successfully prevented.

For columns with thinner tubes, an inclined shear failure was observed, that failure disappeared when the thickness was bigger. The reason may be that more confinement was offered by the thicker tube. In addition, Yang et al also found that columns with thicker EHS tube owned high load-bearing capacity and improved ductility, while those with higher concrete strength can only be enhanced on ultimate bearing load and the ductility decreased; the effect of concrete shrinkage had little effect on the ultimate load of the EHS composite columns. For those specimens loaded only on core concrete, it was found that

both the static strength and ductility of core concrete were higher than the unconfined concrete.

From all the above conclusions, it can be easily summarized that composite EHS columns under axial compression work better than any of the individual member, EHS tubes or the core concrete. Zhao and Packer [29] expanded the experimental study to stub columns with self-consolidating concrete (SCC). In the test programme, both normal concrete and SCC were used and the above mentioned three loading cases were considered.

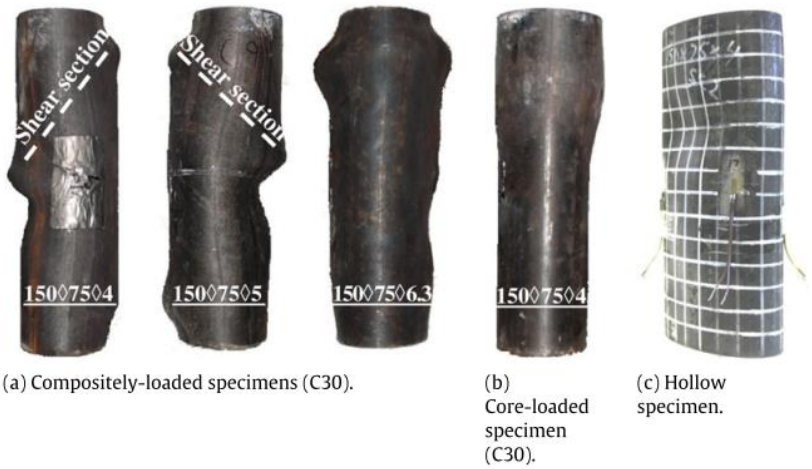

Figure 2.10 Typical failure modes of EHS columns [8]

Different failure modes can be found in Figure 2.11. It can be concluded that the inward local buckling of EHS is eliminated by the concrete infill as similar with those in Figure 2.10. In addition, Zhao and Packer [29] compared the test results of load bearing capacity with those predicted equations in Eurocode 4 and CAN/CSA-S16 for CHS columns and found them applicable to EHS short columns. Moreover, a simple superposition approach to predict the ultimate load carried by the EHS and that by the core concrete was proved to be suitable by all test data. Equations are shown below:

$$P_{ss} = A_s f_y + A_c f_c \tag{2.6}$$

$$P_{ss} = A_s f_y + 0.85 A_c f_c \tag{2.7}$$

where A_c and A_s refer to loading area of concrete and steel tube, respectively; f_c denotes the compressive cylinder strength of concrete; 0.85 is a reduction factor

on concrete strength which is often used in design rules. Load bearing capacities calculated by Equation (2.6) slightly overestimate the tested results while those from Equation (2.7) were slightly conservative.

Figure 2.11 Failure modes in different loading cases: (a) uniform compression loading of entire cross-section, (b) compression loading of concrete only and (c) compression loading of steel only. [29]

For axial compressive behavior of both stub and slender composite columns with EHSs, Jamaluddin et al [31] provide more test data covering a wider range of specimen dimensions. Column lengths (300, 400, 1500, 1800, 2500mm), sectional sizes (150×75×4, 200×100×5mm) and concrete strength (C30, C60, C100) were all taken into consideration. As expected, load bearing capacity was enhanced due to the confinement of steel tube to core concrete and inwards local buckling failure occurring in stub columns was eliminated or delayed. Failure modes of all slender column specimens was characterized by global buckling though most cases got the local steel yielding before the buckling. A review of current design rules on composite columns with CHSs in Eurocode 4 was presented by Jamaluddin et al and then new provisions on EHS columns were proposed to predict the load bearing capacities of elliptical composite columns.

Figure 2.12 Deformation of slender columns [31]

Uenaka [32] investigated the concrete-filled thin-walled elliptical stub columns subjected to pure compression. Overall 21 specimens (EHS: 2a=160mm) with different wall thicknesses (1.0, 1.6, and 2.3) and column lengths (160, 200, and 250mm) were tested covering different aspect ratios (1.5, 2.0, and 2.5). Local buckling of steel tube and shear failure of core concrete can be observed from failed specimens which are similar to those mentioned above. It was found that the thinnest specimen with an aspect ratio of 2.5 bulged within 1% of the initial load. Deformability of elliptical stub columns increased with the increasing of diameter-to-thickness ratio reasoning that the confinement of steel tube to core concrete turned to weaker.

Sheehan et al [30] complemented the experiments on concrete-filled EHS stub columns under eccentric compression. Eight stub columns with two different tube thicknesses were tested to failure and various eccentricities were taken into consideration. The structural behavior of columns under eccentric compression was found to be sensitive to tube thickness, loading eccentricity as well as axis of bending. Typical failure modes (Figure 2.13) obtained from specimen MI25-5

and MI75-5 were found to be local buckling of steel tube at either mid-height of the column or the position that below the mid-height.

A 3D finite element model was developed to simulate the exact behavior of tested specimens and was found to have successfully captured their failure modes and load vs. lateral displacement curves. Combined axial force vs. bending moment interaction curves were also derived for EHSs though a plastic analysis which was proved to be efficient to most of the EHS stub members.

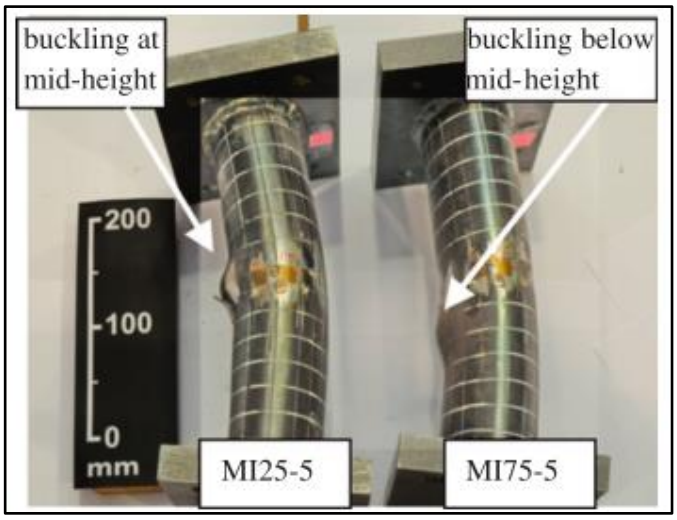

Figure 2.13 Typical failure modes [30]

Dai and Lam [33] proposed a new confined concrete stress-strain model for the concrete-filled EHSs which can be used in finite element analysis provided by ABAQUS software. The numerical results obtained from finite element models using the new confined concrete stress-strain relationship were found to be successful to repeat the stub column tests in literature on failure modes, maximum axial compressive and the full load vs. end-shortening curve. Thus the proposed stress-strain model is accurate but needs to be validated by a wider range of experiments to expand its application.

Dai and Lam modified the stress-strain curves for concrete confined by CHS from “three parts” to “four parts” by adding a “quick softening” section after the concrete crushed and the effect of section deformation, which is depicted in Figure 2.14 where $0.5f_{cc}$ means the proportional limit stress, f_{cc} refers to the maximum confined strength and ε_{cc} is the corresponding strain. The curve before 0.5fcc is

the first part where $E_{cc} = 4700\sqrt{f_{cc}}$; the curve starts from 0.5f_{cc} to f_{cc} is the second part, where the stress-strain relationship can be obtained by Equations (2.8). The third part beginning from f_{cc} to f_e is the new portion introduced by Dai and Lam, where f_{cc} can be calculated using the same equations but with different parameter values, as listed in Equation (2.9). And $f_e = \nu_3(f_{cc} - f_u) + f_u$ in which $\nu_3 = 0.3$ when a/b=2 and $15 \le (a+b)/t \le 30$, the corresponding strain $\varepsilon_e = 10\varepsilon_{ck}$. The fourth part begins from f_e to f_u where $f_u = \nu_4 f_{cc}$ and the corresponding $\varepsilon_u = 30\varepsilon_{ck} = 0.09$, and the parameter ν_4 is 0.3 for C30 concrete and 0.7 for C100 concrete (linear interpolation may be used between C30 concrete and C10 concrete).

$$f = \frac{E_{cc}\varepsilon}{1 + (R + R_E - 2)\left(\frac{\varepsilon}{\varepsilon_{cc}}\right) - (2R - 1)\left(\frac{\varepsilon}{\varepsilon_{cc}}\right)^2 + R\left(\frac{\varepsilon}{\varepsilon_{cc}}\right)^3} \tag{2.8}$$

where $R_E = \frac{E_{cc}\varepsilon_{cc}}{f_{cc}}$, $R = \frac{R_E(R_\sigma - 1)}{(R_\varepsilon - 1)^2} - \frac{1}{R_\varepsilon}$, $R_\sigma = R_\varepsilon = 4$.

$$f_{cc} = f_{ck} + k_1 \cdot f_1 \tag{2.9a}$$

$$\varepsilon_{cc} = \varepsilon_{ek}\left(1 + k_2 \frac{f_1}{f_{ck}}\right) \tag{2.9b}$$

$$k_1 = 6.770 - 2.645(a/b) \tag{2.9c}$$

$$k_2 = 20.5 \tag{2.9d}$$

$$f_1^{'} = f_y\{\nu_1 - \nu_2[(a+b)/t]\} \tag{2.9e}$$

where $\nu_1 = 0.043646$, $\nu_2 = 0.000832$ for $21.7 \le (a+b)/t \le 47$;

$\nu_1 = 0.006241$, $\nu_2 = 0.0000357$ for $47 \le (a+b)/t \le 150$.

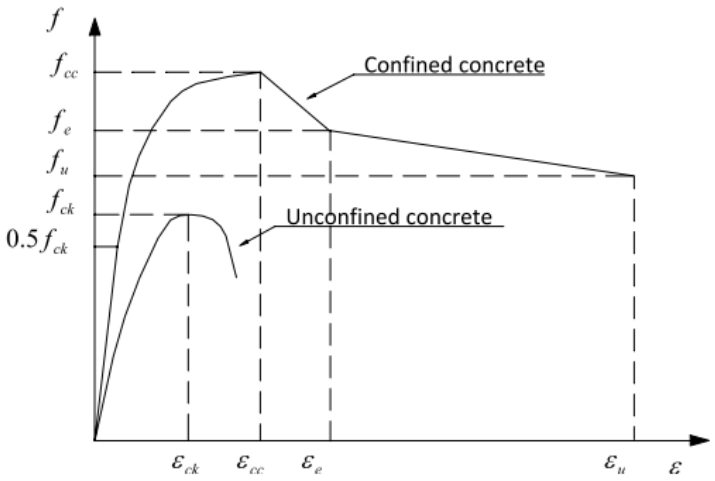

Figure 2.14 Stress-strain curves of concrete unconfined and confined by EHSs [33]

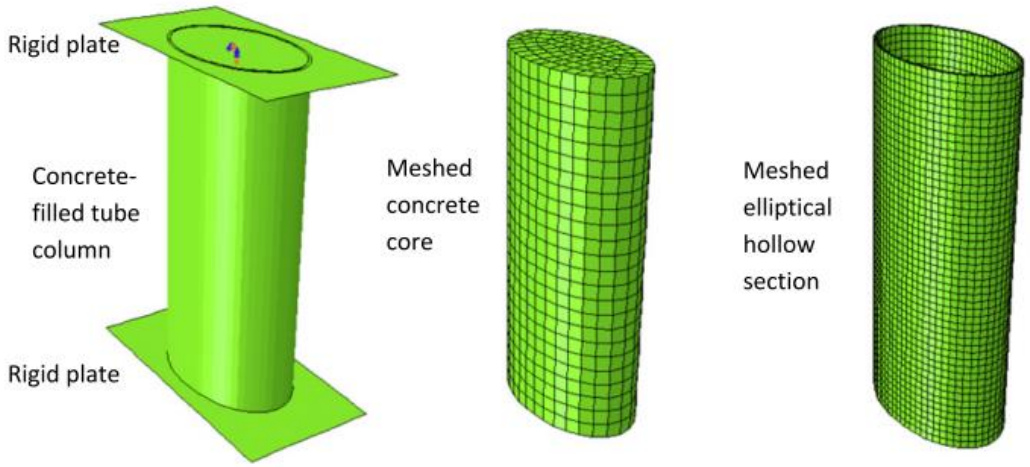

Figure 2.15 Typical FEM used in numerical modelling [33]

In addition, it is suggested that an appreciate mesh size for steel tube can be 5-10mm while 10-20mm for the core concrete, and the concrete element size is better to be twice that of the steel tube mesh size. Finite element model adopted in their numerical study can be seen from Figure 2.15, in which two rigid plates were used on both the top and the bottom end of the column; solid element C3D8 were selected for both steel tube and concrete infill as it can reflect the real mechanical response. The contact between rigid plate and end column was defined as a surface-to-surface contact with “Hard contact” in normal direction and “rough” option (no slip once contact) in tangential direction; “Hard contact” was also adopted for contact between the inner surface of EHS tube and concrete surface while “penalty” with friction factor of 0.2 or 0.3 was suggested in the

tangential direction. All the above suggestions may be used to develop the finite element models for composite columns of elliptical column to I-beam connections.

A numerical modelling method for slender elliptical concrete-filled columns under axial compression was then reported by Dai et al [34] to supplement the previous study on stub columns. As the stress-strain relationship described above for confined concrete is only suitable for the stub columns, hence another model was adopted into FE modelling. As global buckling will govern the failure of a slender column, both compression and tension will occur. Therefore, the tensile stress-strain model for confined concrete was introduced to be 10% of the corresponding compressive stress and strain. The compressive relationship can be obtained using the following Equation (2.10):

$$y = \begin{cases} 2x - x^2 \\ \dfrac{x}{\beta_0 (x-1)^2 + x} \end{cases} \tag{2.10}$$

where $x = \varepsilon/\varepsilon_0$, $y = \sigma/\sigma_0$, $\sigma_0 = f_{ck}$, $\varepsilon_0 = \varepsilon_c + 800\xi^{0.2} \times 10^{-6}$;

$\varepsilon_c = (1300 + 12.5 f_{ck}) \times 10^{-6}$;

$\beta_0 = \left(2.36 \times 10^{-5}\right)^{\left[0.25 + (\xi - 0.5)^7\right]} (f_{ck})^{0.5} \times 0.5 \geq 0.12$.

In the above equations, f_{ck} means the cylinder compressive strength of concrete and ξ is the confinement factor which can be calculated by $A_s f_y / (A_c f_{ck})$ in which f_{ck}=0.8f_{cu}, and f_{cu} is the cube compressive strength of unconfined concrete. The concrete material properties suggested for stub columns by Dai and Lam [33] will be adopted to develop the numerical models in this thesis, as no global buckling failure was observed in the columns after experiments.

Figure 2.16 shows the comparison of failure modes of slender columns between experimental results and modelling results which proves that the FE modelling method adopted can successfully predict the deformation of slender EHS columns filled with concrete.

As illustrated in this figure, both loading plate and roller were simulated to capture the actual response of the specimen which is a good way that can then be applied in this report when simulating the loading part at beam ends of the connections. Also, an imperfection value of L_e/2000 was assumed in the geometrical models for slender columns.

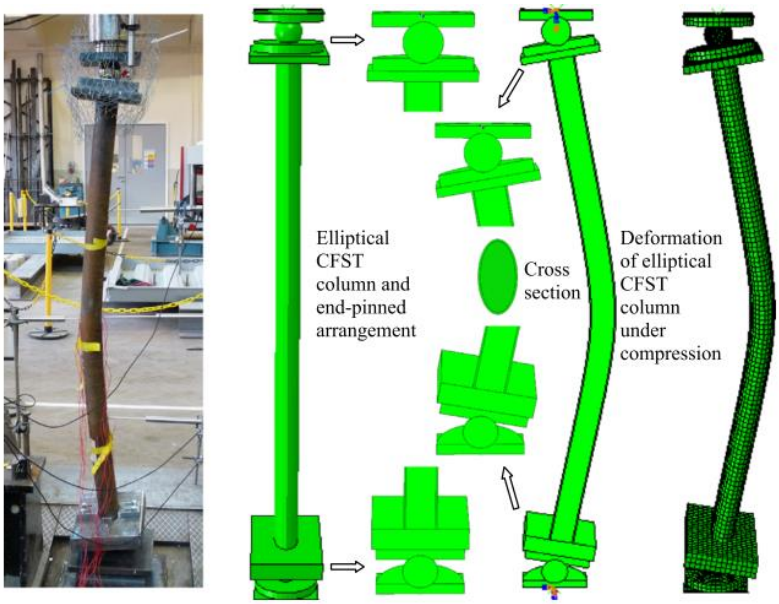

Figure 2.16 Comparison between tested specimen and FEM [34]

Additionally, an innovative type of composite column, stainless steel-concrete-carbon steel double-skin tubular columns, has been introduced by Han et al [35]. Overall eighty stub columns tests have been conducted in which the main parameters are the sectional type (CHS, SHS, RHS, and EHS), the column type (straight, inclined and tapered) and the hollow ratio (from 0.5 to 0.75) of the composite section. This research has pushed the application of composite columns further widespread. Thus mechanical behavior of the corresponding connections need to be investigated as well in the future to obtain economical connection details as well as design provisions.

2.2.2 Connections with composite tubular columns

Connections with composite tubular columns have been studied for decades due to its widespread use in building structures. The connection types involved has varied significantly depending on the tube sectional shape and desired connection requirements [36]. Some very early research had been focused on various connections which either with beams attached to the face of the steel

tube only [37-41] or with elements embedded into the concrete core [42-44]. All the connections showed good ductile behavior. Conclusions from these studies suggest that connections with beam directly on the columns demand exclusive deformation on tube wall as well as the connection, and connections with embedded components may own better static and seismic behavior because that the high shear force is alleviated to the tube wall. Shakir-Khalil [37] demonstrated those conclusions by conducting six large-scale connection experiments, saying that it was efficient in alleviating the high stress concentration existing on the tube wall by using embedded elements to distribute the beam flange force to the core concrete.

From then on, extensive studies were carried out on framed connections with tubular composite columns on their monotonic loading behavior [45-47], seismic behavior [49-52], and fire resistance [53, 54], etc. Through beam connection is one of those framed connections being tested by Elremaily and Azizinamimi [55] to help comprehend the behavior of this ideal-rigid connection (shown in Figure 2.17).

The beam web was attached to the web cleat plate through two fabrication bolts and fillet welds. Column failure, beam failure, and joint shear failure were found among seven two-thirds scale connection specimen. Based on the experiments, column failure would happen when the column flexural capacity is less or equal than that of the beam, and failure initiates at the tearing zone on the fillet weld that attaches to the beam flange. Beam failure, with plastic hinge formation, would occur when the column is strong enough while if the joint portion cannot stand the high shear force, failure would take place by joint shear failure.

Static behavior of this kind of connection was also investigated by Beutel et al [46], with four straight reinforcing bars welded to the top and bottom flanges of the beam and embedded into the core concrete. It was found that the there is no connection failure due to the embedded bars and failure occurred in the beam by a plastic hinge outside the zone of influence of the bars.

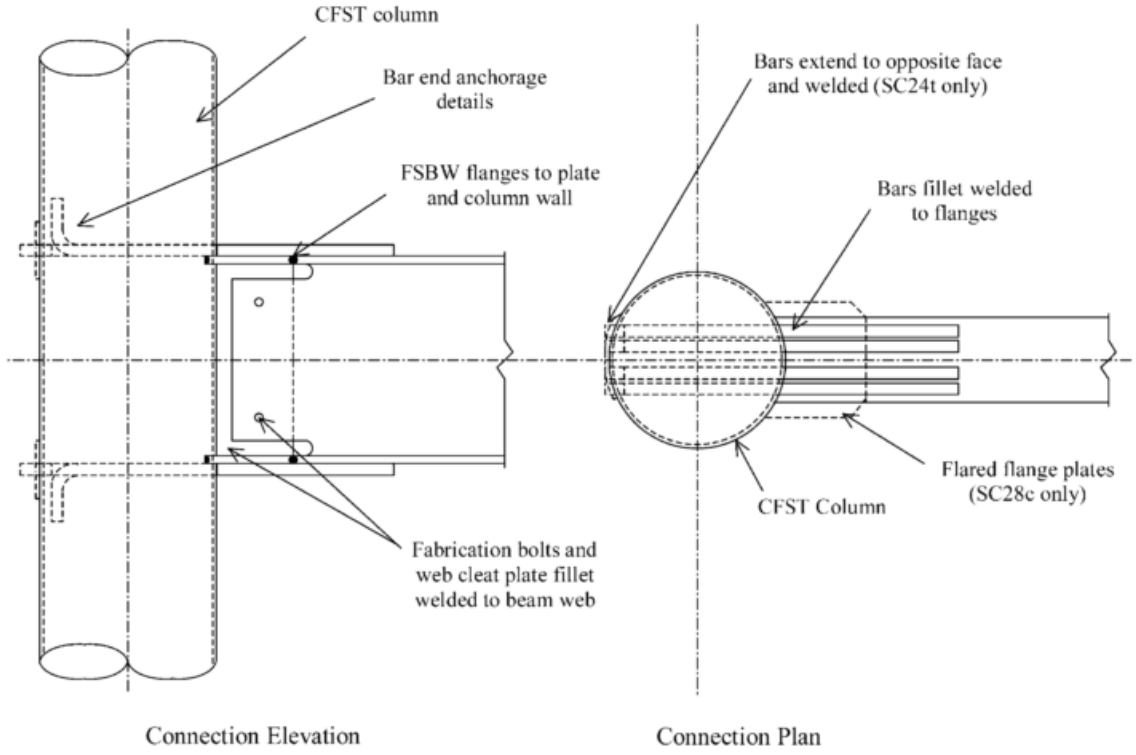

Figure 2.17 Connection configuration [46, 50, 55]

Although through beam connections will have better performance under seismic load, they may cause difficulty in field construction owing to their complexity in the panel zone. In contrast, through column connections can be characterized that utilize diaphragms or other stiffeners to connect steel beams to the CFST columns, which have received much attention on improving their mechanical performance. Figure 2.18 shows a typical bolted CFST connection with either square column or circular column, which are also named by flush end plate joints compared with those comprised of I-beams and H-section columns reported in some publications [56-59].

Wang et al [48] conducted an experimental study to demonstrate the good moment-rotation behaviour of this kind of joint with blind bolts. All the tested connections show good ductility when subjected to monotonic loading, the stiffness and strength of the blind bolted connections are definitely affected by the thickness of end plate.

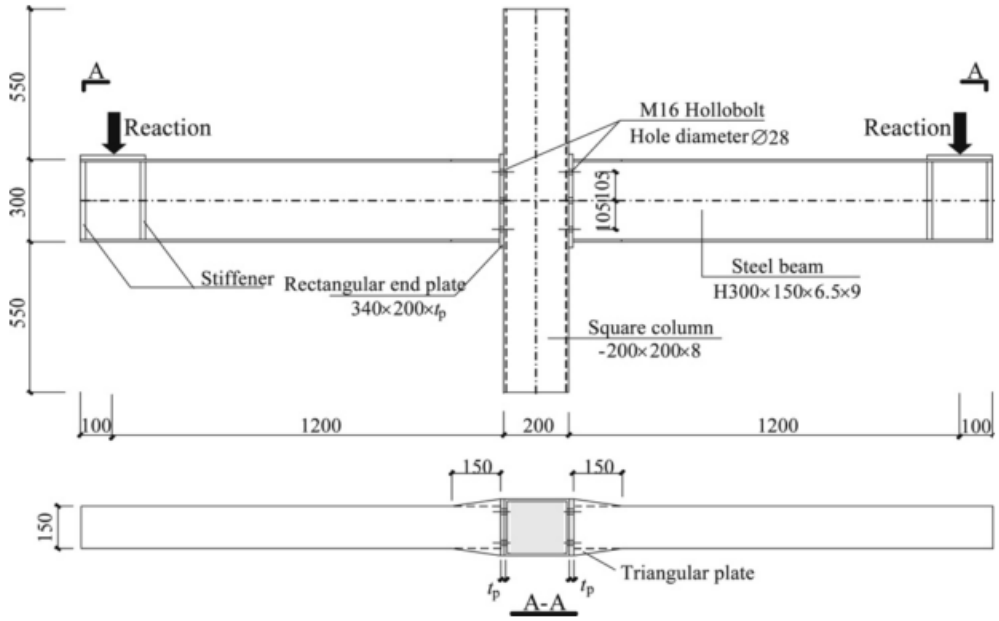

(a) Square CFST connection

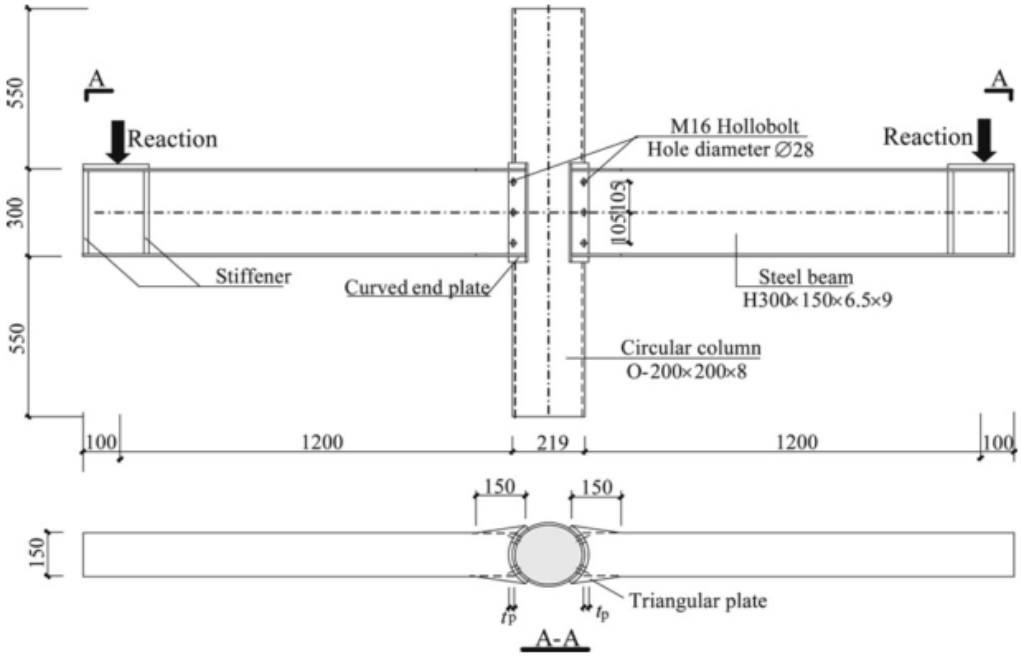

(b) Circular CFST connection

Figure 2.18 Typical bolted CFST connection [48]

Another through column connection-CFST connection with external diaphragm is depicted in Figure 2.19, where the diaphragm is like a ring and connects the beam ends together. Han and Li [49] investigated the seismic behavior of such connection with reinforced concrete (RC) slab experimentally. Overall six connections, four of which had interior joints and two of which had exterior joints,

were tested to failure. Favorable performance were obtained by assessing the ductility, strength degradation and energy dissipation of the joints.

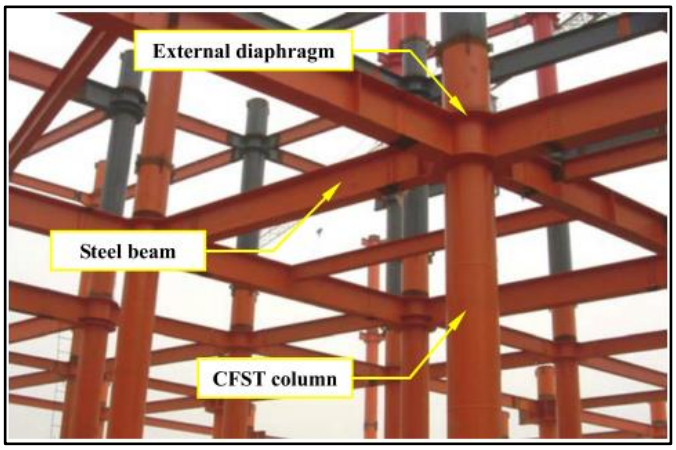

Figure 2.19 CFST connection with external diaphragm [49]

In case of column failure in these connections, the reduced beam section (RBS) steel beam to CFST circular column was designed based on the weak-beam-strong column approach and was investigated by different scholars, such as Chen and Chao [60], Jin and El-Tawil [61]. Wang et al [52] conducted an experimental study which comprised five connections of reduced beam section (RBS) steel beam to CFST circular column using the external ring, tested connection configuration can be seen in Figure 2.20. In general, all of the specimens were failed with beam failure which initiated at the reduced section of beam. It was found that the RBS beam to CFST column owns better seismic performance and ductility compared to their weak-column connection counterparts whilst the ultimate load may be reduced slightly.

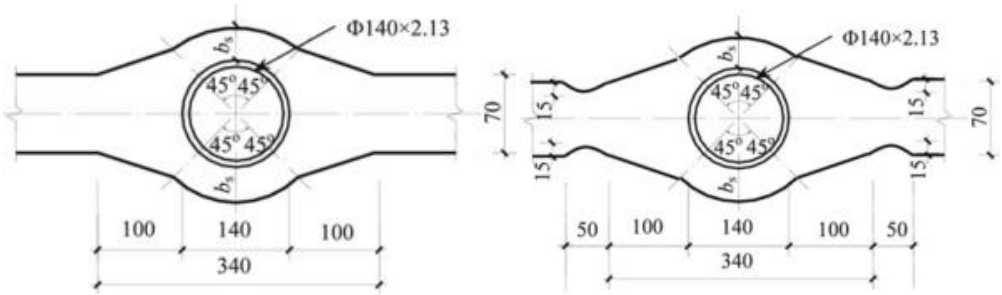

Figure 2.20 CFST connections with external ring [52]

However, for CFST columns with a sectional size exceeding a large value, e. g. 500mm, it will be difficult to fabricate and incorporate a larger ring plate outside the column. Therefore, such a stiffening method will be not suitable for CFST connections in this case which enables the adoption of an internal stiffening method. Joint specimens with internal diaphragms were tested to failure by Cheng et al [62]. Four steel beams to CFST column joint with RC slabs were tested, two of which had exterior joints and two with interior joints. A simplified analytical model was proposed based on the experiments to simulate the envelope of force-deformation behavior for the connections. The details of panel zone of tested specimens are shown in Figure 2.21.

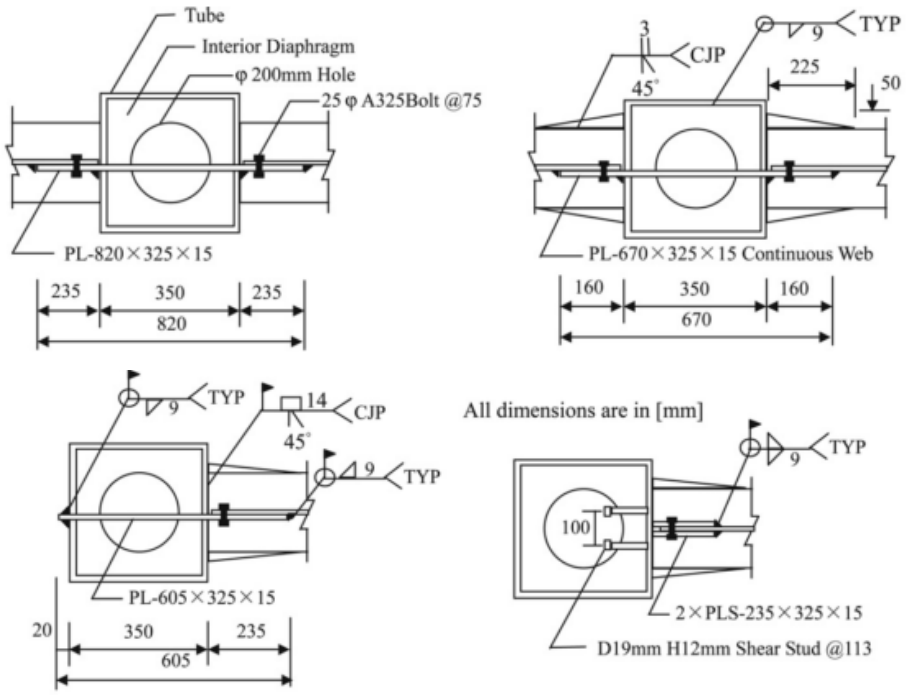

Figure 2.21 Details of panel zone in connections with internal rings [62]

Although the connection mentioned above may provide better stiffness, static strength, etc., there are fabrication difficulties which are time consuming and expensive due to the complexity of these connections. Simple connections such as fin plate connections are easy to fabricate and install, and thus they have gained popularity owing to their economical cost and fast construction.

2.3 Fin plate connections

A fin plate beam-to-column connection consists of a piece of steel plate welded in the workshop to the outer face of the column, to which the supported beam

web is bolted on site. Fin plate beam to column connections are illustrated in Figure 2.22 where the beams are bolted either to H column, SHS column or CHS column. Design of such connections is based on BS EN 1993-1-8 [59] and its accompanying national annex with supplementary recommendations presented in the 'Green Book' [63] which is a joint publication of the Steel Construction Institute and the British Constructional Steelwork Association Limited. With the emergence of EHS column, the current design method of fin plate connections should be evaluated and extended to be applicable to the connections with EHS columns.

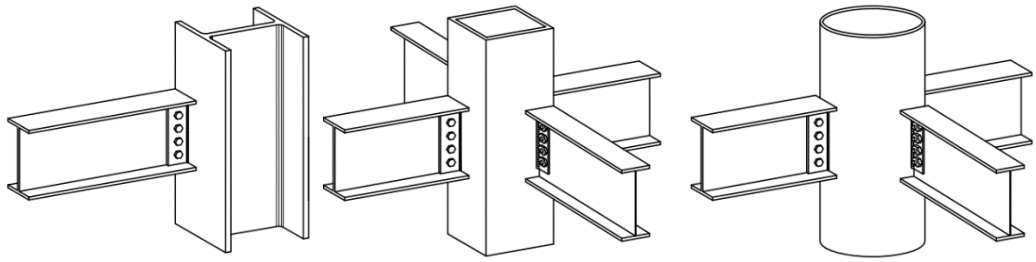

Figure 2.22 Fin plate beam to column connections [63]

2.3.1 Early research work

Early research on fin plate connections with tubular column dates back to 1960's. White and Fang [64] conducted forty-two tests in regarding to five configurations (shown in Figure 2.23) under combined shear and bending load and also scenario of shear force only. Connection configuration of Type A (fin plate) and Type E (through plate) are most relevant to the current research. Type A connection was mentioned as the easiest connection type in terms of fabrication among the cases analyzed. Five parameters were considered for this kind of connection: ratio between the width of tube wall to tube thickness, ratio between the connection length to tube size, material, shape of tube, and type of fastener. Different failure modes were obtained for Type A connections under shear force, which were local buckling of the column, tearing of the weld and web crippling of the beam. It is noted that the distortion of the tubular column walls caused by loading transferred from connections might decrease the capacity of the column. This may reside in the fact that the effective area of the column tube decreased when the large distortion has formed. In terms of stress, it was found that the magnitude of stress near the connection zone was high at a relatively low load level.

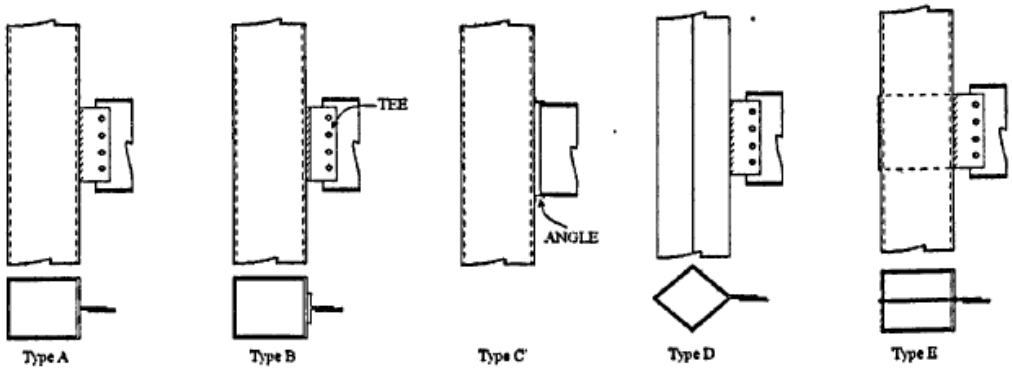

Figure 2.23 Connection types [64]

Sauerwine [65] conducted further experimental tests in comparison with those performed by White and Fang. Four tests of double-sided connections with symmetrical beams connected to the sides of the square tubular columns were studied. The columns in the connections were not subjected to axial loading in the longitudinal direction of the column, so they only carried the load transferred from the beams through connections. It was found from the test results that the tube wall above the connection was compressed in, the wall below was pulled out, while the unloaded tube wall was buckled both above and below the connection. Final failure of the connection was found as tension tear of the weld originated from the bottom of the fin plate. When analysing the strain data, Sauerwine found that the strain at the fin plate was generally lower than the strains in the tube wall.

Sherman [66] conducted twenty-four tests on a series of connections with hollow structural section columns. Nine connections were tested in regards to fin plates with different lengths subjected to combined shear and bending. The column width/thickness ration ranged from 5 to 45. Punching shear failure was found as the only limit state for connections with a relatively thin-walled column joined by a thick fin plate. Two tested connections failed around the perimeter of the welds – the fin plate was pulled out from the column wall. CIDECT design guide 9 [10] has included the criterion to avoid this failure, which is that to endure the tension resistance of the shear plate under axial load (per unit plate length) is less than the shear resistance of the column wall along two planes (per unit plate length). The inequality to express this criterion is given as follows [66, 67],

$$\emptyset_1 f_{p,y} t_p(unit\ length) < 2\emptyset_2(0.60 f_{c,u}) t_c(unit\ length) \quad (2.11)$$

where $\emptyset_1$ is the resistance factor for plate yielding, equals to 0.9; $\emptyset_2$ is the resistance factor for punching shear failure of the tube wall [67], equals to 0.75.

Jarrett & Grantham [68] conducted eighteen tests on fin plate connection with rectangular hollow section columns subjected to tensile force, to investigate the effect of column cross-section geometry and axial load on the tying behaviour of the connections. Failure modes were identified as follows: fracture of the column wall around the weld between the wall and the fin plate and buckling of the column for connections with a thinner tube wall, fin plate fracture, bolt shearing failure and beam web pulling out failure for connections with a thicker tube wall. It can be thus concluded that the tube wall thickness has great influence on the behaviour of the studied connections under tension.

The simple connections are nominally deemed as pinned connections, however, they can sustain moment to some extent in reality, especially when large beam rotation occurs. Richard et al [69] investigated the moment-rotation capacity in the fin plate connections considering the parameters of bolt numbers and bolt diameter in the experimental scheme. The test setup is illustrated in Figure 2.24. Based on both experimental and numerical results, they concluded that the outer bolts of the bolt group will reach the maximum capacity at a lower beam load with the bolt number increasing.

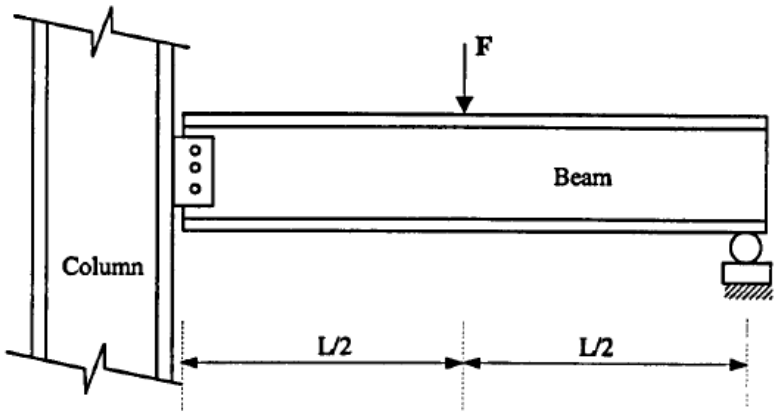

Figure 2.24 Fin plate connection setup [69]

2.3.2 Recent research work

Astaneh-Asl [70] summarized a number of research in the investigation of fin plate connections to develop design procedures for both gravity and lateral load (seismic and wind). It was found that the considered connections were sufficiently ductile in accommodating the end rotation demands of simply supported beams. The maximum rotation increased when the number of bolts in the connection decreased. Astaneh-Asl also concluded that the limit states of fin plate connections were established as follows:

- plate yielding in gross area
- bearing yielding of the bolt holes in fin plate or beam web
- edge distance failure
- net-section fracture of fin plate
- bolt fracture
- weld fracture

Jones and Wang [71, 72] conducted both numerical and theoretical studies upon the behaviour of single-sided fin-plate to concrete-filled tubular columns subjected to tensile force and bending combined with shear. The current design deformation limit of 3% of the tube width for similar connections in CIDECT Guide 9 [10] was found inadequate, when determining the ultimate strength of such connections under tension. As a result, numerical models were developed and adopted to conduct extensive parametric studies to establish a simple hand calculation method, to evaluate the strength of the steel column component of rectangular concrete-filled columns. Considered parameters include column cross-section size, column wall thickness and length of fin plate. The procedure of the simple hand calculation was according the definition of a rigid plate deformation pattern for the column face and then using the virtual work principle.

Lam and Dai [73] conducted a numerical study through ABAQUS solver on four types of beam to elliptical column connections, considering the EHS orientation, concrete infill and stiffener plate. The four simple joint assemblies are shown in Figure 2.27. Beams are bolted to columns via fin plates which are welded on the outer face of the EHSs in either the major axis direction or minor axis direction. A separate stiffener plate was used in the case of Joint-A to enhance the stiffness

of column in the minor axis direction as well as restrict possible bulge or concave deformation, while the stiffener plate in the minor axis direction and the two fin plates combined to be a whole plate in the case of Joint-C.

By analyzing numerical results, the failure modes and effect of component arrangement to the moment rotation behavior of the connections were obtained, and the through plate connection was recommended for minor axis elliptical column to I-beam joints due to its better moment behaviour. However, finite element modelling results needs to be verified by experimental data to be more convincible which turns to be one of the objectives of this thesis.

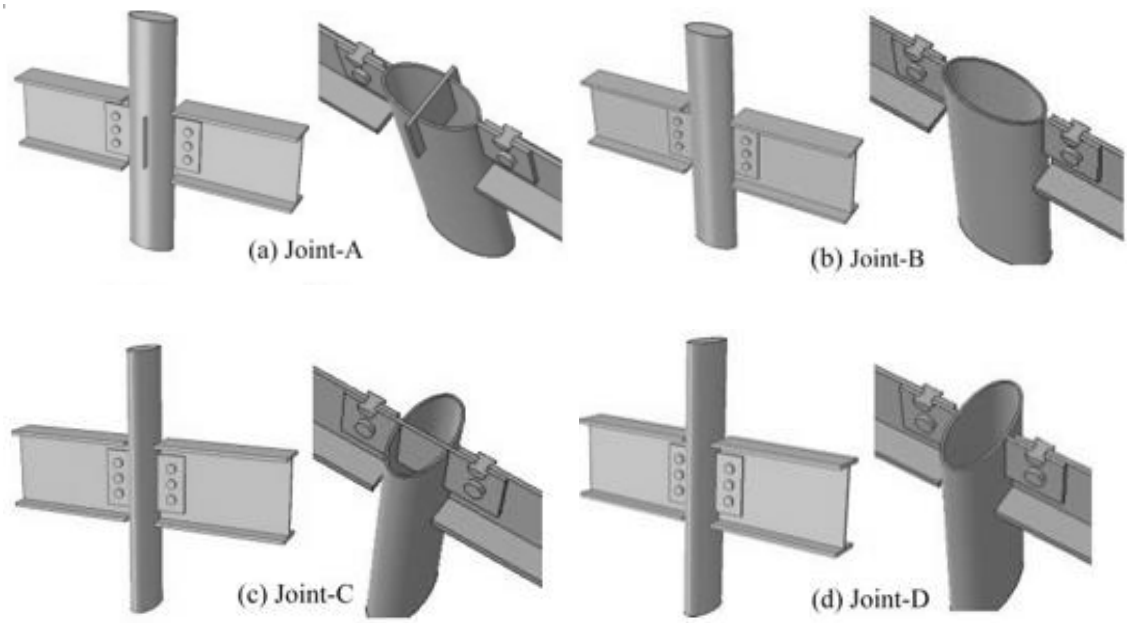

Figure 2.25 Joint assemblies [73]

2.4 Conclusions

As a new cross-sectional shape being introduced in building construction, EHS has drawn much attention among designers and researchers. Research in regards to EHS members, welded joints between EHSs, and concrete-filled elliptical columns can be found, which involved analytical, experimental and numerical studies to investigate the nonlinear response of components and truss-type joints with EHSs.

In the past decades, structural behaviour of beam to column connections with CHS and SHS have been studied thoroughly, regarding to various joint types,

load level in columns, and loading conditions, etc. However, there is limited research to date on framed-type elliptical column to beam connection which restricts widespread the use of the EHS and even threaten the safety of applications in practical structures. Especially, there is a research gap on the moment behaviour of fin plate connections with elliptical columns, which is normally deemed as pinned joints.

Chapter 3

Experimental Programme

This chapter presents an experimental programme to investigate the structural performance of a number of I-beam to elliptical steel column connections using fin plates and through plates. Design consideration of the connections and specimen details are given; material property tests for both steel and concrete are described; connection test setup, instrumentation and test procedure are provided. Relevant test results will be discussed in Chapter 4.

3.1 Design of the connections

In multi-story frame structures, the connections linking the basic structural components such as columns and beams are extensively used. It is reasonable to assume that many of these connections are those of beams to tubular columns. The design of such connections is crucial to ensure the structural stability and robustness, economical, easy and rapid construction. With all those merits, fin plate connections have been very popular and widely adopted as an optimum connection solution, especially when it is necessary to bolt beams to tubular columns. By simply welding a plate to an Elliptical Hollow Section (EHS) column face, the difficulty and complexity of fitting connection components to curved face of the columns can be avoided.

Figure 3.1 illustrates a typical double-sided beam to EHS column connection using fin-plates under a combination of bending moment and shear force, which is the main research focus of the experiments on beam to elliptical column connections. In such an assembly, fin plates are welded to the EHS column face by using fillet welds on each side, while the two beams are connected to the fin plates by using a single vertical-row of bolts.

The upper portion of the EHS column near the connection area is subjected to tensile forces transferred from the fin plates, while the lower portion sustains the compressive force not only from the fin plates but also the direct compression from the end of the beam flange (when the joint rotation exceeds a certain value). Consequently, failures of such a connection may arise in the EHS column once

there is no sufficient strength or stiffness in the transverse direction of the EHS. Possible failure modes which may occur in the column are yielding, local buckling or fracture of the column face near the fillet welds between fin plates and the column. In practical design, the column should be stronger than any other components to prevent the whole structure from collapse, thus in this chapter, a stiffener plate is adopted in the EHS column to strengthen its ability to resist internal forces and moments mainly in its transverse direction.

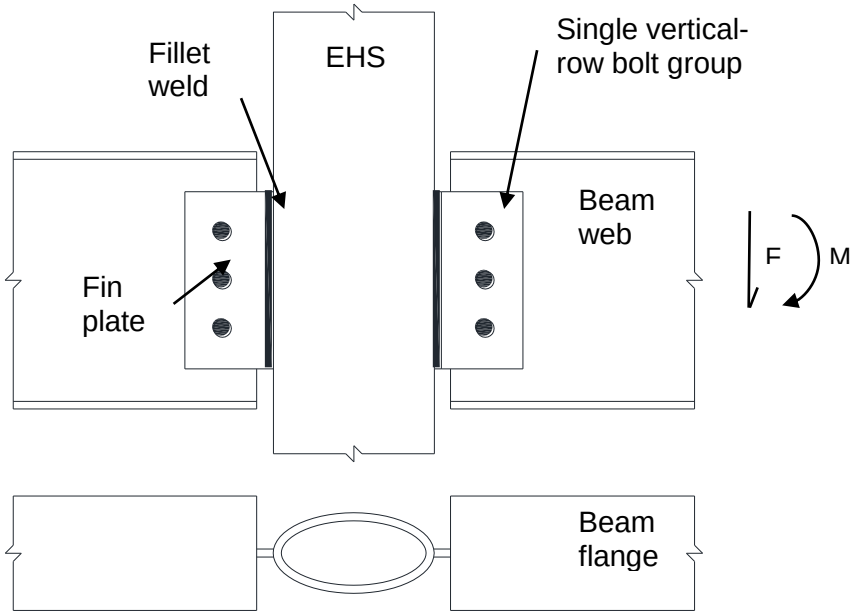

Figure 3.1 A typical beam to EHS column fin plate connection

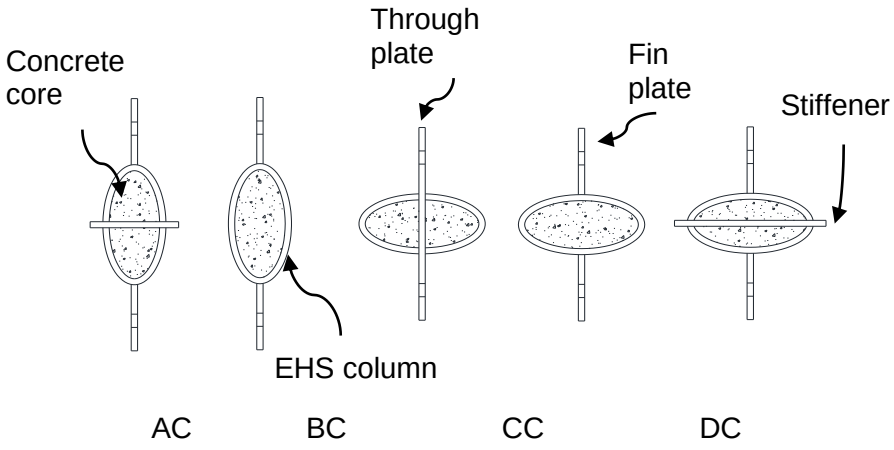

Figure 3.2 Joint assemblies (Cross-sectional view; concrete-filled ones)

As there are two main principle axes in an elliptical hollow section - the major axis and the minor axis, the arrangement of stiffeners may differ due to the orientation of the EHS. Joint assemblies considered in this chapter are illustrated in Figure 3.2. Overall, ten fin-plate connections were designed and manufactured based on these joint types (described here as Type A, B, C, D and E). Each type has a connection (e.g. Joint-AC) with a concrete-filled EHS column and another connection (e.g. Joint-AH) with an empty column, to highlight the benefit of adopting concrete on the structural behaviour of fin-plate connections.

For joint Type-A, a stiffener plate is inserted vertically at the middle of the pre-slotted EHS column in the minor axis direction to enhance its transverse stiffness. Due to the complexity and difficulty of installing stiffeners in both major and minor directions, only one stiffener plate is used, and this stiffener plate should be inserted in the minor axis direction due to its weaker stiffness. Thus, a through plate (combination of fin plates and a stiffener plate) major axis connection is not considered in this thesis. To study the effect of the stiffener, a corresponding un-stiffened joint type, Type-B is adopted. The above two types of joints are subjected to bending in their major axis direction. In practice, a connection may sustain bi-axial forces and moments, the structural behaviour of the connection in the minor axis direction is thus more crucial.

Therefore, it is necessary to investigate and improve the capability of the connections in the minor axis direction in resisting the loads. By inserting a stiffener plate, it is expected to enhance the minor axis stiffness to obtain similar or even better moment-rotation behaviour compared to the major axis. The connections of Type-C, D and E are thus designed, in which the stiffener plate and fin plates are replaced by a whole steel plate to get a continuous stiffness in the Type-C connection; the Type-E connection employed a stiffener plate in the major axis direction for comparison, while the Type-D connection is the corresponding un-stiffened connection. By investigating the above-described types of fin-plate connections experimentally, this research aims to provide reliable test data to reference in developing and verifying numerical models, simplified analytical models and component models.

The five joint assemblies are simply described as follows:

Type-A: Major axis connections with stiffeners

Two fin plates in the major axis direction and a stiffener plate in the minor axis direction; one connection with concrete-filled EHS column (Joint-AC) and another connection with empty EHS column (Joint-AH);

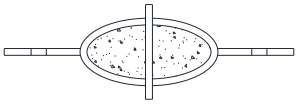

Type-A

Type-B: Major axis connections without stiffener

Two fin plates in the major axis direction and no stiffener plate; one connection with concrete-filled EHS column (Joint-BC) and another connection with empty EHS column (Joint-BH);

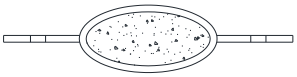

Type-B

Type-C: Minor axis through plate connections

A whole plate through the column functions as both fin plate and stiffener plate in the minor axis direction; one connection with concrete-filled EHS column (Joint-CC) and another connection with empty EHS column (Joint-CH);

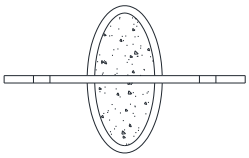

Type-C

Type-D: Minor axis connections without stiffener

Two fin plates in the minor axis direction and no stiffener plate; one connection with concrete-filled EHS column (Joint-DC) and another connection with empty EHS column (Joint-DH);

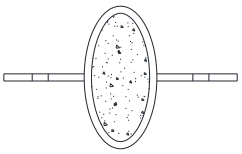

Type-D

Type-E: Minor axis connections with stiffeners

Two fin plates in the minor axis direction and a stiffener plate in the major axis direction; one connection with concrete-filled EHS column (Joint-EC) and another connection with empty EHS column (Joint-EH);

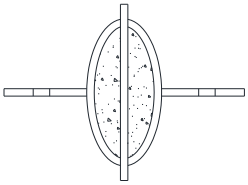

Type-E

3.2 Specimen details

Figure 3.3 shows a typical view of a beam to elliptical column fin-plate connection tested. The specimen is composed of one EHS column, two I-beams, and one end plate, and each beam is connected to the wide side of the column through a fin plate using a single vertical-row of M20 Gr.8.8 bolts or Gr.10.9 bolts. The fin

plate is welded by using fillet welds (weld size is 6mm) at the mid-height of the elliptical column (1500mm in height); the end plate used to fix the specimen is welded on to the bottom of the columns whereas the top end of the column has no end plate. The manufacturing procedure of the stiffened EHS column is, firstly, to slot a suitable hole at the designated position in the column, and then, to insert a stiffener plate and connect it with the external face of the column by using fillet welds.

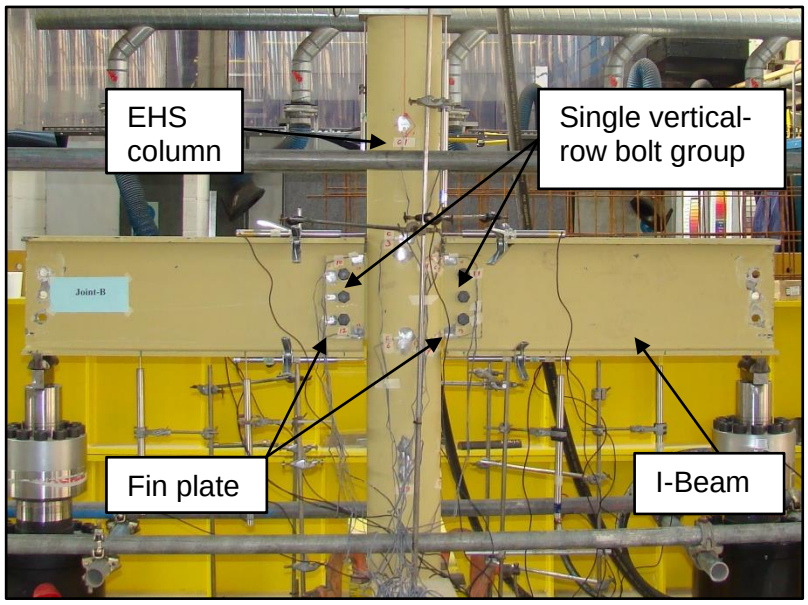

Figure 3.3 Elliptical column to I-beam fin plate connection

For the concrete-filled columns, plaster was filled in the gap at the top column end caused by shrinkage of the concrete after casting, to make sure the compressive load could be applied evenly to both steel tube and concrete.

For all of the specimens, the EHS column is made from a hot-finished EHS steel tube (S355J2H) with a section size of 200 × 100 × 5mm and length of 1500mm; the I-beam with section size of 305 × 127 × 48UB (S355JR) is 900mm in length, providing enough space to set up measuring and loading devices. Detailed specimen geometries (columns & fin and stiffening plates; I-beam) can be seen from the design drawings in appendix I; Figure 3.4 depicts the cross-sectional dimensions of the adopted I-beam. Concrete-filled specimens have the same designed dimensions with their hollow counterparts.

Prior to conducting the experiments, the actual dimensions of EHS columns were measured. Mean values are listed in Table 3.1, where 2*a*, 2*b*, *t* and *L* refer to the larger outer diameter, smaller outer diameter, thickness and length of the EHS column, respectively; hollow joints are named as Joint-AH, Joint-BH, etc., while the concrete-filled counterparts were represented by Joint-AC, Joint-BC, etc.

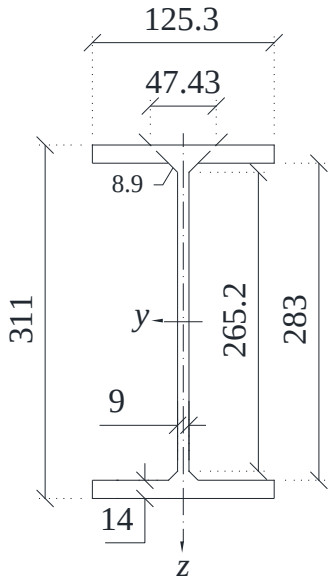

Figure 3.4 Cross-sectional dimensions of I-beam (mm)

Table 3.1 Mean measured values of EHS dimensions (mm)

Specimen ID	2*a*	2*b*	*L*	*t*
Joint-AH	198.43	99.52	1500	5.05
Joint-BH	200.01	101.51	1487	4.92
Joint-CH	198.50	100.50	1498	4.88
Joint-DH	197.78	102.03	1497	4.54
Joint-EH	197.82	102.10	1495	4.75
Joint-AC	198.60	101.89	1499	4.97
Joint-BC	198.47	101.57	1498	5.01
Joint-CC	198.21	101.42	1498	5.02
Joint-DC	198.50	101.62	1500	5.05
Joint-EC	198.11	101.58	1495	5.17

3.3 Material property tests

3.3.1 EHS steel

A series of tensile coupon tests was performed for EHS steel tubular columns. The coupon specimens were designed and tested in accordance with BS EN ISO 6892-1 [74]. Figure 3.5 (a)-(b) depict the coupon dimensions designed for EHS column and fin plate/stiffener plate, respectively.

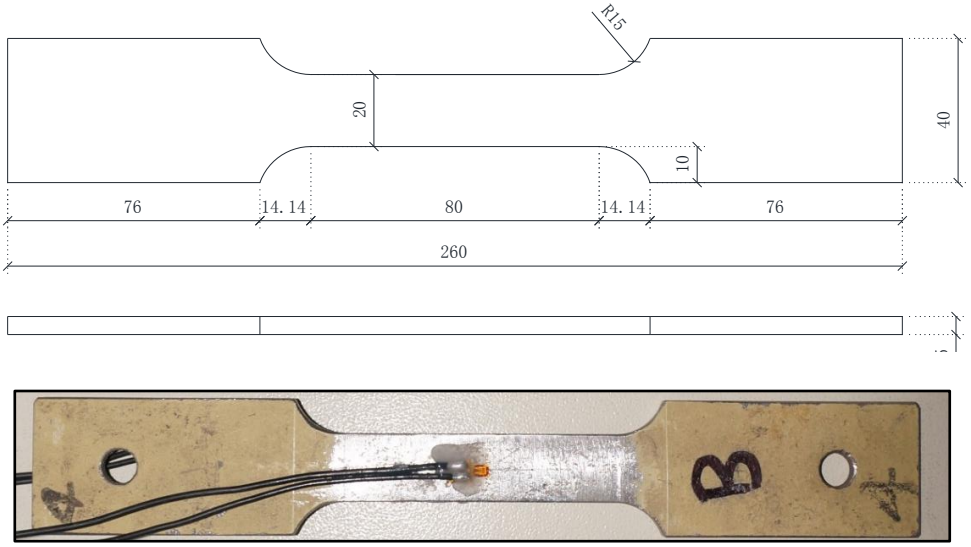

(a) Coupon from EHS column (Grade S355)

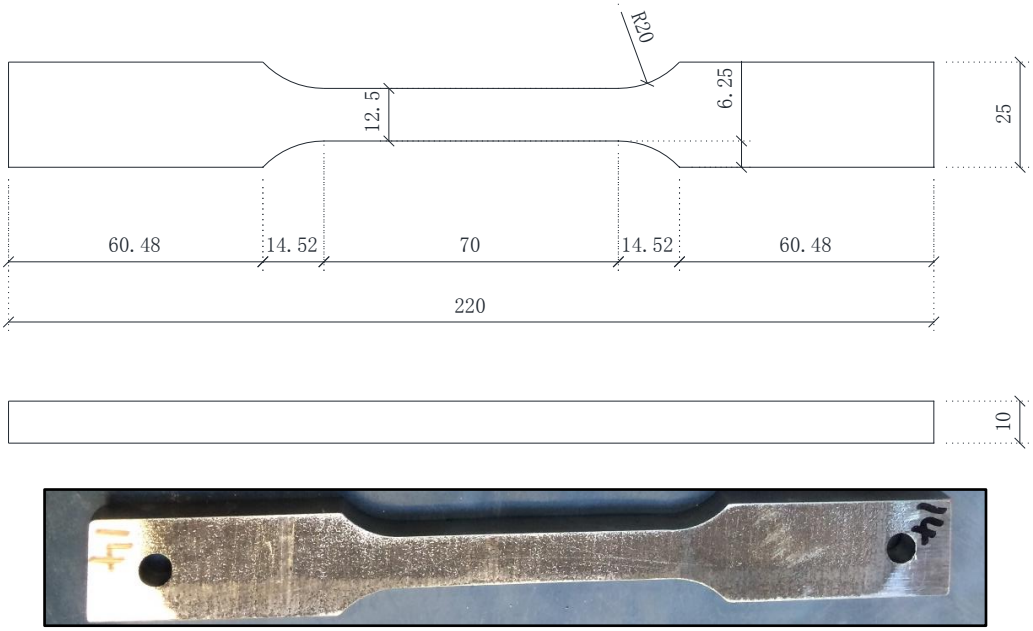

(b) Coupon from fin/stiffener plate (Grade S275)

Figure 3.5 Steel coupon schematic (mm)

Overall eight coupons were manufactured which were taken longitudinally from the EHS tube. Sampling positions from the cross-sectional view of the EHS and corresponding coupon ID are shown in Figure 3.6 where the coupon X1 has a width of 18 mm at the parallel length which is 2 mm smaller than the others. Coupons A1 and A2 were extracted from the minimum radius of curvature region of the EHS; coupons B1 and X1 were created from the maximum radius of curvature region; and coupons C1, C2, D1, D2 were taken from intermediate positions. A total of three coupons (denominated by P1, P2 and P3) were manufactured from Grade 275 steel plate which was adopted as the fin plate or stiffener plate. Table 3.2 and 3.3 illustrate the mean value of dimensions for coupons from EHS column and those from fin/stiffener plate measured prior to conduct the tensile tests.

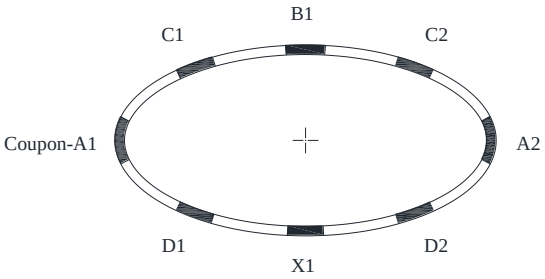

Figure 3.6 Sampling positions and coupon ID (EHS column)

Table 3.2 Mean value of coupon dimensions (EHS column coupons)

Coupon ID	Width (mm)	Thickness (mm)	Gauge length (L_0) (mm)	Original Area (A_0) (mm^2)
A1	20.12	4.52	80.01	90.94
A2	20.09	4.55	79.98	91.41
X1	18.13	4.63	80.04	83.94
B1	20.15	4.54	80.08	91.48
C1	20.15	4.60	80.03	92.69
C2	20.11	4.60	79.99	92.51
D1	20.11	4.57	79.87	91.90
D2	20.13	4.61	80.13	92.80

Table 3.3 Mean value of coupon dimensions (fin/stiffener plate coupons)

Coupon ID	Width (mm)	Thickness (mm)	Gauge length (L_0) (mm)	Original Area (A_0) (mm^2)
P1	12.64	9.84	50.33	124.38
P2	12.50	9.77	50.19	122.13
P3	12.60	9.73	49.89	122.60

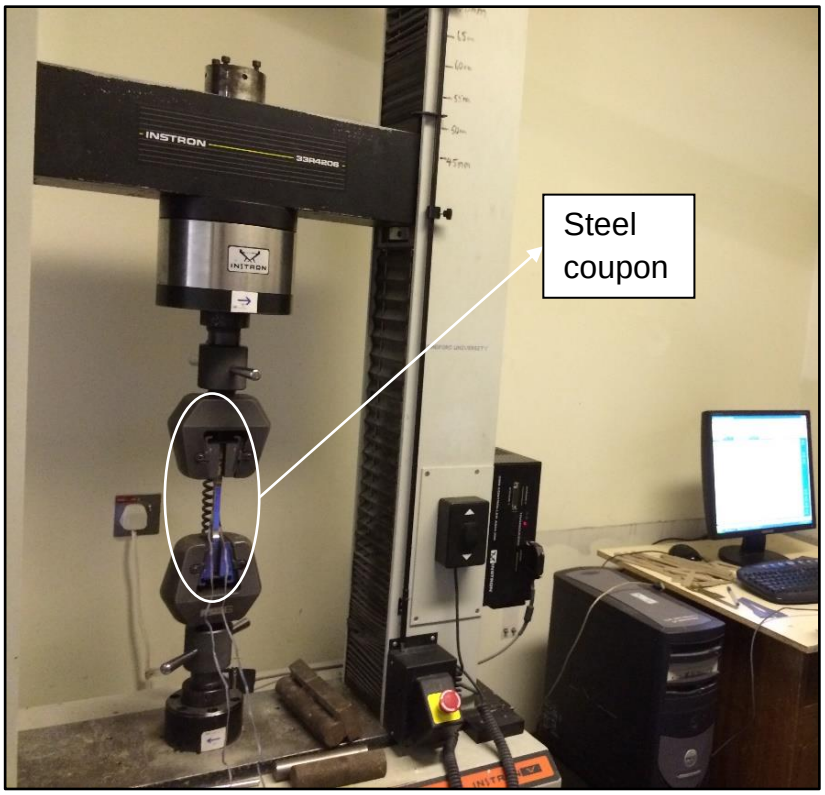

Figure 3.7 Tensile test rig

The tensile test rig is shown in Figure 3.7. Tensile test procedures adopted in this chapter are listed below, which are basically referred to in the proposed procedures suggested in Huang and Young's publication [75]; some changes have been made according to circumstances.

Step-1: Preparation of specimen

1.1 Manufacture specimens according to design schematic shown in Figure 3.5.

1.2 Remove surface coating (e.g. paint) using sander machine or sand paper (selection of tools depending on difficulty and time-spending of coating removing).

1.3 Clean the surface and measure the original cross-sectional area (three cross-sections, using mean values to minimize error measuring as recommended in BS EN ISO 6892-1), based on cross-sectional shape, thickness, width.

1.4 Mark the original gauge length, parallel length and strain gauge positions (strain gauges locate at mid-length, on both sides of the specimens) by using fine lines or scribed lines; measure the gauge length and parallel length.

1.5 Clean the surface again and then attach strain gauges in the longitudinal direction of the specimens.

Step-2: Set-up

2.1 Clamp the upper grip end of a specimen, ensure the specimen is vertical or in line with the load applying direction.

2.2 Set loading and strains to zero and then clamp the other end of the specimen, ensure the grip lengths at both ends are equal, then set the extension to zero.

Step-3: Pre-load

3.1 Apply tensile load to the specimen, which is lower than a value corresponding to 5% of the expected yield strength [74].

3.2 Observe the loading, extension and strains, ensure the loading versus extension curves are correct, and that the strain gauges work well.

3.3 Unload the specimen, set the loading, extension and strains to zero.

Step-4: Loading procedure

4.1 The loading rate of the tensile tests is controlled by crosshead separation rate at a velocity equal to the desired strain rate multiplied by the parallel length; in the initial range from the beginning up to the end of yielding, the separation rate is 0.005mm/s (estimated strain rate is 0.00007/s); after the yielding stage, this rate increases to a constant value of 0.2mm/s (estimated strain rate is

0.00286/s) according to the specified strain rates given in BS EN ISO 6892-1 [74].

4.2 Stress relaxation is applied twice during the tensile tests achieved by pausing the loading for 100s each time to obtain the static material properties; the first holding point is during the yielding stage and the second holding point is near the ultimate strength.

4.3 Stop the test after entire fracturing of the specimen; extract test data of load and strains; remove the two pieces from the testing machine, measure the gauge length and parallel length again as well as the fractured cross-sectional area.

3.3.2 Bolts

Two one-meter-long fully-threaded studs were machined to dog-bone shape tensile samples for the material testing of M20 Grade 8.8 and 10.9 bolts. Three samples were made in each grade in accordance with Annex D in BS EN ISO 6892-1 [74] which is applicable to bars with its diameter greater than 4mm. Figure 3.8 depict the sample dimensions designed for the bolts. In the parallel segment, bolt diameter was machined to be 10mm while in the gripped portion it was 16mm.

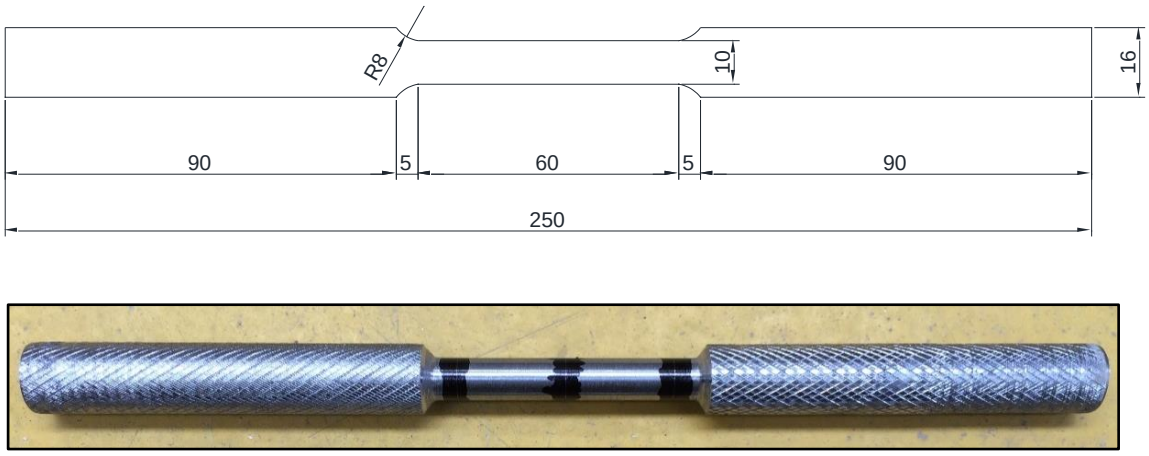

Figure 3.8 Bolts tensile coupon schematic (mm)

Table 3.4 illustrates the mean value of bolts coupon dimensions measured prior to conducting the tensile tests. The tensile test rig for bolts testing is shown in Figure 3.9. This machine has 50-tonne capacity which could satisfy the tensile loading to the bolt coupons.

Table 3.4 Mean value of bolts coupon dimensions

Coupon ID	Diameter (mm)	Gauge length (L_0) (mm)	Original Area (A_0) (mm^2)
G8.8-1	9.72	50.01	74.17
G8.8-2	9.88	50.00	76.58
G8.8-3	9.94	49.91	77.51
G10.9-1	10.00	50.02	78.50
G10.9-2	9.99	50.00	78.29
G10.9-3	9.92	49.98	77.25

Figure 3.9 Tensile test rig for bolts testing

3.3.3 Concrete

Two batches of concrete were made with the same mix design given in Table 3.2, to cast all of the specimens. A series of cube tests were conducted through a crushing machine in the Heavy structures lab of the School of Engineering, University of Bradford. The 28-day strength and test-date strength of concrete

cubes were tested, average values of the testing results will be given in Chapter 4. Figure 3.8 depicts a concrete cube specimen after the crushing test.

Table 3.5 Concrete mix specification design (per m^3)

Water	Cement	Coarse aggregate	Fine aggregate
225	402	1027	715

Figure 3.10 Concrete cube specimen

3.4 Test setup

The typical test setup is illustrated in Figure 3.11. Overall three actuators were employed to apply loads to the specimen, of which, one 250-tonne actuator was fixed to the loading frame and the other two 100-tonne actuators were placed on the strong floor upside down. The upper 250-tonne actuator was used to exert a compressive force at the top end of the EHS column, generating the working load within the column. The two 100-tonne actuators were adopted to apply an upward load at the beam ends, replacing the distributed load that would occur from a concrete floor slab in a real frame structure. The actuators were controlled by Servocon software in three independent PCs. The loading data and other measurements, e.g. beam travel displacements and strains, were recorded by data loggers during the tests.

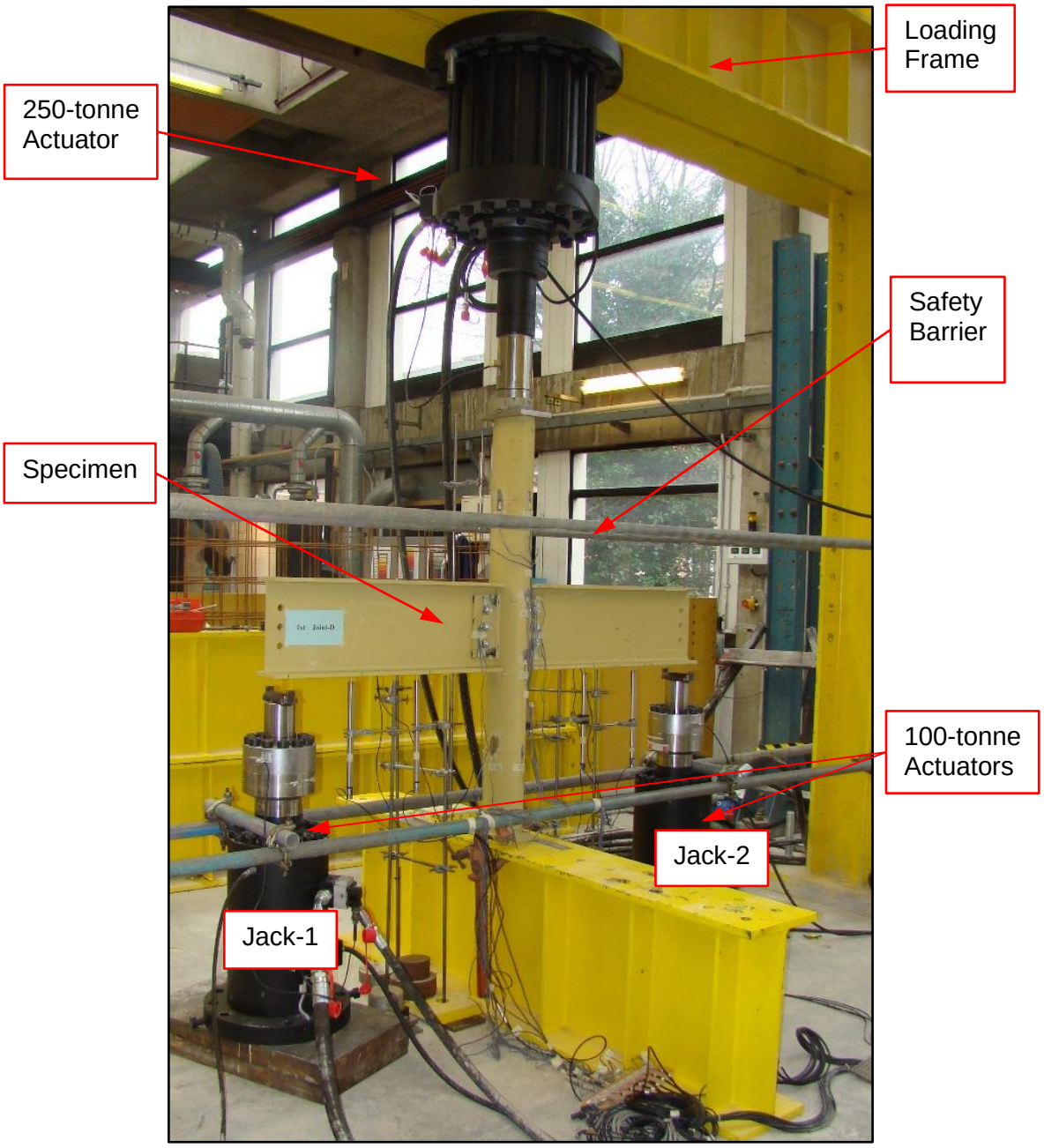

Figure 3.11 Test setup (joint tests)

Figure 3.12 (a)-(d) shows boundary conditions of the tests. A slotted and reusable steel cap was adopted at the top end of the column, see Figure 3.12 (a)-(b). On the top of this special cap, as depicted in Figure 3.12 (a), a circular groove slightly bigger than the load cell was carved to slot the loading cell into it while an elliptical slot, see Figure 3.12 (b), was made on the opposite side to cover the top of the EHS column to constrain sliding in the orientation of the I-beams and out-of-plane movement of the column. For the EHS column bottom end, two clamps were employed as shown in Figure 3.12 (c), providing a semi-rigid boundary condition

for the joints. The curved rollers shown in Figure 3.12 (d) allowed the beams to rotate in the plane of the test-rig and plates welded at the sides of the rollers were adopted to constrain out-plane freedoms of the beam bottom flanges to some extent. The initial distance between the ends of the beam to the loading point was 50 mm.

(a) steel cap top view: connecting the 250 tonne actuator

(b) steel cap bottom view: connecting the EHS column end

(c) EHS column bottom end (clamping)

(d) beam ends (roller bearing)

Figure 3.12 Boundary conditions (joint tests)

3.5 Instrumentation

Several linear variable displacement transducers (LVDTs) and strain gauges were used to measure displacements and strains of selected locations, separately. Figure 3.13 illustrates the arrangements for Type-A connections.

Symbols, e.g. L1 and C1 represent the first LVDT and the first strain gauge on the column face, respectively. Gauges named from C1 to C9 were used to measure either longitudinal or circumferential strains on the column face, while gauges named from “10” to “16” were those located on fin plates, either near fillet welds connecting the fin plates to the column or adjacent to bolt holes to monitor the critical strain. Similar arrangements were adopted for the other nine specimens which are shown in Figure 3.14-17.

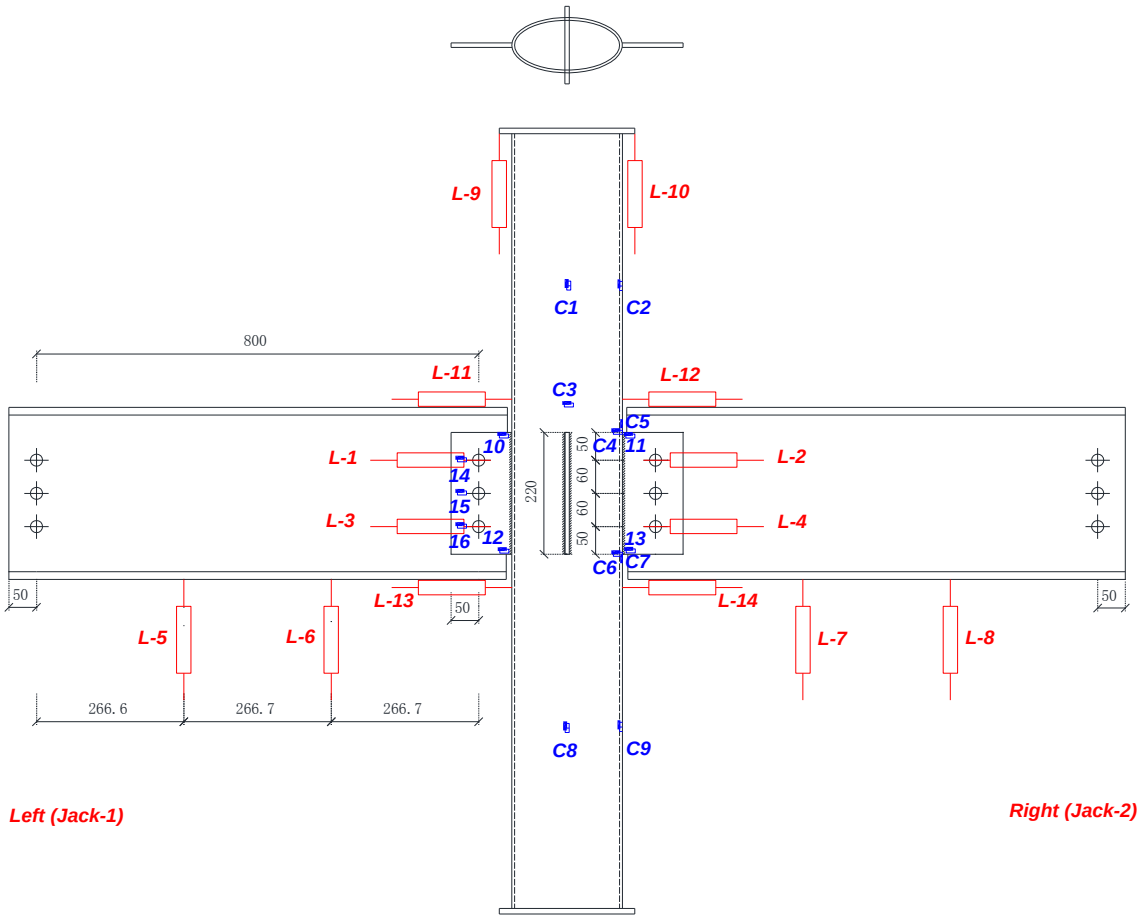

Figure 3.13 Positions of strain gauges & LVDTs (Type-A; mm)

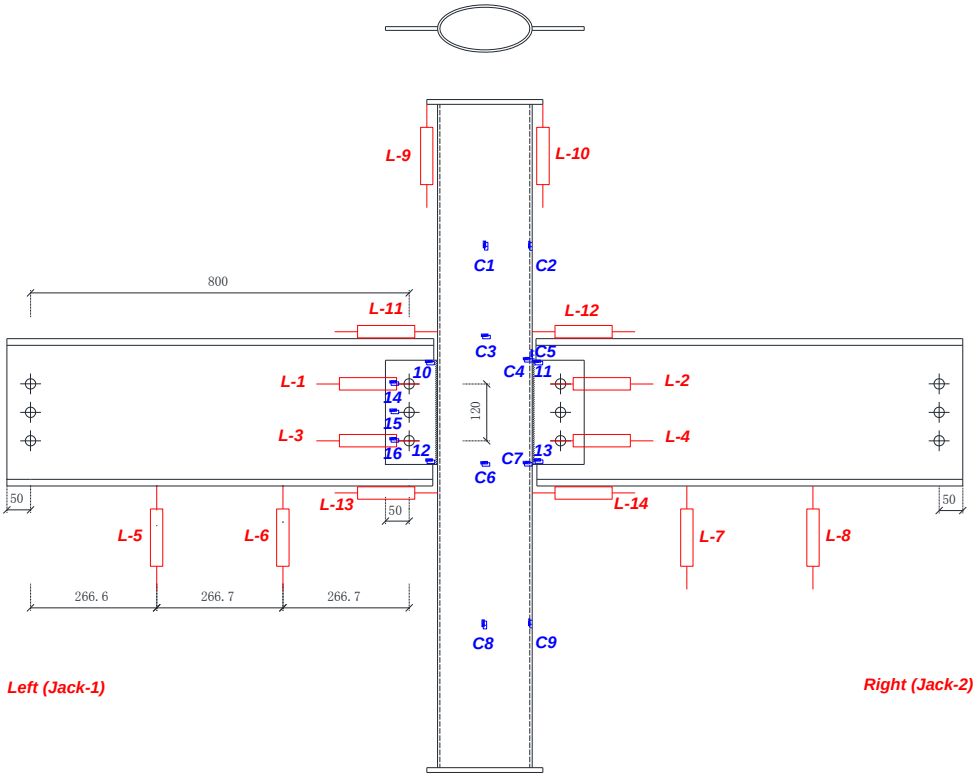

Figure 3.14 Positions of strain gauges & LVDTs (Type-B)

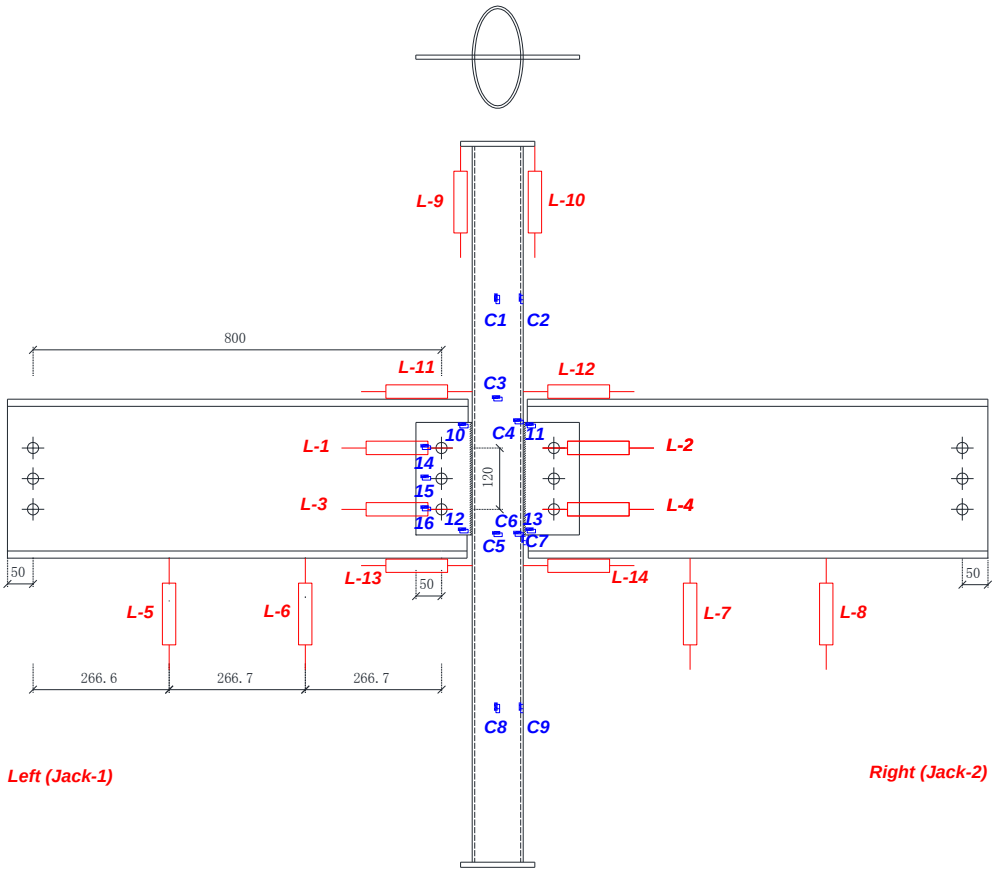

(a) Unfilled

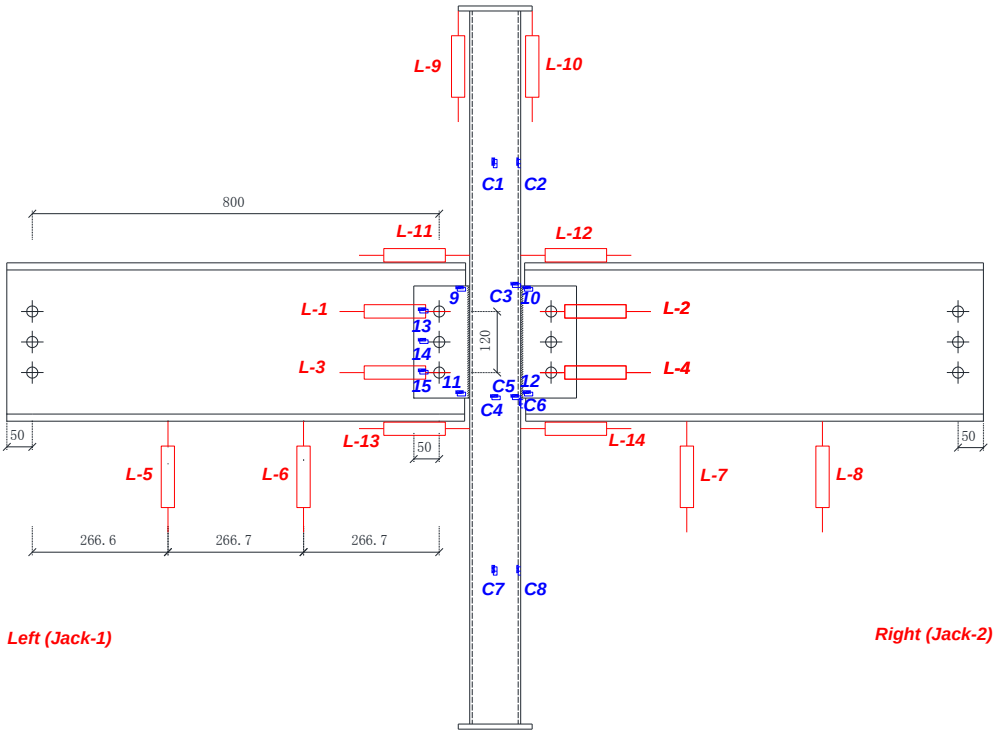

(b) Concrete-filled

Figure 3.15 Positions of Strain Gauges & LVDTs (Type-C)

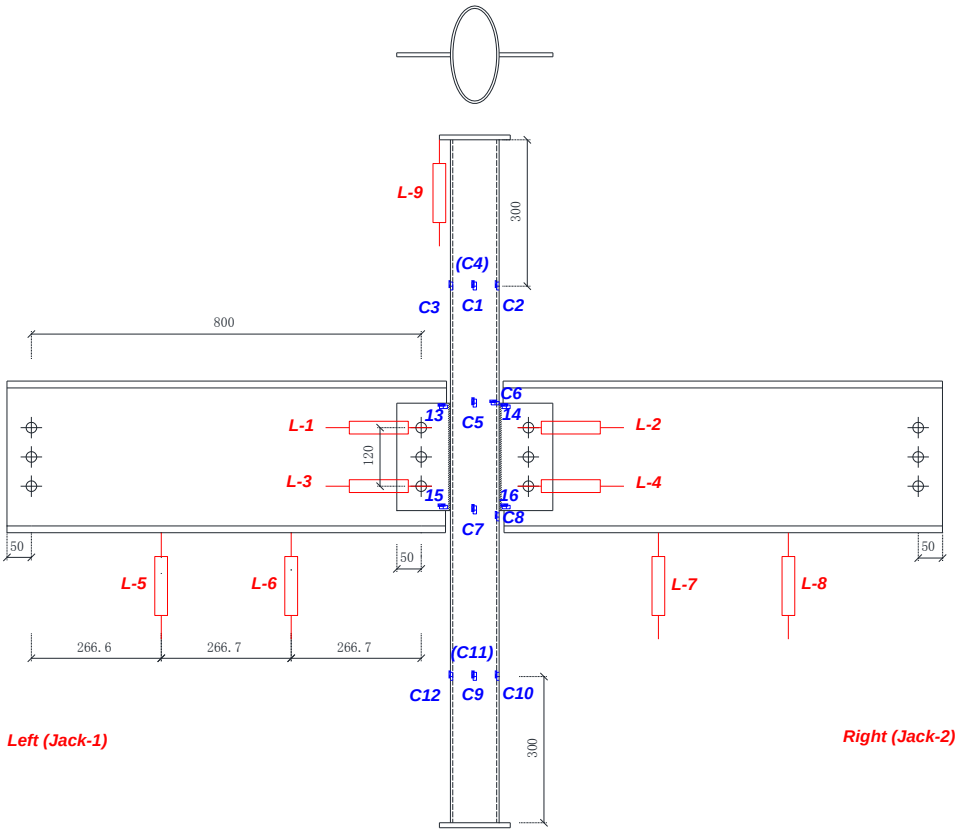

(a) Unfilled

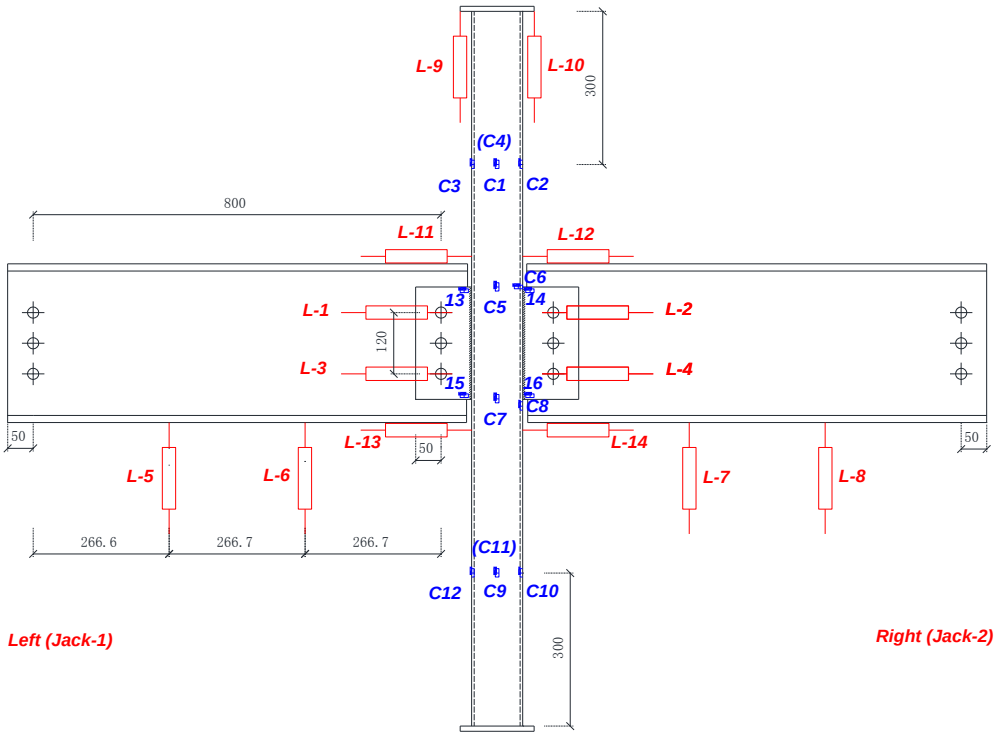

(b) Concrete-filled

Figure 3.16 Positions of strain gauges & LVDTs (Type-D)

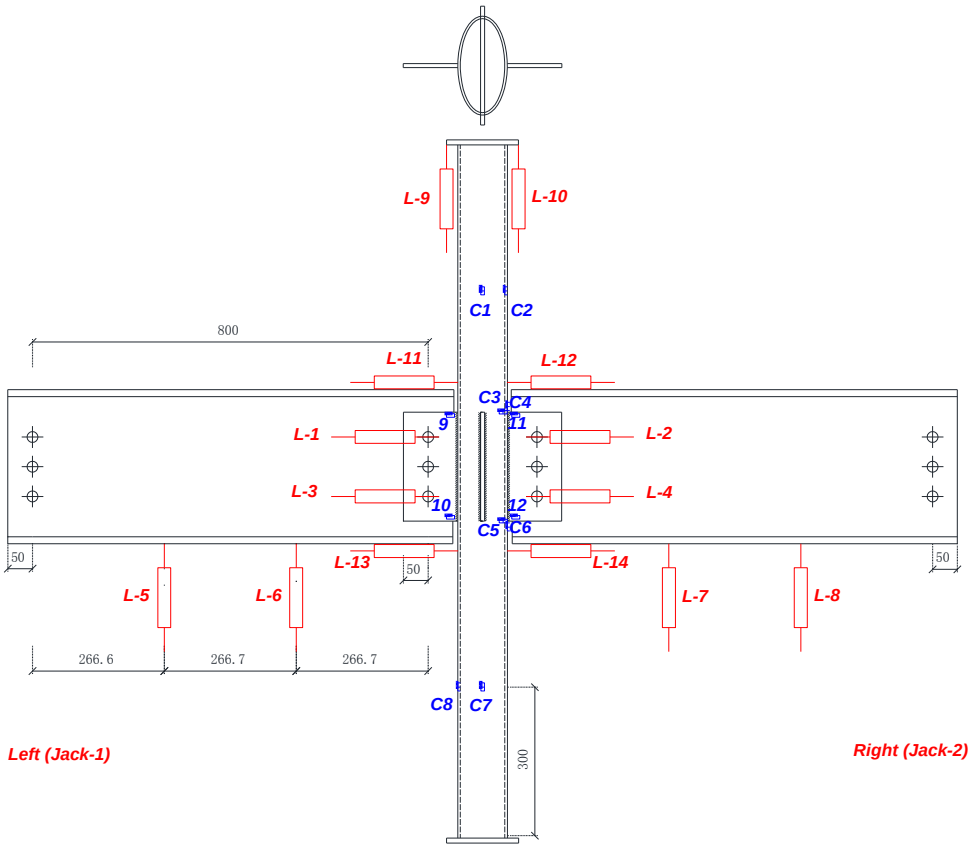

(a) Unfilled

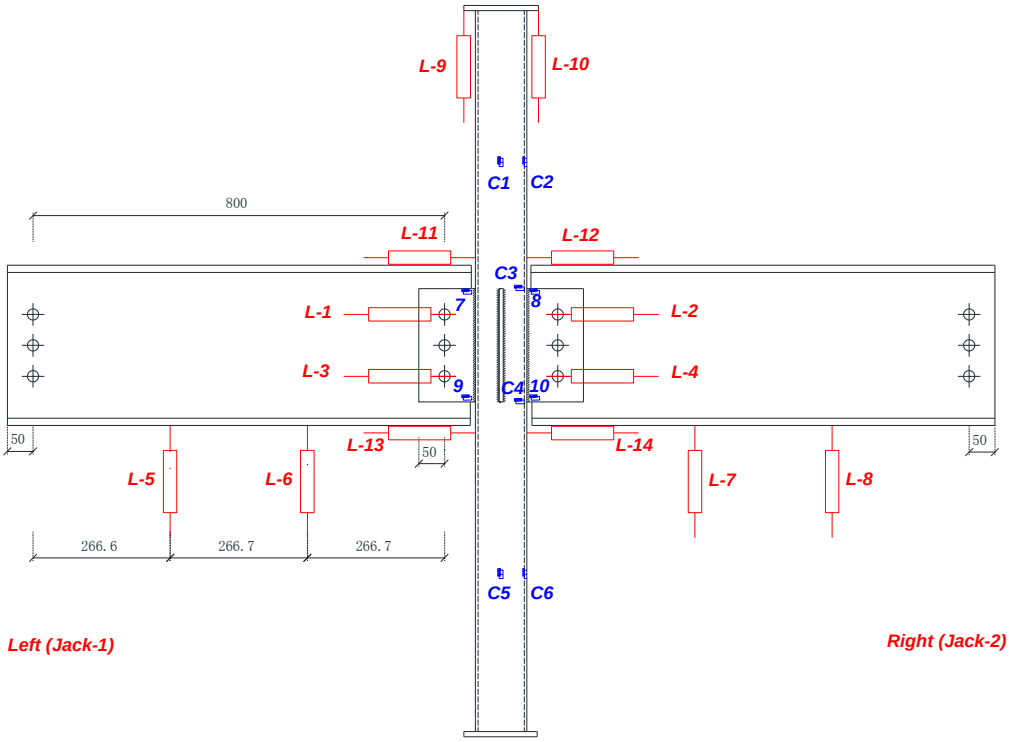

(b) Concrete-filled

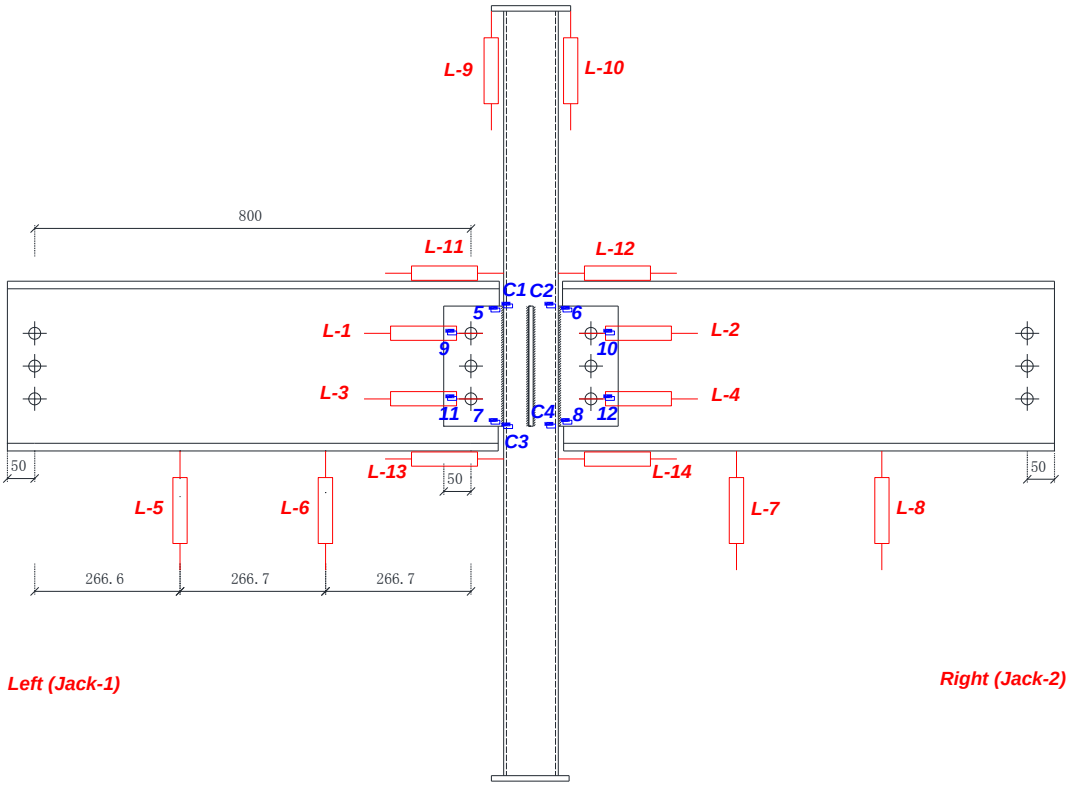

(c) Concrete-filled (Repeat)

Figure 3.17 Positions of strain gauges & LVDTs (Type-E)

In general, in most cases of the connection tests, four groups of LVDTs were employed to calculate the rotation of connections as well as to obtain the axial shortening of the columns, respectively, which are depicted in Figure 3.18 (a)-(d).

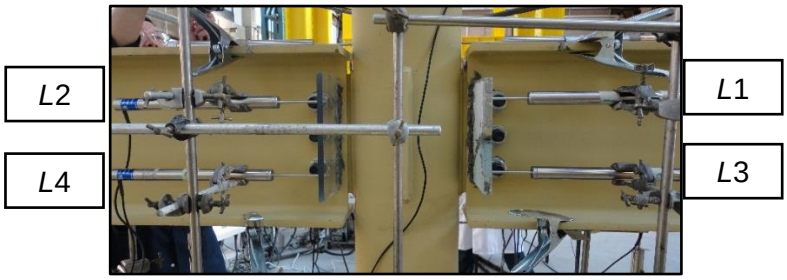

(a) *L*1 - *L*4

(b) *L*5 - *L*14

(c) Close view of *L*9 and *L*10

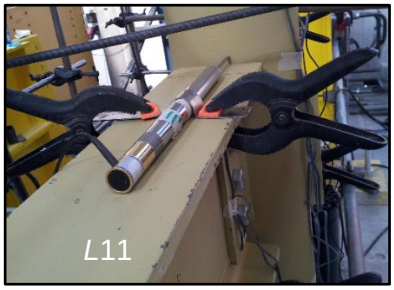

(d) Close view of *L*11

Figure 3.18 Arrangements of LVDTs

LVDTs named from L1 to L4 were placed perpendicular to vertical plates, which had previously been glued onto the fin plates, as depicted in Figure 3.18 (a), with the aim of obtaining the rotation of beams. L5-L8 were placed underneath the bottom flanges of the beams in order to check whether or not the beam underwent bending and measurements taken by L5-L8 were also used to derive the rotations of the joints using the difference between the vertical displacements. L9 and L10, employed to obtain the shortening of the elliptical columns, were placed directly underneath the steel cap. And L11-L14 were used trying to capture the concave or convex deformation of EHS column tubes.

Rotations of the beam to elliptical column connections can be calculated using the displacements measured by L1-L8, and equation is listed as follows:

$$\theta = \frac{1}{2}\left(\theta_{1-4} + \theta_{5-8}\right) = \frac{1}{2}\left[Arc\tan\left(\frac{D^{+}}{120}\right) + Arc\tan\left(\frac{D^{-}}{800/3}\right)\right] \tag{3.1}$$

where θ denotes the rotation of the elliptical column to beam connection; $\theta_{1\text{-}4}$ and $\theta_{5\text{-}8}$ refer to rotations calculated by displacements from L1-L4 and L5-L8, *respectively;* D^{+} is the sum of displacements obtained from L1, L3 or L2, L4; D^{-} is the difference between displacements measured by L5, L6 or L7, L8.

3.6 Test procedure

The basic test procedure including the preparation of test connection, test setup, loading method is listed as follows.

Step-1 Preparation of test connection

a. Place the EHS column beneath the head of the 250 tonne actuator (fixed to the test-rig), move the actuator head until it is close to the column end and put the specially made steel cap on top of the column. Adjust the column position to make sure that the central line of the column is in line with that of the actuator's in both major and minor axis direction by using a levelling instrument; use clamps to fix the bottom column end to base. For concrete-filled columns, infill plaster in the gap at the column end caused by concrete shrinkage to ensure load is evenly applied on both steel tube and concrete core prior to positioning the column in the test-rig.

b. Use a crane to hang a steel beam close to a fin plate which was previously welded onto the column face in the workshop; insert a bolt into the central bolt hole of the fin plate and beam web and tighten this bolt firstly to a relatively small preload; insert another two bolts into the top and bottom bolt hole separately, then using a levelling instrument again to level the steel beam by changing the beam hanging position; tighten all the three bolts manually to a torque value of 200 N·m. Carry out the same procedure to fix the second beam to the other side.
c. Locate the positions of the strain gauges, remove the coating from these locations, clean the surface and then attach the strain gauges in the pre-designed directions; arrange the LVDTs to certain positions as illustrated in Figure 3.14 by using either clamps or fixing devices, make sure the LVDTs are vertical or horizontal.

Step-2 Set-up

a. Move the two 100 tonne actuators close to the beam end until the central line of the actuators reaches the pre-set loading point which is 50 mm away from the beam end.
b. Use four parallel safety barriers (steel bars; two on the top and two on the bottom) attached to the loading frame to protect observers in the event of out-of-plane movement of the specimen. Add another four shorter bars across the bottom two bars to prevent the 100 tonne actuators from lateral movement.
c. Connect the strain gauge cables and LVDT cable to the data logging system; set reading to zero and start to record before loading.

Step-3 Loading procedure

a. Apply a compressive load which was approximately equal to 40% of the column resistance at the top column end using the 250-tonne actuator.
b. Use the two 100-tonne hydraulic actuators to exert upwards concentrated forces simultaneously at each beam end through displacement control at constant loading rate of 2mm or 0.5kN intervals.

c. Continue to apply upwards load until one or more components fail, or large deformation is observed.
d. Stop the tests and extract test data.

3.7 Conclusions

An experimental programme is presented in detail in this chapter, including designed specimens of the I-beam to elliptical steel column connections, material property tests of steel components and concrete core, test setup and instrumentation, and finally the full procedures of the experimental tests.

Chapter 4

Experimental Results and Comparisons

This chapter presents the results of ten elliptical column to beam connection tests, which include failure modes of the connections and moment vs. rotation curves. Material properties obtained from experiments are also provided. Comparisons of the connection test results between hollow and concrete-filled connections and among joint types are also given and discussed. Some conclusions are highlighted at the end of this chapter.

4.1 Material properties

4.1.1 Steel - EHS and fin/stiffener plate

Table 4.1 and 4.2 show the tensile test results of the coupons from EHS column and fin/stiffener plate. In the tables, f_y, f_u and E denote the yield strength, ultimate strength and elastic modulus, respectively; f_y and f_u are extracted based on stress relaxation and E is determined from the slope of the initial stress vs. strain curve where the stress equals to the applied tensile load divided by the measured original cross-sectional area (A_0) and the strain is the average strain measured by the two strain gauges attached on the two sides of the test coupon. Fracture strain $\varepsilon_{frac,elon}$ is calculated according to elongation of the gauge length (L_0) of the coupon specimen after tests, while the strain designated by $\varepsilon_{frac,aera}$ is based on the reduction of the cross-sectional area. The stress at fracture is denoted by σ_f. Equations to calculate $\varepsilon_{frac,elon}$, $\varepsilon_{frac,aera}$ and σ_f are given below:

$$\varepsilon_{frac,elon} = \ln(\frac{L_f}{L_0}) \times 100\% \quad (4.1)$$

$$\varepsilon_{frac,area} = \ln(\frac{A_0}{A_f}) \times 100\% \quad (4.2)$$

$$\sigma_f = \frac{F_{frac}}{A_{frac}} \quad (4.3)$$

where L_f is the final gauge length of the coupon specimen after fracture; A_f is the smallest cross-sectional area after fracture; F_{frac} and A_{frac} are the load and the smallest cross-sectional area when the coupon is fully fractured.

Table 4.1 Steel properties of the EHS column

Coupon ID	f_y (MPa)	f_u (MPa)	E (MPa)	f_u/f_y	$\varepsilon_{frac,elon}$ (%)	$\varepsilon_{frac,aera}$ (%)	σ_f (MPa)
A1	381.5	508.7	xx	1.3	25.6	93.3	902.7
A2	380.9	500.2	xx	1.3	24.2	97.2	996.8
X1	348.7	527.6	206178.2	1.5	26.9	104.0	1010.4
B1	353.7	526.9	205794.4	1.5	26.1	98.9	958.3
C1	349.3	523.6	209347.0	1.5	26.5	91.1	872.0
C2	356.8	527.2	204421.1	1.5	26.3	89.8	850.8
D1	329.9	529.7	191855.1	1.6	25.2	100.0	970.4
D2	341.5	532.5	212369.8	1.6	23.7	96.8	962.2
Average	355.3	522.1	204994.3	1.5	25.6	96.4	940.5

Note: For A1, A represents the location which is shown in Fig. 3.6; subscript 1 means the number of the specimen.

Table 4.2 Steel properties of the fin/stiffener plate

Coupon ID	f_y (MPa)	f_u (MPa)	E (MPa)	f_u/f_y	$\varepsilon_{frac,elon}$ (%)	$\varepsilon_{frac,aera}$ (%)	σ_f (MPa)
P1	331.3	438.1	204971.6	1.3	31.8	100.6	932.8
P2	334.5	451.4	204931.8	1.3	31.6	102.9	957.6
P3	333.6	444.1	205199.9	1.3	33.2	105.21	940.8
Average	333.1	444.5	205034.4	1.3	32.2	102.9	943.7

The obtained stresses and strains are the so-called engineering results which ignore the deduction of the cross-sectional area that would occur after yielding of steel up to facture. In fact, the cross-sectional area decreases dramatically after necking initiates which normally results in the climbing of the stress as the tensile load increases. The true stress-strain relationship is then consequently converted from the engineering values via the following recognized expressions according to the principle of constant-volume:

$$\sigma^t = \sigma^n(1 + \varepsilon^n) \tag{4.4}$$

$$\varepsilon^t = ln(1 + \varepsilon^n) \tag{4.5}$$

where σ^t and ε^t denote the true stress and true strain, respectively; whereas σ^n and ε^n refer to the nominal stress and strain. The average converted true values will be adopted to define the plastic range of steel in the proposed finite element model (FEM) to simulate the non-linear structural behaviour of the connection specimens which will be described and discussed in Chapter 5.

4.1.2 Bolts

Table 4.4 illustrates the tensile test results for grade 8.8 and 10.9 coupons and the mean values of each item which will be treated as the actual mechanical properties of the bolts utilized in the beam to column connections in Chapter 3.

Table 4.3 Bolts properties

Coupon ID	f_y (MPa)	f_u (MPa)	E (MPa)	f_u/f_y	$\varepsilon_{frac,elon}$ (%)	$\varepsilon_{frac,aera}$ (%)	σ_f (MPa)
G8.8-1	674.5	858.8	209300.0	1.3	16.1	98.2	1581.4
G8.8-2	678.5	854.7	207960.4	1.3	16.2	101.1	1620.6
G8.8-3	679.7	854.9	209185.0	1.3	18.2	102.0	1592.3
Average	677.6	856.1	208815.1	1.3	16.8	100.4	1598.1
G10.9-1	1095.2	1190.1	204374.2	1.1	10.3	73.3	1760.8
G10.9-2	1126.2	1216.7	206759.7	1.1	9.9	70.0	1818.5
G10.9-3	1122.6	1214.9	206760.4	1.1	11.0	70.9	1811.1
Average	1114.7	1207.2	205964.7	1.1	10.4	71.4	1796.8

4.1.3 Concrete

For the concrete, an average of 28-day strength of 37.5 MPa and test-date strength of 42.1 MPa are obtained in terms of cube compressive tests, which are illustrated in Table 4.3 where C1 and C2 refer to the first and second batch of concrete mixing, respectively.

Table 4.4 Concrete cube strength (MPa)

Batch	28-day strength	Test-date strength
C1	37.8	43.1
C2	37.1	41.1
Average	37.5	42.1

4.2 Test results and comparisons of the connections

In this section, moment versus rotation relationships, failure modes and mechanism, deformation of the EHS and strains at designed measuring points will be provided and discussed to depict the moment behavior and capacity of the specimen in different joint type group.

The connection moment was calculated using the concentrated force at the beam end multiply by the lever arm (distance between loading line and vertical bolt line; 0.8 meters); the concentrated force was recorded automatically during the experimental tests; beam rotation was calculated using the equation (3.1) provided in section 3.5, Chapter 3.

The following failures were observed in the tests: inward and outward deformations of the EHS column (hollow connections); fracture of the fillet weld between fin plate and the EHS column; yielding at the tension zone of the EHS column (concrete-filled connections); distortion of the bolt holes; cracks in the concrete core and shear failure of the bolts.

4.2.1 Type-A: Major axis connection with stiffener

4.2.1.1 Specimen AH

Figure 4.1 illustrates the moment versus rotation curve of Joint-AH. In this figure, the solid line refers to the result from Jack-1 side of the unfilled AH connection, while the other dash line with hollow circles represent the result from the Jack-2 side. Deviations of this two sides were found which may be caused by the initial gap between the beam end and the column face. Design value of this gap is 10 mm, but differences of the gap size were observed between the left hand side and right hand side of each connection after being assembled. The lower

maximum moment between the two sides is adopted as the ultimate bending moment (22.3 kN·m with a rotation of 0.20 rad) of the connection for safety concerns which is illustrated with a red circle in Figure 4.1. The moment capacity of the connection is determined regardless of beam deflection limit in service state.

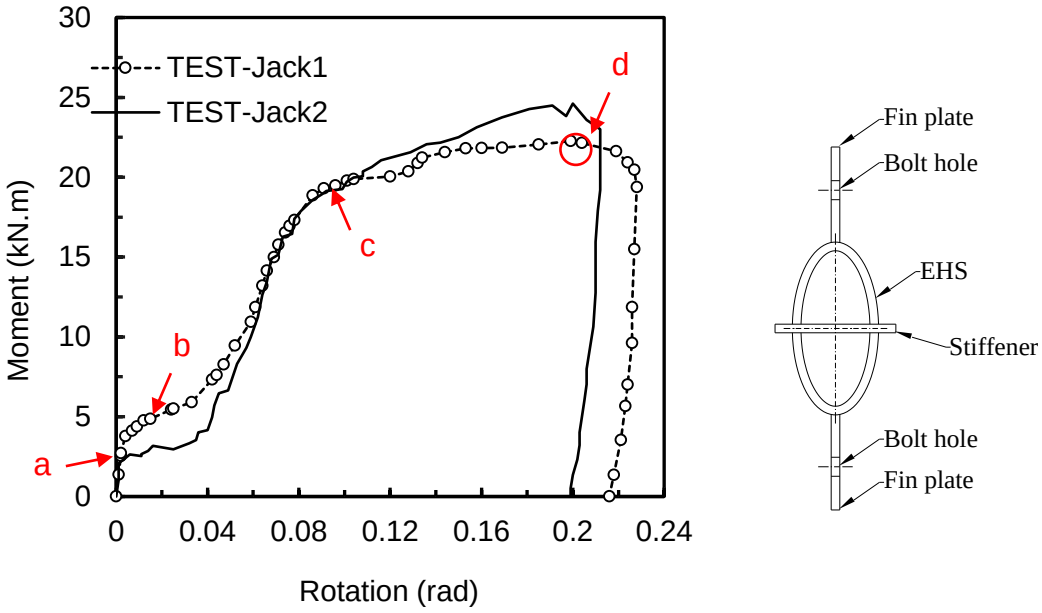

Figure 4.1 Moment versus rotation curves (Joint-AH)

By analysing the moment vs. rotation relationships, connection behaviour can be described in the following stages as shown in Figure 4.1:

a) Friction stage, during which the friction existing between bolts, fin plates and beams was in control. In this stage, the connection's rotation was quite low and the curve slope was nearly constant, with the components, e.g. fin plates, beams and bolts working well together.

b) Then, the moment climbed slowly with increasing of the rotation, showing that slip occurred after the applied load exceeding the friction force. This phenomenon mainly because of the clearance between the bolt shank and the bolt holes in fin plates and beam webs as the diameter of the bolt hole is 2mm larger than that of the bolt shank.

c) The curves progressed to the next phase where the slope increased, and direct bearing between the bolts and holes in the fin plate and beam webs initiated.

When the rotation exceeded a certain value, the beam end compressed the column face, and finally resulted in failure of the EHS column in its transverse direction which is deemed as local buckling failure.

d) Failure of the connection is determined at the point at which the maximum moment capacity occurred.

As can be seen from the moment-rotation curve, Joint-AH has an obviously large rotation capacity. In this case, the rotation drives mainly from the EHS column outward deformation in the tension zone of the connection and the column inward deformation in the upper portion after the beam end compressed the EHS column outer face.

Failures of Joint-AH are depicted in Figure 4.2. No obvious overall deformation of the beams and column was observed, as shown in Figure 4.2(a). The hollow connection failed in the following local areas which can be seen in Figure 4.2(b): the EHS column face near the upper portion (cross-section A) of the connection (local buckling) and the weld area between the left-hand-side fin plate and the column (weld fracture). The local buckling failure was caused by the direct compression of the beam end after the beam rotation exceeded a certain value. This failure was mainly because of the weakness of the transverse stiffness of the thin-walled column tube. The inserted stiffener plate constrained the expansion of the EHS in the minor axis direction to some extent which may delay the failure process but did not eliminate the buckling failure mode eventually. The reason is that the force and moment were transferred from the fin plates firstly to the EHS column and then to the stiffener.

The weld fracture was observed at the final stage of the experiment as during this stage the tensile force finally reached a large value that was beyond the weld capacity. However, this failure did not lead to a sudden drop of the moment as can be seen from Figure 4.1 (curve TEST-Jack1). Instead, the moment increased gradually with the increase of rotation in the static loading situation. The experiment was terminated after that the ultimate moment was obtained and that the rotation was large enough or the travel distance of the actuator reached its limit.

(a) Front elevation of failed Joint-AH

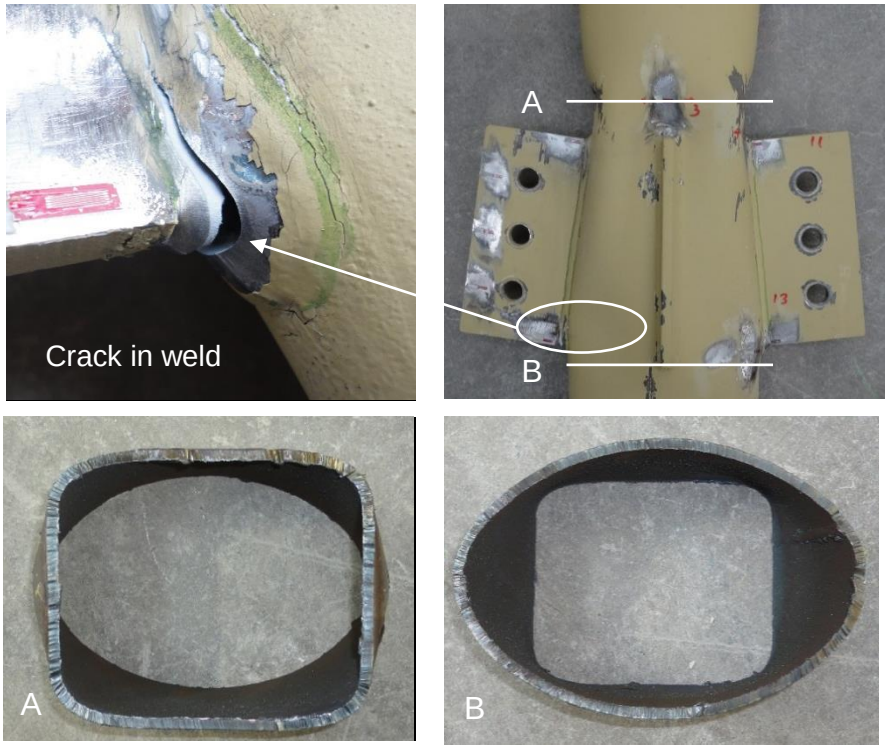

(b) Local failure

Figure 4.2 Failure modes of Joint-AH

After the test, the deformed cross-sections of the EHS column were extracted which are illustrated in Figure 4.2(b). The upper cross-section (A) was compressed from ellipse to a squared shape while the lower section (B) was formed into an ellipse with a higher aspect ratio by the tensile forces transferred from the fin plates.

Overall sixteen strain gauges were attached either on the column face or the fin plate to detect the critical positions of the connection. Positions of all set of strain gauges can be found in Figure 3.13. Figure 4.3 illustrates the critical ones based on the recorded data during experiments. It is found that the strains at gauges C3, C4, C6, 13 and 16 were relatively critical compared with the others which are given in Figure 4.4, where "-" means in compression. C3, C4 and 16 were all in compression but apparently the 16 located near the fin plate bolt hole was less critical than the C3 and C4 which were on the EHS column.

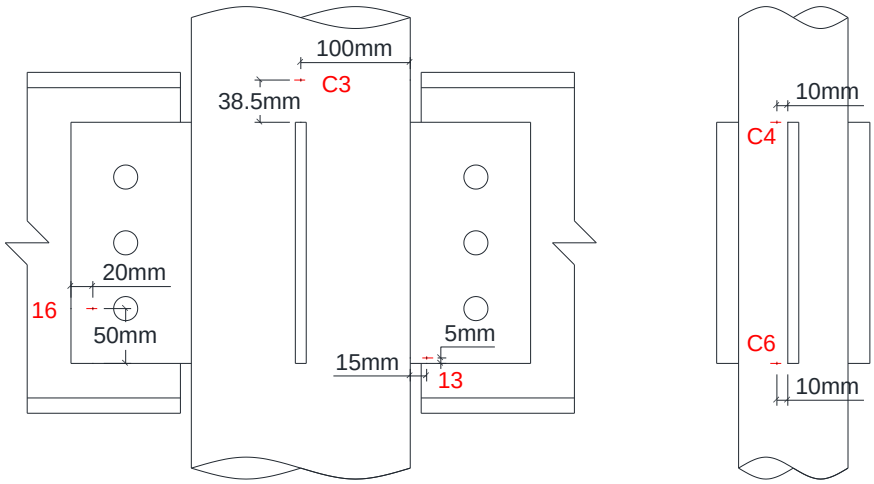

Figure 4.3 Critical strain positions of Joint-AH

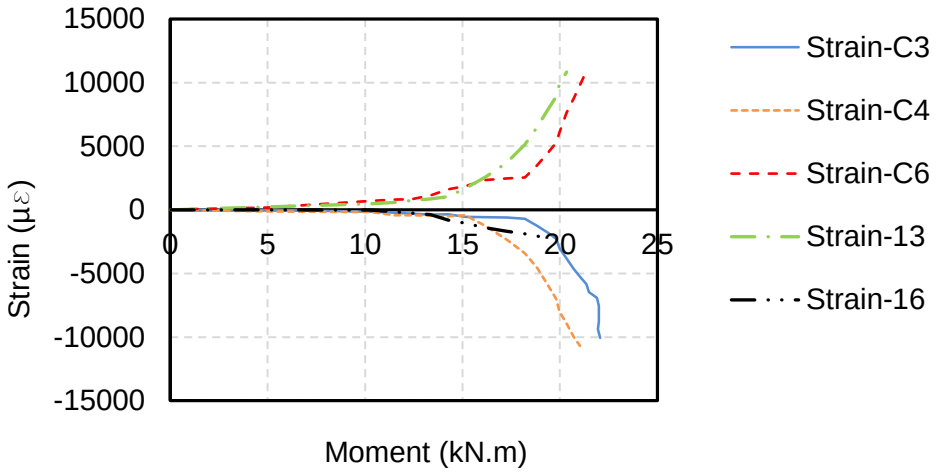

Figure 4.4 Strain vs. moment curves (AH)

4.2.1.2 *Specimen AC*

Figure 4.5 illustrates the moment vs. rotation relationship of the Joint-AC connection. The ultimate moment capacity is found as 43.8 kN·m with a rotation of 0.11rad in the Jack-1 side which is circled in the figure. This is determined by the lower value of the moment at bolt failure. Similar with Joint-AH, the moment-rotation curve experienced the stages of friction and slip initially. However, the moment increased significantly after slip stage with the rising of the rotation and finally underwent a sudden drop. Jack-1 side could not carry further load after failure of the bottom bolt while the Jack-2 side could pick up even higher load after stress redistribution since the bolts of this side did not fail. This phenomenon demonstrates that each side of the double-sided fin plate connection could work individually without interacting each other. With this reason, the connections will be simulated using half model adopting symmetrical loading and boundary conditions. The connection was unloaded after full moment vs. rotation profile was obtained.

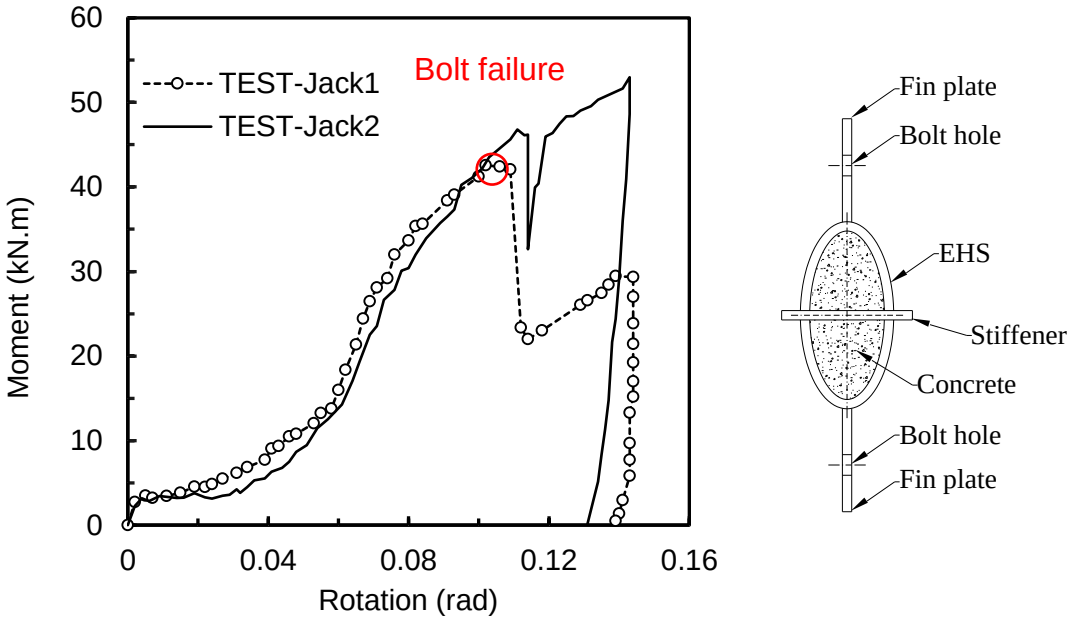

Figure 4.5 Moment versus rotation curves (Joint-AC)

The moment-rotation behaviour can be explained through the failure modes provided in Figure 4.6. As is shown from the front elevation of the AC connection after failure, the beam rotation is relatively smaller than that of the hollow connection as in this case the core concrete stiffened the EHS column and eliminated its inward and outward deformations around the fin plate, which

contributed to the increase of the moment capacity. No obvious overall deformation of the beams and column was observed for Joint-AC. After test, the tube wall around connection portion was cut off and showed that there was no obvious local failure and no cracks in the core concrete which means the stiffener, core concrete and steel tube worked absolutely well in this connection during the experiment. Instead of local buckling observed in the EHS column of the AH connection, bolt shearing failure occurred in AC connection as depicted in Figure 4.6(c) which caused a sudden drop in the moment versus rotation curves. Obvious distortion of the bottom hole in the fin plate was observed after the experiment which is given in Figure 4.6(d).

(a) Front elevation of failed Joint-AC

(c) Bolt failure

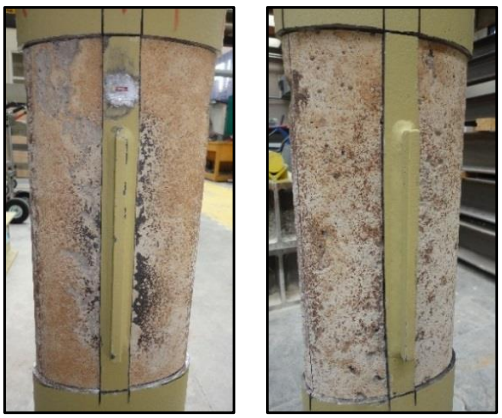

(b) Core concrete

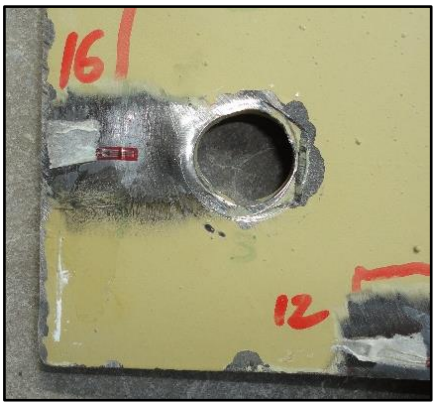

(d) Distortion of the bottom bolt hole in the fin plate

Figure 4.6 Failures of Joint-AC

Figure 4.7 illustrates the critical strain positions of Joint-AC. These positions were all located in the tension zone of the connection though the position 16 was

compressed. It thus can be drawn that the EHS column failure caused by compression was prevented by the infill concrete. Among all, position 16 underwent a relatively big strain at the same moment capacity of the connection, indicating that distortion of the bottom bolt hole was more severe compared with other regions.

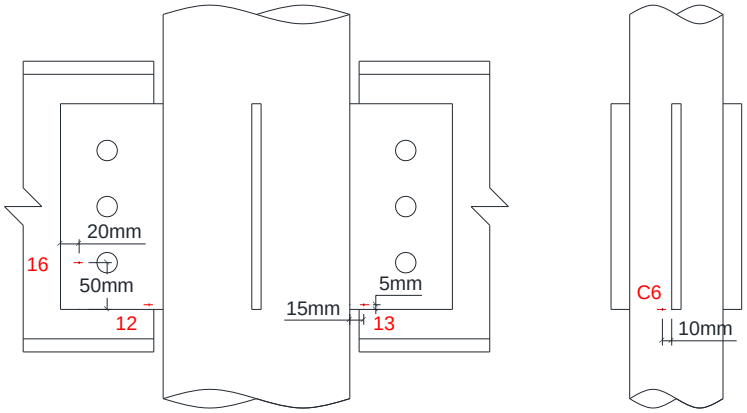

Figure 4.6 Critical strain positions of Joint-AC

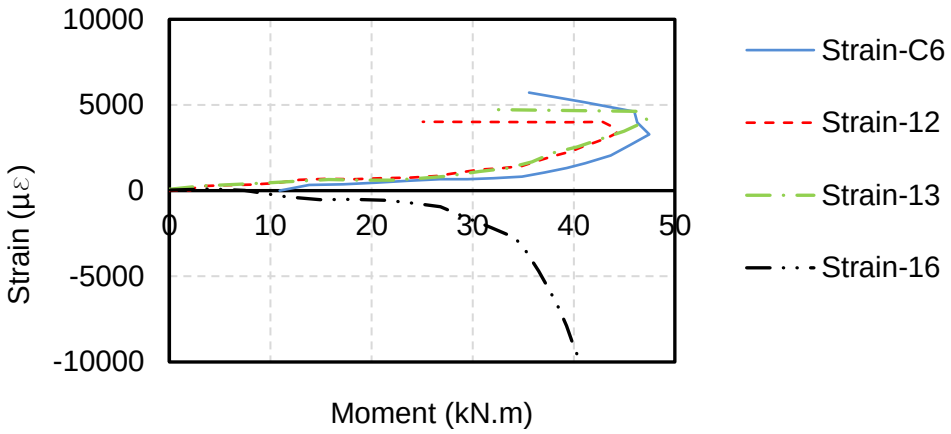

Figure 4.7 Strain vs. moment curves (AC)

4.2.1.3 Comparisons

Figure 4.9 illustrates the comparison of moment versus rotation curves between AH ad AC connection. As seen in this figure, the friction and slip stage is nearly identical and deviations occurred at around 0.04rad, after which, AC curve went beyond over the AH curve. The significant increase of the curve slope is contributed by the core concrete which stiffened the transverse stiffness of the EHS column. But the infill concrete decreased the ductility of the connection.

Table 4.4 summarizes the ultimate moments, rotations and failure modes of the Type-A connections. It indicates that the concrete infill enhanced the moment capacity of the connection by 96%. In addition, the concrete infill changed the column failure mode to the component failure mode. In the case studied, the brittle failure of bolt rupture may be avoided by decreasing the thickness of the fin plate in practical design.

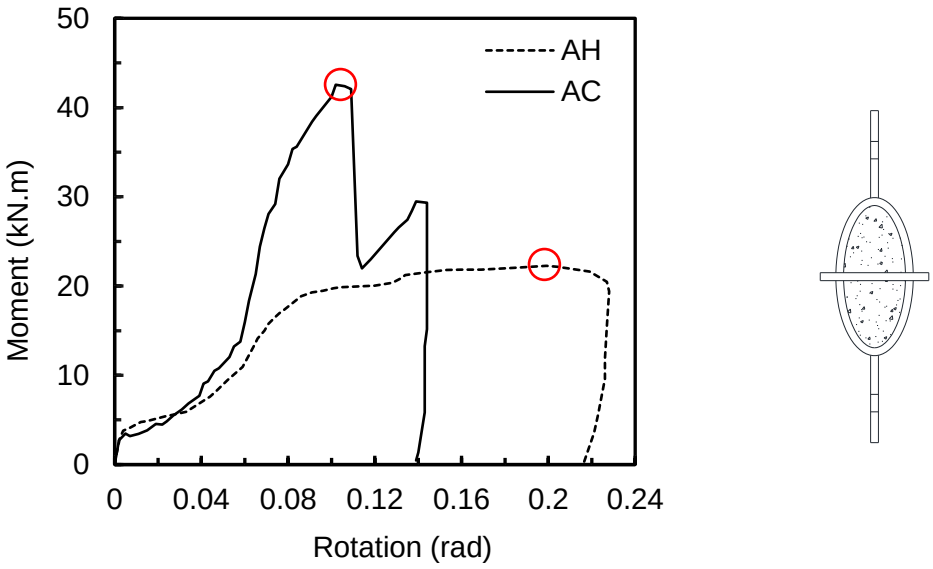

Figure 4.8 Comparison of moment-rotation curves (A)

Table 4.5 Ultimate moments, rotations and failure modes of Type-A connection

ID	M_u (kN·m)	θ_u (rad)	M_{uc}/M_{uh}	Failure mode
Joint-AH	22.3	0.20	-	Local buckling
Joint-AC	43.8	0.11	1.96	Bolt shear failure

Besides, concrete infill stiffened the EHS column to resist axial load showing from that the maximum shortening of the concrete-filled column during the test was 2.5 mm which is much smaller than that of the hollow one whose was 8.0 mm at the same loading level (about 40%) of the corresponding column's capacity, as shown by the red circles in Figure 4.9. The horizontal axis refers to the deflections at column end which was the average results measured by LVDTs *L*9 and *L*10, while the vertical axis was the concentrative load at column end exerted by Jack-

3. The concentrative load was maintained during the experiments after reaching the designed value and then was released after test. As can be seen from the profiles, stiffness of the EHS column was increased after filling in concrete.

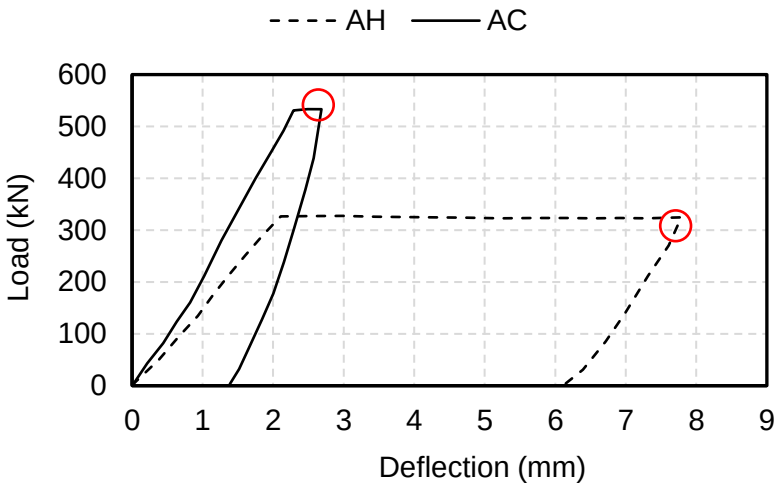

Figure 4.9 Comparison of the load vs. deflection profiles (A)

4.2.2 Type-B: Major axis connection without stiffener

4.2.2.1 Specimen BH

Figure 4.11 depicts the moment versus rotation relationships of Joint-BH where the dash line with circles and solid line represent the Jack-1 side and Jack-2 side of the connections, respectively. As seen from this figure, the slip stage of this two sides are markedly different which indicates that this stage is sensitive with the bolt positions. The lower maximum moment (16kN.m with a rotation of 0.10rad) of the two sides is redeemed as the connection's moment capacity which is shown in a red circle in the graph. In contrast to Joint-AH, the moment capacity of BH experienced decreasing stage after the maximum capacity was achieved due to the absence of the stiffener plate. Figure 4.12 shows the failures of Joint-BH. Apparently, there is no obvious general deformation on both beams and column of BH. Portion 'A' of the un-stiffened EHS column encountered inwards local buckling failure same with the stiffened AH; while the tension zone 'B' experienced more extensive deformation compared with AH and the column section turned to be oval with a really high eccentricity.

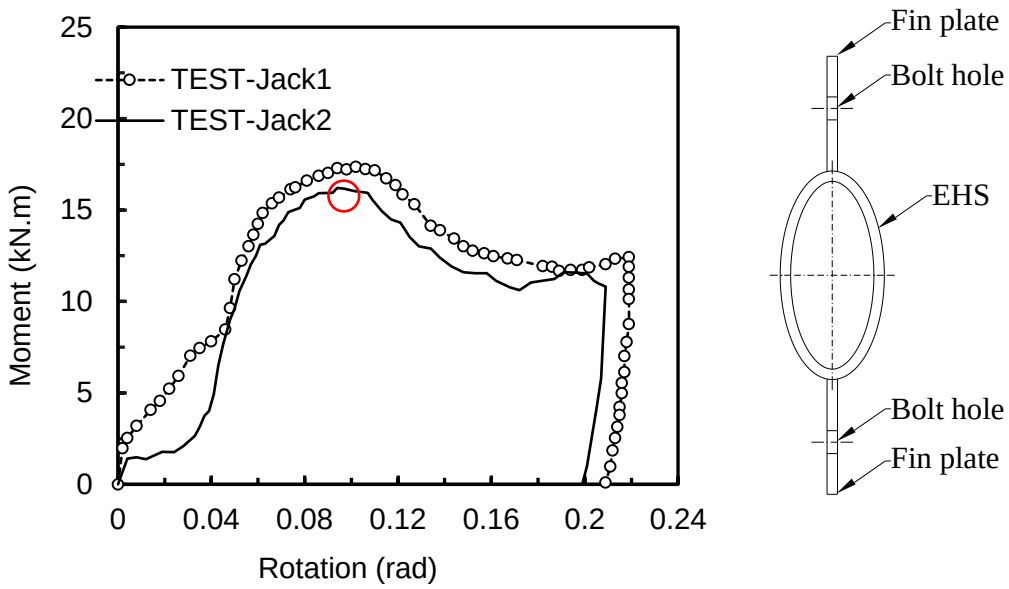

Figure 4.10 Moment versus rotation curves (Joint-BH)

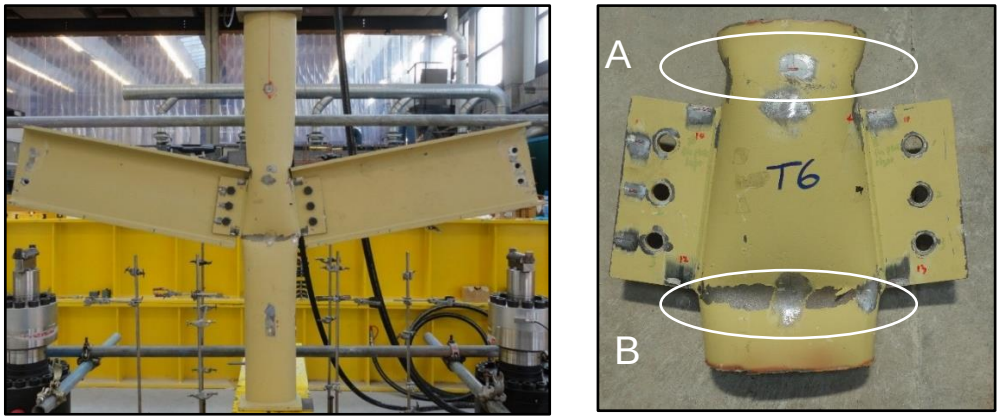

(a) Front elevation of Joint-BH

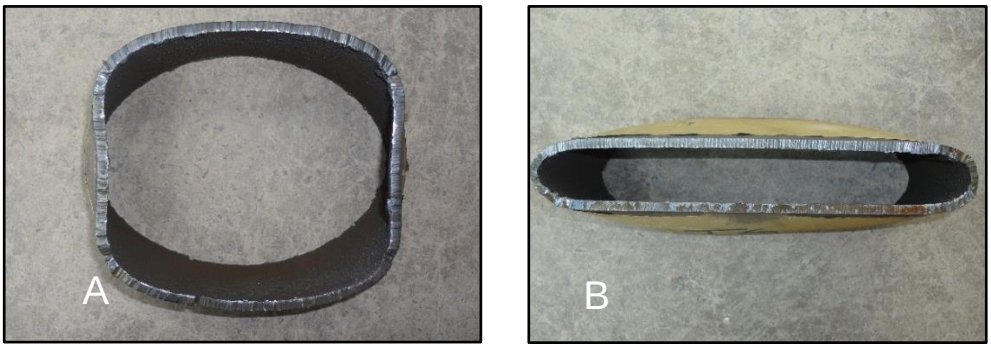

(b) Local failure in the EHS column

Figure 4.11 Failures of Joint-BH

Figure 4.13 and 4.14 illustrate the critical stain positions and the corresponding strain data of Joint-BH. As can be seen from this two figures, critical area of such connection locates in the EHS column at the intersection between fin plate and

the EHS as well as the worst section of the EHS in tension zone. As for the compression zone of the EHS, the strain gauge at C3 recorded relatively small tensile strain value in the transverse direction, which was interfered with by the bending effect of the side wall caused by a deep compression.

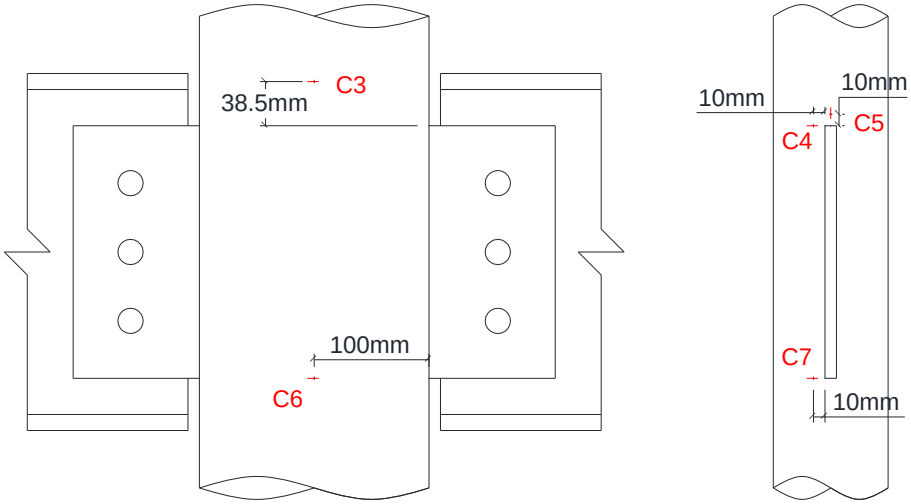

Figure 4.12 Critical strain positions of Joint-BH

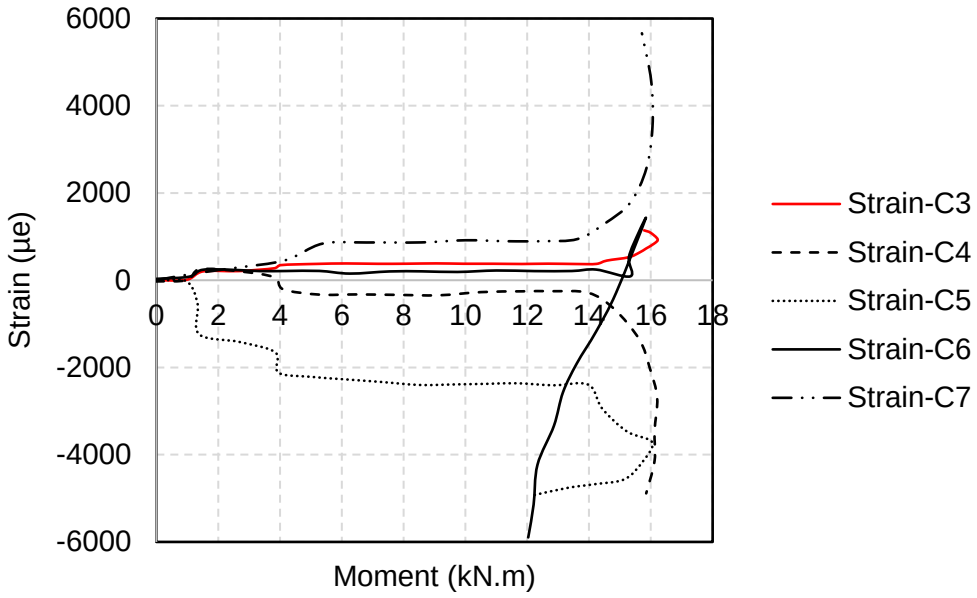

Figure 4.13 Strain vs. moment curves (BH)

4.2.2.2 Specimen BC

The moment vs. rotation relationship of the Joint-BC connection was drawn in Figure 4.15. The ultimate moment capacity is found as 49.6 kN·m with a rotation of 0.12 rad at the Jack-2 side which is shown in a red circle in the figure. This is determined by the lower value of the moment at bolt failure. In this case, the bottom bolt at both sides fractured in sequence, thus caused the sudden drop in the curves profile. The moment-rotation curve experienced the stages of friction and slip initially and then deviations was observed between both sides. This phenomenon may be caused by different initial gap between the beam end and the EHS column after installation. Both sides could not carry further load after the failure of bolts.

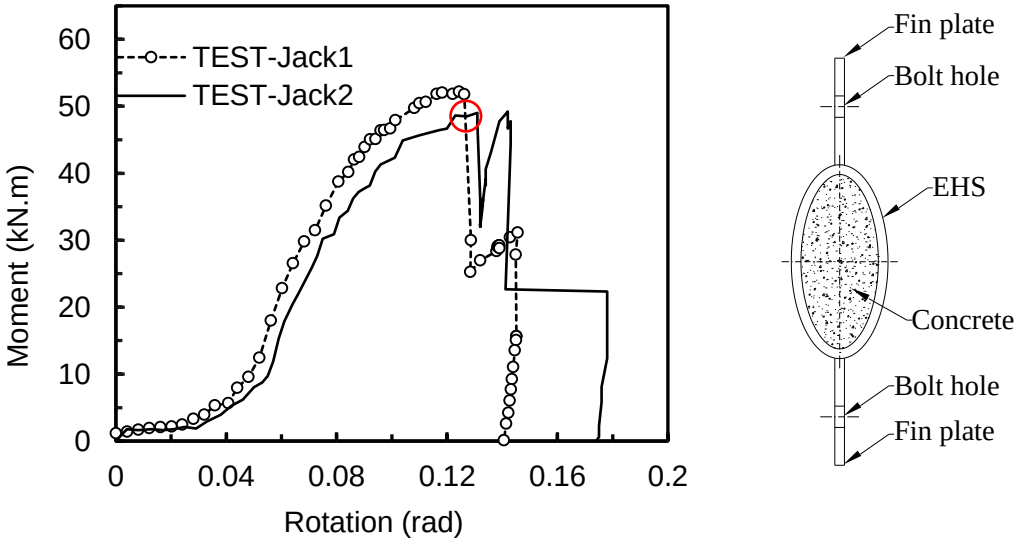

Figure 4.14 Moment versus rotation curves (Joint-BC)

The failures of Joint-BC are given in Figure 4.16. As is shown from the front elevation of the BC connection after failure, no obvious overall deformation of the beams and column was observed. Instead of extensive deformation found in the EHS column of Joint-BH, there is no obvious failure in the steel tube. Unlike Joint-AC, several cracks were found in the concrete core of BC which were caused by direct compression from the beam end. Bolt shear failure is illustrated and obvious distortion of the bottom hole in the fin plate also occurred.

(a) Front elevation of Joint-BC

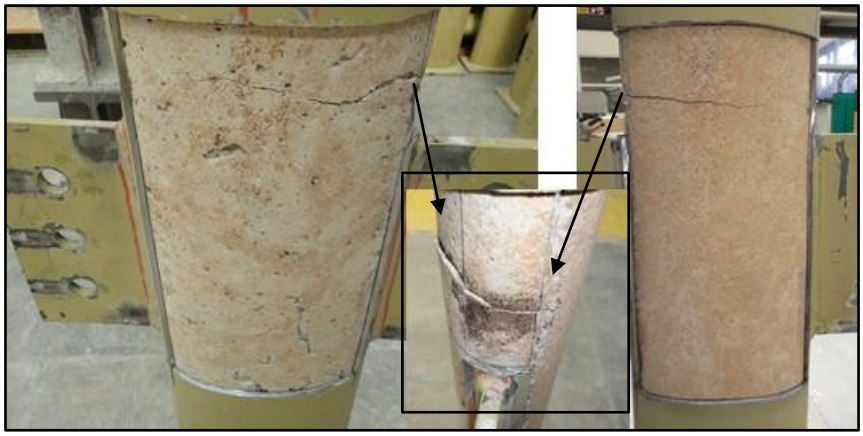

(b) Cracks in concrete core

(c) Bolt shear failure

(d) Distortion of the bottom bolt hole in fin plate

Figure 4.15 Failures of Joint-BC

Figure 4.17 and 4.18 illustrate the critical strain positions and the corresponding strain data of Joint-BC, respectively. As can be seen that the strains at C7 and '16' are more distinct compared to the others. Thus in this connection, the tension

zone in the EHS tube at the intersection and the bottom bolt hole in the fin plate are more critical. As can be seen from strain-15, failure of the middle bolt hole in the fin plate only occurred after the peak moment was achieved which means the bottom bolt bore most of the load before its fracture.

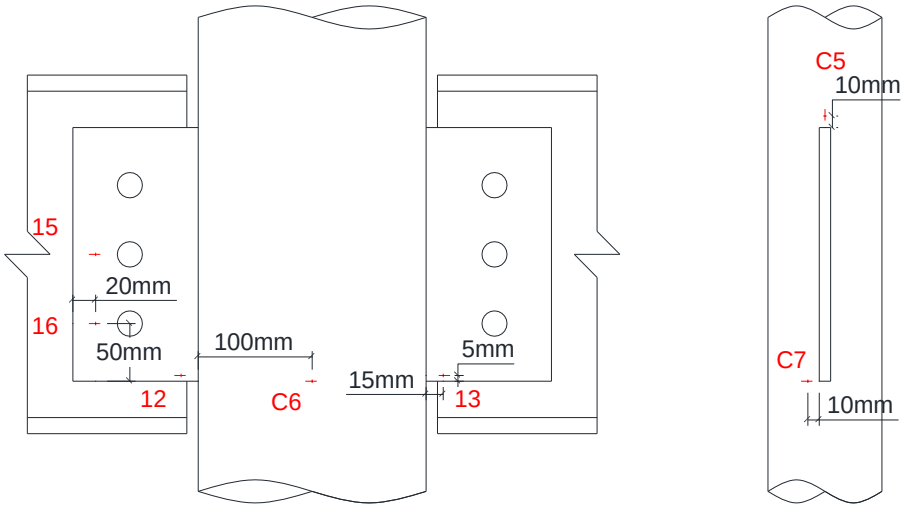

Figure 4.16 Critical strain positions of Joint-BC

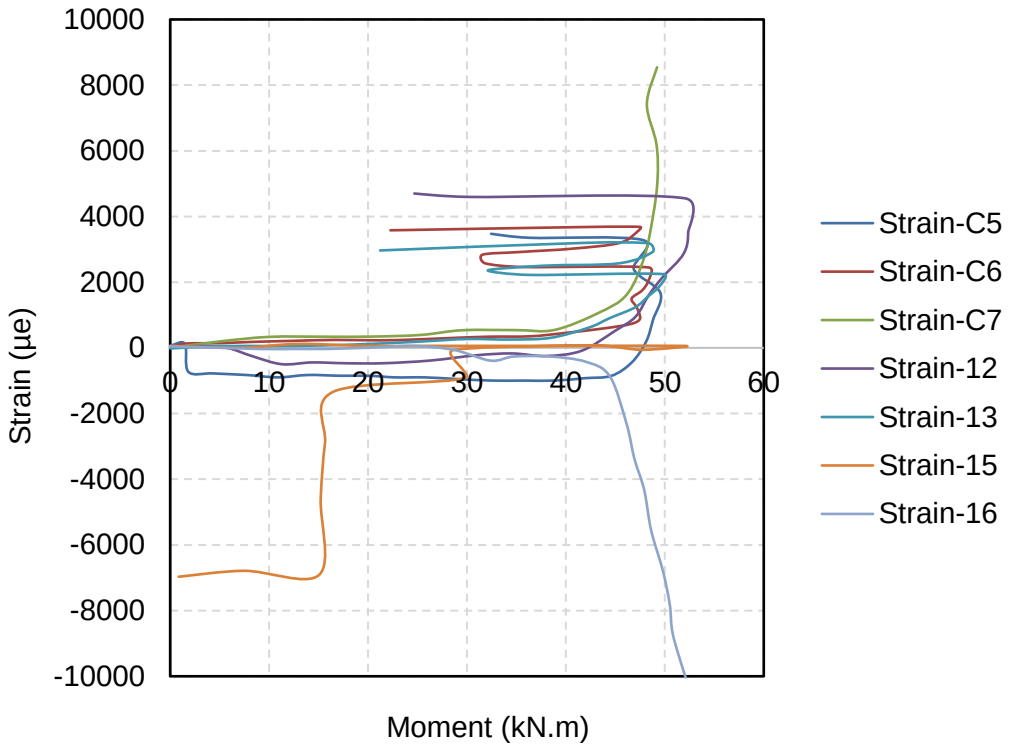

Figure 4.17 Strain vs. moment curves (BC)

4.2.2.3 Comparisons

Figure 4.19 illustrates the comparison of moment versus rotation curves between BH and BC connection. As can be seen in this figure, the increase of both the stiffness and the peak moment is significant after the slip stage of the curves. Table 4.6 summarizes the ultimate moments, rotations and failure modes of the Type-B connections.

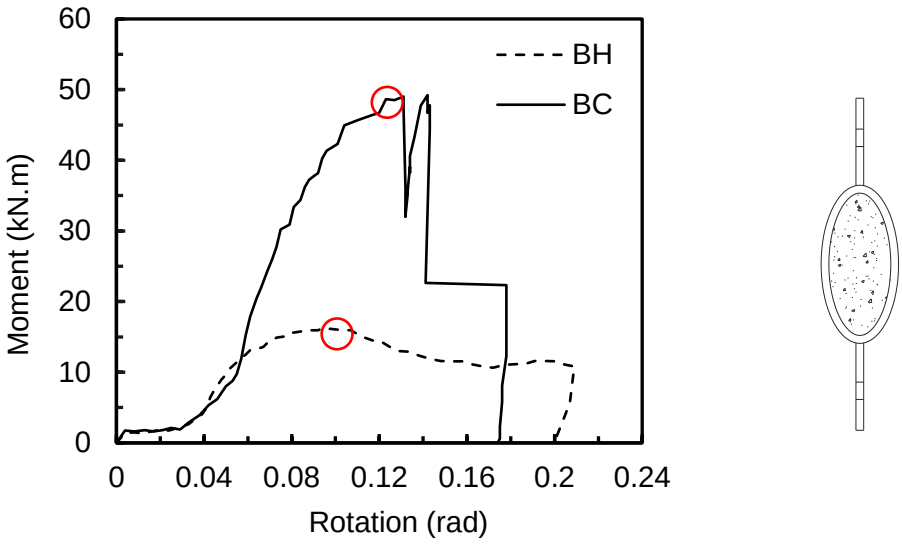

Figure 4.18 Comparison of moment-rotation curves (B)

Table 4.6 Ultimate moments, rotations and failure modes of Type-B connection

ID	M_u (kN·m)	θ_u (rad)	M_{uc}/M_{uh}	Failure mode
Joint-BH	16.0	0.10	-	Local buckling
Joint-BC	49.6	0.12	3.10	Bolt shear failure

Comparison of the load versus deflection of the column was drawn in Figure 4.20. The horizontal axis refers to the deflections at column end which was the average results measured by LVDTs *L*9 and *L*10, while the vertical axis was the concentrative load at the column end exerted by Jack-3. The concentrative load was maintained during the experiments after reaching to the designed value and then was released after the test. As shown in the figure, the maximum shortening of the concrete-filled column after test was 2.6 mm which is much smaller than

that of unfilled one whose was 14.3 mm. Obviously, the stiffness and the load carrying capacity of the EHS column was increased after filling in concrete.

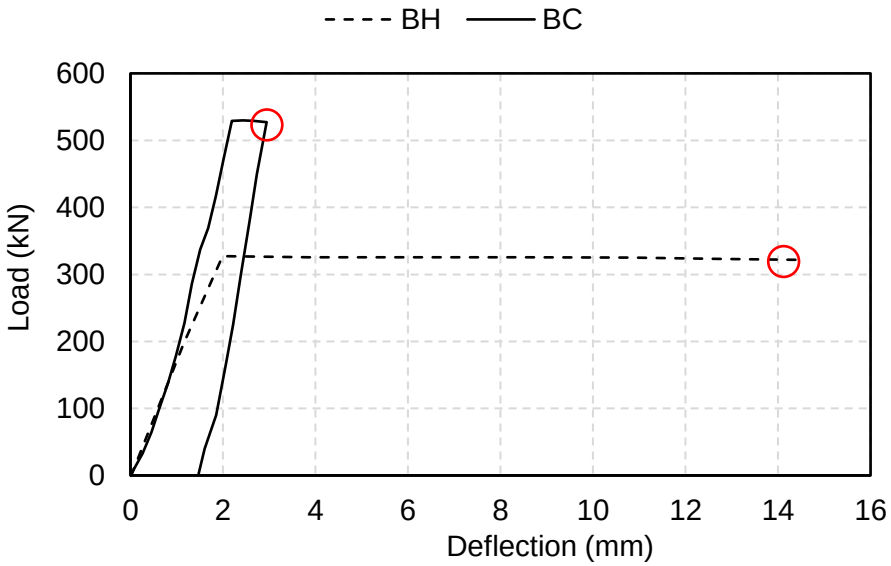

Figure 4.19 Comparison of the load vs. deflection profiles (B)

4.2.3 Type-C: Minor axis connection with through plate

4.2.3.1 Specimen CH

The moment versus rotation curves of Joint-CH at both sides are given in Figure 4.21. As is shown, the curves underwent friction and slippage stages as well but the deviations between the two sides afterwards are more remarkable. This may be explained that the load transferred from beams was resisted directly by the through plate rather than detached fin plates, thus the influence of bolt positions within the bolt holes and the initial gap between the fin plate and the EHS column on the load carrying capacity of the connection were more evident. Lower value of the peak moment (30.0 kN.m at beam rotation of 0.11 rad) at both sides was taken as the ultimate moment capacity for safety concern.

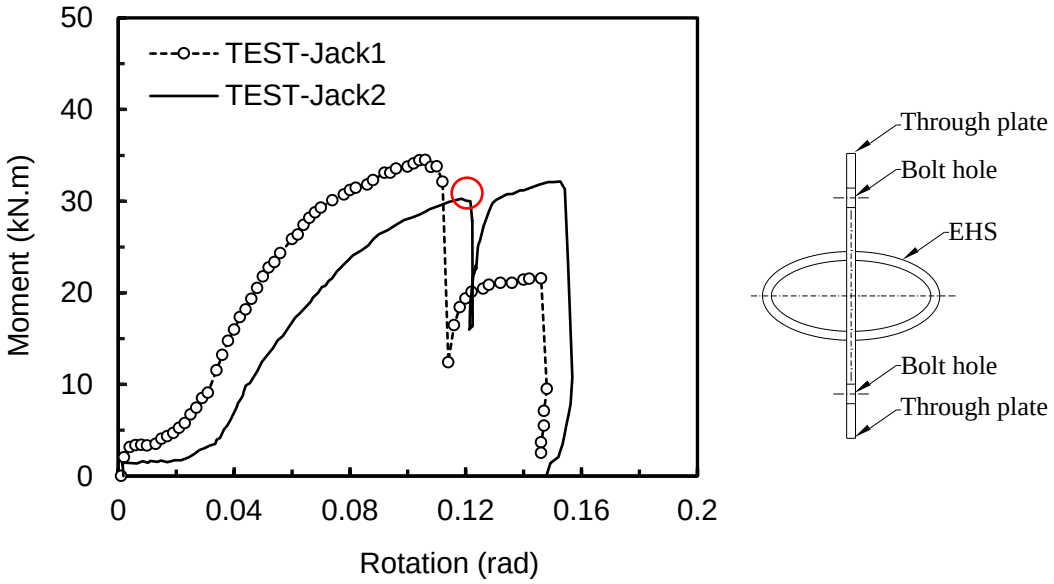

Figure 4.20 Moment versus rotation curves (Joint-CH)

Failures of Joint-CH specimen are shown in Figure 4.22. No obvious general failure was observed in the beams and the EHS column. Local failure occurred in the upper portion of the connection in the EHS column which was caused by direct compression from the beam ends, while there was no obvious tensile deformation in the tension zone of the column. The worst section of the EHS was extracted after the test which illustrates that the curved face at higher radii of the EHS was compressed to a relatively flat face. As shown in figure 4.22 (c), the through plate was not flat but slightly bended due to compression. Distortion of the bottom bolt hole was more severe compared to the AH and BH cases. And bolt shearing failure was observed during the test which caused a sudden decrease of the moment/load. After which the connection could not pick up further load at both sides of the connection.

Figure 4.23 and 4.24 illustrate the critical strain position and corresponding strain data of Joint-CH respectively. It is found that the strain in the compression zone of the EHS column at the intersection between the fin plate and the column was more critical compared with the tension zone. The reason is that tensile force was resisted by the through plate and the area around the bottom bolt hole in the fin plate yielded as a consequence.

(a) Front elevation of Joint-CH

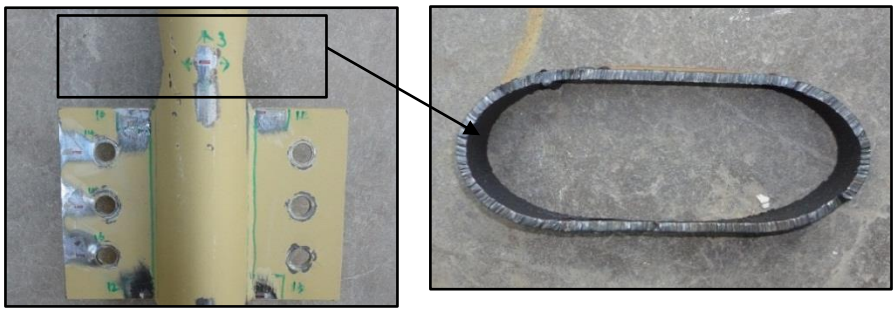

(b) Local failure of the EHS

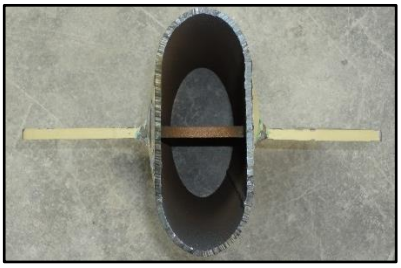

(c) Top view of the EHS and through plate

(d) Bolt hole distortion (e) Bolt shear failure

Figure 4.21 Failures of Joint-CH

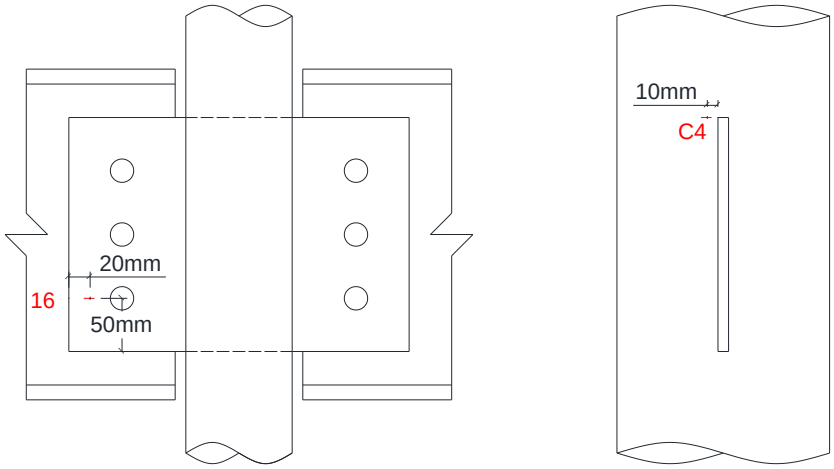

Figure 4.22 Critical strain positions of Joint-CH

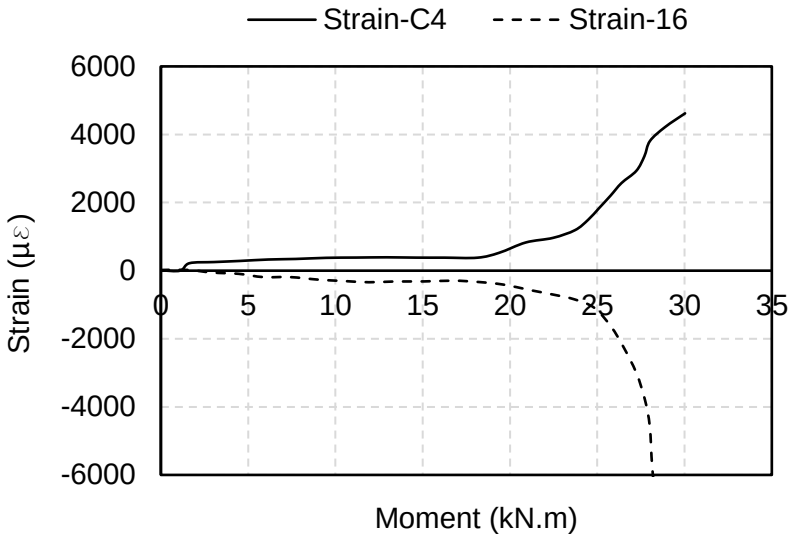

Figure 4.23 Strain vs. moment curves (CH)

4.2.3.2 Specimen CC

Figure 4.25 gives the moment versus rotation curves of the Joint-CC specimen. The slippage stage of the curves was relatively longer than the AH and BH connections as the through plate is stiff in its longitudinal direction, thus the load transferred from beam can only be picked up until the bolts fully touched with the bolt holes in both the fin plates and the beam webs.

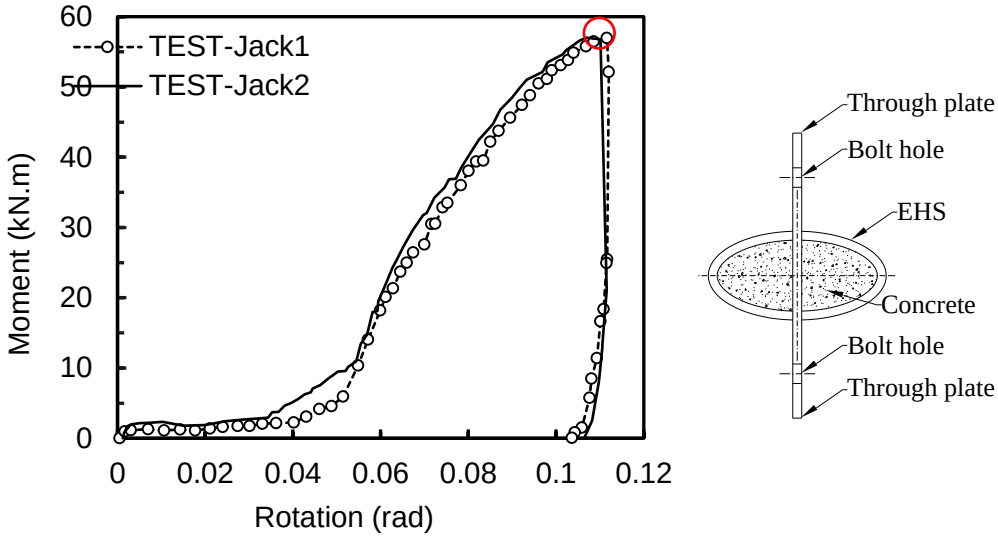

Figure 4.24 Moment versus rotation curves (Joint-CC)

Figure 4.26 shows the failures of Joint-CC after test. No obvious global deformation was observed in the beams and the EHS column. And no large cracks were observed in the concrete core as the stiffener resisted most of the tensile force rather than the EHS column, indicating that the stiffener prevented the core concrete from cracking failure and thus demonstrated that the stiffener, core concrete and the EHS worked well in this case. Both bole hole distortion and bolt shear failure occurred at the final stage of the experiment.

The critical strain positions and the corresponding strain data are given in Figure 4.27 and 4.28, respectively. As is shown, the critical area is found at the compression zone near the bottom bolt hole in the fin plate. From strain versus moment profile, it can be seen that the fin plate yielding occurred at the final stage of the experiment when the peak moment was about to be achieved.

(a) Front elevation of Joint-CC

(b) Core concrete after connection failure

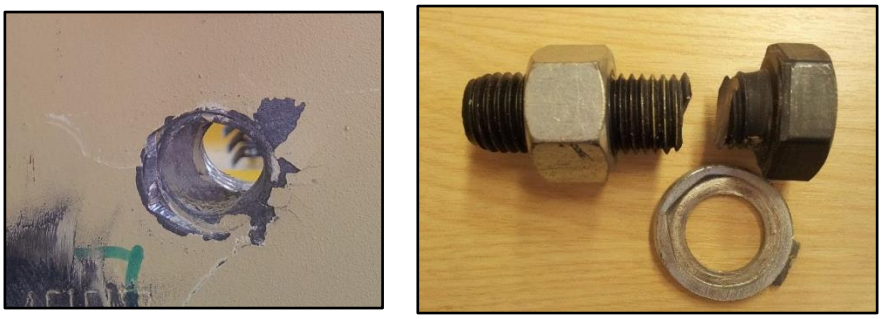

(c) Bolt hole deformation (d) Bolt shear failure

Figure 4.25 Failures of Joint-CC

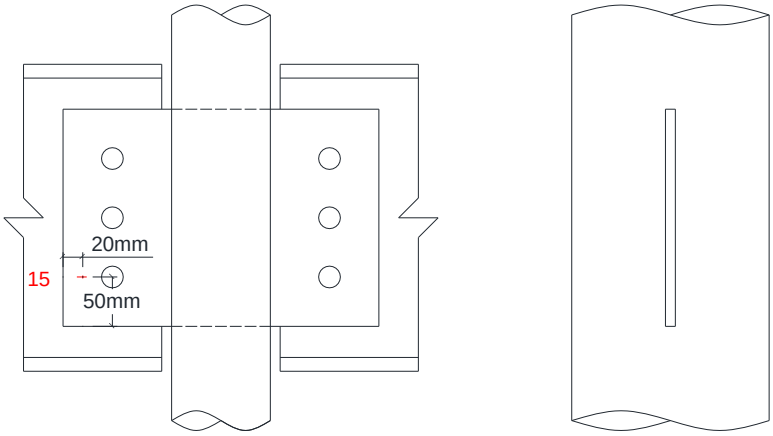

Figure 4.26 Critical strain positions of Joint-CC

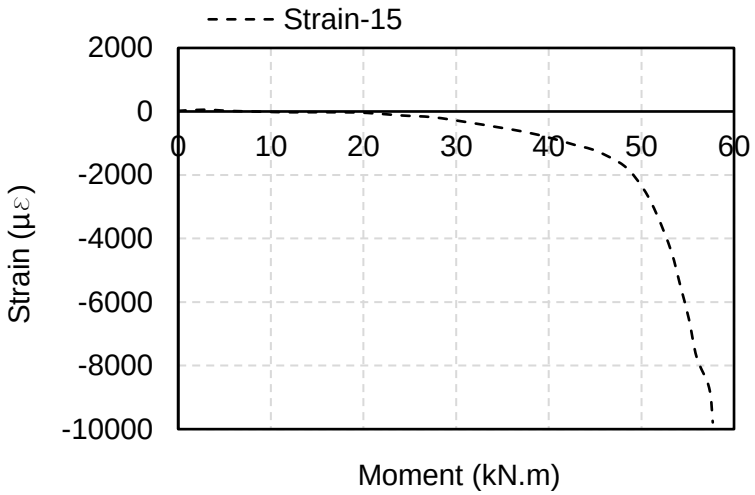

Figure 4.27 Strain vs. moment curves (CC)

4.2.3.3 Comparisons

Comparison of the moment versus rotation curves of the Type-C connections is illustrated in Figure 4.29. The ultimate moments, rotations and the failure modes of the connections are listed in Table 4.7. Load versus deflection profiles of the columns are drawn in Figure 4.30. Maximum deflections after the test were 2.9 mm and 1.9 mm for the hollow and the concrete-filled columns, respectively, which shows that the concrete-filled column deformed less easily under the same loading level at column end. Additionally, it had larger stiffness compared with the hollow column based on the curved slope of the linear part.

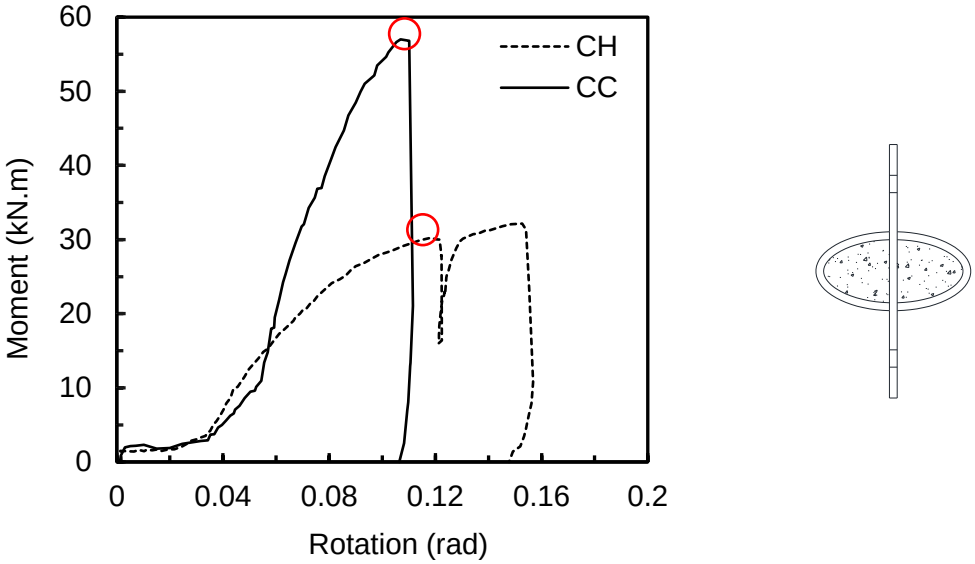

Figure 4.28 Comparison of moment-rotation curves (C)

Table 4.7 Ultimate moments, rotations and failure modes of Type-C connection

ID	M_u (kN·m)	θ_u (rad)	M_{uc}/M_{uh}	Failure mode
Joint-CH	30.0	0.11	-	Local buckling
Joint-CC	57.2	0.11	1.91	Bolt shear failure

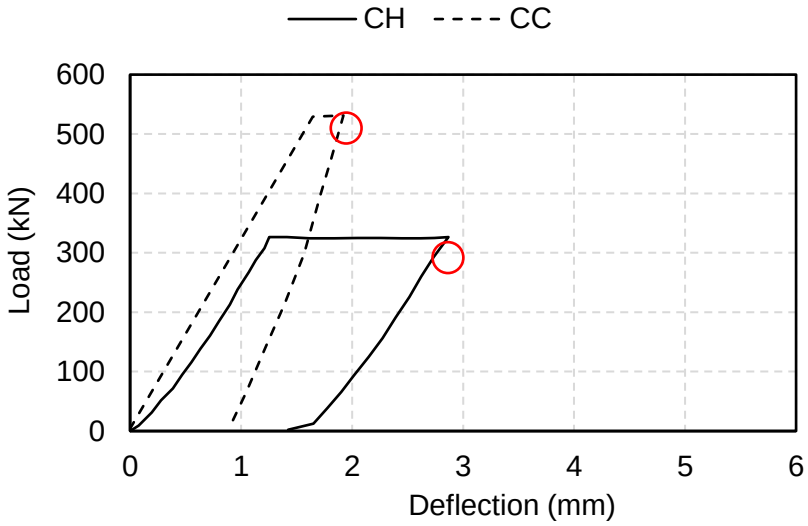

Figure 4.29 Comparison of the load vs. deflection profiles (C)

4.2.4 Type-D: Minor axis connection without stiffener

4.2.4.1 Specimen DH

Figure 4.31 presents the moment versus rotation curves of Joint-DH specimen. The two sides are almost identical before failure of the connection. The relatively lower peak moment of the two sides is deemed as the ultimate moment of the DH connection which is circled in the graph (8.4 kN.m at 0.12 rad). Failures of the connection are provided in Figure 4.32. No global deformation was observed in both the beams and the EHS column, while local buckling was found near the upper portion of the connection in the EHS column. As can be seen, this connection type failed at a low moment value since the stiffness of the EHS in the minor direction is weak.

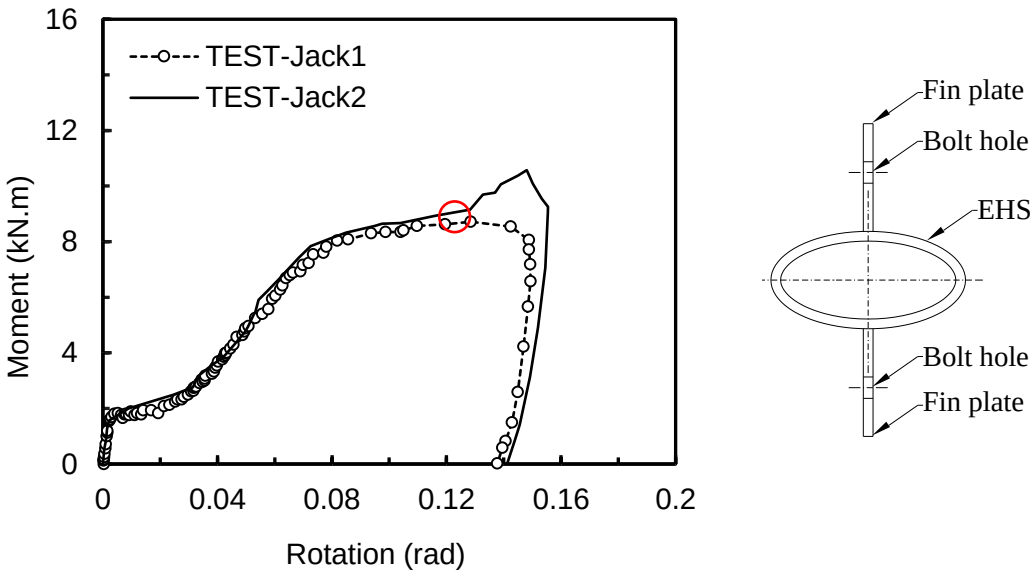

Figure 4.30 Moment versus rotation curves (Joint-DH)

(a) Front elevation of Joint-DH

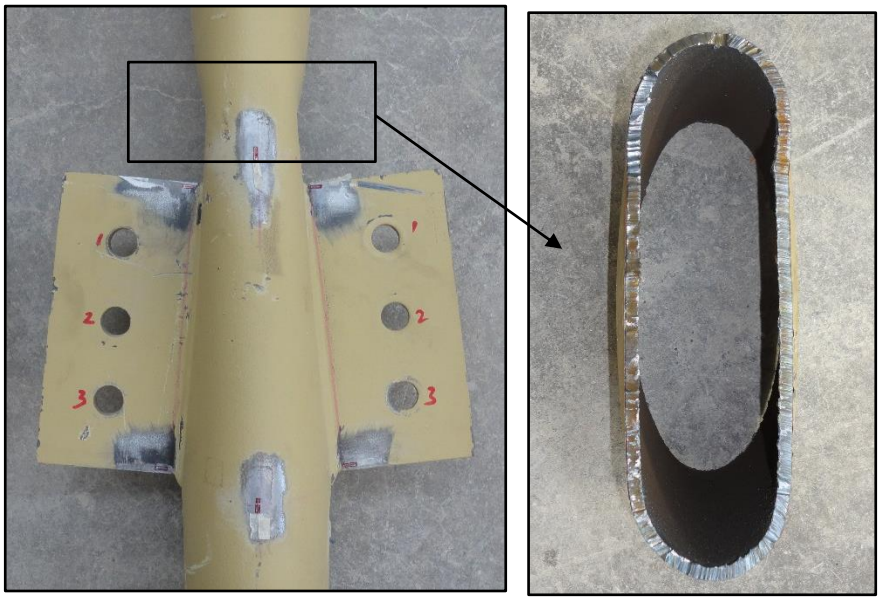

(b) Failure mode of the EHS

Figure 4.31 Failures of Joint-DH

4.2.4.2 Specimen DC

Figure 4.33 gives the moment versus rotation curves of Joint-DC. The relatively lower peak moment of the two sides is 43.6 kN.m at beam rotation of 0.11 rad. Failures of the connection are provided in Figure 4.34. No global deformation was observed in both the beams and the EHS column. Large cracks occurred in the concrete core caused by direct compression of the beam end due to lack of the stiffness in the minor axis direction of the EHS. The lower portion of the EHS column was pulled out, which caused fracture around the weld between the fin plate and the EHS column at the right hand side, while in the other side, the bottom and middle bolts failed in shearing.

Based on strain recording data at limited positions in the connection, the critical area was found at the tension zone of the EHS column which is given in Figure 4.35, while the strain versus moment curves are illustrated in Figure 4.36. As shown by the strain data, position of 'C8' yielded prior to the ultimate moment capacity of the connection reached.

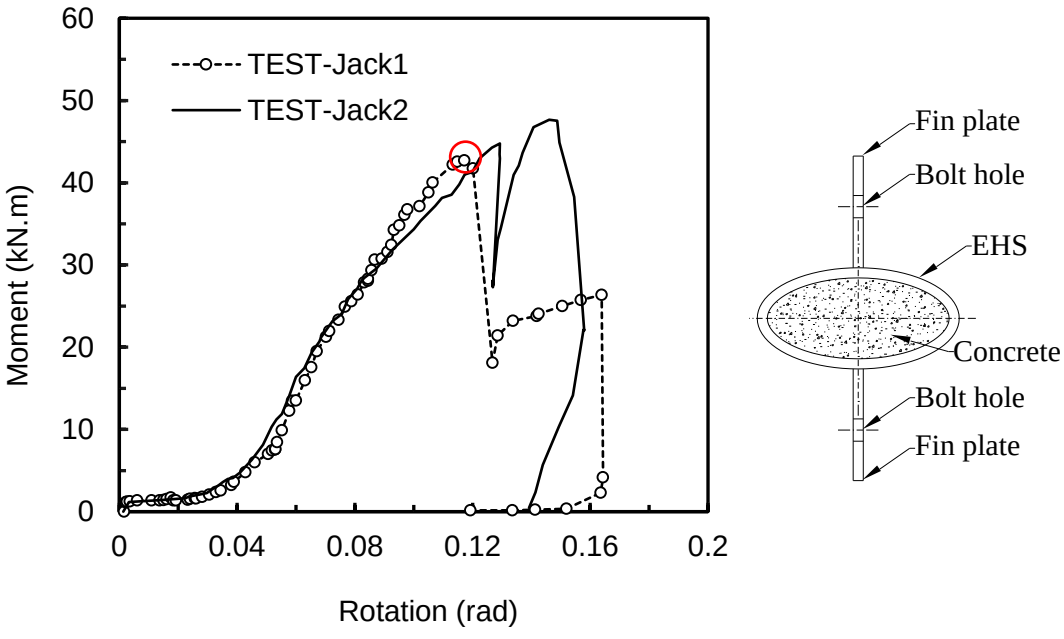

Figure 4.32 Moment versus rotation curves (Joint-DC)

(a) Front elevation of Joint-DC

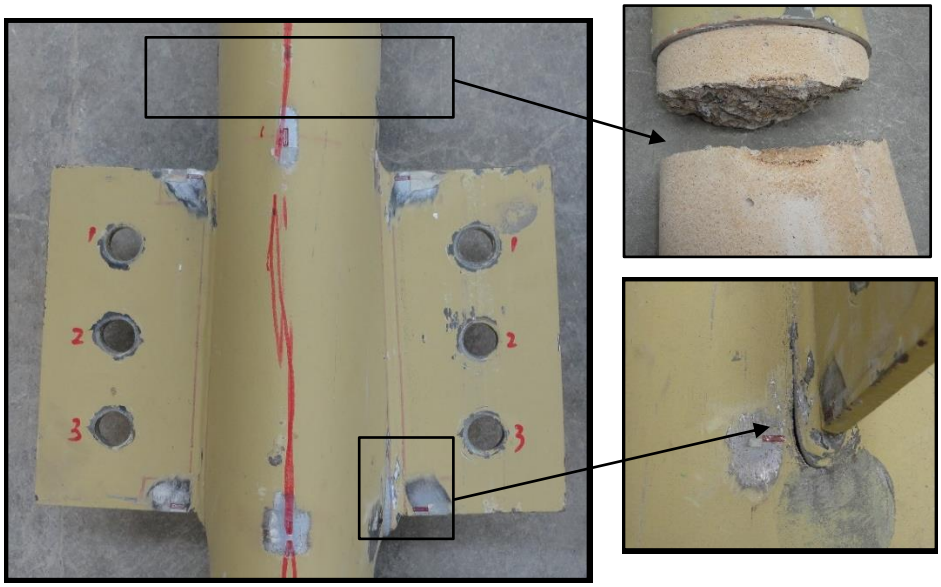

(b) Local failure of the column

Figure 4.33 Failures of Joint-DC

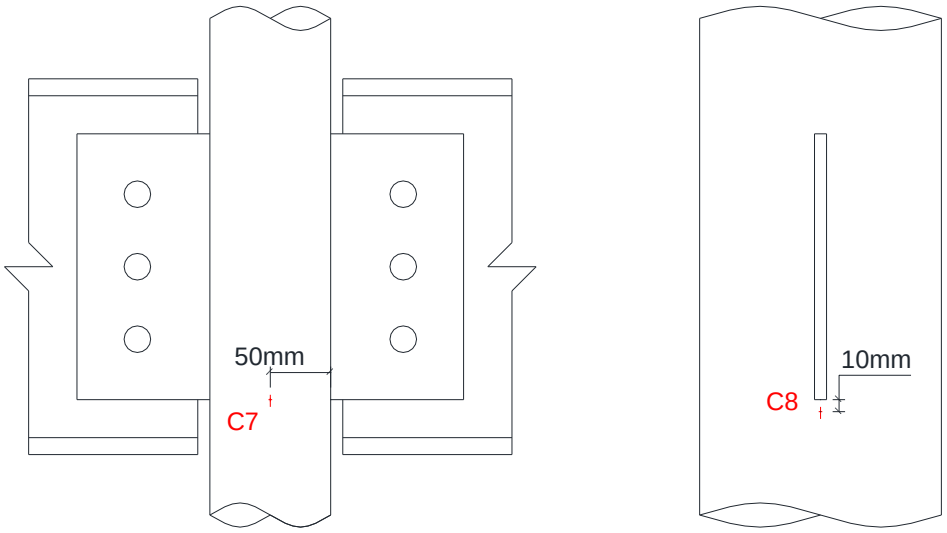

Figure 4.34 Critical strain positions of Joint-DC

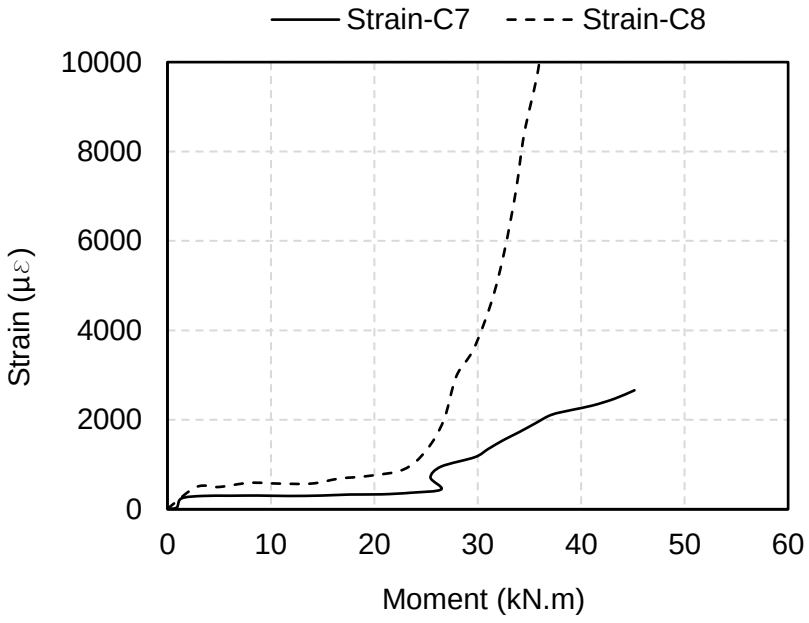

Figure 4.35 Strain vs. moment curves (DC)

4.2.4.3 Comparisons

Comparison of the moment versus rotation curves of Type-D connections is given in Figure 4.37, while the ultimate moment, rotations and failure modes of the connections are listed in Table 4.8. It is found that the infill concrete enhanced both the stiffness and the moment capacity significantly in this case. Also, the concrete core changed the failure of the EHS column to the components failure. Bolt shearing failure occurred in the connection with concrete infill.

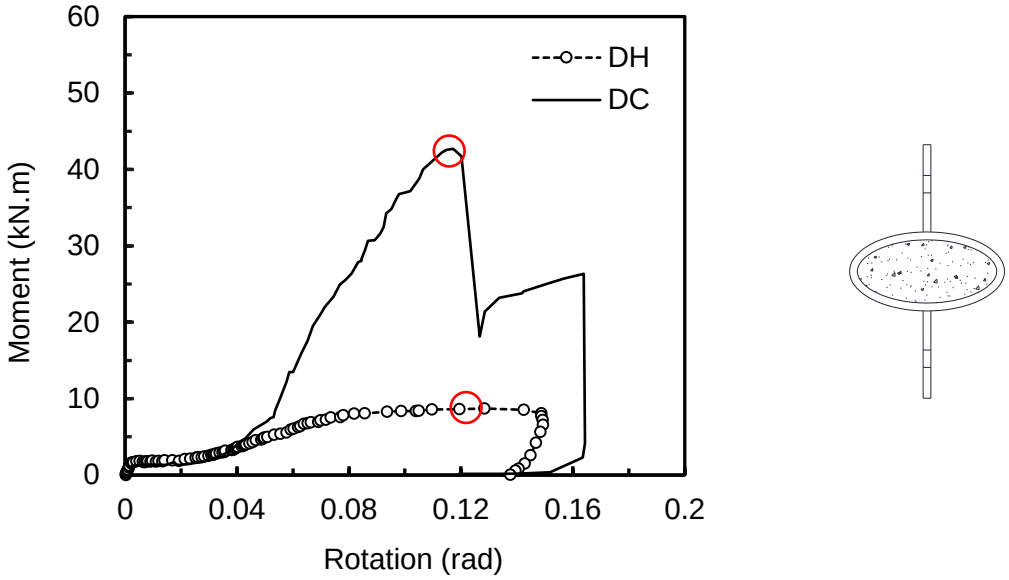

Figure 4.36 Comparison of moment-rotation curves (D)

Table 4.8 Ultimate moments, rotations and failure modes of Type-D connection

ID	M_u (kN·m)	θ_u (rad)	M_{uc}/M_{uh}	Failure mode
Joint-DH	8.4	0.12	-	Local buckling
Joint-DC	43.6	0.11	5.19	Bolt shear failure

4.2.5 Type-E: Minor axis connection with stiffener

4.2.5.1 Specimen EH

Figure 4.38 presents the moment versus rotation curves of Joint-EH specimen. Deviations of the initial stages can be seen between the both sides, which may be caused by the difference of the bolt positions in the holes (due to clearance) and the initial gap between the beam end and the EHS column. The ultimate moment of the connection was found as 13.3 kN.m at the beam rotation of 0.18 rad which is shown in the red circle in the graph.

Failures of Joint-EH are provided in Figure 4.39. It is found that there is no obvious global deformation in the beams and the column but local failures in the compression zone of the connection observed which possibly were caused by the direct compression from the beam ends. The stiffener plate inserted in the

major direction of the EHS did not prevent the column from buckling failure but decreased the deformation to some extent.

The critical strain positions and the corresponding strain versus moment curves are illustrated in Figure 4.40 and 4.41, respectively. It can be seen that both the tension (C5 and C6) and compression (C3 and C4) zones around the intersection between the fin plate and the EHS column yielded prior to the peak moment achieved while position '12' failed right after the peak moment was achieved.

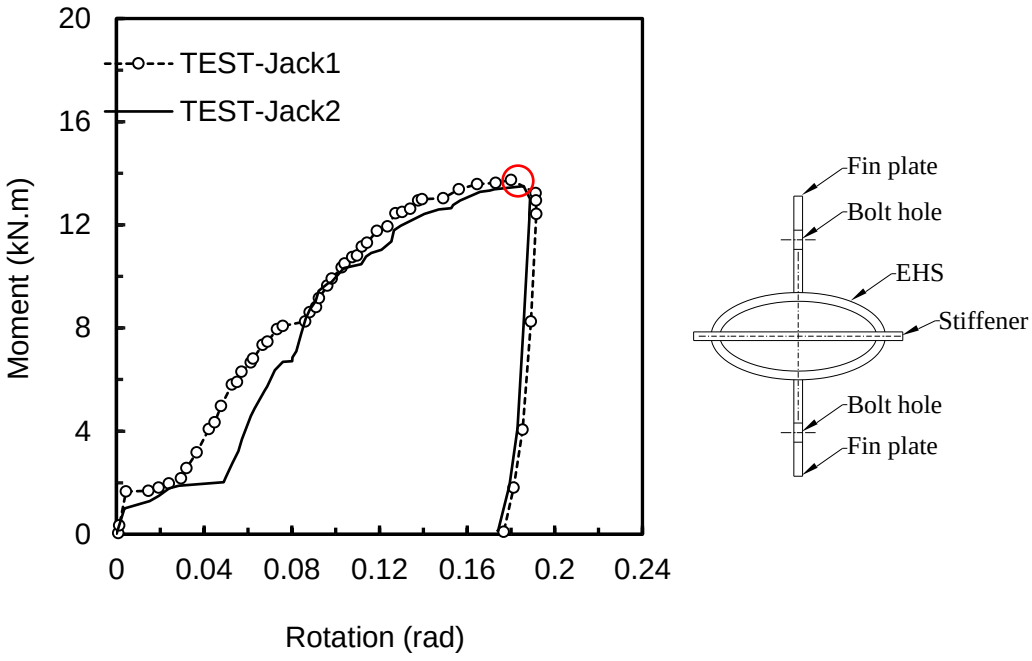

Figure 4.37 Moment versus rotation curves (Joint-EH)

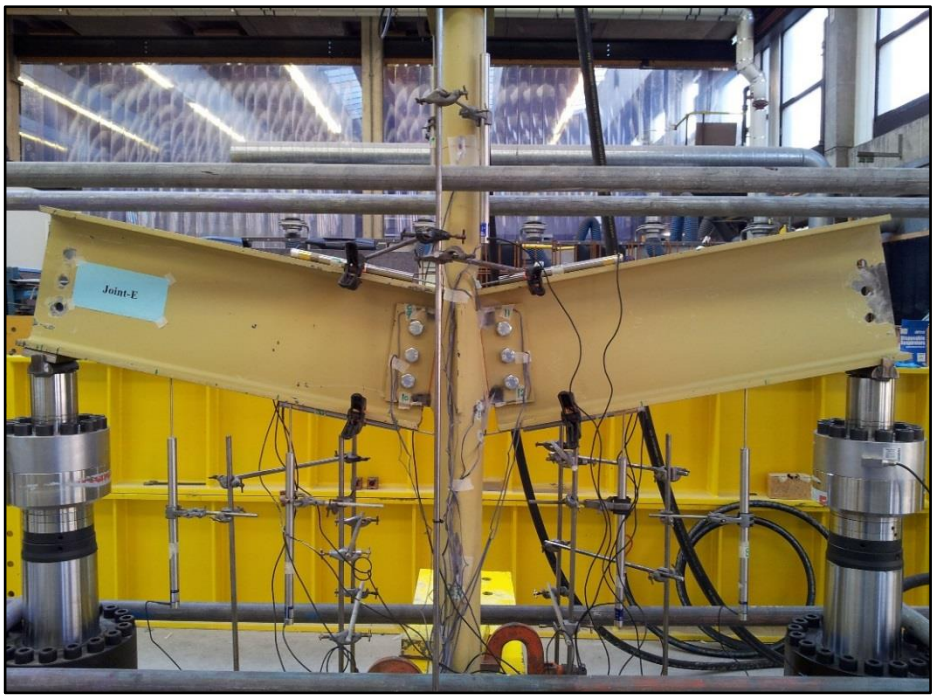

(a) Front elevation of Joint-EH

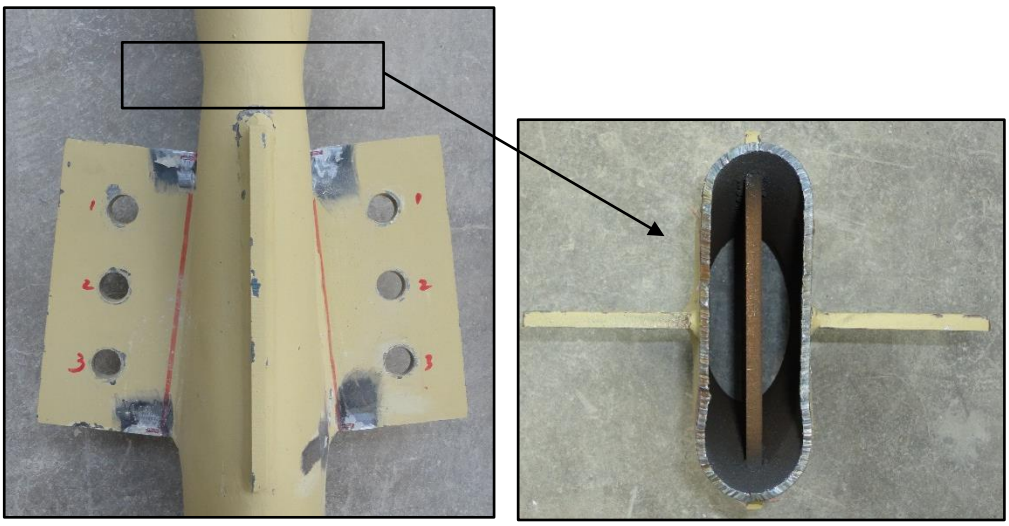

(b) Local failure of the EHS column

Figure 4.38 Failure modes of Joint-EH

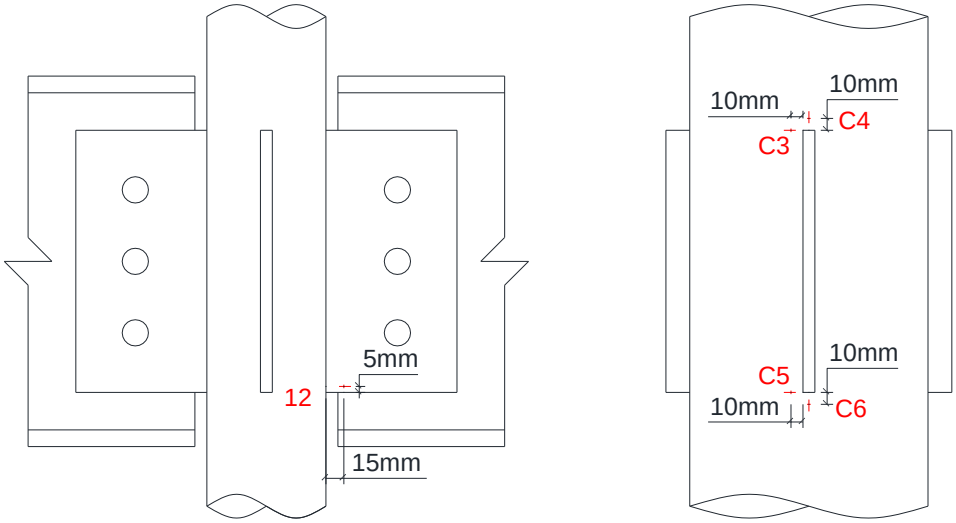

Figure 4.39 Critical strain positions of Joint-EH

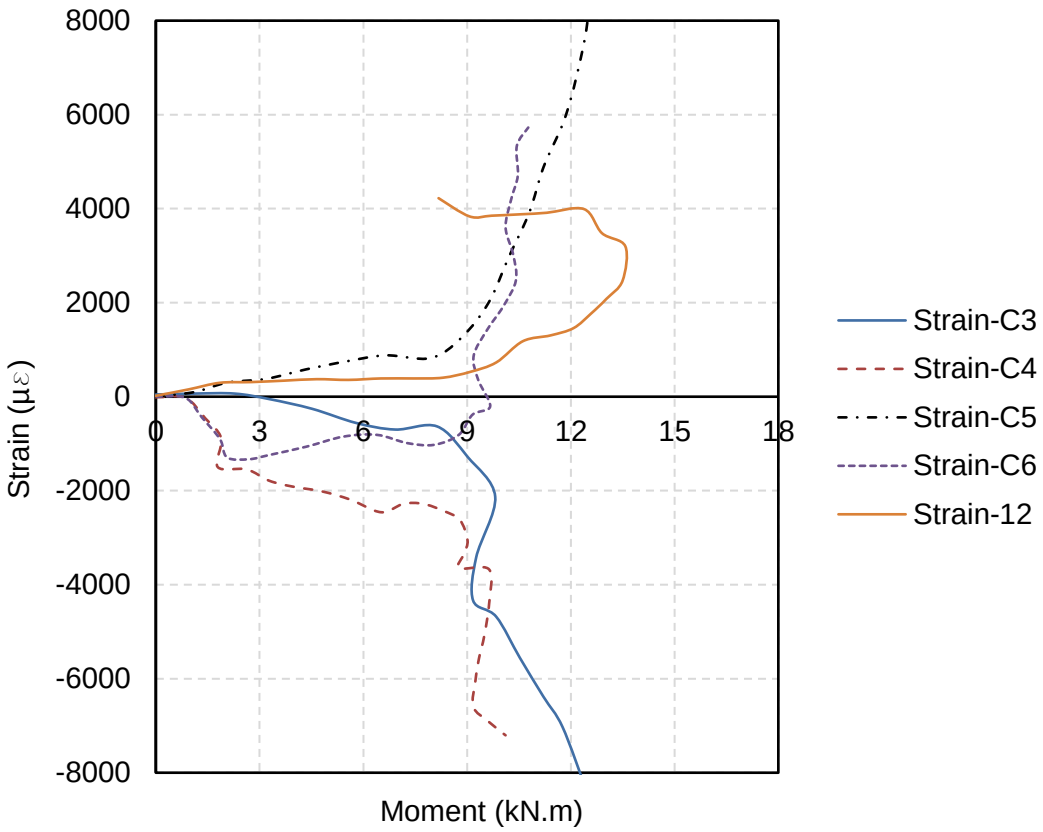

Figure 4.40 Strain vs. moment curves (EH)

4.2.5.2 Specimen EC

Figure 4.42 presents the moment versus rotation curves of Joint-EC specimen. The curves at both sides before failure are almost identical, which indicate that the tolerance in installation is not sensitive in this case. The lower peak moment of the connection was 33.8 kN.m at a beam rotation of 0.13 rad which is shown in the red circle in the graph. The sudden drop of the curve was caused by shearing failure of the bottom bolt at Jack-1 side. After this failure occurred, loading was carried on to achieve the full moment-rotation profile, while the bottom bolt of the other side failed as well right after the first bolt, after which both sides could not bear further loads. Failures of Joint-EC are shown in Figure 4.43. There is no obvious global deformation in the beams and the column, while initial cracks was found in the tension zone of the weld between the fin plate and the EHS column. Distortion of the bottom bolt was found in the fin plate. In this case, Gr. 8.8 bolts were adopted. To demonstrate the possible increase on the moment by utilising higher strength of bolts, Gr. 10.9 bolts were used in the repeat test for Joint-EC.

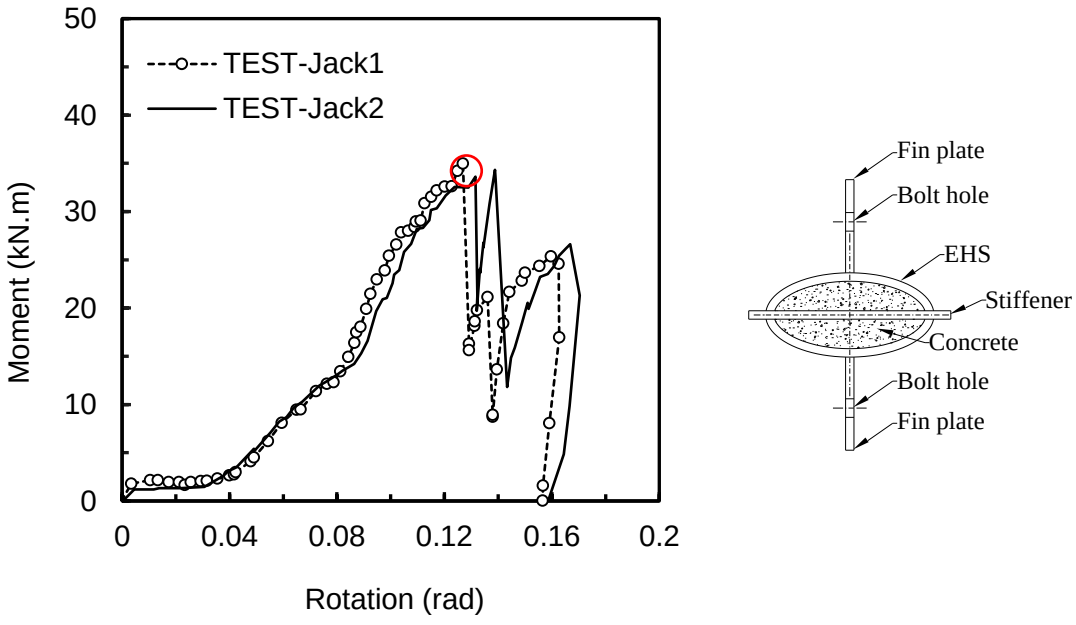

Figure 4.41 Moment versus rotation curves (Joint-EC)

(a) Front elevation of Joint-EC

(b) Close view of the connection

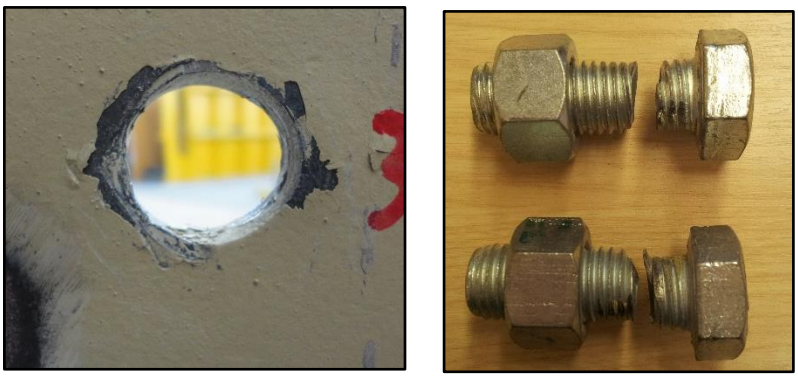

(c) Bolt hole deformation and bolt shear failure

Figure 4.42 Failures of Joint-EC

Figure 4.44 and 4.45 illustrates the critical strain positions and the corresponding strain data of Joint-EC. As can be seen, when the stiffener was inserted, although the compression zone of the EHS column near the weld between the fin plate

and the EHS yielded, the yielding of the compression zone of the EHS was prevented. Instead, the compression area of the fin plate shown in positions ‘7’ and ‘8’ yielded, indicating that the stiffener plate adopted in the major axis direction of the EHS prevented the column from failure to some extent.

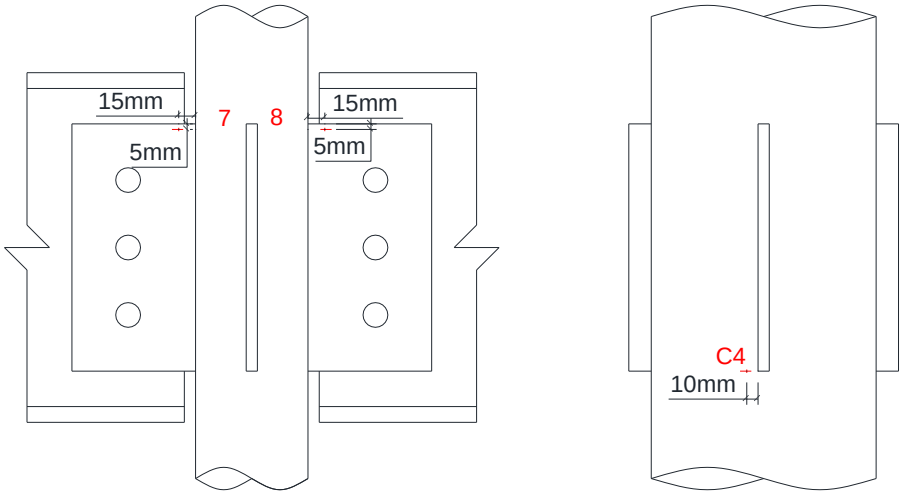

Figure 4.43 Critical strain positions of Joint-EC

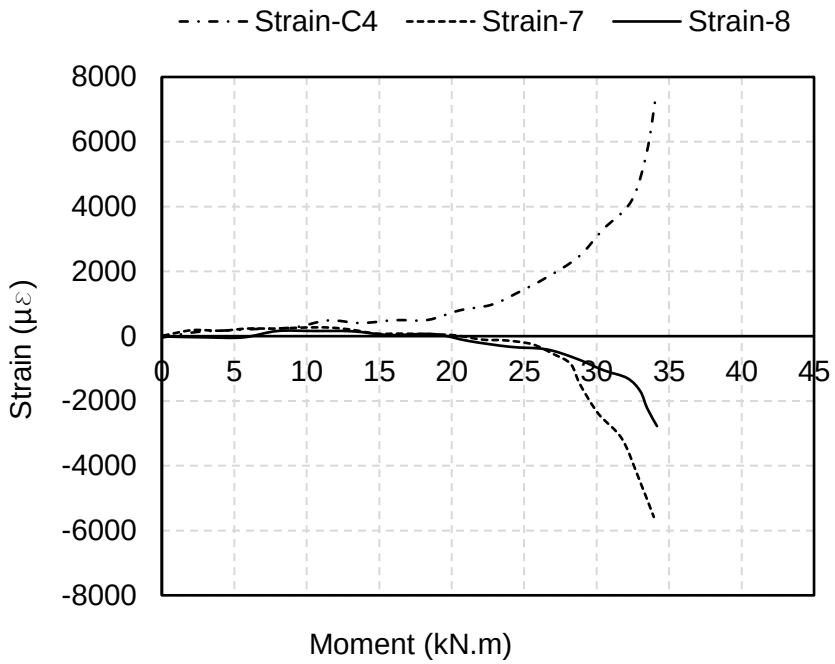

Figure 4.44 Strain vs. moment curves (EC)

Figure 4.46 and 4.47 presents the moment versus rotation curves and failures of the repeat test of Joint-EC, respectively. As is shown in the curve profiles, the connection experienced relatively long period of slippage as the bolt holes were enlarged after the initial test. Bolt failure occurred as well in this case, and the first fractured bolt was the bottom bolt of Jack-1 side, which caused the sudden drop in the moment versus rotation curves. Further load was picked up at the Jack-2 side although the cracks generated in the initial test grew and lead to tearing out of the EHS tube around the weld as show in Figure 4.47(b). The middle bolt of Jack-1 side failed afterwards, the shear failure of the bolts can be seen in Figure 4.47(c). No global deformation was observed in both the beams and the column. After the initial and the repeat test, only small cracks were generated in the concrete core which demonstrated that the stiffener plate, the concrete and the EHS column worked really well in this case.

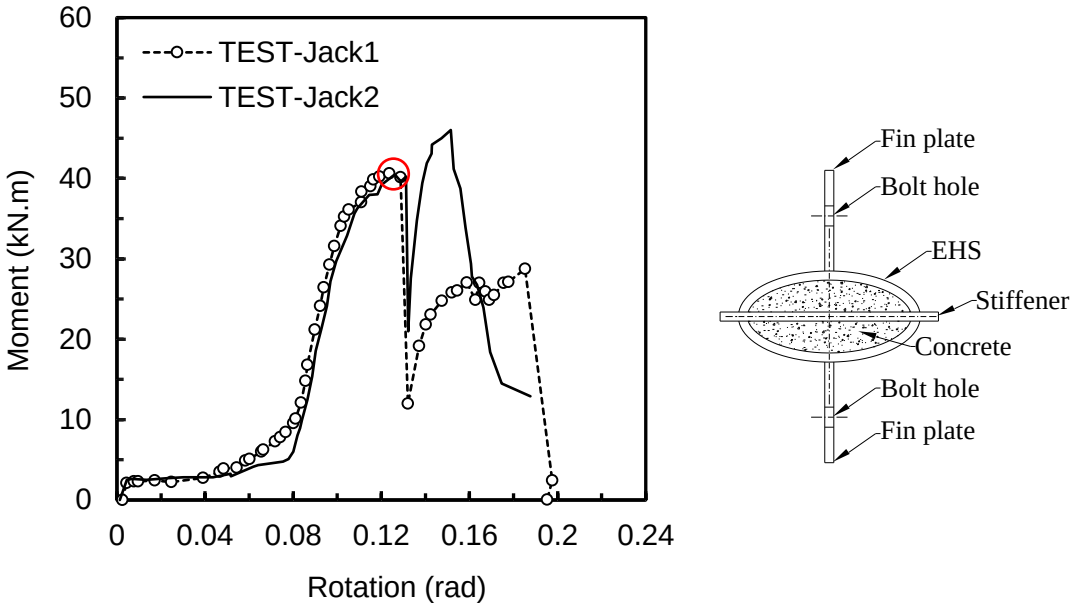

Figure 4.45 Moment versus rotation curves (Joint-ECR)

(a) Front elevation of Joint-EC after the repeat test

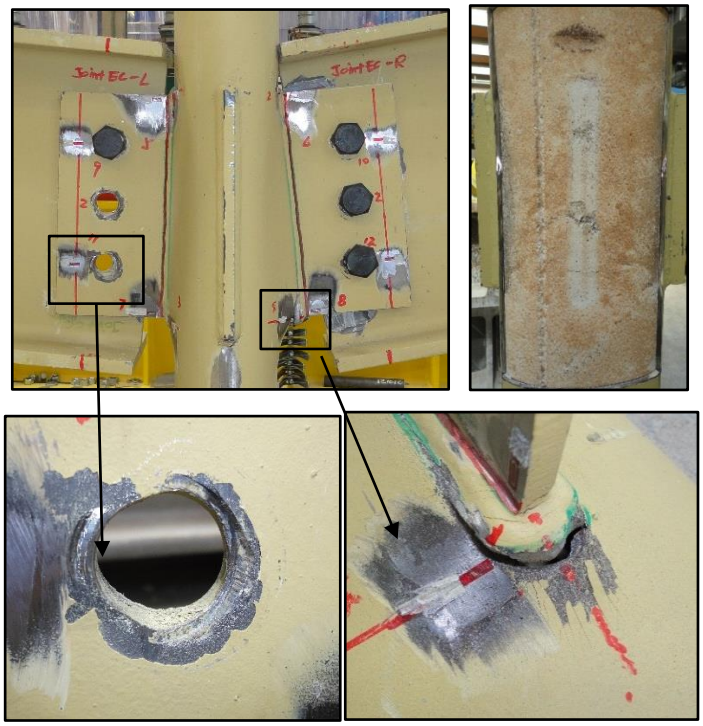

(b) Local failure

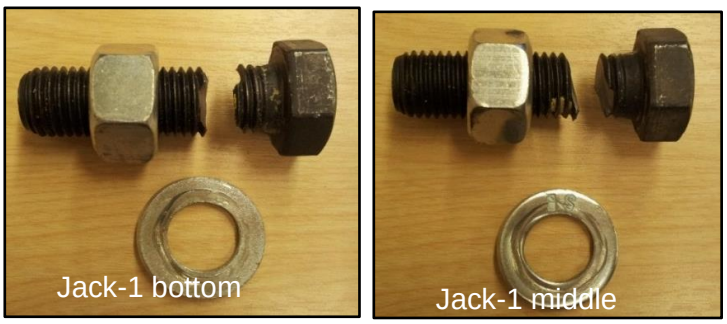

(c) Bolt shear failure

Figure 4.46 Failures of Joint-EC after the repeat test

4.2.5.3 *Comparisons*

Figure 4.48 and Table 4.9 gives the comparison of moment versus rotation curves and the comparison of ultimate moments and failure modes of Type-E connections. As can be seen, the moment capacity could be enhanced significantly by infilling concrete into the EHS column. Stiffness could also be increased after the slippage stage. The ultimate moment capacity of the connection could be improved by adopting higher strength of bolts based on the comparison between EC connection and its repeat test. The concrete core eliminated the buckling failure of the EHS column but lead to the bolt shear failure in both the EC connection and the repeat rest with higher strength of bolts.

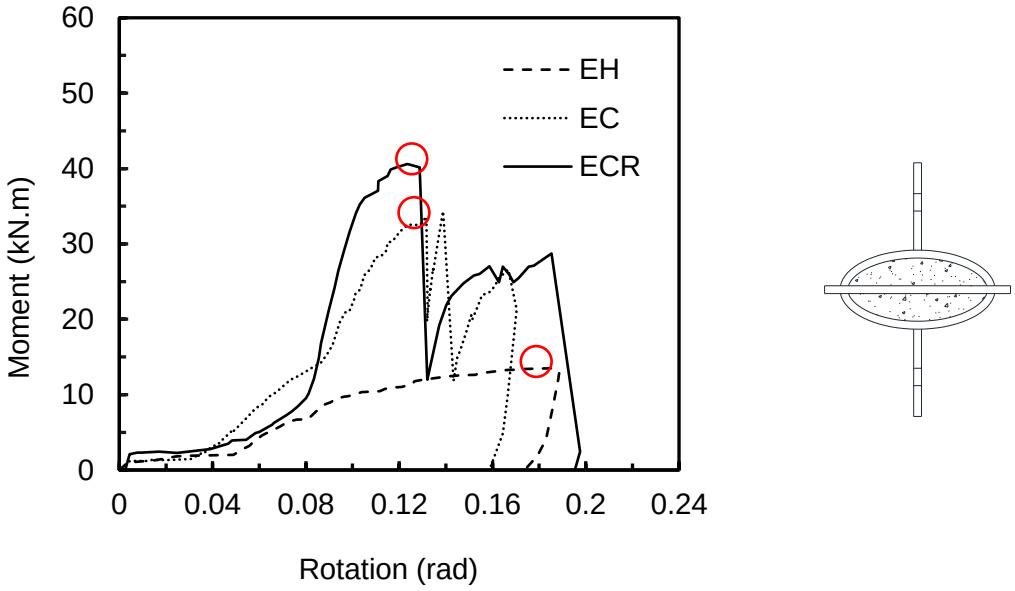

Figure 4.47 Comparison of moment-rotation curves (E)

Table 4.9 Ultimate moments, rotations and failure modes of Type-E connection

ID	M_u (kN·m)	θ_u (rad)	M_{uc}/M_{uh}	Failure mode
Joint-EH	13.3	0.18	-	Local buckling
Joint-EC	33.8	0.13	2.55	Bolt shear failure
Repeat-EC	41.4	0.13	3.11	Bolt shear failure

A comparison of the load versus deflection profiles of Type-E connections is given in Figure 4.49. Maximum deflections after the tests were 4.7 mm, 2.7mm and 2.3 mm for the hollow, the concrete-filled columns and the column in the repeat test, respectively. The different values in the concrete-filled column between the initial and repeat test occurred because that there was plastic deformation existing in the concrete-filled tube in the initial test and thus the deflection of the column in the repeat test was relatively smaller. It can be concluded that the concrete core could increase the stiffness of the column by comparing the results of the hollow column and the concrete-filled ones.

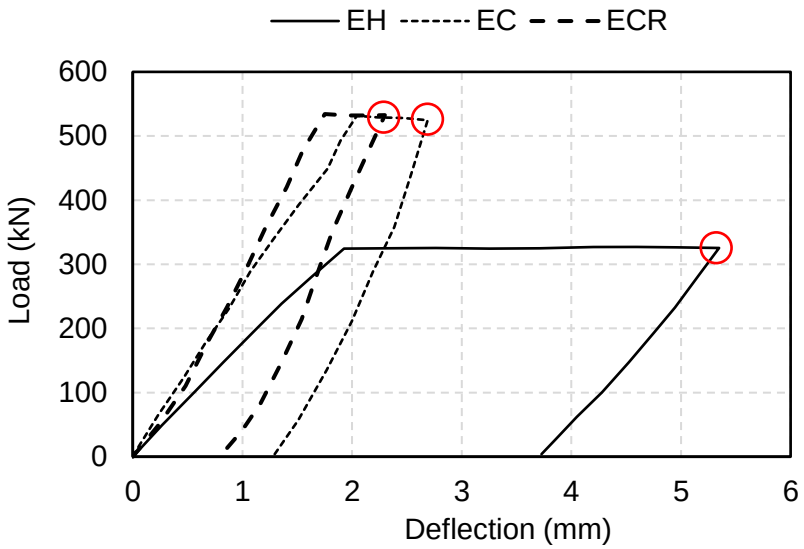

Figure 4.48 Comparison of the load vs. deflection profiles (E)

4.3 Comparisons among joint types

Summary of the moment vs. rotation curves is illustrated in Figure 4.50. The ultimate moments, rotations and failure modes obtained from experimental results are given in Table 4.10. It can be concluded that concrete infill can improve the moment behavior of the connections considerably and the most notable cases tested in this research were those without stiffener plates (Type-B and Type-D). The ultimate moment capacity of Joint-AC and Joint-EC was slightly lower than that of the unstiffened counterpart Joint-BC and Joint-DC, respectively. The reason may be that the failure of the connection with core concrete was governed by bolt failure and the inserted stiffener plate contribute to earlier failure of the bolts.

For connections with hollow columns, the moment capacity could be increased significantly due to the enhancement of the stiffener plate, e.g. in the minor axis direction of the EHS tube (Type-A and Type-C). It was found that the moment capacity of the minor axis connection could also be improved by inserting the stiffener plate in the major axis direction of the EHS tube, although the stiffness of the major axis direction of the EHS is higher than that in the minor axis direction. Evidence could be found from the results of connections of Type-D and Type-E. All of the cases failed in local buckling at the upper portion of the EHS tube around the connection, though stiffener plates were adopted in some cases either in the minor or the major axis direction of the EHS tube. The explanation is that failure of the hollow column was caused by direct compression from the beam ends while the thin-walled tube has relatively weak stiffness in the transverse direction. In the case of Joint-C, bolts failure occurred additionally compared with the other cases. The reason is that the loads was transferred from beam ends to the bolts and then to the through plate and the bolts plus the through plate endured almost the whole shear force and moment before beam end touched the EHS column face.

Among all of the tested specimens, through plate connections (Type-C) exhibited the highest capacity in both the hollow connections group and the concrete-filled group, although they failed at a lower joint rotation. The above reason for the bolts failure of Joint-C could also be adopted to explain this phenomenon. The EHS tube wall was subjected to compressive force near the upper section and tensile force near the bottom portion. Since the through plate endured most of the compressive or tensile load, large concave or convex deformations in the EHS column around the connection and cracks that might occur in the core concrete of the connections with concrete-filled columns were prevented.

In addition, for the concrete-filled connections with stiffener plate in the columns (AC, CC, EC), no severe cracks were observed in the core concrete which demonstrates the benefit of the stiffeners. Moreover, the concrete failure of Joint-DC was more severe than that of Joint-BC because it was subjected to bending in the weaker axis direction.

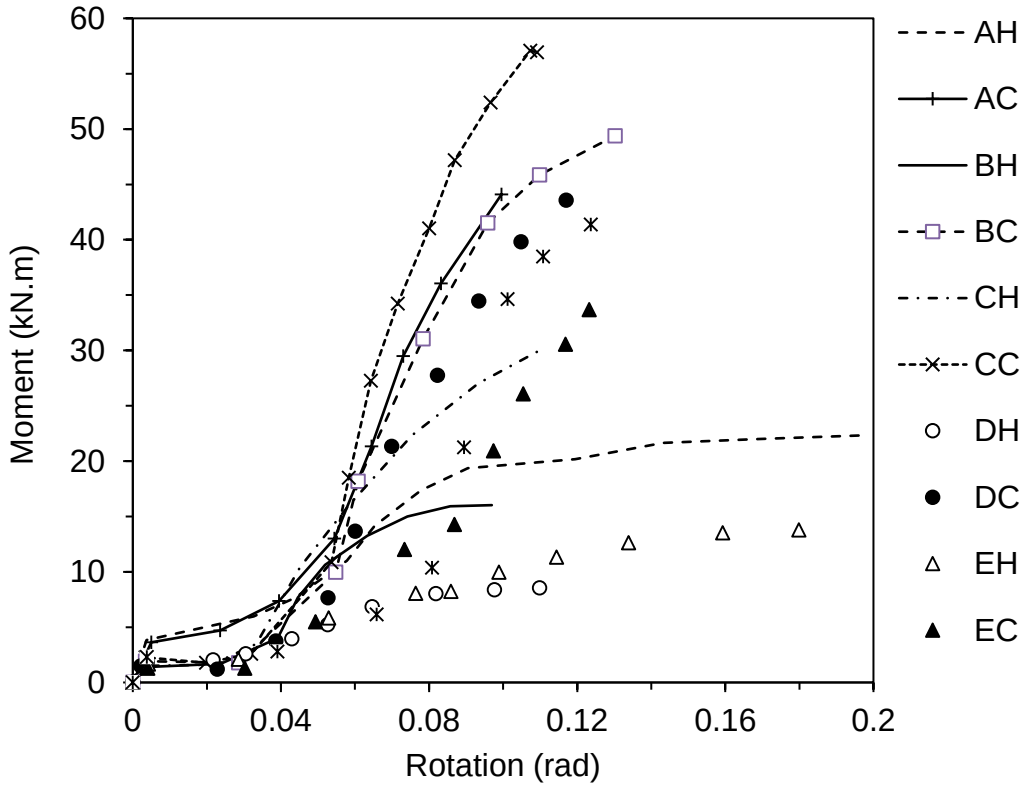

Figure 4.49 Summary of moment vs. rotation curves

Table 4.10 Summary of ultimate moments, rotations and failure modes

Specimen ID	M_u (kN·m)	θ_u (rad)	M_{uc}/M_{uh}	Failure mode
Joint-AH	22.3	0.200	-	Local buckling
Joint-AC	43.8	0.110	1.96	Bolt shear failure
Joint-BH	16.0	0.100	-	Local buckling
Joint-BC	49.6	0.120	3.10	Bolt shear failure
Joint-CH	30.0	0.110	-	Local buckling
Joint-CC	57.2	0.110	1.91	Bolt shear failure
Joint-DH	8.4	0.180	-	Local buckling
Joint-DC	43.6	0.110	5.19	Bolt shear failure
Joint-EH	13.3	0.180	-	Local buckling
Joint-EC	33.8	0.130	2.55	Bolt shear failure
Joint-ECR	41.4	0.130	3.11	Bolt shear failure

4.4 Conclusions

In this chapter, both material test results and connections experimental results are provided. Based on the experimental results, it is found that concrete infill can increase the connections moment capacity significantly, the enhancement ratio ranging from 1.91 to 5.19. The stiffener plate could increase the ultimate moment capacity of the hollow connections but may cause decrease in the relevant concrete-filled connections. The minor axis connection with the through plate was found to have higher stiffness and moment capacity, and thus this joint type was recommended for minor axis connection with EHS column.

Failure mode of the hollow connection was observed as local buckling of the EHS column while this failure was not eliminated by the stiffener plate but the filling concrete. Shearing failure of the bolts occurred in all the cases of connections with concrete infill and also the case of minor axis through plate connection with hollow EHS column.

According to the moment versus rotation profiles of the connections, friction was in control in the initial stage with the friction force existing between fin plates, beams and bolts. In this section, the rotation of the connection was quite low but the slope of the moment-rotation curves was nearly constant, with the column, beam and bolts working well together. Then, slippage occurred when the load applied exceeded the friction force, and the moment climbed slowly with the increase of rotation. Afterwards, the bolts, the bolt holes in the fin plates and the beam webs acted together in resisting the load until the joints failed in one of the modes described previously.

Chapter 5

Development of the numerical model and validation

In this chapter, the experiments described in the previous chapters are simulated numerically by ABAQUS/standard server. The developed finite element (FE) model is described in detail and is validated against the observed/measured experimental results given in Chapter 4.

5.1 Introduction

Apparently, full-scale experiments can reflect nearly real response of the connections and provide trustworthy test data. However, it is time consuming and expensive to conduct extensive parametric studies to cover various connections profiles and loading cases only based on laboratory tests. A general and well-recognized method to solve this problem is finite element simulation which has been proved to be successful to capture the failure modes, loading response, and loading resistance of both members and connections. In this chapter, the general purpose finite element analysis package ABAQUS is employed due to its superb performance in simulating complex non-linear structural response.

5.2 Geometric model and mesh

A three-dimensional finite element model (FEM) was developed to simulate the moment behaviour of the beam to elliptical column connections. In order to reduce the size of the finite element model (FEM) and to achieve computational efficiency, only half of each specimen was modelled in which appropriate symmetry boundary conditions were applied. The geometric model with mesh is shown in Figure 5.1, including the symmetry plane and the applied loads. A loading endplate was modelled to touch the top faces of both the EHS tube and the concrete core to fully transmit the applied axial load. The loading plate was controlled via a reference point and only longitudinal deflection of the EHS column was allowed at the top whereas the freedoms in all directions of the bottom end plate were constrained. The bearing roller adopted in the experiments to apply load at beam end was introduced in this model.

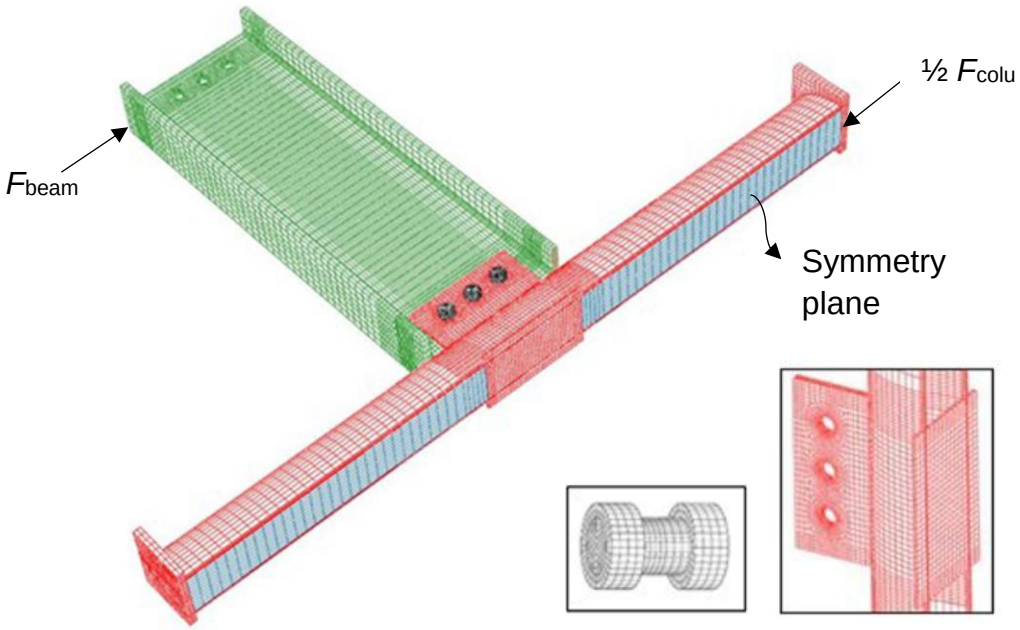

Figure 5.1 Finite element model with mesh (1/2 model)

The actual gap between end of the beam flange and the EHS column face was set according to the measurements. In order to provide more accurate predictions for the experiments, bolt positions were assumed based on the test setup; adopted positions were illustrated in Figure 5.2 as an example.

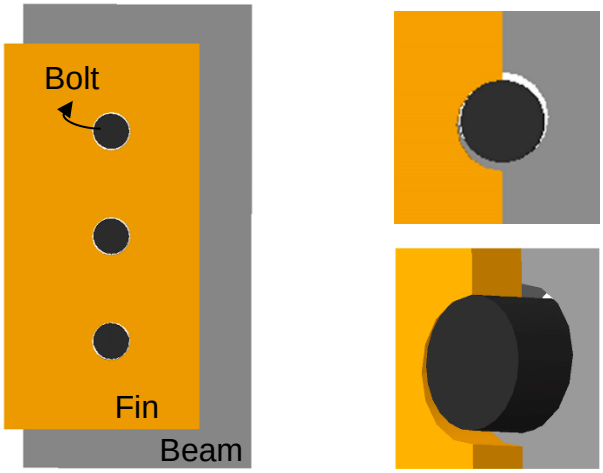

(a) Central position (b) Off center (Joint-AC)

Figure 5.2 Bolt positions in FE models

It was observed that both bolt heads and nuts were embedded into the fin plates around the bottom bolt holes after tests, which was caused by tensile force in the bolts occurred in the late stage of the experiments. In order to avoid possible convergence problem when calculating by using ABAQUS/standard solver,

hexagonal bolt heads and nuts were simplified as cylinders. This simplification was also adopted by other researchers [76, 77]. Fillet welds and washers were not considered in all of the FE models.

5.3 Element type and mesh

Three-dimensional 8-node solid element - C3D8 was employed to establish the column, beam, plate, bolts, concrete core and the roller. This element is suitable for complex non-linear analysis in regards to extensive contacts and large deformations. Incompatible mode was selected for steel component elements to avoid possible hourglass phenomenon while ‘reduced integration’ was used for the concrete core elements to reduce computational cost.

For the tested specimens, failure normally occurred around the connection, thus a finer mesh was used to obtain accurate simulation while a coarser mesh was adopted further away from the connection area to save computational time. No global buckling of the EHS column was observed during the tests, therefore the following mesh size recommendations which has been proved to be suitable and sufficient for stub concrete-filled columns were followed: 5-10 mm for EHS and 10-20 mm for concrete; the concrete element size was set as twice the element size of the EHS column where applicable [33]. Also, a mesh size of 20 mm was adopted for both steel and column of the through-plate concrete-filled connection [78], which gave sufficiently accurate results with quick convergence and reasonable computational time.

Taking the above findings into consideration, global mesh sizes of 20mm were adopted for both the EHS and concrete core while mesh sizes of 10 mm and 5 mm were used in the connection area for concrete and EHS, respectively. The hoop direction of the EHS column was meshed using a single bias meshing technique with a minimum mesh size of 10 mm (curved side of EHS) and maximum of 20 mm (flat side, this value may be reduced accordingly); same technique was used in the longitudinal direction of the EHS column. The steel components had two layers of mesh in their thickness directions.

A bolt mesh size of 3 mm was recommended by Yu et al. [79] and was thus adopted as the global size for the bolts in this chapter. In particular, mesh size

was minimized to 2 mm along part of the bolt shank longitudinal edges where the surface was defined as ‘slave surface’ in one of the contact pairs. In the circumferential direction of the bolts/bolt holes, 32 elements were adopted. Mesh sensitivity analysis was conducted in terms of this element quantity. Figure 5.3 illustrates the equivalent plastic strain distribution along the critical bolt hole in fin plate (Joint AC-4mm-Fin, model details can be found in the parametric study of section 5.9), where the results obtained from 16 elements, 32 elements and 48 elements are compared. The x-axis represents the angle initiating from 0° to 360°. The strain distribution profiles of 32 and 48 elements are nearly identical, however, in contrast, the profile from 16 elements has noticeable deviation, which proves that the FE model could adopt the 32 elements as the optimum option regarding computational efficiency and result convergence.

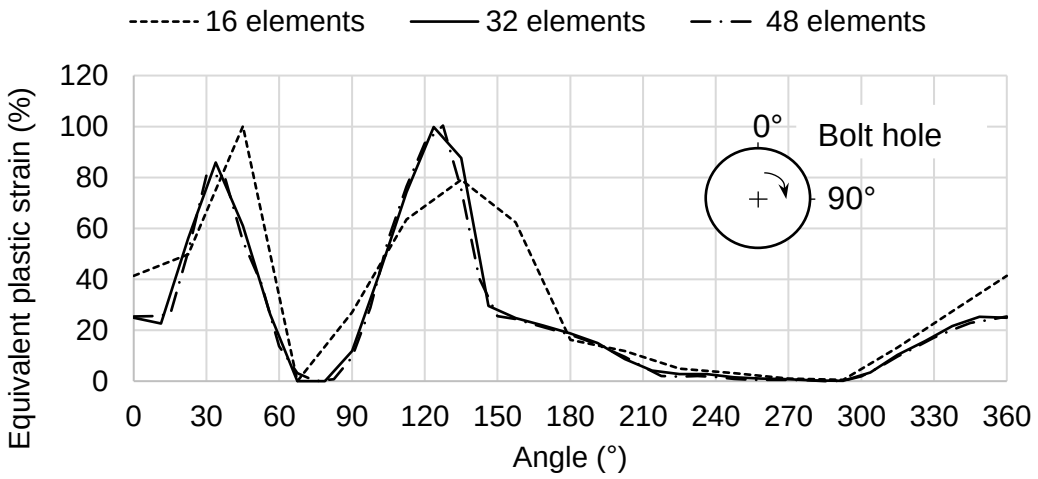

Figure 5.3 Equivalent plastic strain distribution

5.4 Material properties

For characterizing the mechanical behavior of concrete, damage plasticity model was selected among all the model options in ABAQUS. This model is based on the assumption of scalar (isotropic) damage and is designed for applications in which the concrete is subjected to arbitrary loading conditions. The model takes into consideration the degradation of the elastic stiffness induced by plastic straining both in tension and compression.

For the compression behavior, a four-part stress-strain model provided by Dai & Lam [33] for ABAQUS analysis was adopted for the EHS confined concrete in

this chapter, and the calculated compressive stress vs. strain relationship is shown in Figure 5.4; key parameters are listed below: maximum un-confined compressive cylinder strength was 33.2 MPa; initial elastic modulus was 30826 MPa; maximum confined compressive strength was 43 MPa. Fracture energy option was selected to define the tensile behavior of concrete, with a failure stress of 2 MPa (approximately equal to 0.1 times the corresponding compressive stress) and a fracture energy of 0.08 N/mm which was obtained through linear interpolation between 0.04 N/mm for C20 concrete and 0.12 N/mm for C40 concrete [80].

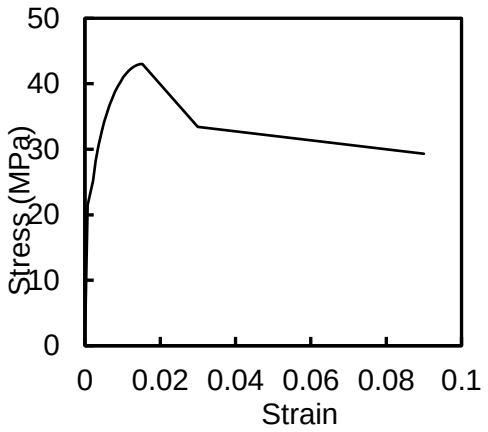

Figure 5.4 Stress-strain curves of EHS confined concrete

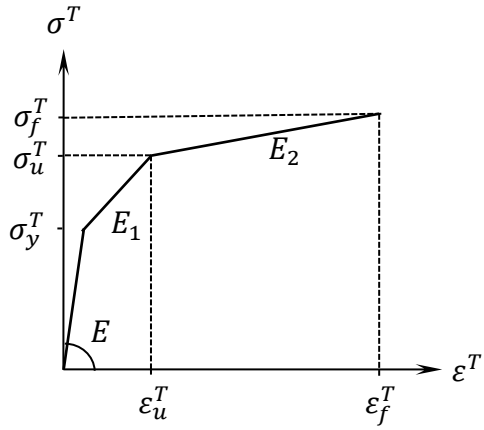

Figure 5.5 Stress-strain model of steel [81]

The stress-strain model of steel is illustrated in Figure 5.5 where the vertical and horizontal axes represent the true stress and strain converted from the tested

nominal values via the following recognized expressions based on the principle of constant-volume:

$$\sigma^t = \sigma^n(1 + \varepsilon^n) \quad \text{(a)}$$

$$\varepsilon^t = ln(1 + \varepsilon^n) \quad \text{(b)}$$

where σ^t and ε^t denote the true stress and true strain, respectively; σ^n and ε^n refer to the nominal stress and strain. The true stress and strain at fracture are obtained by using the following equations:

$$\sigma_f = \frac{F_{frac}}{A_{frac}} \times 100\% \quad \text{(c)}$$

$$\varepsilon_f = \ln(\frac{A_0}{A_f}) \quad \text{(d)}$$

where F_{frac} and A_{frac} are the load and smallest cross-sectional area when the coupon is fully fractured; A_f is the smallest cross-sectional area after fracture. Tested σ_f and ε_f are 940.5 MPa and 96.4% for S355 steel; 943.7 MPa and 102.9% for S275 steel.

5.5 Failure criteria

To verify the accuracy and reliability of the FE models, it is essential to determine the failure modes and ultimate strength of the connections. Therefore, selection of failure criteria becomes crucial. In this thesis, the strain based failure criterion for bolted connections adopted by Salih et al [82] were employed to define the bolt shear and plate failure in the numerical studies. In this thesis, bolt failure is deemed to occur when the equivalent plastic strain over the full critical cross-section of the bolt exceeds 1%. The possible plates bearing failure and net section failure are adopted with the criterion that the localized equivalent plastic strain reaches the true fracture strain [82] to identify the failure modes and the failure moment of the bolted connections regardless of the deformation limit of bolt holes.

For the true fracture strain, experiments have been carried out by Khoo et al. [83], Dowling [84], Huns et al [85] and Nip et al [86] and an average value of 100% was obtained for structural carbon steels [82]. Based on the uniaxial tension test

results of 96.4% for S355 steel and 102.9% for S275 steel obtained in Chapter 4, this value of 100% is reasonable and therefore will be used in the parametric studies conducted in the next chapter. However, in the verification of the FE models, tested results of the true fracture strain of the plates will be adopted in this chapter.

For connections with thick fin plate welding to thin-walled RHS column, punching shear failure of the tube wall along the perimeter of the weld between fin plate and the column was found the only limit state according to the observation from early tests conducted by Sherman [66]. However, in the range of tests presented in Chapter 4, sign of punching shear failure of EHS tube wall was only observed in the test of Joint-AH, Joint-DC and the repeat test of Joint-EC. Determination of this failure in the FE models will be based on the identification of yield failure of tube wall along the welds.

For hollow connections, the main failure was found to occur in the EHS column near compression zone of the connections, caused by direct compression from the beam end. Determination of the ultimate capacity of the column in such scenario could be similar to the case of a chord member in a welded tubular joint, when failure occurs in the chord member. Hence, two failure criterions could be adopted: peak load/moment or the corresponding load/moment at the deformation limit. For circular hollow sections, 3% of the tube diameter (D_{CHS}) is generally used as the deformation limit. In this chapter, the solution of EHSs is that using the largest diameter of the EHS for the connections subjected to bending in the major axis direction, while, the smallest diameter will be used for the connections subjected to moment in the minor axis direction.

5.6 Contact

Contact interaction is complicated when conducting the nonlinear analysis of concrete-filled bolted connections by using the ABAQUS standard solver. Proper definitions of master and slave surfaces in contact pairs (in accordance with the below two criteria: 1) stiffer material is normally set as the master surfaces; 2) a surface should not be used as slave surface in two or more different interactions) and contact properties were essential to avoid possible convergence problems and to successfully capture the moment-rotation behavior of the connections.

Surface-to-surface contact command with a finite sliding option was used in this thesis for the following contact pairs: beam-fin plate, beam/fin plate-bolt, stiffener plate/through plate-concrete, rigid plate-concrete, EHS-concrete. 'Hard contact' in the normal direction was defined to fully transfer the load from beam to column through fins and bolts; the frictional effect between contact surfaces was considered by incorporating the classical isotropic Coulomb friction model with a friction coefficient of 0.3 was assumed for all of the contact surfaces in the tangential direction as there is little effect when different coefficient is used [33].

5.7 Verification of the numerical models

5.7.1 Concrete-filled connections

The three-dimensional numerical models of concrete-filled connections were validated against the experimental results provided in Chapter 4. In the first stage, the rotation behaviour of the connections was validated by comparing the moment vs. rotation curves obtained from the experiments and the numerical simulations, see the comparisons shown in Figure 5.6. In general, the whole curves prior to the maximum point (caused by bolt shear failure) can be well captured by the FE modeling with the exception of Joint-ECR. The EC connection underwent yielding along the intersection between the fin plate and the EHS column during the initial testing, however this was not considered in the FE modeling. The friction and slippage between beam and fin plate can be predicted reasonably in all specimens based on the initial stages of these moment vs. rotation curves from the FE simulation and experimental results.

Nevertheless, there was a gentle transition phase in the experimental curve before the bolt shanks fully contacted the surface of the bolt holes, which was governed by bolt positions. The positions of bolts in the holes could not always locate in the center of holes and thus bolt positions were adjusted. Good agreement of the transition phase of the curves were obtained, e.g. Joint-AC, which means the actual bolt positions were correctly assumed. However, the bolt positions could have a number of combinations and therefore leads to the differences on the moment-rotation curves at around 0.04 rad to 0.06 rad for the rest of connections. But this phenomenon will not affect the subsequent stage of

the moment behaviour of the connections nor the ultimate moment capacities after beam end touching the column sides.

The gap between beam end and column face affected the slope of the curve in the later stage: a smaller gap caused the slope to change at an earlier stage. The gaps used in the concrete-filled FE models are listed as follows: AC, 9.1 mm; BC, 9 mm; CC, 8.5 mm; DC, 7 mm; EC, 12mm, ECR, 11mm.

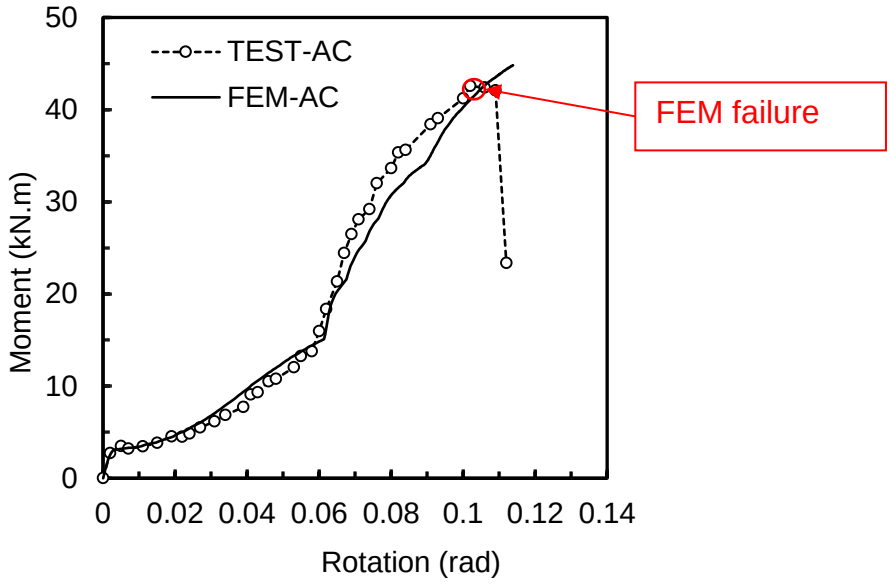

(a) Joint-AC

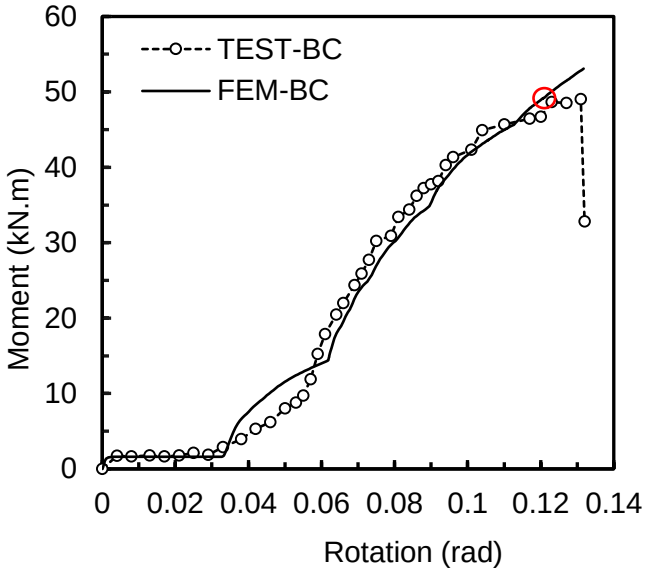

(b) Joint-BC

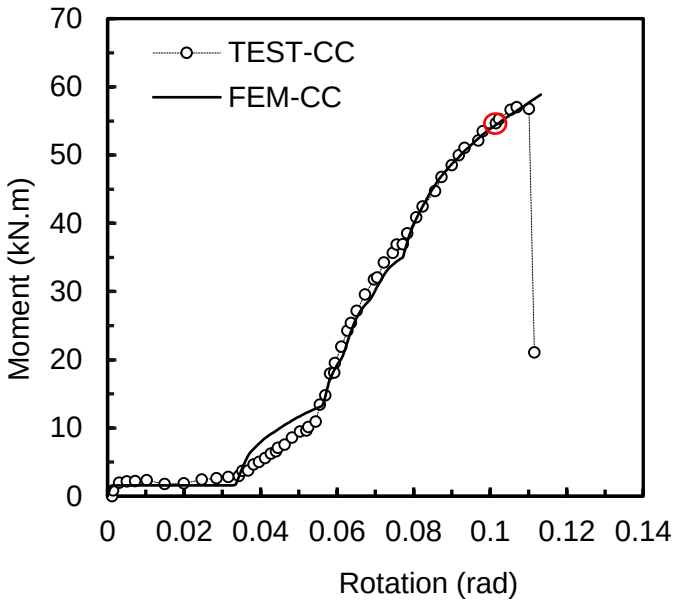

(c) Joint-CC

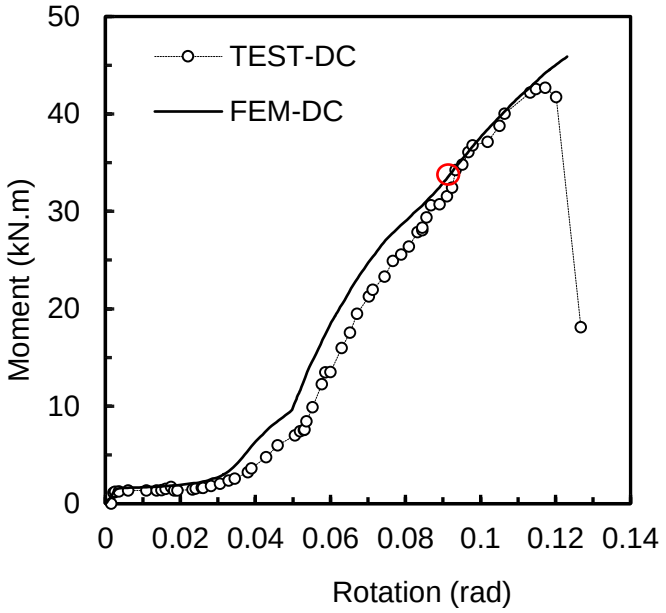

(d) Joint-DC

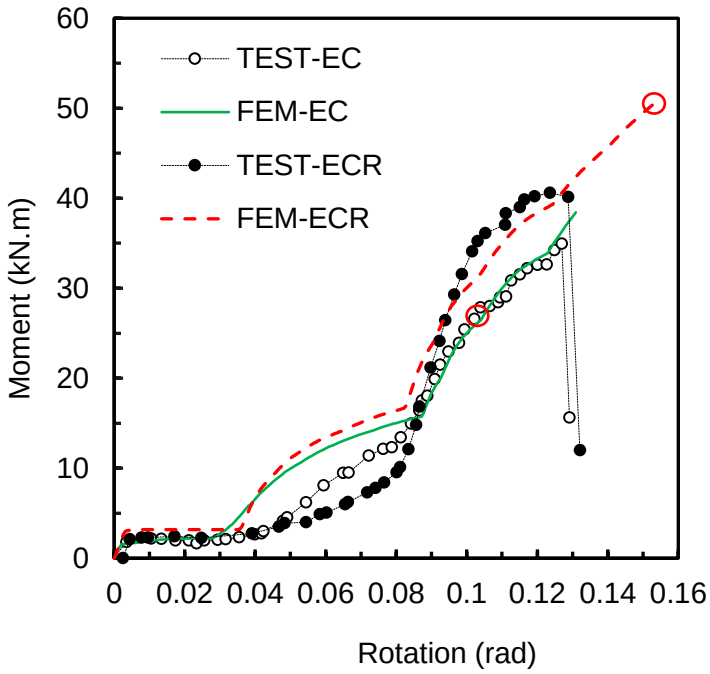

(e) Joint-EC & ECR

Figure 5.6 Comparisons of moment vs rotation relationships (concrete-filled)

In the second stage, the ultimate moment capacities obtained from the numerical simulations using the adopted failure criteria was compared with those extracted from the experimental results. The comparisons illustrated in Table 5.1 shows that the developed FE models could reasonably replicate the failure of the connections which proves the validity of the described FE modeling method. Good agreement within a satisfied accuracy of 7% has been obtained for Joint-AC, BC and CC which utilized the Gr. 10.9 bolts, which means that the developed FE model, adopted material properties and failure criteria could reasonably determine the moment capacities of the concrete-filled connections adopting Gr. 10.9 bolts. For the cases of Joint-DC and EC in which Gr. 8.8 bolts were utilized, the simulation results are in the safe side which means the adopted bolt nominal properties and the equivalent plastic strain limit of 1% underestimated the connection capacities based on the comparison in Table 5.1.

Comparisons of failures between tested specimens and the corresponding FE models is shown in Figure 5.7. It can be concluded that the developed FE models are able to capture the specimens' behavior and therefore can be employed to generate moment-rotation data by means of parametric studies.

Table 5.1 Comparison of ultimate moments from experiments and FE simulations (concrete-filled connections)

Specimen ID	M_{TEST} (kN.m)	M_{FEM} (kN.m)	M_{TEST}/M_{FEM}
Joint-AC	43.8	44.5	0.98
Joint-BC	49.6	48.5	1.02
Joint-CC	57.2	53.3	1.07
Joint-DC	43.6	32.8	1.33
Joint-EC	33.8	27.6	1.23
Joint-ECR	41.4	50.6	0.82
		Average	1.08
		Stand deviation	0.18
		Coefficient of variation	0.1667

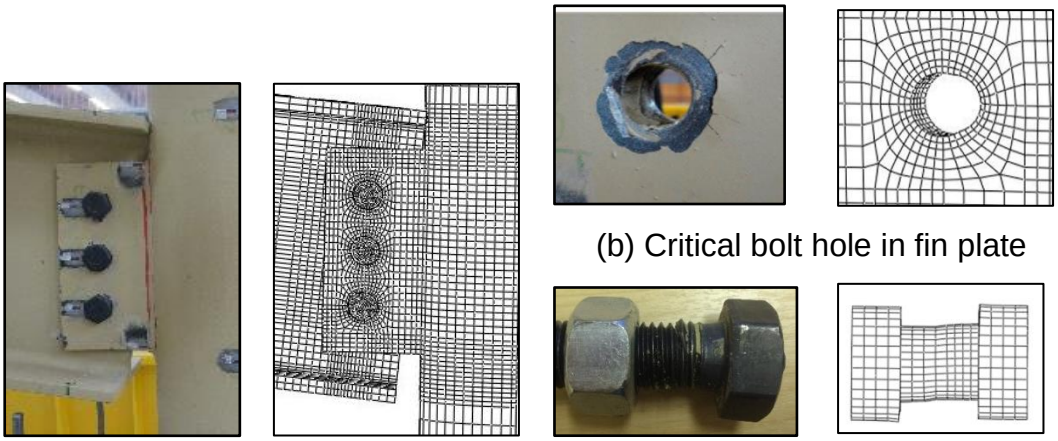

(a) Connection rotation (b) Critical bolt hole in fin plate (c) Bolt (deformation scale: 1.5)

Figure 5.7 Comparison of failures (Joint-BC)

5.7.2 Hollow connections

For hollow connections, the comparisons of the moment vs. rotation relationships obtained from the experimental and numerical results are illustrated in Figure 5.8. In general, the numerical curves are in good agreement with the experimental ones, which demonstrates the ability of the FE models to replicate the moment-rotation behaviour of the hollow connections. Deviations was observed to occur after the slippage stage in some cases. One of the reasons may be measuring error of the EHS tube thickness, as the thin-walled tube is quite sensitive with the

tube thickness when subjected to loading in the transverse direction. Similar with the concrete-filled connections, the gap between beam end and the EHS column face affect the slope changing of the curves. The gaps of the hollow connections in the FE models are adopted as follows: AH, 9.5 mm; BH, 9 mm; CH, 8.5 mm; DH, 7 mm; EH, 11mm. Ultimate moments obtained for each hollow connection from both the experiments and numerical modeling are given in Table 5.2.

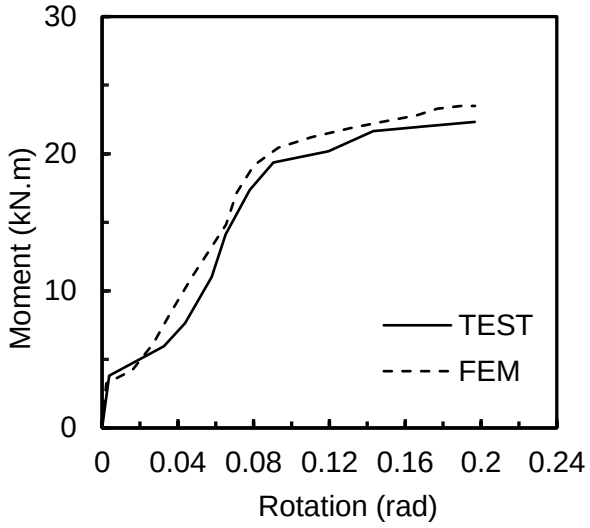

(a) Joint-AH

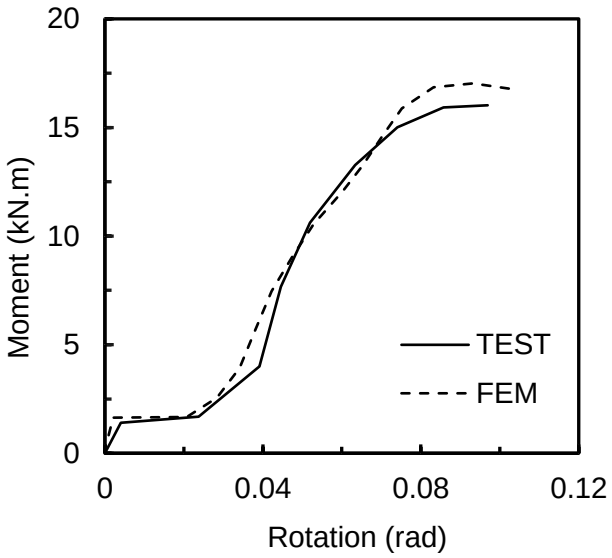

(b) Joint-BH

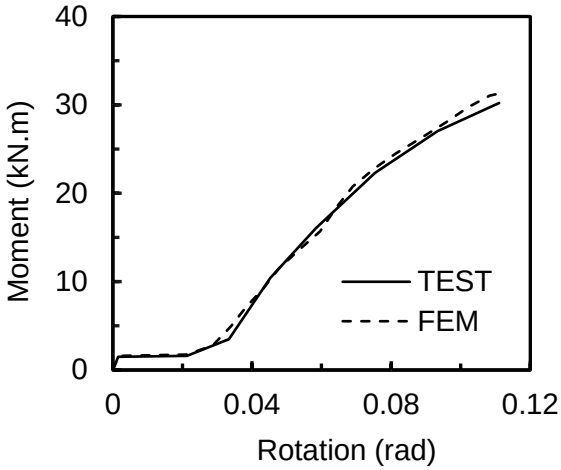

(c) Joint-CH

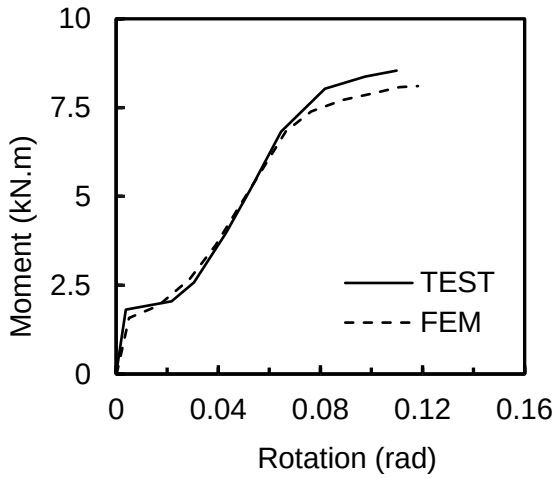

(d) Joint-DH

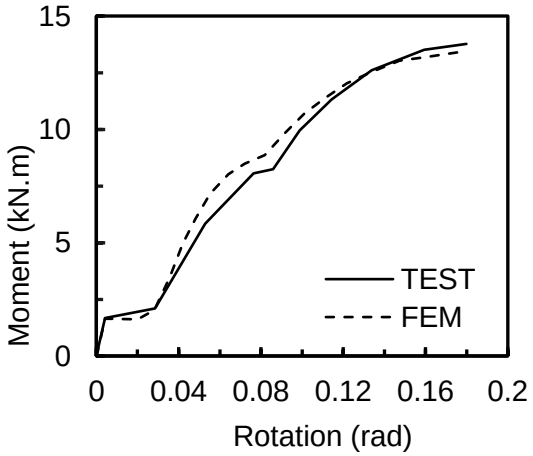

(e) Joint-EH

Figure 5.8 Comparisons of moment vs rotation relationships (hollow)

Moment vs. deformation curves of the tested connections with EHSs are given in Figure 5.9, where the horizontal axis denotes the EHS column's concave deformation at the worst cross-section after the beam end touched the EHS column face, while the vertical axis represents the moment calculated by the concentrated force at beam end multiplied by the level arm. The deformation limit for EHS mentioned in Section 5.5 is used to extract the ultimate moment capacity, which is denoted by $M_{3\%}$. Relevant results are illustrated in Table 5.2 and are compared with the test results which were obtained by shear failure of the bolts for Joint-CH and peak moments for the rest of hollow connections.

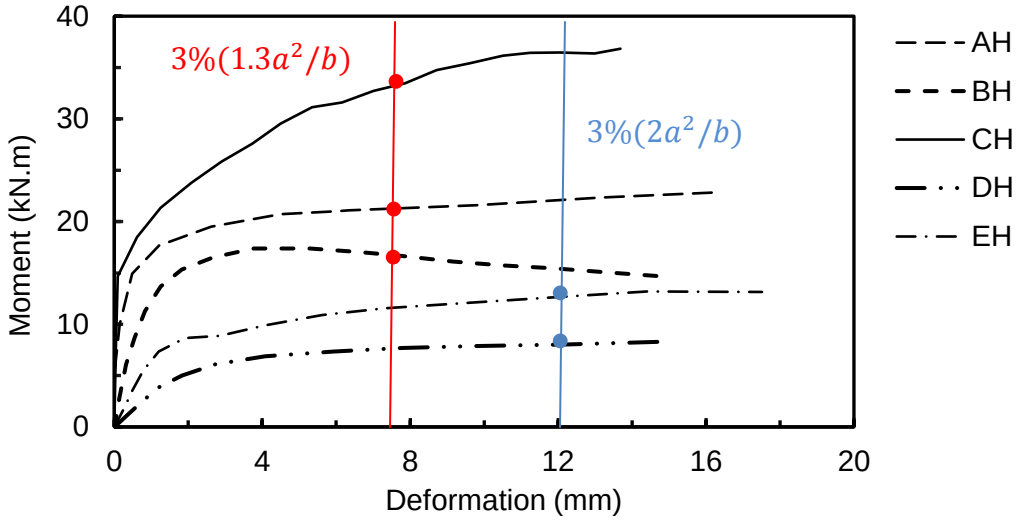

Figure 5.9 Moment vs. deformation curves (hollow connection)

The comparisons of the ultimate moment capacities between experimental and numerical results were illustrated in Table 5.2, where M_{FEM} denotes the numerical results obtained by shear failure of bolts for Joint-CH and peak moments for the rest of the hollow connections. By comparing M_{FEM} and M_{TEST}, it is shown that the developed FE models could reasonably predict moment capacities of the connections within a satisfied accuracy of 6%, which proves the accuracy and validity of the described FE modelling method. Note that there is difficulty of measuring the worst concave deformation of the EHS during the experiments, thus this deformation was extracted from the FE modelling results after the accuracy and validity of the FE models being proved.

Ultimate moments obtained by strength limit criteria (M_{FEM}) and deformation limit criteria ($M_{3\%}$) is compared, which shows that the 3%D_{CHS} deformation limit for circular hollow section is suitable for the investigated fin plate connections with EHS column, where D_{CHS} is replaced by selected equivalent diameter (D_e) of the EHS: 1) $D_e = 2\ a^2\ /\ b$, for minor axis bending [13]; 2) $D_e = 1.3\ a^2\ /\ b$ for major axis bending [15]. Note that, in the case of Joint-CH which is a through plate minor axis connection, the ultimate moments determined from the 3%($2a^2\ /\ b$) deformation limit and from the bolt shear failure criteria are in good agreement.

Table 5.2 Comparison of ultimate moments from experiments and FE simulations (hollow connections)

Specimen ID	M_{TEST} (kN.m)	M_{FEM} (kN.m)	$M_{3\%}$ (kN.m)	M_{TEST}/M_{FEM}	$M_{FEM}/M_{3\%}$
Joint-AH	22.3	21.0	21.1	1.06	1.00
Joint-BH	16.0	17.0	16.8	0.94	1.01
Joint-CH	30.2	31.4	33.2	0.96	0.95
Joint-DH	8.5	8.1	7.9	1.05	1.03
Joint-EH	13.8	13.5	12.6	1.02	1.07
	Average			1.01	1.01
	Stand deviation			0.05	0.04
	Coefficient of variation			0.0495	0.0396

Comparisons of failures between specimens with hollow columns and the corresponding FE models are shown in Figure 5.10. It can be seen that the developed FE models are able to capture the specimens' deformation behavior and therefore can be employed to conduct further parametric studies.

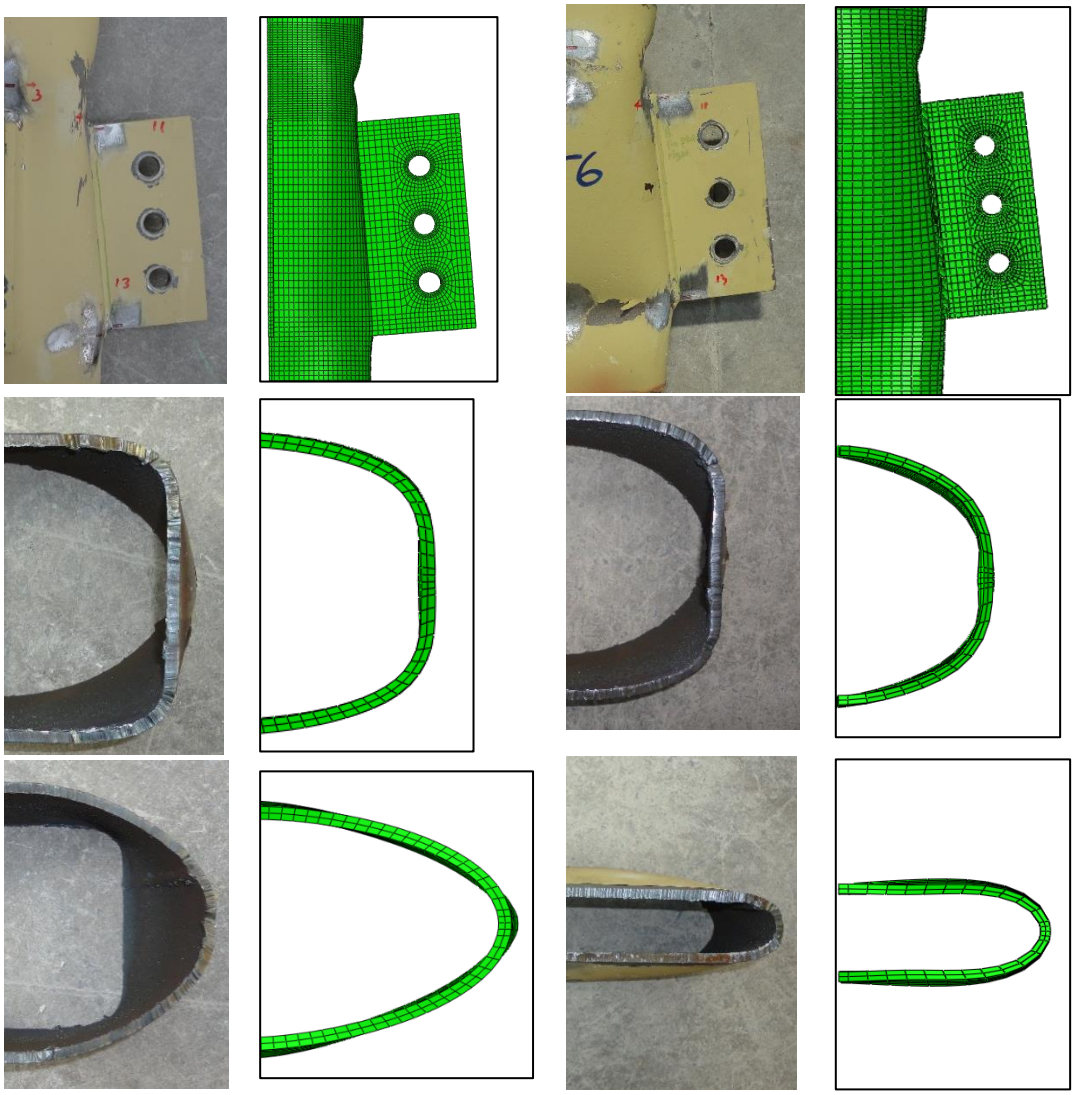

(a) Joint-AH

(b) Joint-BH

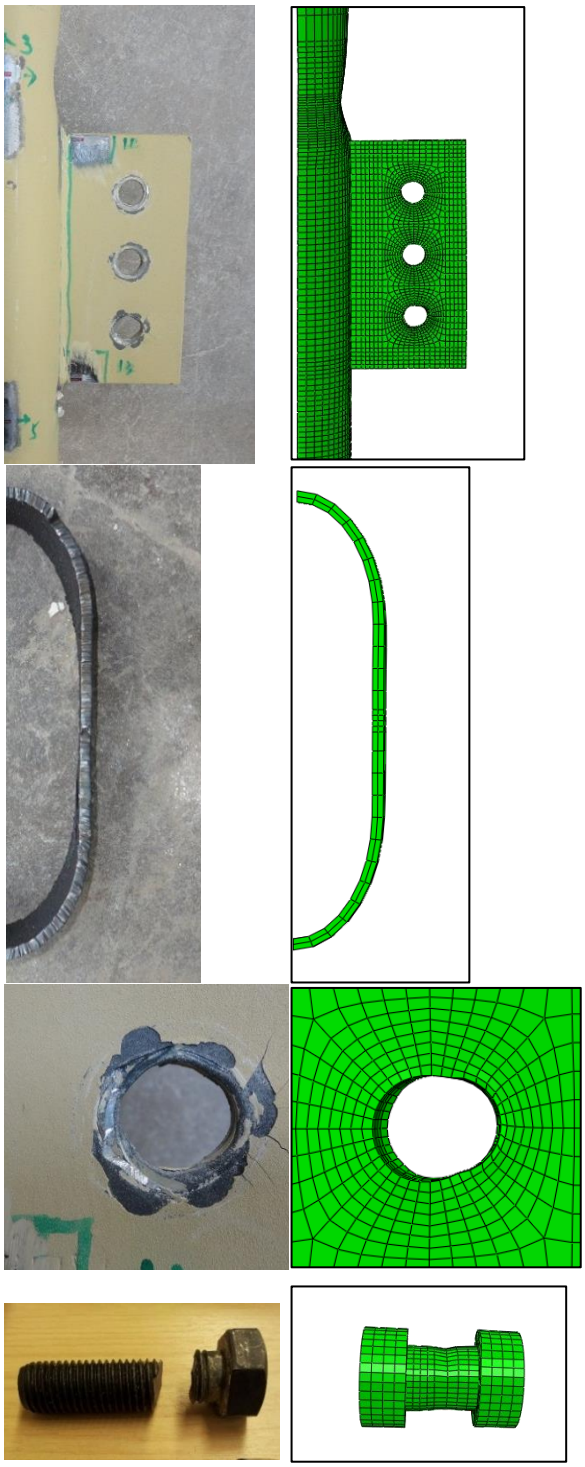

(c) Joint-CH (bolt deformation scale: 1.5)

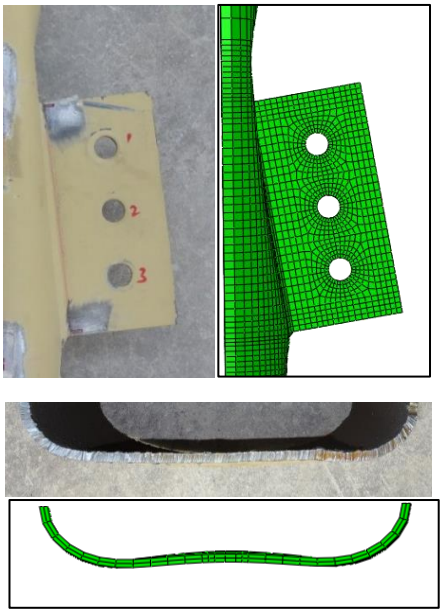

(d) Joint-DH

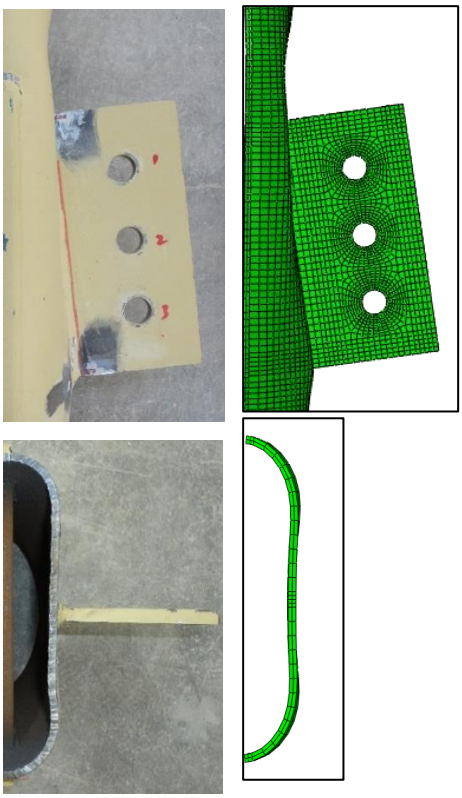

(e) Joint-EH

Figure 5.10 Comparison of failures (hollow connections)

5.8 Conclusions

A three-dimensional finite element model developed by using ABAQUS software is presented in this chapter, along with its validation process against with obtained experimental results, which shows acceptable accuracy and reliability in predicting failures of the connections, moment vs. rotation relationships and the moment capacities. The FE models are therefore can be employed to generate further results in regards to investigating the parameters that may affect the failures and the rotation capacity of the connections. The failure criterion adopted in the verified FE models will be used in the parametric studies covered in Chapter 6.

Chapter 6

Parametric studies and capacity prediction using simple hand calculation methods

In this chapter, parametric studies for both concrete-filled connections and hollow connections are conducted by using the verified FE models described in Chapter 5. Effect of some important parameters on the structural behaviour of the connections is highlighted. Simple calculation methods to predict the moment capacity of beam to elliptical column connections with and without concrete infill is presented as well. Test results and numerical results obtained are utilized to adjust and evaluate the methods.

6.1 Parametric studies

6.1.1 Concrete-filled connections

Parametric studies for the concrete-filled connections in this sub-section were conducted for the joint type-AC (major axis fin plate connection with stiffener in the minor axis direction), type-BC (major axis fin plate connection without stiffener) and type-CC (minor axis through plate connection). Considered geometrical parameters are: end distance e_1 (1.5d, 2.0d, 2.5d, 3.0d, 3.5d), end distance e_2 (1.5d, 2.0d, 2.5d, 3.0d, 3.5d), bolt spacing p_1 (2.0d, 2.5d, 3.0d, 3.5d, 4.0d), fin plate thickness t_p (4mm, 6mm, 8mm), where d is the diameter of the bolt (20mm). Symbols are given in Figure 6.1. Beam sections and EHS column are identical in dimensions with those tested in the experiments. The bottom column end was fixed while only axial shortening was allowed at the top end. Three M20 Gr. 10.9 bolts were used with bolt tightening load of 20 kN. No weld and washers are modeled in the FE analysis. Summary of the parameters and values selected for the parametric studies is listed in Table 6.1.

S355 steel was used for the EHS columns and beams with a nominal yield strength of 355MPa and a nominal minimum ultimate strength of 470MPa [87]. S275 steel was adopted for the plates which has a nominal yield strength of 275MPa and nominal minimum ultimate strength of 410MPa. True stress-strain

relationships in three-part linear line were used, assuming $E_2=\sigma_u$ [81]. C30 concrete was adopted in the EHS columns.

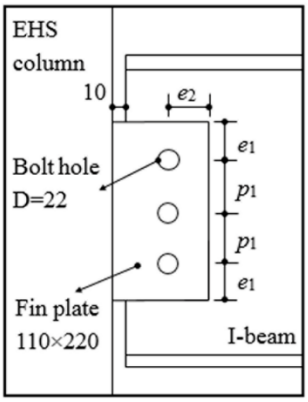

Figure 6.1 Symbols of the connections dimensions

Table 6.1 List of parameters and values selected for the parametric studies in Chapter 6 (mm)

Connection type		Fin plate	Parameters and Values	
Concrete-filled	AC, BC, CC	220×110×t_p	t_p:	4.0, 6.0, 8.0
	BC, CC	220×110×6	e_1 & p_1	1.5d & 4.0d; 2.0d & 3.5d; 2.5d & 3.0d; 3.0d & 2.5d; 3.5d & 2.0d
	BC, CC	220×(60+ e_2)×6	e_2	1.5d, 2.0d, 2.5d, 3.0d, 3.5d
Hollow	AH, BH,CH, DH,EH	220×110×10	t	5.0, 6.3, 8.0, 10.0, 12.5

Note: External dimensions of EHS adopted are 200mm×100mm×5mm; t_p, e_1, p_1,e_2, d and t denote the fin plate thickness, end distance parallel to column, bolt spacing, edge distance perpendicular to column, diameter of the bolt and EHS tube wall thickness, respectively.

6.1.1.1 Effect of fin plate thickness

A set of thickness values of 4mm, 6mm and 8mm was selected for Joint types-AC, BC and CC to address the effect on failures of the connections, since the tested connections with a 10 mm fin plate failed in bolts. Bolts arrangement and fin plate dimensions can be found in Figure 6.1.

Failures of fin plate are determined by using the equivalent plastic strain obtained from the FE model. Distribution of the equivalent plastic strain along the critical bolt hole in both fin plate and beam web is illustrated in Figure 6.2. The horizontal axis denotes an angle initiating from 0° to 360°. This figure demonstrates that the critical position along bolt hole in the beam web and fin plate is approximately locates at around 120°-135°. It can be seen that the connections with fin plate thickness of 4mm and 6mm failed in fin plate, since the equivalent plastic strain at the critical position reached the limit of 100%. The bolts did not fail in this cases since the shear resistance of the bolts is less critical than the fin plate bearing resistance. In contrast, bolt shear failure occurred prior to the fin plate failure in the connection with an 8mm fin plate. Evidence was shown in Figure 6.3 which indicates that the critical equivalent plastic strain of the fin plate is lower than the limit of 100%.

Since fin plate failure occurred in the connection, the stiffener plate inserted into the concrete-filled column of type-AC connection could not provide obvious enhancement to the resistance on the connection level. Thus there would be no significant difference in the moment response between the stiffened type-AC connections and type-BC connections.

The moment vs. rotation curves of the connections analyzed are illustrated in Figure 6.4, where the curves were cut at the failure points to clarify the comparisons within the graph. Obviously, the fin plate thickness has great influence on the structural performance of these types of connections. The higher the fin plate thickness, the higher the ultimate moment of the connections, even through failure mode might change.

The numerical results of the connections analyzed in this sub-section were summarized in Table 6.2 in terms of the failure moment, corresponding rotation and failure mode.

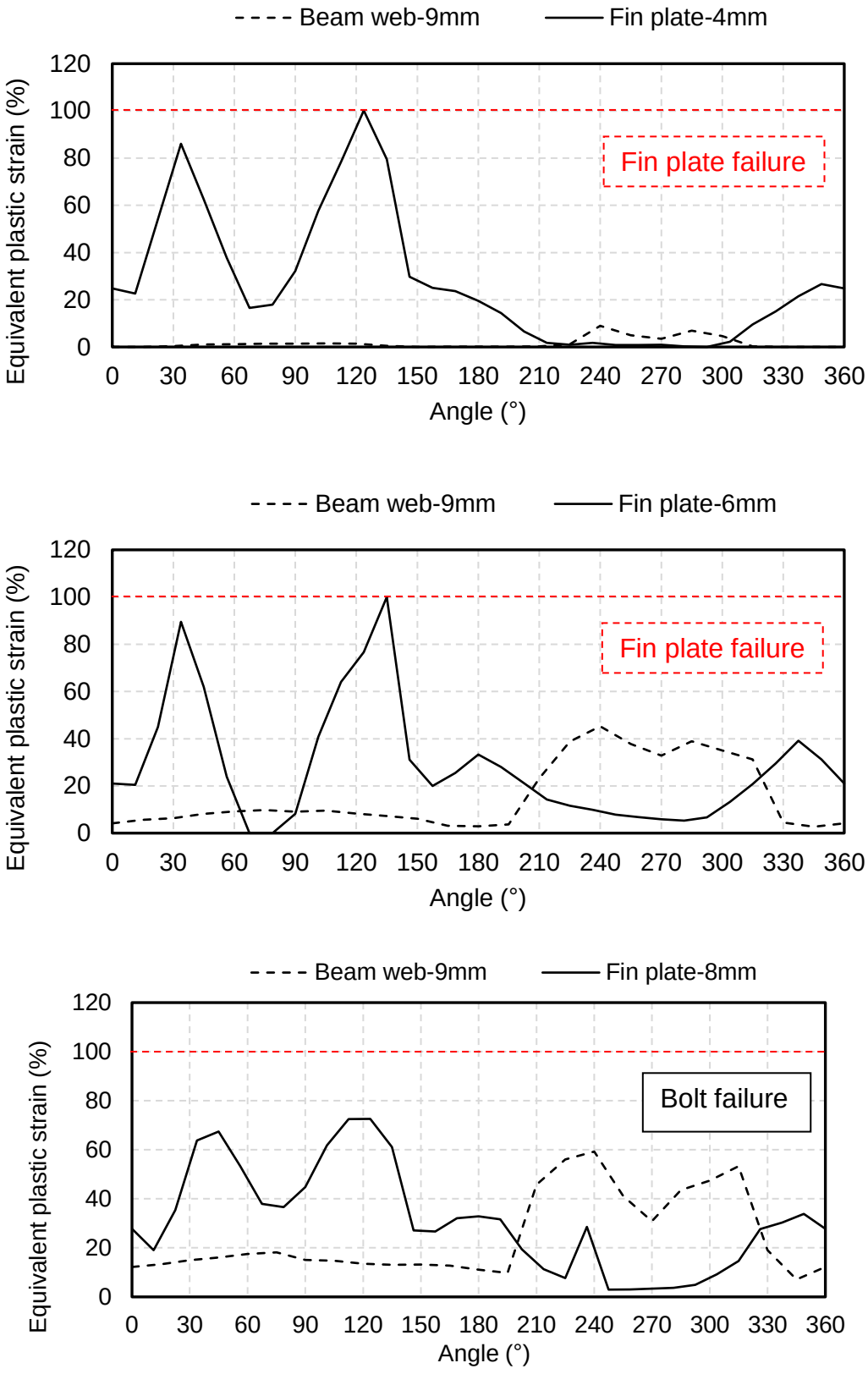

Figure 6.2 Equivalent plastic strain distribution along the side bolt hole at failure (AC)

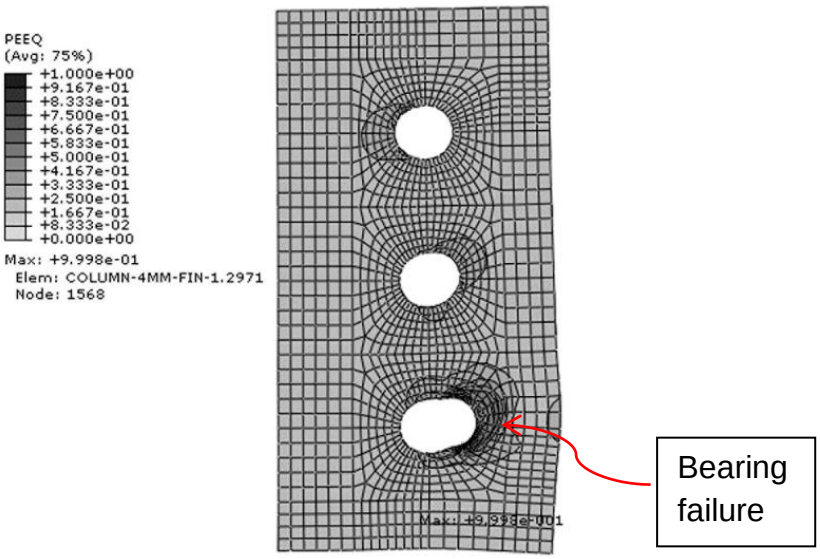

Figure 6.3 Equivalent plastic strain contour in fin plate (AC-4mm-Fin)

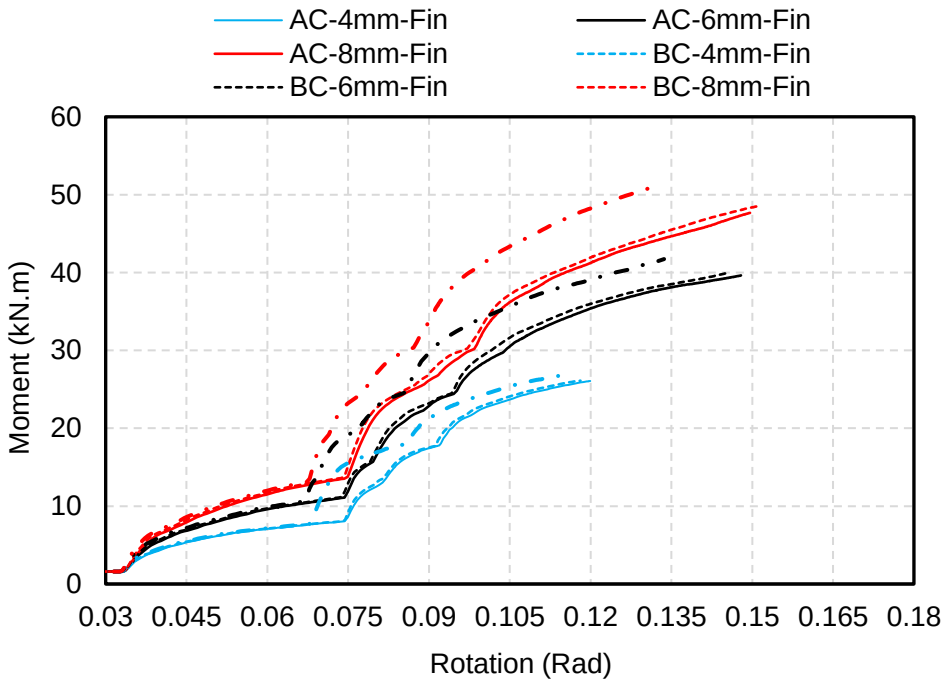

Figure 6.4 Moment vs. rotation relationships

Table 6.2. List of beam to elliptical connections analysed in section 6.1.1

Connection ID	t_p (mm)	Failure moment (kN.m)	Rotation at failure (Rad)	Failure mode
AC-4mm-Fin	4	26.08	0.120	PF
AC-6mm-Fin	6	39.63	0.148	PF
AC-8mm-Fin	8	47.66	0.150	BF
BC-4mm-Fin	4	26.11	0.118	PF
BC-6mm-Fin	6	39.95	0.146	PF
BC-8mm-Fin	8	48.58	0.151	BF
CC-4mm-Fin	4	26.72	0.114	PF
CC-6mm-Fin	6	41.70	0.134	PF
CC-8mm-Fin	8	50.78	0.131	BF

Note: Connection ID, e.g. AC-4mm-Fin denotes type-AC connection with a 4mm fin plate; BF - bolt failure and PF - fin/through plate failure.

6.1.1.2 Effect of end distance-e_1 and bolt spacing-p_1

In this sub-section, the optimum arrangement of the bolts in the fin plate (the fin plate outer dimensions is set to be constant - 110mm in width and 220 mm in length) was investigated by changing the end distance e1 and vertical bolt spacing p1. Considered combinations of e1 and p1 are given as follows: 1.5d & 4.0d; 2.0d & 3.5d; 2.5d & 3.0d; 3.0d & 2.5d; 3.5d & 2.0d.

Ultimate moment capacities obtained from type-BC and CC FE models are presented in Figure 6.5 and are also summarized in Table 6.3. It can be seen that bolt spacing p1 is more influential than the end distance e1 on the moment capacities of the connections. Based on the comparison within and between graphs, vertical bolt spacing is suggested to be at least 2.5d; the minimum e1 could be 1.5d in type-BC connection but this value should be increased to 2.0d in type-CC connection; and the combination of e1=2.0d and p1=3.5d may be the optimum option for the bolts arrangement in the cases studied.

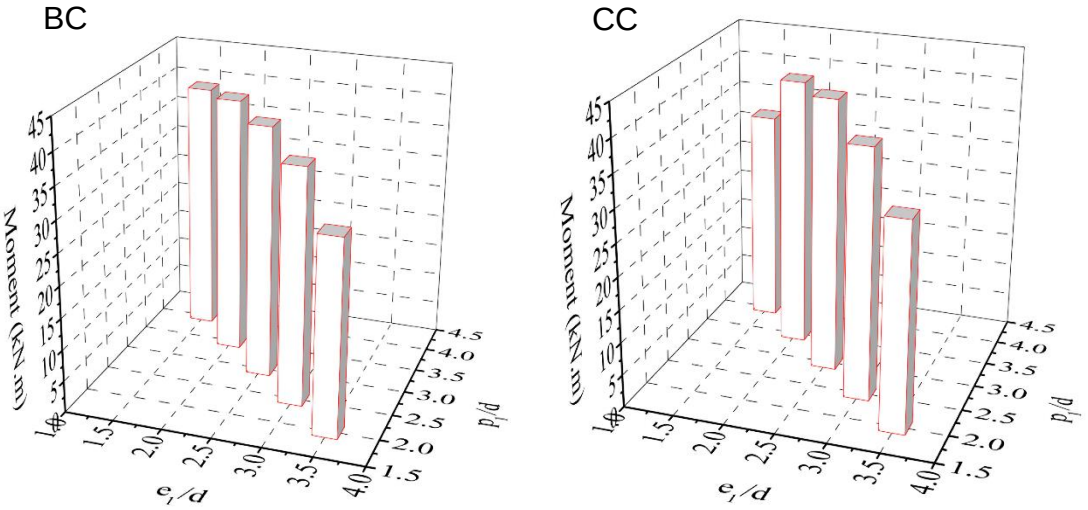

Figure 6.5 Effect of end distance e_1 and bolt spacing p_1 (type-BC and CC)

Table 6.3. List of beam to elliptical connections analysed in section 5.3 (e_2=2.5d)

Connection ID	t_p (mm)	Failure moment (kN.m)	Rotation at failure (Rad)	Failure mode
BC-6-E1-15-P1-40	6	39.63	0.125	PF
BC-6-E1-20-P1-35	6	40.81	0.135	PF
BC-6-E1-25-P1-30	6	39.95	0.146	PF
BC-6-E1-30-P1-25	6	37.36	0.146	PF
BC-6-E1-35-P1-20	6	30.85	0.130	PF
CC-6-E1-15-P1-40	6	32.67	0.111	PF
CC-6-E1-20-P1-35	6	41.32	0.116	PF
CC-6-E1-25-P1-30	6	41.84	0.134	PF
CC-6-E1-30-P1-25	6	38.31	0.134	PF
CC-6-E1-35-P1-20	6	31.79	0.124	PF

Note: Connection ID, e.g. BC-6-e1-15-p1-40 denotes type-BC connection with a 6mm fin plate; end distance e1 equals to 1.5d while vertical bolt spacing p1 equals to 4.0d; PF - fin/through plate failure.

6.1.1.3 Effect of edge distance-e_2

Selected e2 equals to 1.5d, 2.0d, 2.5d, 3.0d and 3.5d, respectively, and the corresponding fin plate width was (60 + e2) mm while the length is kept constant as 220 mm. Table 6.4 lists the corresponding FE results of the connections. Figure 6.6 illustrates the moment capacities of analyzed BC and CC connections

in terms of edge distance e2. It was found that, the moment capacities increased with the increasing of the edge distance e2 while the increment was not obvious after e2 reaching 3d; the difference between the ultimate moments between connection types BC and CC is not significant but the capacity of the CC connection is always slightly bigger than that of the BC connection. The minimum value of e2 is suggested to be at least 2.5d in both cases.

Table 6.4. List of beam to elliptical connections analysed in section 5.4 (e_1=2.5d; p_1=3d)

Connection ID	t_p (mm)	Failure moment (kN.m)	Rotation at failure (Rad)	Failure mode
BC-6-E2-15	6	30.30	0.119	PF
BC-6-E2-20	6	36.75	0.135	PF
BC-6-E2-25	6	39.95	0.146	PF
BC-6-E2-30	6	41.33	0.148	PF
BC-6-E2-35	6	42.03	0.147	PF
CC-6-E2-15	6	31.13	0.111	PF
CC-6-E2-20	6	37.6	0.122	PF
CC-6-E2-25	6	41.84	0.134	PF
CC-6-E2-30	6	42.96	0.134	PF
CC-6-E2-35	6	43.55	0.132	PF

Note: Connection ID, e.g. CC-6-E2-15 denotes type-CC connection with a 6mm fin plate,edge distance e2 equals to 1.5d ; PF - fin/through plate failure.

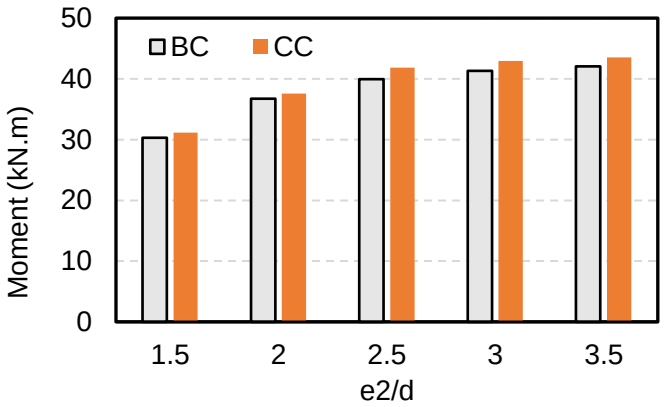

Figure 6.6 Effect of end distance e_2

6.1.2 Hollow connections

Parametric studies conducted in this section explores the effect of EHS tube thickness and joint type on the moment behaviour of the hollow connections.

Dimensions of the beams are identical with those adopted in the experiments. EHS outer dimension is constant as 200mm×100mm. The column end was fixed on the bottom while only axial shortening was allowed at the top end. Three Gr. 10.9 bolts were adopted with a constant diameter of 20mm. The beam flange and fin plate/through plate was tightened with bolt load of 20 kN. No weld and washers are included in the FE models. S355 steel was adopted for the EHS columns and beams while S275 steel was selected for the fin plates, which is the same with the concrete-filled connections. The load level at column end is selected as 40% of the axial compression resistance of the EHS.

The ultimate moment with corresponding joint rotation at failure and failure mode of the connections analyzed in this section are illustrated for each joint type in Tables 6.5 - 6.9, where *t* is the thickness of the EHS tube.

Table 6.5 List of beam to elliptical connections analysed in section 6.2 for Type A connection

Connection ID	*t* (mm)	Failure moment (kN.m)	Rotation at failure (Rad)	Failure mode
A-EHS5	5.0	23.4	0.113	SCF
A-EHS63	6.3	31.5	0.124	SCF
A-EHS8	8.0	42.6	0.138	SCF
A-EHS10	10.0	53.2	0.154	BF
A-EHS125	12.5	54.3	0.142	BF

Note: Connection ID, e.g. A-EHS5 denotes type-A connection with an EHS tube of 5mm in thickness; SCF - steel column failure; BF - bolt failure.

Table 6.6 List of beam to elliptical connections analysed in section 6.2 for Type B connection

Connection ID	*t* (mm)	Failure moment (kN.m)	Rotation at failure (Rad)	Failure mode
B-EHS5	5.0	21.1	0.109	SCF
B-EHS63	6.3	28.2	0.122	SCF
B-EHS8	8.0	38.4	0.134	SCF
B-EHS10	10.0	54.9	0.163	BF
B-EHS125	12.5	54.0	0.144	BF

Note: Connection ID, e.g. B-EHS5 denotes type-B connection with an EHS tube of 5mm in thickness; SCF - steel column failure; BF - Bolt failure.

Table 6.7 List of beam to elliptical connections analysed in section 6.2 for Type C connection

Connection ID	*t* (mm)	Failure moment (kN.m)	Rotation at failure (Rad)	Failure mode
C-EHS5	5.0	35.2	0.147	BF
C-EHS63	6.3	38.8	0.171	BF
C-EHS8	8.0	44.9	0.168	BF
C-EHS10	10.0	46.3	0.163	BF
C-EHS125	12.5	51.1	0.154	BF

Note: Connection ID, e.g. C-EHS5 denotes type-C connection with an EHS tube of 5mm in thickness; BF - bolt failure.

Table 6.8 List of beam to elliptical connections analysed in section 6.2 for Type D connection

Connection ID	*t* (mm)	Failure moment (kN.m)	Rotation at failure (Rad)	Failure mode
D-EHS5	5.0	9.5	0.106	SCF
D-EHS63	6.3	13.8	0.109	SCF
D-EHS8	8.0	21.4	0.108	SCF
D-EHS10	10.0	29.7	0.133	SCF
D-EHS125	12.5	42.1	0.147	SCF

Note: Connection ID, e.g. D-EHS5 denotes type-D connection with an EHS tube of 5mm in thickness; SCF - steel column failure.

Table 6.9 List of beam to elliptical connections analysed in section 6.2 for Type E connection

Connection ID	*t* (mm)	Failure moment (kN.m)	Rotation at failure (Rad)	Failure mode
E-EHS5	5.0	12.9	0.118	SCF
E-EHS63	6.3	15.8	0.087	SCF
E-EHS	8.0	26.5	0.119	SCF
E-EHS10	10.0	40.3	0.156	SCF
E-EHS125	12.5	44.5	0.121	SCF

Note: Connection ID, e.g. E-EHS5 denotes type-E connection with an EHS tube of 5mm in thickness; SCF - steel column failure.

6.1.2.1 Effect of EHS tube thickness

The influence of EHS tube thickness on the moment-rotation behaviour of the beam to elliptical hollow column connections is investigated in this section, by fixing the outer dimension of the EHS to 200×100mm. The analyzed thickness range covers all the available values of the selected EHS in the current manufacturing market, which are 5.0mm, 6.3mm, 8.0mm, 10.0mm and 12.5mm.

The effect of tube thickness on the moment capacity of the connections is illustrated in Figure 6.7(a)-(e). It is found from the graphs that the thickness of the EHS tube wall has significant effect on the ultimate capacity of the hollow connection of all the joint assemblies considered - the higher the thickness of the EHS tube wall, the higher the ultimate moment capacity of the connection. Note that the curves are nearly linear before the failure mode changed from steel column failure to bolt failure, e.g. type-A and B connections. For this two joint assemblies, the limit tube wall thickness of failure mode changing is found as 10mm which means the transverse stiffness of the EHS tube is large enough at this stage. In other words, the yield strength of the EHS cross-section is bigger than the shear capacity of the bolt group.

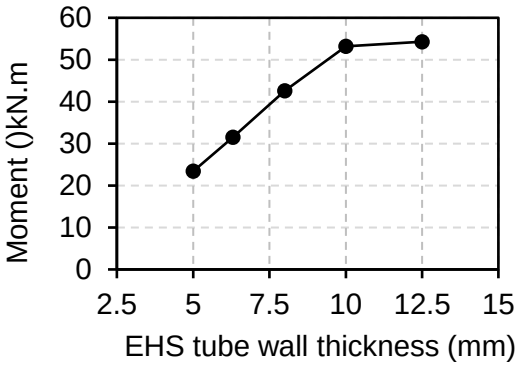

(a) A-major axis connection with stiffener in the minor axis direction

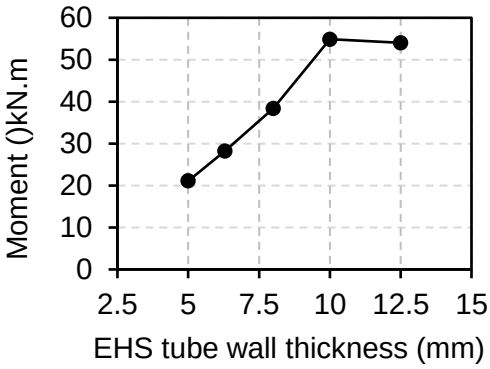

(b) B-major axis connection without stiffener

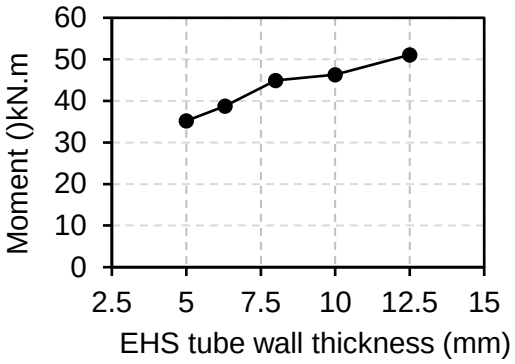

(c) C-minor axis connection with through plate

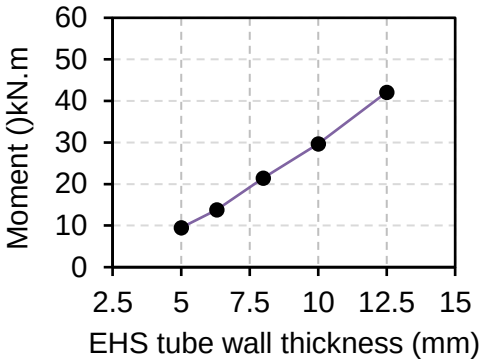

(d) D-minor axis connection without stiffener

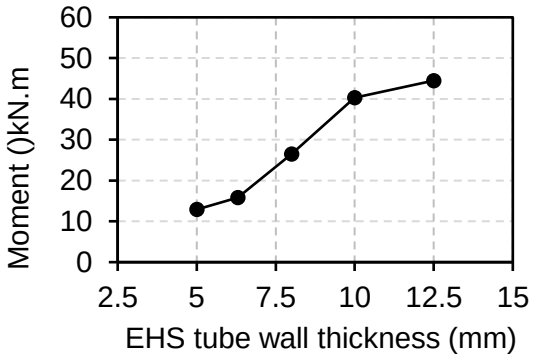

(e) E-minor axis connection with stiffener in the major axis direction

Figure 6.7. Effect of the tube wall thickness on the moment capacity of the connections.

For type-C connection which is a through plate connection, although shear failure of the bolts is predominant in all the cases analyzed, the moment capacity of the connections get higher with the increasing of the tube wall thickness. This is because that the bigger the tube wall thickness (the higher the transverse stiffness of the EHS tube), the more contribution of each bolt, after beam end touched the column face. Recall from the experimental result presented in sub-section 4.2.3.2 that not only the end bolt of the connection fractured but the middle bolt failed as well after continuous loading in the final stage of the test. This means the end bolt is fully engaged in regards to the moment capacity while the middle bolt contributed a large portion.

For type-D and E connections, steel column failure is predominant throughout the thickness range. The linear phenomenon of the moment-wall thickness curve is more notable for type-D connection. In addition, the tube wall thickness has more significant effect on the moment capacity of the connections, revealed by the enhancement degree of the capacity when comparing the results at 5mm and 12.5mm. The enhancement ratios are 1.32, 1.56, 0.45, 3.43, 2.45 for the connections from type-A to E, respectively. It turns out that the lower the stiffness of the connection in the transverse direction, the higher the enhancement degree on the moment capacity.

6.1.2.2 Effect of Joint type

The above sub-section has given part of the difference among different joint types. This sub-section will address the influence of stiffener plate and EHS orientation on the moment capacity of the connections. Figure 6.8 illustrates the comparisons of moment capacities among difference joint types for each tube wall thickness analysed.

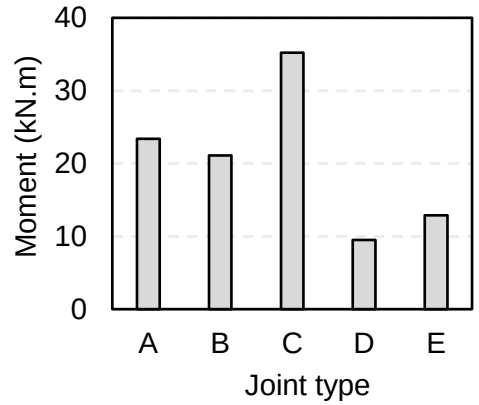

(a) t = 5mm

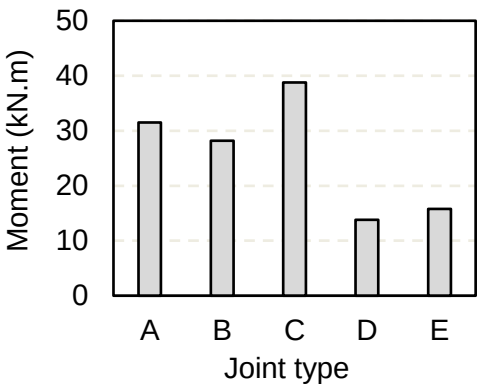

(b) t = 6.3mm

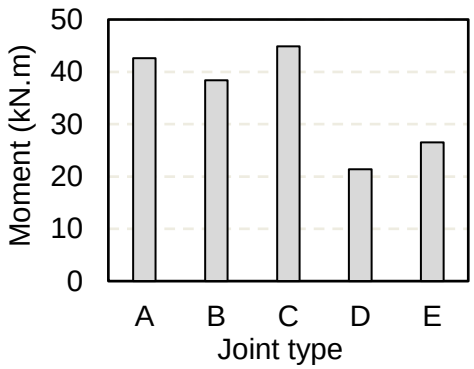

(c) t = 8mm

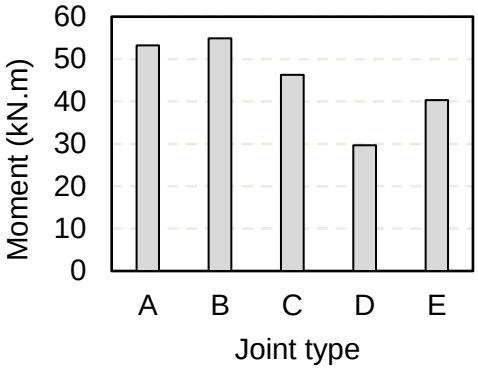

(d) t = 10mm

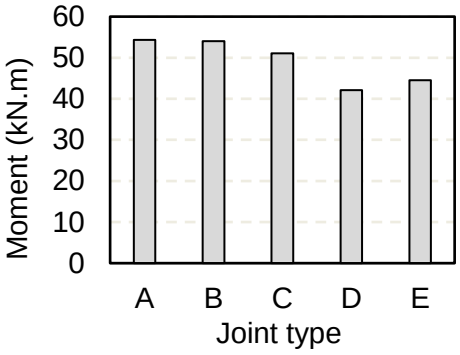

(e) t = 12.5mm

Figure 6.8 Effect of joint type

It was found from the above graphs that the higher the tube wall thickness, the less notable difference among the joint types on the moment capacity of the connections. This arises from the fact that the column will have higher transverse stiffness with higher thickness which will reduce the benefit of using stiffener plate.

For type-A and B connections, the stiffener plate placed in the minor axis direction of the EHS tube increased the moment capacity of the connection. However, this increase disappears when the tube wall thickness is bigger than 10mm. Explanation to this may be that it is less easy to deform in the minor axis direction when the thickness is big enough, thus let the stiffener has minor contribution. When comparing the type-D and E connections, it was found that the moment capacity of minor axis connection can be enhanced by inserting a stiffener plate in the major axis direction, which is in agreement with the observation from the experimental result given in section 4.3.

Normally, the through plate connection (type-C) has the highest moment capacity as the through plate endure much of the load transferred from the fin plate rather than the column wall. However, for connections with a column tube wall thickness bigger than 10mm, there seems no benefit of adopting through plate connection (type-C) in regards to the moment capacity within the scope of this research. So it is thus not recommended to use through plate connection in this situation since this kind of connection is much more expensive than the normal fin plate connection.

6.2 Capacity prediction using simple hand calculation methods

6.2.1 Limit states for fin plate connections with concrete-filled columns

A number of limit states are applicable to fin plate connections with concrete-filled columns covered in this thesis, associated with the bolts, beam webs and fin plates. Adopted beams in this thesis are designed sufficient in resisting load compared to fin plates. Therefore, the fin plates will be more critical in failures. Concrete crushing failure and weld failure are assumed to occur after the failures in bolts, fin plates to simplify the calculations. Therefore, potential failure modes will be shear failure of the bolts and bearing failure of the fin plates based on the observations from the experiments.

Table 6.10 illustrates the design shear and bearing resistance for bolts subjected to shear force provided in Eurocode 3 (EN1993-1-8).

Table 6.10 Design shear resistance for individual bolts subjected to shear in Eurocode 3

Failure mode	Design equations
Shear resistance per shear plane (bolts)	$F_{v,Rd} = \frac{\alpha_v f_{ub} A}{\gamma_{M2}}$ - where the shear plane passes through the threaded portion of the bolt (A is the tensile stress area of the bolt): - for classes 4.6, 5.6 and 8.8: $\alpha_v = 0.6$ - for classes 4.8, 5.8, 6.8 and 10.9: $\alpha_v = 0.5$ - where the shear plane passes through the unthreaded portion of the bolt (A is the gross cross section of the bolt): $\alpha_v = 0.6$ - where $f_{ub}$is the ultimate tensile strength of bolts; γ_{M2} is a safety factor and deemed as 1.0 when predicting moment capacities of the connections in this thesis
Bearing resistance (fin plates and beam webs)	$F_{b,Rd} = \frac{k_1 \alpha_b f_b d t}{\gamma_{M2}}$ - where $\alpha_b$is the smallest of α_d; $\frac{f_{ub}}{f_b}$or 1.0; in the direction of load transfer: - for end bolts: $\alpha_d = \frac{e_1}{3d_0}$; for inner bolts: $\alpha_d = \frac{p_1}{3d_0} - \frac{1}{4}$ perpendicular to the direction of load transfer: - for edge bolts: $k_1$is the smallest of $2.8\frac{e_2}{d_0} - 1.7$, $1.4\frac{p_2}{d_0} - 1.7$and 2.5 - for inner bolts: $k_1$is the smallest of $1.4\frac{p_2}{d_0} - 1.7$ or 2.5 - where $f_b$is the ultimate strength of fin plate; d is the nominal bolt diameter; d_0 is the bolt hole diameter; t is the thickness of the fin plate; e_1 and e_2 are the bolt hole edge distance; p_1 and p_2 are bolt spacing

6.2.2 Moment capacity calculation and comparisons against test results

The moment capacity calculation mechanism is illustrated in Figure 6.9, where the connection is assumed pivot at the edge of the bottom beam flange. This calculation method is proposed for through plate connection (Joint-CC). The column is redeemed rigid enough in this case since the load transferred from beam end is endured mainly by the through plate. Moment of the connection can then be obtained by using the following equation 6.1,

$$M = FD + F'D' + F''D'' \quad (6.1)$$

where *F* denote the shear resistance of the top bolt or bearing resistance of the fin plate depends on the critical failure mode; *D* is the corresponding lever arm; F' and F'' are the assumed forces existing in the middle and the bottom bolt, respectively, when the top end bolt or the bolt hole in fin plate reach to the limit state; D' and D'' are the corresponding lever arms, which can be obtained by linear interpolation.

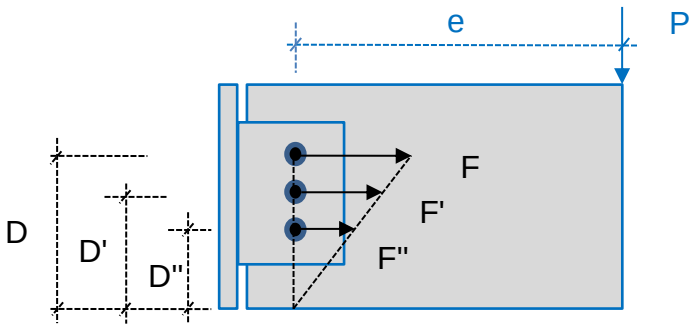

Figure 6.9 Moment capacity calculation mechanism (for through plate connection – Joint-CC)

For fin plate connections – Joint-BC and DC which bending in the major and minor axes direction of the EHS column, respectively, pivot center is assumed to be locating at the fin plate bottom edge. Then the moment calculation mechanism will be the one shown in Figure 6.10. Moment of the connection can then be calculated using the following equation 6.2,

$$M = FD + F'D' + F''D'' + F'''D''' \quad (6.2)$$

where F''' denote the reaction force at the beam bottom flange and equals to the sum of the reversed forces F', F'', and F'''.

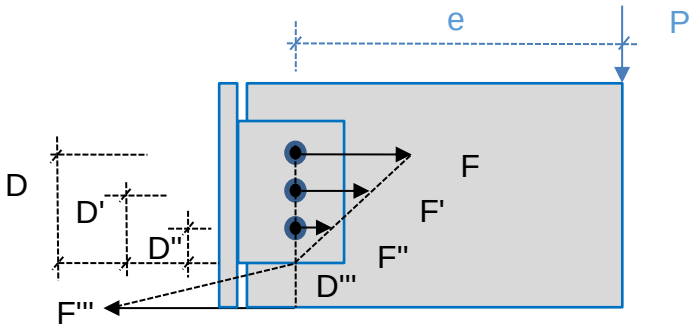

Figure 6.10 Moment capacity calculation mechanism (for fin plate connections – Joint-BC and Joint-DC)

For fin plate connections with stiffener plate in the minor axis direction of the EHS – Joint-AC which bending in the major axis direction, pivot center is assumed at the bottom bolt. The moment calculation mechanism is shown in Figure 6.11. Moment of the connection will be calculated using equation 6.3,

$$M = FD + F'D' + F''D'' \tag{6.3}$$

where F'' is assumed as the sum of the forces F' and F''.

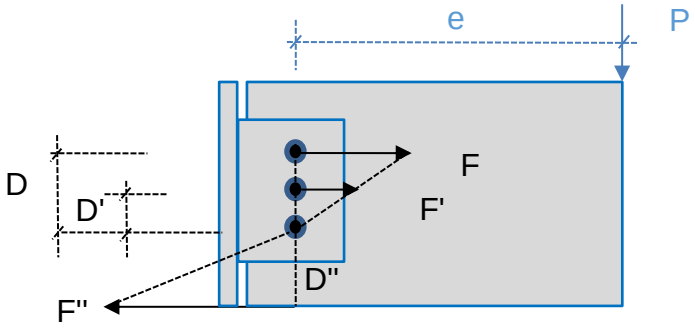

Figure 6.11 Moment capacity calculation mechanism (for fin plate connections with stiffener – Joint-AC)

For fin plate connections with stiffener plate in the minor axis direction of the EHS – Joint-EC and it's repeat test which bending in the minor axis direction, pivot center is assumed at a point between the middle and the bottom bolt. The moment calculation mechanism is illustrated in Figure 6.12. Calculation of the moment capacity are based on the following equations 6.4-6.7.

$$M = FD + F'D' + F''D'' + F'''D''' \tag{6.4}$$

where the lever arms are calculated as follows,

$$\Sigma F = 0,\ F + F' = F'' + F''' \tag{6.5}$$

Using linear interpolation to obtain F', F' and F' in terms of F, then equation 6.5 will be,

$$F + FD'/D = FD''/D + FD'''/D \tag{6.6}$$

Then an equation of the lever arms will be,

$$D + D' = D'' + D''' \tag{6.7}$$

where $D = D' + 60$, $D' + D'' = 60$, $D + D''' = 215.5$, then the solution is $D = 98.875$; $D' = 38.875, D'' = 21.125, D''' = 116.625$. The unit of lever arms is millimetre.

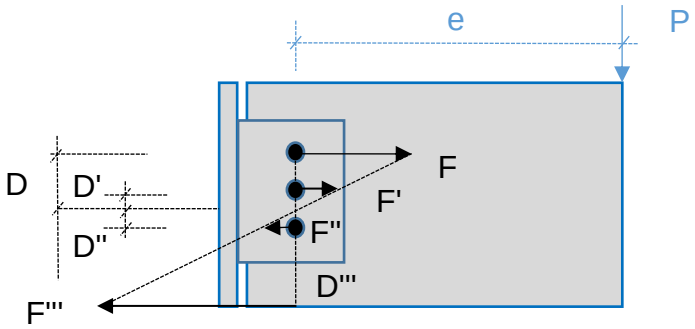

Figure 6.12 Moment capacity calculation mechanism (for fin plate connections with stiffener – Joint-EC and repeat Joint-EC)

For the connection specimens being tested in Chapter 4, the bolt shear resistance F_v and plate bearing resistance F_b are calculated shown as follows based on the principles given in Table 6.11, regardless of the safety factor γ_{M2},

M20 Gr. 8.8 bolts:

Shear resistance, $F_{v,1} = \alpha_v f_{ub1} A_s$=0.6×856×245=125.83 kN

Bearing resistance, $F_{b,1} = k_1 \alpha_b f_b dt$=2.5×0.659×444.5×20×10=146.46 kN

M20 Gr. 10.9 bolts:

Shear resistance, $F_{v,2} = \alpha_v f_{ub2} A_s$=0.5×1207×245=147.86 kN

Bearing resistance, $F_{b,2} = k_1 \alpha_b f_b dt$ =2.5×0.659×444.5×20×10=146.46 kN.

As a result, bolt shear failure is predominant for the tested concrete-filled connections adopting M20 Gr. 8.8 bolts according to the calculated results. In contrast, shear failure of bolts and bearing failure of plates are both critical as the difference between shear and bearing resistance is within 1%. Therefore, in the cases with M20 Gr. 10.9 bolts, shear failure of bolts is deemed as dominant failure of the connections as observed from the experimental results. Then the force F in equation 6.1 can be replaced by the shear resistance of individual bolt. Comparisons of test results and corresponding calculated results are illustrated in Table 6.10. It was found that the moment capacities can be well predicted by using the proposed calculation methods within a satisfactory error of 10%.

Table 6.11 Comparisons of moment capacities between test results and hand calculation results

Connection ID	M_{TEST} (kN.m)	M_{EURO} (kN.m)	M_{TEST}/M_{EURO}
Joint-AC	43.8	42.9	1.02
Joint-BC	49.6	50.4	0.98
Joint-CC	57.2	54.6	1.05
Joint-DC	43.6	43.3	1.01
Joint-EC	33.8	32.3	1.05
Joint-ECR	41.4	37.5	1.10
	Average		1.04
	Standard deviation		0.04
	Coefficient of Variation		0.0385

6.3 Conclusions

This chapter presents preliminary parametric studies for both concrete-filled connections and hollow connections, to explore the influence of main geometrical variables on the connections' structural behaviour. Capacities of the tested concrete-filled connections are predicted by using simple hand calculation method based on limit state of bolt shear failure or bearing failure of fin plates.

From the numerical results obtained from the parametric studies based on concrete-filled connections, it is found that:

- The fin plate thickness affects the moment capacity of the connections significantly. Normally, the higher the fin plate thickness, the higher the ultimate moment capacity of the connections, although the failure mode may change when the thickness reaches a certain value, e.g. 8 mm.
- Vertical bolt spacing is suggested to be at least 2.5d for both type-BC and CC connections; the minimum value of edge distance e1 could be 1.5d in type-BC connection and 2.0d in type-CC connection. The minimum value of edge distance e2 is suggested as at least 2.5d in both cases.

From the numerical results obtained from the parametric studies based on hollow connections, it is found that:

- The thickness of the EHS tube wall has significant effect on the ultimate capacity of the hollow connection - the higher the thickness of the EHS tube wall, the higher the ultimate moment capacity of the connection.
- The higher the tube wall thickness, the less notable difference among the joint types in terms of the moment capacity of the connections. This can be explained that the column will have higher transverse stiffness with higher thickness which will reduce the benefit of using stiffener plate.
- For major axis connections, the inserted stiffener plate in the minor axis direction of the EHS tube could increase the moment capacity of the connection. However, this increase disappears when the tube wall thickness is bigger than a certain value, e.g.10mm.
- For minor axis connections, the through plate has significant contribution in enduring the load, resulting in the highest moment capacity among corresponding joint assemblies. However, for connections with a column tube wall thickness bigger than 10mm, there is no advantage of adopting through plate in regards to the moment capacity.
- It is also found that the moment capacity of the minor axis connection, can be enhanced by inserting a stiffener plate in the major axis direction.

Limit states of the concrete-filled connections covered in this thesis are found as bolt shearing failure and bearing failure of the fin plates. A simple calculation method is described in this chapter in regards to this two limit states. It is found that the predicted results by using the simple hand calculation method are in good

agreement with the test results given in this Chapter 4. Thus it may be an acceptable calculation method when designing such connections in consideration of moment capacities.

Chapter 7

Conclusions and future work

This chapter presents main conclusions drawn from this thesis. In addition, future work suggestions are given at the end of this chapter.

7.1 Conclusions

This research work presents a series of experimental tests on moment-ration behaviour of elliptical column to I-beam connection with concrete-filled columns or hollow columns. A simple finite element model developed by ABAQUS/standard solver was adopted to replicate the experimental results. The simulation results showed good agreement against with the experimental results in regards to moment-ration relationships, ultimate moment capacities and main failures of the tested specimens. Parametric studies were then conducted to check the main parameters that may influence the moment behaviour of the connections considered in this thesis. A simple hand calculation method was provided to predict the moment capacity of the connections limited in this research. Main conclusions summarized from the previous chapters are listed in the following paragraphs.

Based on the experimental results, below conclusions can be drawn:

- Typical failure mode of elliptical column to I-beam connections with hollow section column is inward local buckling of column surface near the upper portion of the joints caused by direct compression from the beam end, with exception of the through plate connection which failed in bolt shearing failure. However, the inward deformation of the hollow column was eliminated by concrete infill, and the failure mode change to shear failure of the bolts.
- In general, the moment-rotation relationship of elliptical column to I-beam connections can be divided into three different stages. First, friction is in control, which exists among fin plate, beam web and bolts. In this section, the rotation of connection was quite low but the slope of moment-rotation curves was nearly constant, column, beam and bolts worked well together;

then, the slippage occurred when the load applied is bigger than friction, the moment increased slowly with the increasing of rotation. After that, the bolts and bolt hole in fin plates and beam web will compress each other till the failure of joints.

- For all the joint assemblies considered in the current research, connections with concrete-filled columns have much higher moment capacity compared to their hollow counterparts, which highlight the benefit of adopting concrete infill.

The following conclusions can be drawn according to the parametric studies limited in this research:

According to the numerical results based on concrete-filled connection,

- The fin plate thickness has great effect on the moment capacity of the connections - the higher the fin plate thickness, the higher the ultimate moment capacity of the connections, although the failure mode may change when the thickness reaches a certain value, e.g. 8 mm for the cases studied in this research.
- Vertical bolt spacing is suggested to be at least 2.5d for both type-BC and CC connections; the minimum value of edge distance e1 could be 1.5d in type-BC connection and 2.0d in type-CC connection. The minimum value of edge distance e2 is suggested as at least 2.5d in both cases.

Based on the numerical results obtained from the parametric studies of hollow connections, it is found that:

- The thickness of the EHS tube wall has significant influence on the ultimate capacity of connection with hollow columns - the higher the thickness of the EHS tube wall, the higher the ultimate moment capacity of the connection.
- The higher the tube wall thickness, the less notable difference among the joint types in terms of the moment capacity of the connections. This is because that the column will have higher transverse stiffness with higher tube wall thickness, which will reduce the benefit of using stiffener plate.

- For major axis connections, the inserted stiffener plate in the minor axis direction of the EHS tube are capable of increasing the moment capacity of the connection. However, when the tube wall thickness reaches a certain value, e.g.10mm, there will be no increase on the moment capacity within the scope of this research.
- For minor axis connections, the through plate endured much of the load transferred from beams, as a result, the moment capacity of the connections is the highest among all the considered joint assemblies. However, when the column tube wall thickness is bigger than 10mm, there is no advantage of adopting through plate in regards to the moment capacity, since this kind of connection is much more expensive compared to normal fin plate connections.
- The moment capacity of the minor axis connection, can be enhanced by inserting a stiffener plate in the major axis direction.

Limit states of the concrete-filled connections covered in this thesis are found as bolt shearing failure and bearing failure of the fin plates. A simple calculation method is described in this chapter in regards to this two limit states. It is found that the predicted results by using the simple hand calculation method are in good agreement with the test results given in this Chapter 4. Thus it may be an acceptable calculation method when designing such connections in consideration of moment capacities.

7.2 Future work

The numerical model and hand calculation method can be verified against supplementary experimental tests extended from those connections tested in this thesis. Suggestions on a wider range of experiments would be:

- Tests on concrete-filled connections with thinner fin plate to check the bearing failure or net section failure of the fin plates.
- Tests on concrete-filled connections with different fin plate length/bolt numbers as the rotation centre will be affected.
- Tests on concrete-filled connections with different EHS geometries, e.g. a larger or smaller external dimension and a different tube wall thickness.

In addition, experimental investigation on such connections in fire condition would be a further study. Finally, another aspect ratio of the EHS tube would be desirable to investigate in the future.

References

[1] CEN. Hot finished structural hollow sections of non-alloy and fine grain steels - Part 1: Technical delivery conditions. 2006.

[2] Packer JA. Going elliptical. Modern Steel Construction, American Institute of Steel Construction. 2008;March.

[3] Chan TM, Gardner L. Compressive resistance of hot-rolled elliptical hollow sections. Engineering Structures. 2008;30:522-32.

[4] Chan TM, Gardner L. Bending strength of hot-rolled elliptical hollow sections. Journal of Constructional Steel Research. 2008;64:971-86.

[5] Nowzartash F, Mohareb M. Plastic interaction relations for elliptical hollow sections. Thin-Walled Structures. 2009;47:681-91.

[6] Bortolotti E, Jaspart JP, Pietrapertosa C, Nicaud G, Petitjean PD, Grimault JP. Testing and modelling of welded joints between elliptical hollow sections. Proceedings of the 10th International Symposium on Tubular Structures, Madrid Taylor & Francis, London. 2003:259–66.

[7] Chan TM, Gardner L, Law KH. Structural design of elliptical hollow sections: a review. Proceedings of the ICE - Structures and Buildings. 2010;163:391-402.

[8] Yang H, Lam D, Gardner L. Testing and analysis of concrete-filled elliptical hollow sections. Engineering Structures. 2008;30:3771-81.

[9] SCI/BSCA. Steel building design: design data in accordance with Eurocodes and the UK national annexes. Steel Construction Institute and British Constructional Steelwork Association, Ascot/London, UK, SCI publication. 2008.

[10] Kurobane Y, Packer JA, Wardenier J, Yeomans NF. Design Guide For Structural Hollow Section Column Connections. 2004.

[11] Gardner L, Chan TM. Cross-section classification of elliptical hollow sections. Steel and Composite Structures. 2007;7:185-200.

[12] CEN. Eurocode 3: Design of steel structures-Part 1-1: General rules and rules for buildings. EN1993: 2005, European Committee for Standardization, Brussels, Belgium. 2005.

[13] Gardner L, Chan TM. Cross-section classification of elliptical hollow sections. Prodeedings of the 11th international symposium on tubular structures. 2006:171-7.

[14] Silvestre N, Gardner L. Numerical study on the ultimate strength of elliptical stub columns. Proceedings of the 13th International Symposium on Tubular Structures, Hong Kong, China. 2010:283-91.

[15] Ruiz-Teran AM, Gardner L. Elastic buckling of elliptical tubes. Thin-Walled Structures. 2008;46:1304-18.

[16] Silvestre N, Gardner L. Elastic local post-buckling of elliptical tubes. Journal of Constructional Steel Research. 2011;67:281-92.

[17] Chan TM, L. G. Flexural buckling of elliptical hollow section columns. Journal of Structural Engineering. 2009;135:546-57.

[18] Gardner L, Chan TM, Abela JM. Structural behaviour of elliptical hollow sections under combined compression and uniaxial bending. Advanced Steel Construction. 2011;7:86-113.

[19] Law KH, Gardner L. Buckling of elliptical hollow section members under combined compression and uniaxial bending. Journal of Constructional Steel Research. 2013;86:1-16.

[20] Pietrapertosa C, Jaspart JP. Study of the behaviour of welded joints composed of elliptical hollow sections. Proceedings of the 10th International Symposium on Tubular Structures, Madrid Taylor & Francis, London. 2003:601–8.

[21] Choo YS, Liang JX, Lim LV. Static strength of elliptical hollow section X-joint under brace compression. Proceedings of the 10th International Symposium on Tubular Structures, Madrid 2003:253–8.

[22] Haque TO. Elliptical hollow section T and X Connections. MSc Thesis, University of Toronto. 2011.

[23] Shen W, Choo YS, Wardenier J, Packer JA, van der Vegte GJ. Static strength of axially loaded EHS X-joints with braces welded to the narrow sides of the chord. Journal of Constructional Steel Research. 2013;88:181-90.

[24] Shen W, Choo YS, Wardenier J, Packer JA, van der Vegte GJ. Static Strength of Axially Loaded Elliptical Hollow Section X Joints with Braces Welded to Wide Sides of Chord. I: Numerical Investigations Based on Experimental Tests. Journal of Structural Engineering. 2014;140:04013035.

[25] Willibald S, Packer JA, Voth AP, Zhao X. Through-plate joints to elliptical and circular hollow sections. Tubular Structures (conference). 2006.

[26] Willibald S, Packer JA, Martinez-Saucedo G. Behaviour of gusset plate connections to ends of round and elliptical hollow structural section members. Canadian Journal of Civil Engineering. 2006;33:373-83.

[27] Martinez-Saucedo G, Packer JA, Zhao XL. Static design of elliptical hollow section end-connections. Proceedings of the Institution of Civil Engineers, Structures and Buildings. 2008;161:103-13.

[28] Bradford MA, Roufeginejad A. Elastic local buckling of thin-walled elliptical tubes containing elastic infill material. 2007.

[29] Zhao XL, Packer JA. Tests and design of concrete-filled elliptical hollow section stub columns. Thin-Walled Structures. 2009;47:617-28.

[30] Sheehan T, Dai XH, Chan TM, Lam D. Structural response of concrete-filled elliptical steel hollow sections under eccentric compression. Engineering Structures. 2012;45:314-23.

[31] Jamaluddin N, Lam D, Dai XH, Ye J. An experimental study on elliptical concrete filled columns under axial compression. Journal of Constructional Steel Research. 2013;87:6-16.

[32] Uenaka K. Experimental study on concrete filled elliptical/oval steel tubular stub columns under compression. Thin-Walled Structures. 2014;78:131-7.

[33] Dai X, Lam D. Numerical modelling of the axial compressive behaviour of short concrete-filled elliptical steel columns. Journal of Constructional Steel Research. 2010;66:931-42.

[34] Dai X, Lam D, Jamaluddin N, Ye J. Numerical analysis of slender elliptical concrete filled columns under axial compression. Thin-Walled Structures. 2014;77:26-35.

[35] Han L-H, Ren Q-X, Li W. Tests on stub stainless steel–concrete–carbon steel double-skin tubular (DST) columns. Journal of Constructional Steel Research. 2011;67:437-52.

[36] Schneider SP, Alostaz YM. Experimental Behavior of Connections to Concrete-Filled Steel Tubes. Journal of Constructional Steel Research. 1998;45: 321–52.

[37] Shakir-Khalil H. Full-scale tests on composite connections. In Composite Construction of Steel and Concrete. 1992:539–54.

[38] Bridge R, Webb J. Thin walled circular concrete filled steel tubular columns. In Composite Construction of Steel and Concrete. 1992:634–49.

[39] Kato B, Kimura M, Ohta H, Mizutani N. Connection of beam flange to concrete-filled tubular columns. In Composite Construction of Steel and Concrete II. 1992:528–38.

[40] Morino S, Kawaguchi, J., Yasuzaki, C. and Kanazawa, S. Behavior of concrete-filled steel tubular three dimensional subassemblages. In Composite Construction of Steel and Concrete II. 1992:726–41.

[41] Ansourian P. Connections to concrete-filled tube columns. International Association of Bridge and Structural Engineers. 1976:1–22.

[42] Prion HGL, McLellan AB. Connecting steel beams to concrete-filled steel columns. In Proc ASCE Structures Congress on Composite Compression Members, San Antonio, TX. 1992:918–21.

[43] Kanatani H, Tabuchi, M., Kamba, T., Hsiaolien, J. and Ishikawa, M. A study on concrete-filled RHS columns to H-beam connections fabricated with HT bolts in rigid frames. In Composite Construction of Steel and Concrete. 1987:614–35.

[44] Azizinamini A, Prakash B. A tentative design guideline for a new steel beam connection detail to composite tube columns. AISC Engineering Journal, 3rd quarter. 1993:108–15.

[45] Winkel GDd. The Static Strength of I-beam to Circular Hollow Section Column Connections. 1998.

[46] Beutel J, Thambiratnam D, Perera N. Monotonic behaviour of composite column to beam connections. Engineering Structures. 2001;23:1152-61.

[47] Wang W-D, Han L-H, Zhao X-L. Analytical behavior of frames with steel beams to concrete-filled steel tubular column. Journal of Constructional Steel Research. 2009;65:497-508.

[48] Wang J-F, Han L-H, Uy B. Behaviour of flush end plate joints to concrete-filled steel tubular columns. Journal of Constructional Steel Research. 2009;65:925-39.

[49] Han L-H, Li W. Seismic performance of CFST column to steel beam joint with RC slab: Experiments. Journal of Constructional Steel Research. 2010;66:1374-86.

[50] Beutel J, Thambiratnam D, Perera N. Cyclic behaviour of concrete filled steel tubular column to steel beam connections. Engineering Structures. 2002; 24:29-38.

[51] Cheng C-T, Chung L-L. Seismic performance of steel beams to concrete-filled steel tubular column connections. Journal of Constructional Steel Research. 2003;59:405-26.

[52] Wang W-D, Han L-H, Uy B. Experimental behaviour of steel reduced beam section to concrete-filled circular hollow section column connections. Journal of Constructional Steel Research. 2008;64:493-504.

[53] Tan Q-H, Han L-H, Yu H-X. Fire performance of concrete filled steel tubular (CFST) column to RC beam joints. Fire Safety Journal. 2012;51:68-84.

[54] Song T-Y, Han L-H. Post-fire behaviour of concrete-filled steel tubular column to axially and rotationally restrained steel beam joint. Fire Safety Journal. 2014;69:147-63.

[55] Elremaily A, Azizinamini A. Experimental behavior of steel beam to CFT column connections. Journal of Constructional Steel Research. 2001;57:1099-119.

[56] Li TQ, Nethercot DA, Choo BS. Behaviour of Flush End-plate Composite Connections with Unbalanced Moment and Variable Shear/Moment Ratios - I. Experimental Behaviour. Journal of Constructional Steel Research. 1996;38:125-64.

[57] Simoes da Silva L, Simoes RD, Cruz PJS. Experimental behaviour of end-plate beam-to-column composite joints under monotonical loading. Engineering Structures. 2001;23:1383-409.

[58] Liew JYR, Teo TH, Shanmugam NE. Composite joints subject to reversal of loading - Part 1: experimental study. Journal of Constructional Steel Research. 2004;60:221-46.

[59] CEN. Eurocode 3: Design of steel structures-Part 1-8: Design of joints. . EN1993: 2005, European Committee for Standardization, Brussels, Belgium. 2005.

[60] Chen S-J, Chao YC. Effect of composite action on seismic performance. Journal of Constructional Steel Research. 2001;57:417-34.

[61] Jin J, El-Tawil S. Seismic performance of steel frames with reduced beam section connections. Journal of Constructional Steel Research. 2005;61:453-71.

[62] Cheng C-T, Chan C-F, Chung L-L. Seismic behavior of steel beams and CFT column moment-resisting connections with floor slabs. Journal of Constructional Steel Research. 2007;63:1479-93.

[63] BCSA. Joints in steel construction: simple joints to Eurocode 3. The Steel Construction Institute. 2014.

[64] White RNaF, P. J. . Framing connections for square structural tubing. Journal of the Structural Division, American Society of Civil Engineers 1966;92.

[65] Sauerwine L. Simple connection for square tubular shapes. Fritz Engineering Laboratory Report No 23761. 1969.

[66] Sherman DR. Simple framing connections to IISS columns. Proc American Institute of Steel Construction, National Steel Construction Conference, San Antonio, Texas, USA. 1995:30.1-.16.

[67] AISC. Hollow structural sections connections manual. American Institute of Steel Construction, Chicago, Ill, USA. 1997.

[68] Jarrett ND, and Granthain, R. I. Robustness tests on fin-plate connections. Client Report No GD 1101 for client Steel Construction Institute, Building Research Establishment, Watford, U K. 1993.

[69] Richard RM, Gillett, P. E., Kriegh, J. D. and Lewis, B. A. The Analysis and Design of Single Plate Framing Connections. Engineering Journal, AISC, Second Quarter. 1980;17.

[70] Astaneh-Asl A, Liu J, McMullin KM. Behavior and design of single plate shear connections. Journal of Constructional Steel Research. 2002;58:1121-41.

[71] Jones MH, Wang YC. Tying behaviour of fin-plate connection to concrete-filled rectangular steel tubular column — Development of a simplified calculation method. Journal of Constructional Steel Research. 2010;66:1-10.

[72] Jones MH, Wang YC. Shear and bending behaviour of fin plate connection to concrete filled rectangular steel tubular column — Development of a simplified calculation method. Journal of Constructional Steel Research. 2011;67:348-59.

[73] Lam D, Dai X. Finite Element modelling of beam to concrete filled elliptical steel column connections. Tubular Structures XIV Gardner (Ed). 2012;Taylor and Francis Group, London, ISBN 978-0-415-62137-3:289-96.

[74] CEN. Metallic materials-tensile testing-Part1: Method of test at ambient temperature. EN ISO 6892-1: 2009. 2009.

[75] Huang Y, Young B. The art of coupon tests. Journal of Constructional Steel Research. 2014;96:159-75.

[76] Sarraj M, Burgess IW, Davison JB, Plank RJ. Finite element modelling of steel fin plate connections in fire. Fire Safety Journal. 2007;42:408-15.

[77] Wang J, Spencer BF. Experimental and analytical behavior of blind bolted moment connections. Journal of Constructional Steel Research. 2013;82:33-47.

[78] Mollazadeh MH, Wang YC. New insights into the mechanism of load introduction into concrete-filled steel tubular column through shear connection. Engineering Structures. 2014;75:139-51.

[79] Yu H, Burgess IW, Davison JB, Plank RJ. Numerical simulation of bolted steel connections in fire using explicit dynamic analysis. Journal of Constructional Steel Research. 2008;64:515-25.

[80] Han LH. Concrete-filled steel tubular structures-theory and practice (2nd ed.). Beijing: China Science Press (in Chinese). 2007.

[81] Fernandez-Ceniceros J, Sanz-Garcia A, Antoñanzas-Torres F, Martinez-de-Pison FJ. A numerical-informational approach for characterising the ductile behaviour of the T-stub component. Part 1: Refined finite element model and test validation. Engineering Structures. 2015;82:236-48.

[82] Salih EL, Gardner L, Nethercot DA. Numerical investigation of net section failure in stainless steel bolted connections. Journal of Constructional Steel Research. 2010;66:1455-66.

[83] Khoo HA, Cheng RJJ, Hrudey TM. Ductile fracture of steel. Structural engineering report no. 233. Canada: Department of Civil & Environmental Engineering, University of Alberta. 2000.

[84] Dowling NE. Mechanical behaviour of materials. New Jersey: Prentice Hall. 1999.

[85] Huns BB, Grondin GY, Driver RG. Block shear behaviour of bolted gusset plates. Structural engineering report no 248 Canada: Department of Civil & Environmental Engineering, University of Alberta. 2002.

[86] Nip KH, Gardner L, Davies CM, Elghazouli AY. Extremely low cycle fatigue tests on structural carbon steel and stainless steel. Journal of Constructional Steel Research. 2010;66:96-110.

[87] CEN. Hot finished structural hollow sections of non-alloy and fine grain steels-Part 1: Technical delivery conditions. EN 10210-1:2006(E), European Committee for Standardization, Brussels, Belgium. 2006.

Appendix I

Design drawings of the specimens

i. Major axis connection with stiffener in the minor axis direction
ii. Major axis connection without stiffener
iii. Minor axis connection with through plate
iv. Minor axis connection without stiffener
v. Minor axis connection with stiffener in the major axis direction
vi. I-beam

i. Major axis connection with stiffener in the minor axis direction

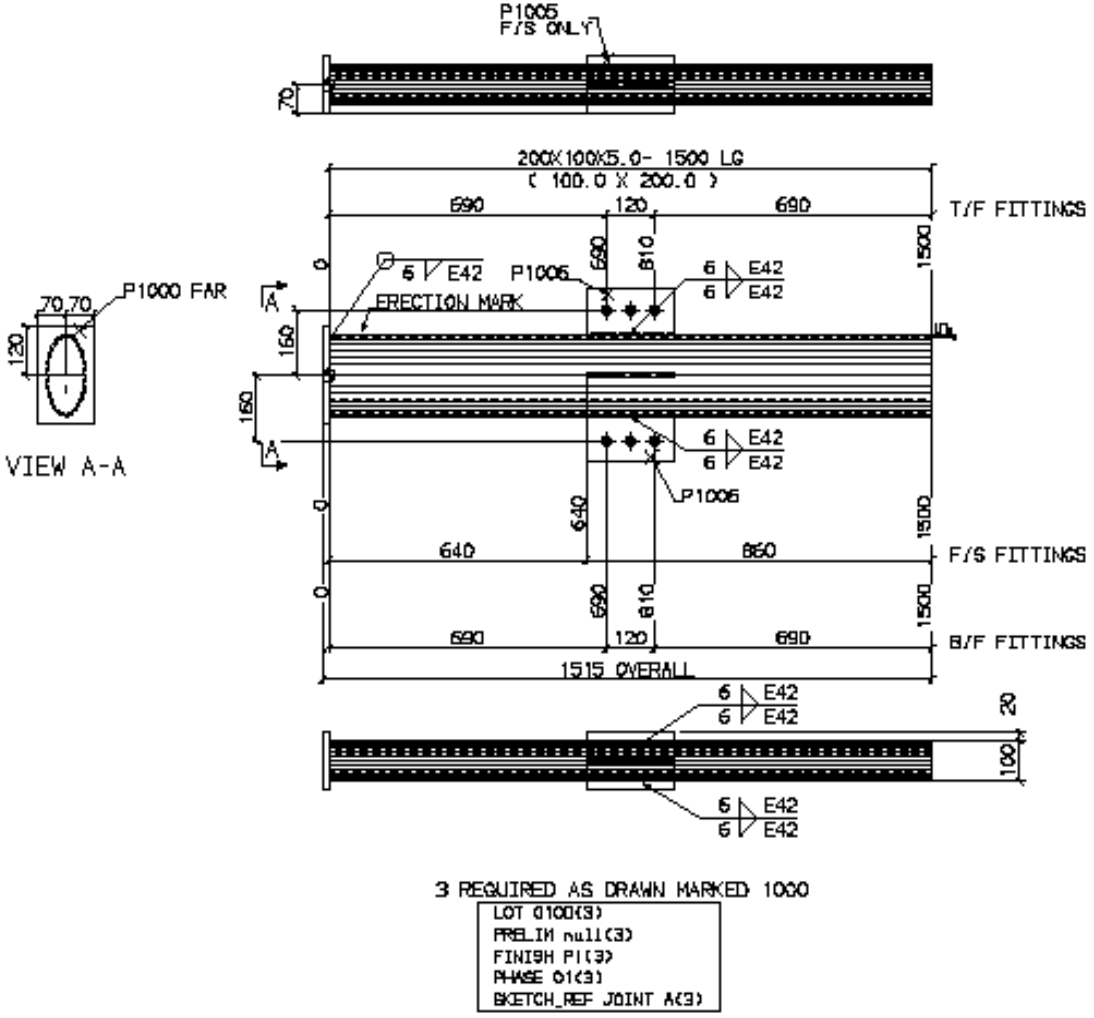

SHOP MATERIAL LIST FOR 1 ASSEMBLY						
MARK	SIZE	GRADE	LENGTH MM	No	AREA M2	WEIGHT KG
1000	200X100X5.0	S355J2H	1500	1	0.71	26.8
P1000	240X15FLT	S275JR	140	1	0.08	4.0
P1005	220X10FLT	S275JR	140	1	0.07	2.4
P1006	220X10FLT	S275JR	110	2	0.11	3.8
				TOTAL	0.97	37.0

LOCATION LIST	
GRID LOC.	GRID LOC.
1/A/0	1/A/1500

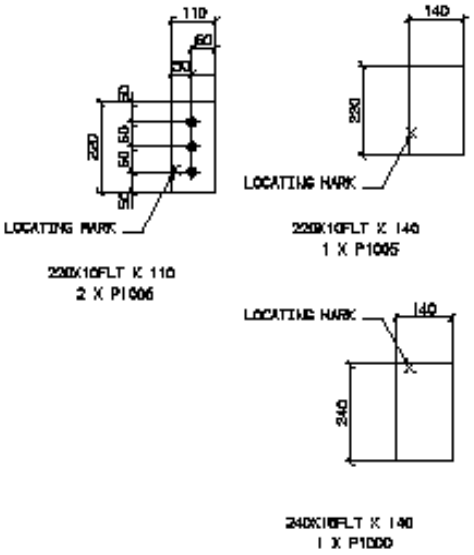

3 REQUIRED AS DRAWN MARKED 1000

LOT 0100(3)
PRELIM null(3)
FINISH P1(3)
PHASE 01(3)
SKETCH_REF JOINT A(3)

ii. Major axis connection without stiffener

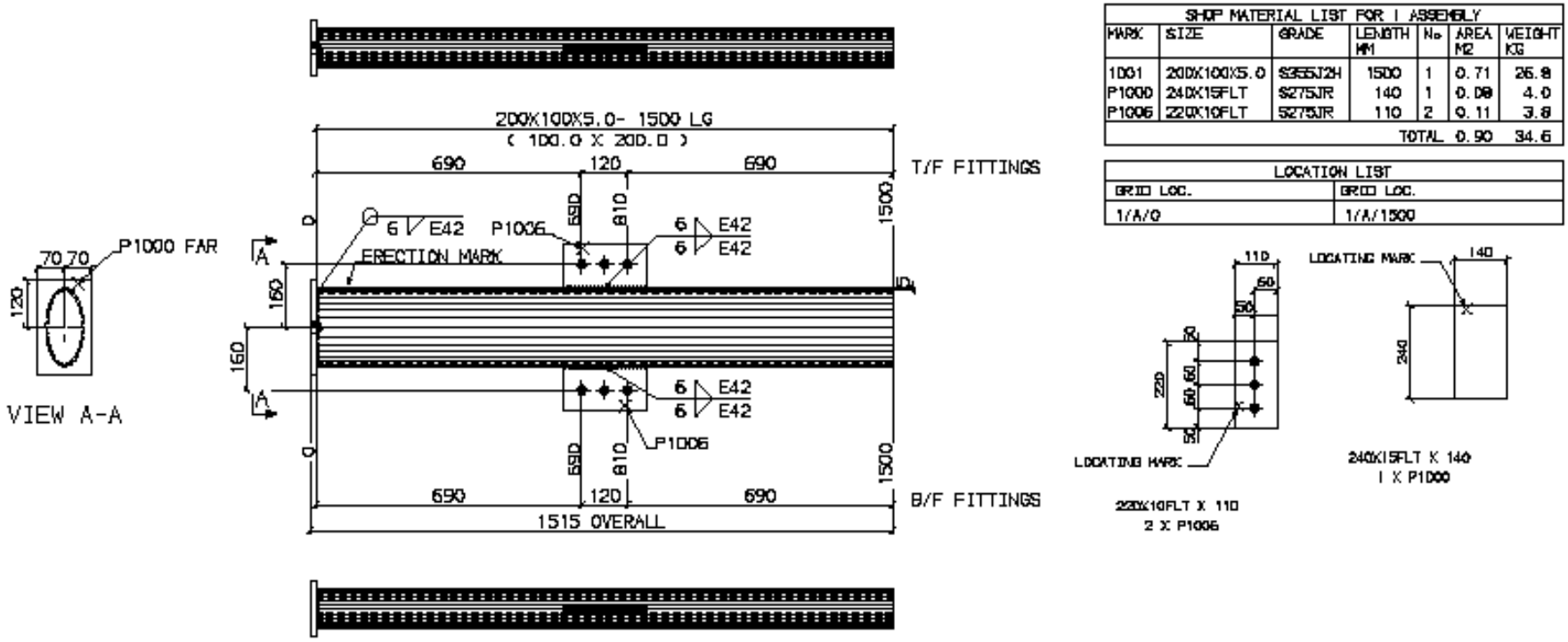

SHOP MATERIAL LIST FOR 1 ASSEMBLY						
MARK	SIZE	GRADE	LENGTH MM	No.	AREA M2	WEIGHT KG
1001	200X100X5.0	S355J2H	1500	1	0.71	26.8
P1000	240X15FLT	S275JR	140	1	0.08	4.0
P1006	220X10FLT	S275JR	110	2	0.11	3.8
				TOTAL	0.90	34.6

LOCATION LIST	
GRID LOC.	GRID LOC.
1/A/0	1/A/1500

3 REQUIRED AS DRAWN MARKED 1001

LOT 0100(3)
PRELIM null(3)
FINISH P1(3)
PHASE 01(3)
SKETCH_REF JOINT B(3)

iii. Minor axis connection with through plate

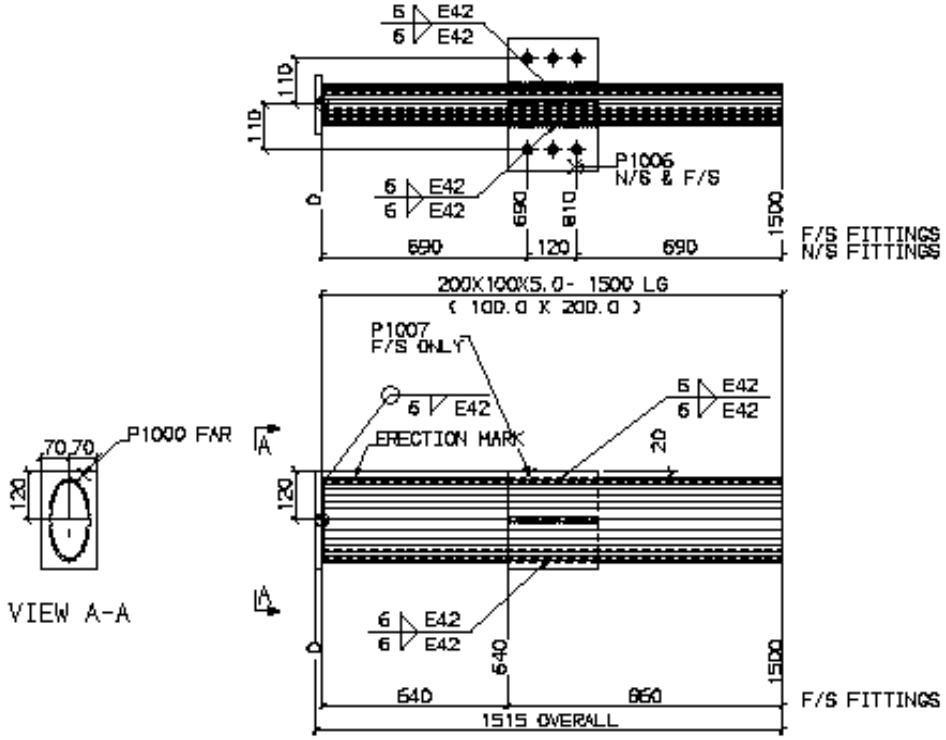

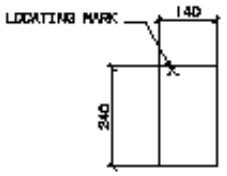

240X15FLT X 140
1 X P1000

SHOP MATERIAL LIST FOR 1 ASSEMBLY						
MARK	SIZE	GRADE	LENGTH MM	No	AREA M2	WEIGHT KG
1002	200X100X5.0	S355J2H	1500	1	0.71	26.8
P1000	240X15FLT	S275JR	140	1	0.08	4.0
P1006	220X10FLT	S275JR	110	2	0.11	3.8
P1007	220X10FLT	S275JR	240	1	0.11	4.1
				TOTAL	1.02	38.8

LOCATION LIST	
GRID LOC.	GRID LOC.
2/A/0	2/A/1500

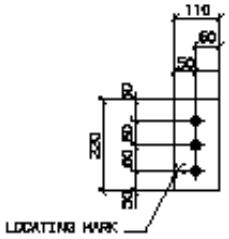

220X10FLT X 110
2 X P1006

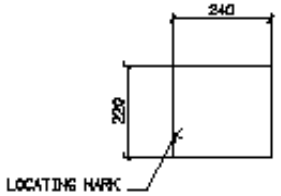

220X10FLT X 240
1 X P1007

3 REQUIRED AS DRAWN MARKED 1002

LOT 0100(3)
PRELIM null(3)
FINISH P1(3)
PHASE 01(3)
SKETCH_REF JOINT C(3)

iv. Minor axis connection without stiffener

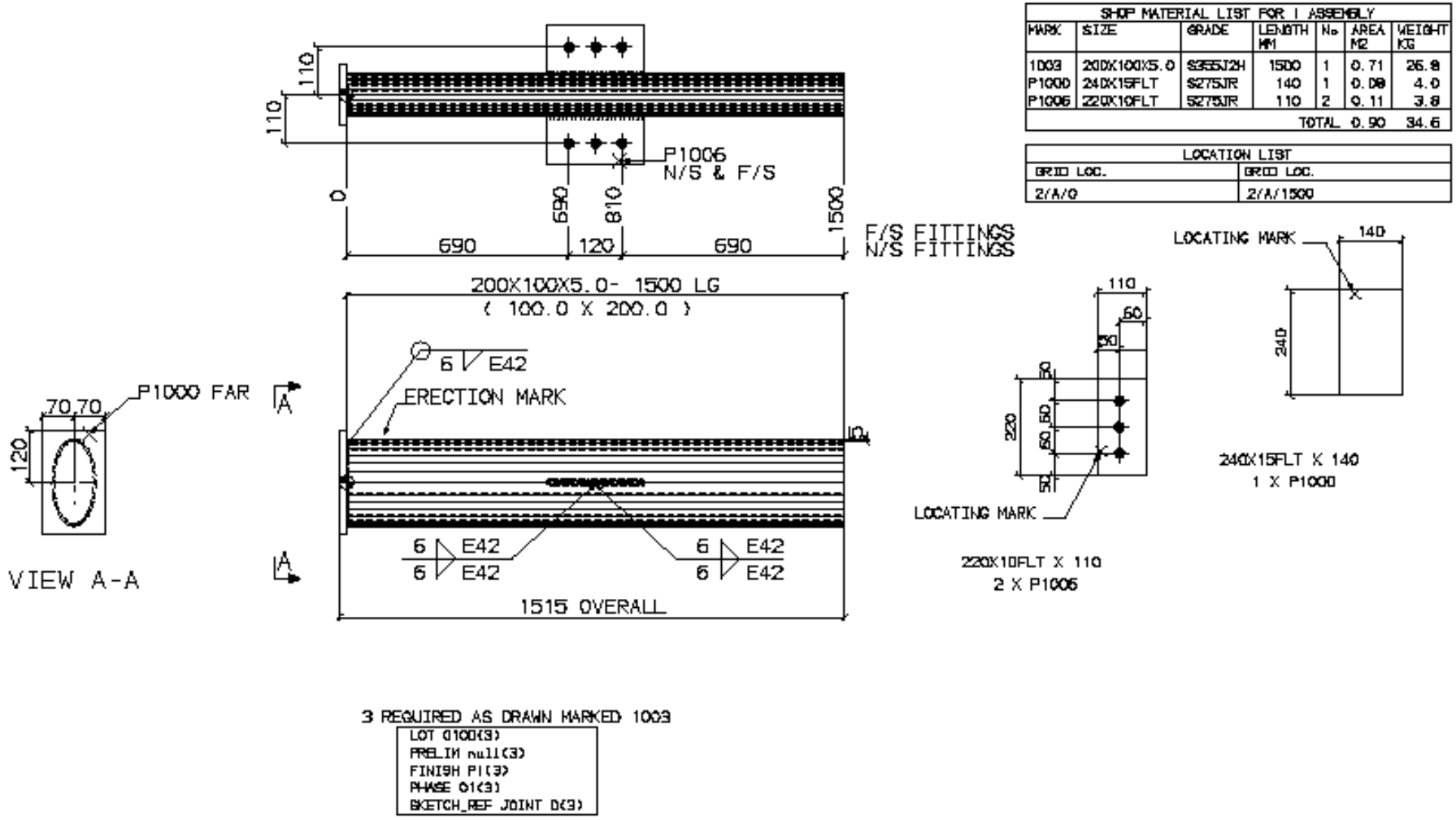

SHOP MATERIAL LIST FOR 1 ASSEMBLY						
MARK	SIZE	GRADE	LENGTH MM	No	AREA M2	WEIGHT KG
1003	200X100X5.0	S355J2H	1500	1	0.71	26.8
P1000	240X15FLT	S275JR	140	1	0.08	4.0
P1006	220X10FLT	S275JR	110	2	0.11	3.8
					TOTAL 0.90	34.6

LOCATION LIST	
GRID LOC.	GRID LOC.
2/A/0	2/A/1500

3 REQUIRED AS DRAWN MARKED 1003

LOT 0100(3)
PRELIM null(3)
FINISH P1(3)
PHASE 01(3)
SKETCH_REF JOINT 0(3)

v. Minor axis connection with stiffener in the major axis direction

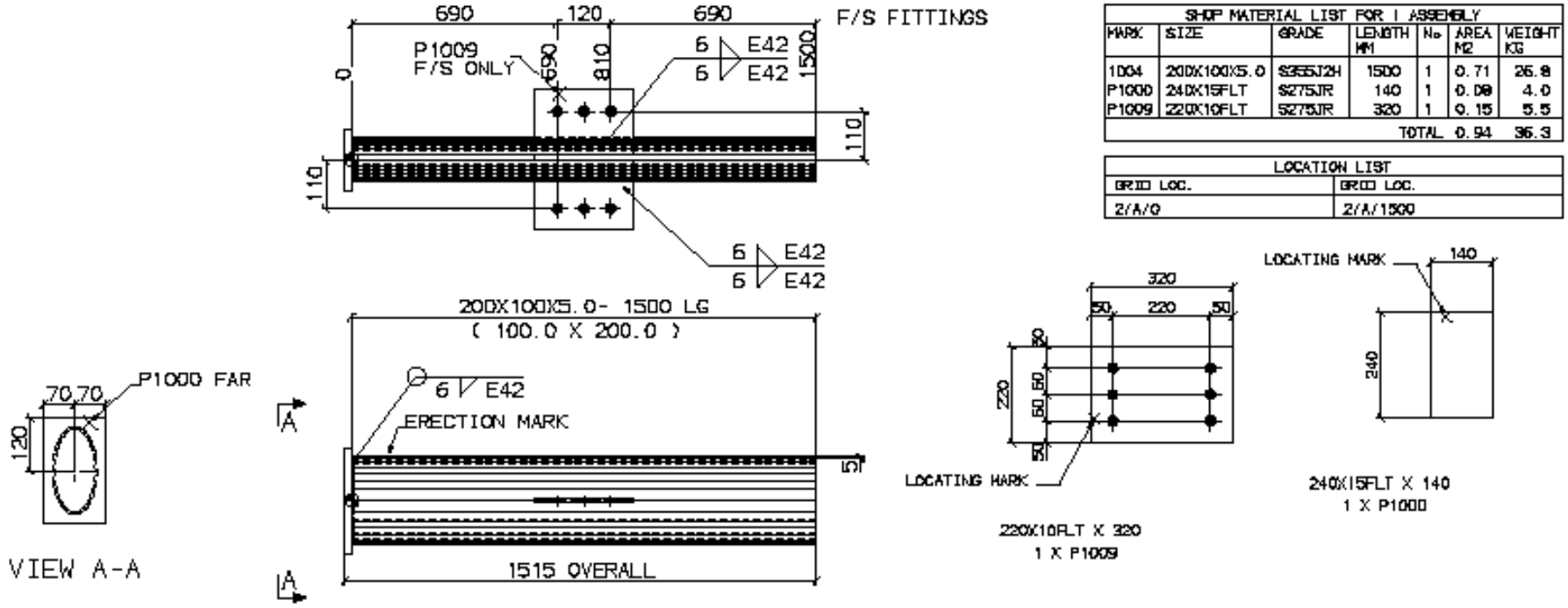

SHOP MATERIAL LIST FOR 1 ASSEMBLY						
MARK	SIZE	GRADE	LENGTH MM	No	AREA M2	WEIGHT KG
1004	200X100X5.0	S355J2H	1500	1	0.71	26.8
P1000	240X15FLT	S275JR	140	1	0.08	4.0
P1009	220X10FLT	S275JR	320	1	0.15	5.5
				TOTAL	0.94	36.3

LOCATION LIST	
GRID LOC.	GRID LOC.
2/A/0	2/A/1500

3 REQUIRED AS DRAWN MARKED 1004

LOT G100(3)
PRELIM null(3)
FINISH P1(3)
PHASE G1(3)
SKETCH_REF JOINT E(3)

vi. I-beam

SHOP MATERIAL LIST FOR 1 ASSEMBLY						
MARK	SIZE	GRADE	LENGTH MM	No	AREA M2	WEIGHT KG
1005	305X127X48UB	S355JR	900	1	1.01	43.3
				TOTAL	1.01	43.3

LOCATION LIST	
GRID LOC.	GRID LOC.
2/A/0 2/B/0	3/A/0 3/B/0

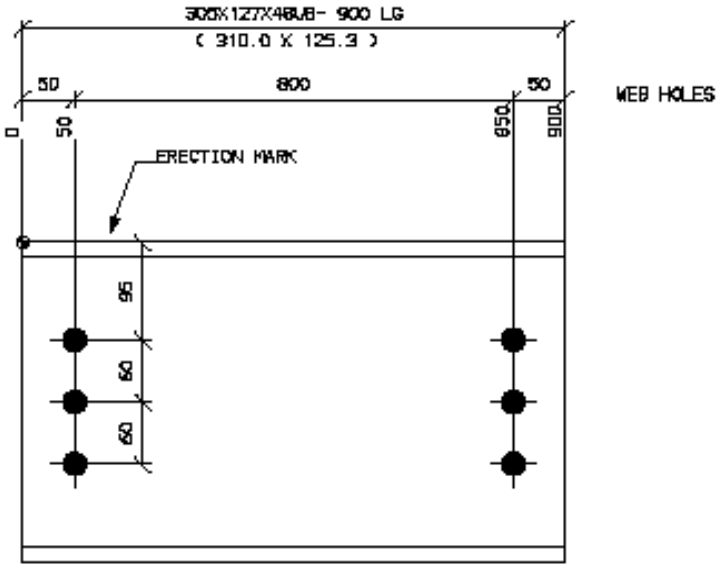

6 REQUIRED AS DRAWN MARKED 1005

LOT 0100(6)
PRELIM null(6)
FINISH P1(6)
PHASE 01(6)
SKETCH_REF STUB BEAM(6)

Appendix II

Journal publications related to this thesis

i. Jie Yang, Therese Sheehan, Xianghe Dai, & Dennis Lam. “Experimental study of beam to concrete-filled elliptical steel tubular column connections”, Thin-Walled Structures, 2015, Vol. 95, pp. 16-23.

ii. Jie Yang, Therese Sheehan, Xianghe Dai, & Dennis Lam. “Structural Behaviour of Beam to Concrete-filled Elliptical Steel Tubular Column Connections.”, Structures, 2016. (Article in Progress)

Thin-Walled Structures 95 (2015) 16–23

Contents lists available at ScienceDirect

Thin-Walled Structures

journal homepage: www.elsevier.com/locate/tws

Experimental study of beam to concrete-filled elliptical steel tubular column connections

J. Yang, T. Sheehan *, X.H. Dai, D. Lam

School of Engineering, University of Bradford, Richmond Road, Bradford BD7 1DP, United Kingdom

ARTICLE INFO

Article history:
Received 10 December 2014
Received in revised form
22 May 2015
Accepted 17 June 2015

Keywords:
Concrete-filled columns
Elliptical hollow section
Beam to column connections
Rotation behavior
Experimental study

ABSTRACT

This paper investigated the rotation behavior of simply bolted I-beam to concrete-filled elliptical steel tubular (CFEST) column connections experimentally. Ten different joint assemblies were tested to failure, with a constant axial compressive load applied to the column and upwards concentrated loads at the beam ends. All of the steel tubes were hot-finished and had a cross-sectional aspect ratio of 2. The orientation of the column and the arrangement of the stiffening plates were taken into consideration. Moment versus rotation relationships and failure modes were compared for each joint, highlighting the benefits of using core concrete and stiffeners in these connections.

1. Introduction

Concrete-filled steel tubular columns (CFST) are widely used in frame structures owing to their superior structural performance. The CFST column is an optimum combination of different materials, steel and concrete. With the confinement effect provided by the steel tube, the core concrete will obtain higher strength, while in turn, the concrete may eliminate or delay the commencement of local buckling in the steel tube. Additionally, the outer steel tube could be the formwork when casting concrete, which is more economic compared with reinforced concrete and enables rapid construction.

The most common cross-sectional shapes of CFST columns until now have been circular, square and rectangular. Only recently did a new range of elliptical hollow sections (EHSs) become available in the manufacturing industry and subsequently be introduced into building structures. The sectional sizes of EHSs range from $120 \times 60 \times 3.2$ mm up to $500 \times 250 \times 16$ mm in Grade S355J2H and the minimum yield strength is 355 MPa [1]. The EHS not only has a varied and interesting appearance which fulfils the esthetic purpose in design, but also provides potential structural efficiency. With two different principal axes, it has better bending capacity compared with a circular hollow section (CHS) of the same area or weight [2]; its closed shape offers high torsional stiffness [3] and high resistance to lateral torsional buckling [4].

With the merits mentioned above, EHS has been applied in several cases, e.g. Heathrow Airport in London and Society Bridge in Scotland. However, there is a lack of appropriate design rules to ensure the safety and economy of utilizing EHS in construction, which hinders its widespread application. Currently, existing research has focused on the behavior of hollow EHSs [5,6] and concrete-filled EHSs [7–10]. However, these investigations did not involve the interaction between members in a connection.

The first experiment on welded EHS tubular joints dates back to 2003; Bortolotti et al. [11] and Pietrapertosa and Jaspart [12] tested the brace-to-chord N- and X-joints where the brace was welded on the wide side of the EHS chord. Choo et al. [13] then furthered the study based on experimental results of welded EHS X-connections covering a wider range of variables through numerical analysis. It is concluded that with appropriate EHS orientation, axially loaded EHS connections can achieve higher capacities than equivalent CHS connections with the same brace and chord sectional areas. Willibald et al. [14] investigated the behavior of gusset–plate connections to EHSs where the branch/through plate was arranged in either the longitudinal or transverse direction of the EHS steel tube; and was connected on the wide/narrow side of the EHS. It is found that the yield strength of the through plate connection is approximately twice that of the branch plate connection or more. Connections with composite tubular columns have also been studied based on varied connection types and loading conditions. Elremaily and Azizinamimi [15] conducted laboratory tests on through beam connections under monotonic loading with the beam web attached to the web cleat plate

* Corresponding author.
E-mail address: t.sheehan@bradford.ac.uk (T. Sheehan).

http://dx.doi.org/10.1016/j.tws.2015.06.009
0263-8231/

through both fabrication bolts and fillet welds. Wang et al. [16,17] investigated the static and hysteretic behavior of flush end plate joints to CFST columns using high strength blind bolts. Cheng et al. [18] reported static behavior of CFST connections with square columns stiffened with internal diaphragms. Han and Li [19] tested connections with a reinforced concrete (RC) slab reinforced by an external ring, under seismic loading; Song and Han [20] provided a numerical investigation on the post-fire behavior of such CFST connections. However, the fabrication of these connection types is always complicated and time-consuming. And it is even more difficult to repeat the investigations for connections with EHSs due to the complexity of geometry. Lam and Dai [21] conducted a numerical study using an ABAQUS solver on four types of easy-to-construct beam to elliptical column connections. The effect of some important parameters on the structural behavior of the connections was observed.

This paper follows on from the above numerical study and starts to explore the behavior of simply bolted I-beam to concrete-filled elliptical column connections experimentally, employing either fin plates or a through plate. The aim is to eventually find out solutions to these kinds of connections for design. Several joint configurations, with or without concrete core/stiffening plates in the columns, were taken into consideration. A total of 10 specimens were tested to failure with the columns bending in the major or minor axis direction. The moment versus rotation relationships and failure modes of 10 specimens were addressed and analysed; the effect of core concrete and stiffening plates on bending behavior of simply bolted beam to elliptical column connections was highlighted.

2. Experimental study

2.1. Specimen types and details

Of all the specimens, five different joint assemblies (named after Type-A, -B, -C, -D, and -E) have been considered, as illustrated in Fig. 1. Each type of assembly comprised one specimen with a hollow EHS column and another specimen with an EHS column filled with concrete, to explore the enhancement of concrete infill on the structural behavior of these joints. All EHS columns were manufactured from Grade S355 steel with a minimum yield strength of 355 MPa. Due to the different axes of the EHS tube, two configurations of joint can be obtained as shown by Type-B and Type-D joints. As it is difficult to arrange stiffeners in both major and minor axis directions, only one stiffener plate is adopted for each joint, as seen in Type-A and Type-E connections. For minor axis connection Type-C, a through plate, functioning as both fin plate and stiffener, is adopted to ensure the continuous stiffness of the joint. The five joint assemblies are described as follows:

Type-A: Major axis connection with stiffener

Two fin plates ($220 \times 110 \times 10$ mm) in the major axis direction and a stiffener plate ($220 \times 140 \times 10$ mm) in the minor axis direction.

Type-B: Major axis connection without stiffener

Two fin plates ($220 \times 110 \times 10$ mm) in the major axis direction and no stiffener plate.

Type-C: Minor axis through plate connection

A whole plate ($220 \times 320 \times 10$ mm) through the column function as both fin plate and stiffener plate in the minor axis direction.

Type-D: Minor axis connection without stiffener

Two fin plates ($220 \times 110 \times 10$ mm) in the minor axis direction and no stiffener plate.

Type-E: Minor axis connection with stiffener

Two fin plates ($220 \times 110 \times 10$ mm) in the minor axis direction and a stiffener plate ($220 \times 140 \times 10$ mm) in the major axis direction.

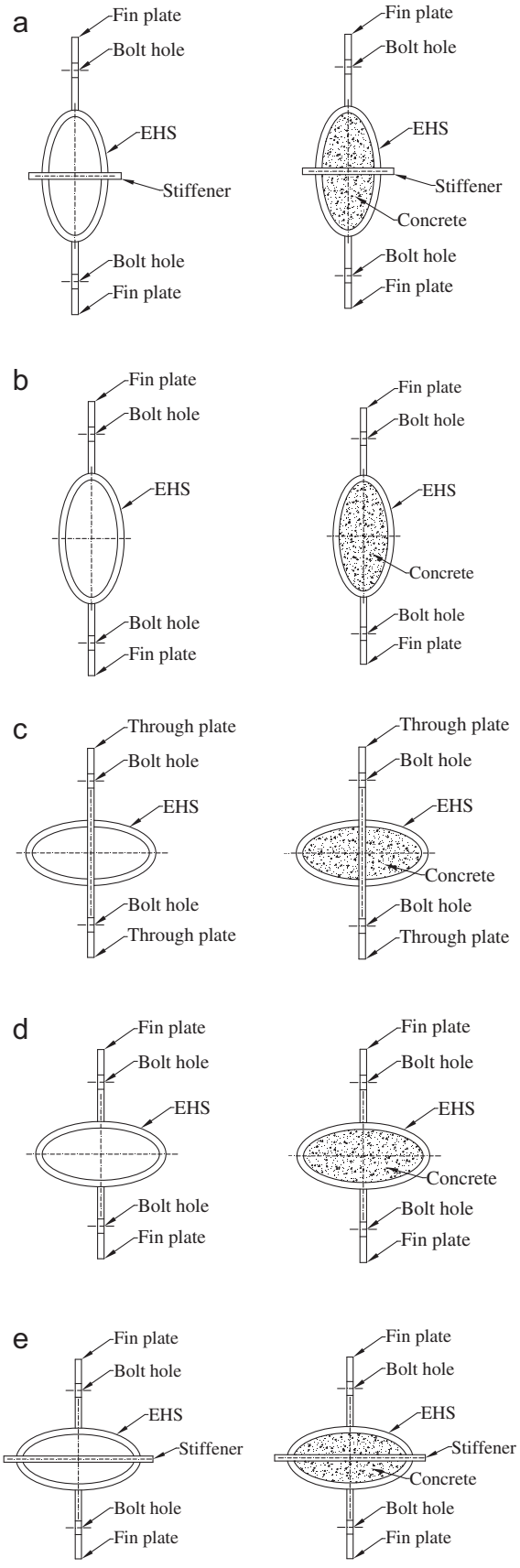

Fig. 1. Joint assemblies (cross-sectional view): (a) Type-A: major axis connection with stiffener; (b) Type-B: major axis connection without stiffener; (c) Type-C: minor axis through plate connection; (d) Type-D: minor axis connection without stiffener and (e) Type-E: minor axis connection with stiffener.

Table 1
Mean measured values of EHS column dimensions (mm).

Specimen ID	2*a*	2*b*	*L*	*t*	Specimen ID	2*a*	2*b*	*L*	*t*
Joint-A	198.43	99.52	1500	5.05	Joint-AC	198.60	101.89	1499	4.97
Joint-B	200.01	101.51	1487	4.92	Joint-BC	198.47	101.57	1498	5.01
Joint-C	198.50	100.50	1498	4.88	Joint-CC	198.21	101.42	1498	5.02
Joint-D	197.78	102.03	1497	4.54	Joint-DC	198.50	101.62	1500	5.05
Joint-E	197.82	102.10	1495	4.75	Joint-EC	198.11	101.58	1495	5.17

For a typical connection, two beams were connected with the column using fin plates with three M20 Gr. 8.8 or Gr. 10.9 bolts on each side; the fin plate is welded by using fillet weld (weld size is 6 mm) at the mid-height of the elliptical column. For Type-C connection, the through plate was run through the pre-slotted EHS column and was then welded to external face of column (6 mm fillet welds). Prior to conducting the experiments, the actual dimensions of EHS columns were measured. Mean values are listed in Table 1, where 2*a*, 2*b*, *t* and *L* mean the shorter diameter, longer diameter, thickness and length of the EHS column, respectively; hollow joints named by Joint-A, Joint-B, etc., while the concrete-filled counterparts were Joint-AC, Joint-BC, etc. All beams adopted in the specimens are 900 mm long, with beam sections of $305 \times 127 \times 48$ UB.

Two batches of concrete were made with the same mix design given in Table 2, to cast all of the specimens. The concrete cube tests were conducted and an average of 28-day strength of 37 MPa and test-date strength of 42 MPa were obtained.

2.2. Testing procedure

The typical test setup can be seen in Fig. 2. All tests were carried out in the heavy structures lab of the School of Engineering, University of Bradford. A compressive load which was approximately equals to 40% of the column resistance was firstly applied at the top column end using a 2500 kN actuator (Jack-3) as shown in Fig. 2. Two 1000 kN hydraulic actuators (Jack-1 and Jack-2) were then employed to exert an upwards concentrated force at each beam end, replacing the distributed load that would occur from a concrete floor slab in a real frame structure. Specially designed roller bearings (see Fig. 3) were employed, connected to the tops of Jacks 1 and 2. The curved rollers allowed the beams to rotate in the plane of the test-rig and plates were welded to the sides of the rollers to constrain out-of-plane freedoms of the bottom flanges to some extent. The initial distance from the edge of the beam flange to the loading point was 50 mm. A slotted and reusable steel cap was adopted at the top end of the column. On the top of this special cap, as depicted in Fig. 4(a), a circular groove slightly bigger than the load cell was carved to slot the loading cell into while an elliptical slot (see Fig. 4(b)) was made on the opposite side to cover the top of the EHS column to constrain sliding parallel to the orientation of the I-beams and out-of-plane movement of the specimen. For the bottom end of the EHS column, two clamps were employed as shown in Fig. 4(c), providing a semi-rigid boundary condition for the connections. It is worth mentioning that for the concrete-filled columns, plaster was used to fill the gap caused by shrinkage of the concrete after casting and to make sure that the compressive load was applied evenly to both steel tube and concrete.

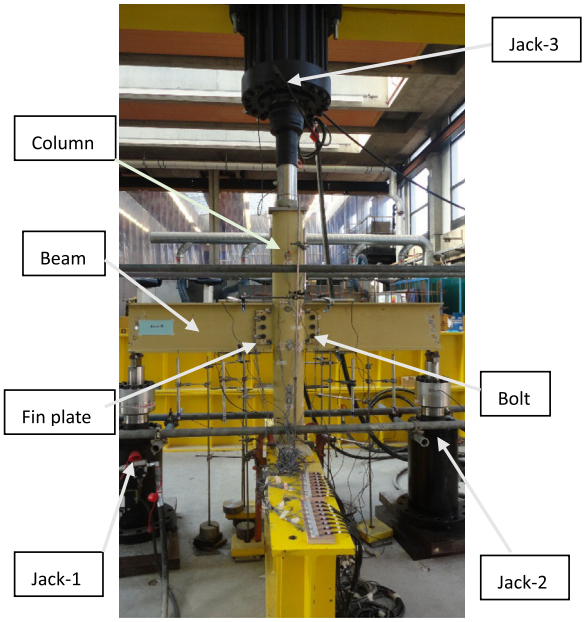

Fig. 2. Typical test setup.

Fig. 3. Roller bearing.

2.3. Instrumentation

Several linear variable displacement transducers (LVDTs) and strain gauges were used to measure displacements and strains of selected locations, separately, as illustrated in Fig. 5. LVDTs named

Table 2
Concrete mix specification design and compressive strength.

Water (kg/m^3)	Cement (kg/m^3)	Coarse aggregate (kg/m^3)	Fine aggregate (kg/m^3)	Compressive strength at 28 days (MPa)	Compressive strength on testing day (MPa)
225	402	1027	715	37	42

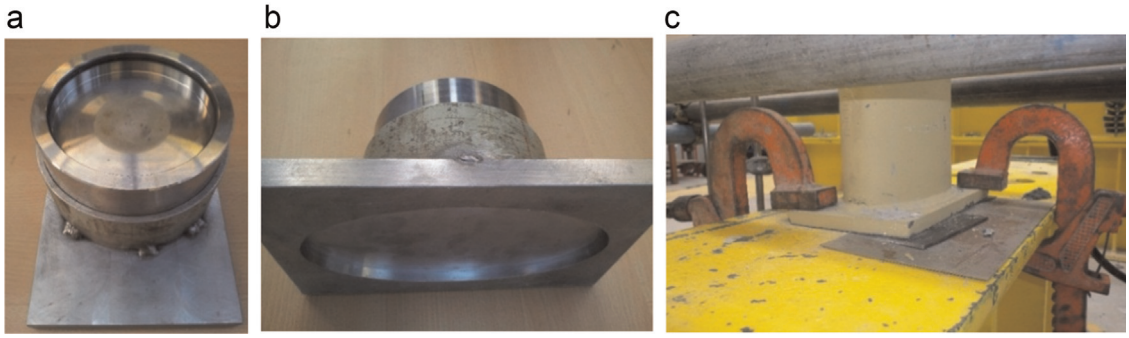

Fig. 4. Boundary conditions: (a) top end: connecting actuator; (b) top end: connecting EHS column and (c) bottom end (using clamps).

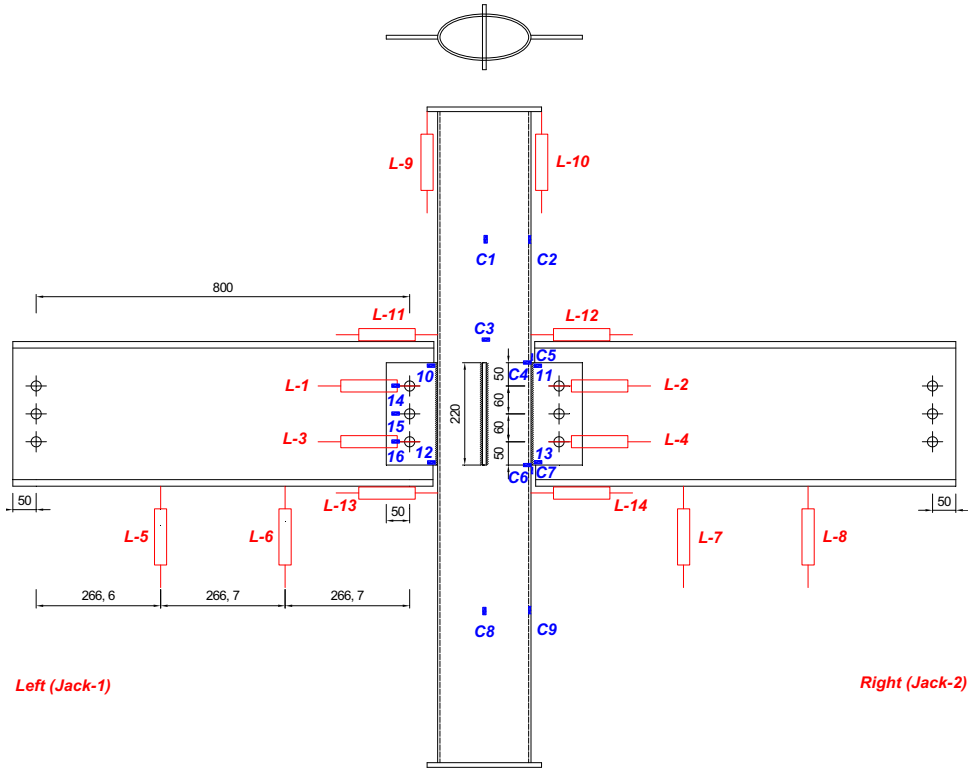

Fig. 5. Positions of strain gauges and LVDTs (Type-A; mm).

from *L*-1 to *L*-4 were arranged to measure the rotation of the beams. *L*-5–*L*-8 were placed at the bottom flanges of the beams to check whether or not beam bending occurred and also to provide an alternative method to derive the rotations of the joints. *L*-9 and *L*-10, employed to measure the shortening of the elliptical columns, were placed directly underneath the top steel cap. *L*-11–*L*-14 were used to capture the concave or convex deformations on the sides of the EHS column tubes directly above and below the connections.

Rotations of the I-beam to column connections can be calculated using the displacements measured by *L*-1–*L*-8 and the equation is listed as follows:

$$\theta = \frac{1}{2}(\theta_{1-4} + \theta_{5-8}) = \frac{1}{2}\left[Arc\ \tan\left(\frac{D^+}{2s}\right) + Arc\ \tan\left(\frac{D^-}{L/3}\right)\right]$$

where θ denotes the rotation of the elliptical column to beam connection; θ_{1-4} and θ_{5-8} refer to the rotations calculated by the displacements from *L*-1–*L*-4 and *L*-5–*L*-8, respectively; D^+ is the sum of the displacements obtained from *L*-1 and *L*-3 (left side, Jack-1) or *L*-2 and *L*-4 (right side, Jack-2); D^- is the difference between the displacements measured by *L*-5 and *L*-6 (left side, Jack-1) or *L*-7 and *L*-8 (right side, Jack-2); *s* is the central spacing of the bolts with a value of 60 mm, *L* equals to 800 mm, which is the horizontal distance between the beam load center to the joint (bolt) center.

Gauges named from *C*1 to *C*9 were used to measure either longitudinal or circumferential strains on the column, while gauges named from "10" to "16" were those located on fin plates, either near fillet welds connecting the fin plates to the column or adjacent to bolt holes to monitor the critical strain. Similar arrangements were adopted for the other nine specimens.

3. Experimental results and comparisons

3.1. Moment versus rotation curves

Fig. 6 shows the comparisons between moment versus rotation relationships for each joint, where the moments are equal to 0.8 m (distance between beam end loading center and beam-column connection center) × the concentrated load at the beam end and the rotation is calculated using the above mentioned equation. The

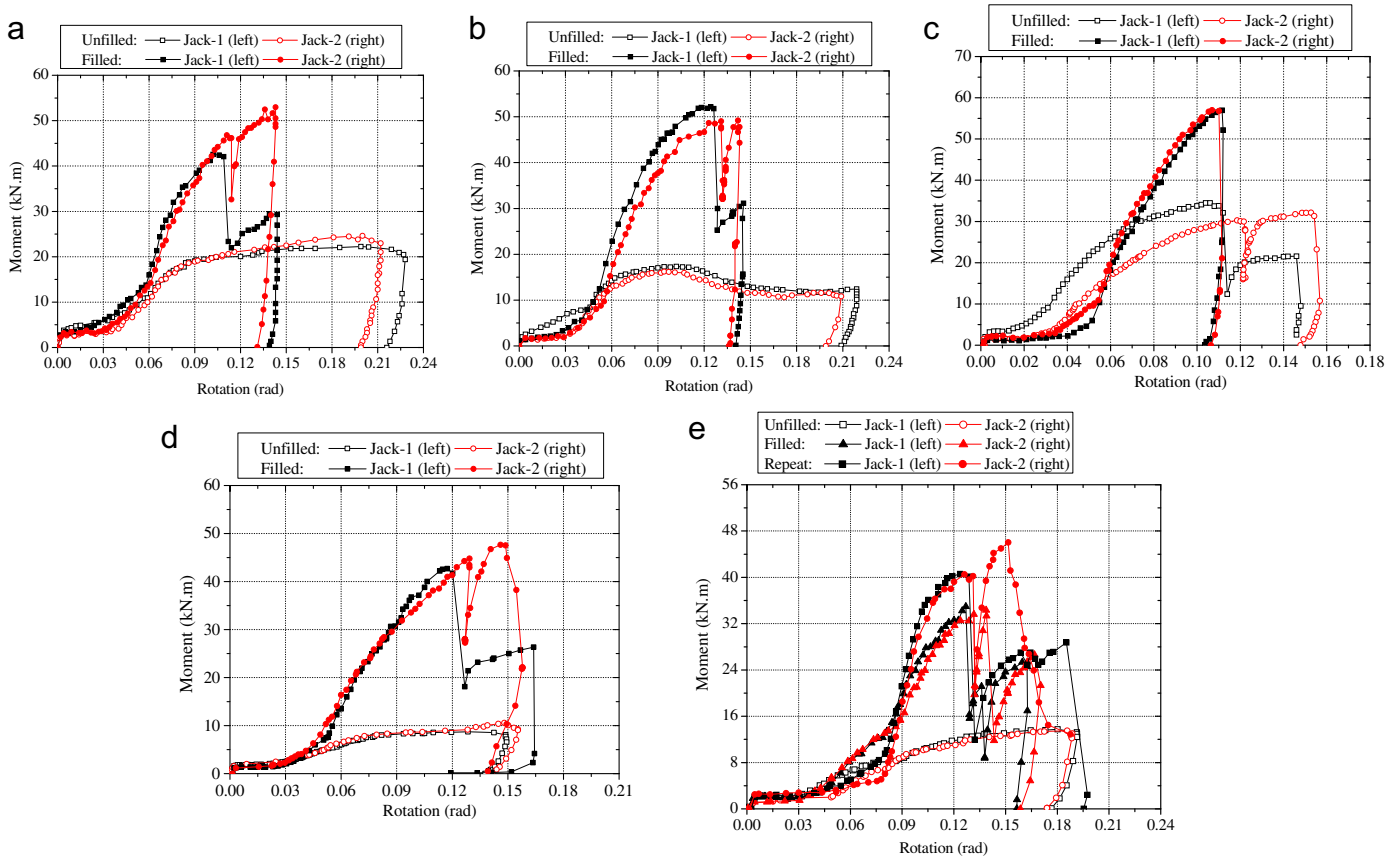

Fig. 6. Moment versus rotation relationships: (a) Type-A connection; (b) Type-B connection; (c) Type-C connection; (d) Type-D connection and (e) Type-E connection. (For interpretation of the references to color in this figure, the reader is referred to the web version of this article.)

lines with hollow square or circle data points represent results of unfilled connections while those with filled points refer to the results from concrete-filled connections; black curves denote results from the left hand actuator Jack-1 and red curves denote results from the right hand actuator Jack-2. The initial gap from the beam end to the column surface for all of the specimens was designed to be 10 mm, but differences in the gap size were observed between the left hand side and right hand side in each connection and between different specimens. This imperfection led to the non-synchronous moment–rotation response of the two sides although the two beams were compressed under same loading scheme. In Fig. 6(e), another set of data, represented by filled triangle data points, was given because a repeat test of Joint-EC was conducted using a higher grade of bolt.

As can be seen from Fig. 6, friction, which existed between the fin plates, beams and bolts, was in control in the initial stage of the test. The rotation of the connection was quite low and the slope was nearly constant, with the column, beam and bolts working well together. Then, the moment climbed slowly with increasing rotation showing that slip occurred after the applied load exceeded the friction. After that, the curves progressed to the next phase where the slope increased, the bolts and holes compressed each other until the failure of the connections. But different curve slopes were observed for concrete-filled and hollow columns after the beam end touched the column surface; the curve slopes of filled connections were steeper due to the enhancement provided by the concrete core to the rotation capacity. The sudden drops seen in the curves were caused by the shear failure of one or more bolts in the final stage of the experiments.

The lower moment between the two sides of joint is adopted to be the ultimate bending moment for safety concerns. The ultimate moments M_u, corresponding to rotations θ_u and the ratio of the ultimate moment between hollow and concrete-filled specimens, $M_{u\text{-hollow}}/M_{u\text{-filled}}$ for all of the specimens are given in Table 3. The enhancement of the ultimate moment ranged from 1.91 to 5.19, and the corresponding rotations of the hollow connections were normally bigger than their concrete-filled counterparts. Therefore, it can be concluded that core concrete in the column can improve the moment behavior of elliptical column to I-beam connections considerably and the most notable cases were those without stiffening plates (Joint-BC and Joint-DC).

As expected, the moment capacity of Joint-A is significantly higher than that of Joint-B owing to the enhancement of the stiffener plate in the minor axis direction of the EHS tube. However, the ultimate moment of Joint-AC was slightly lower than that of

Table 3
Ultimate moments, rotations and failure modes.

Specimen ID	M_u (kN m)	θ_u (rad)	$M_{u,filled}/M_{u,hollow}$	Failure mode description
Joint-A	22.3	0.200	–	Local buckling
Joint-AC	43.8	0.110	1.96	Bolt shear failure
Joint-B	16.0	0.100	–	Local buckling
Joint-BC	49.6	0.120	3.10	Bolt shear failure
Joint-C	30.0	0.110	–	Local buckling
Joint-CC	57.2	0.110	1.91	Bolt shear failure
Joint-D	8.4	0.120	–	Local buckling
Joint-DC	43.6	0.110	5.19	Bolt shear failure
Joint-E	13.3	0.180	–	Local buckling
Joint-EC	33.8	0.130	2.55	Bolt shear failure
Joint-EC (repeat)	41.4	0.130	3.11	Bolt shear failure

Note: Local buckling occurred in EHS column surface near the upper portion of the joints.

the unstiffened counterpart Joint-BC. The reason may be that the failure of the connection with core concrete was governed by bolt failure. Additionally, the benefit of using concrete in the column was more notable in the unstiffened Type-B connections than Type-A connections, due to the contribution of stiffeners to the minor axes of EHS columns.

Among all of the specimens, through plate Type-C connections exhibited the highest capacity in both hollow connections and the concrete-filled group, although they failed at a lower joint rotation. The explanation is that the through plate endured significantly more load transferred from the beam ends. By comparing the results of Joint-D and Joint-E, it can be concluded that although in an EHS tube, the stiffness in the major axis direction is higher than that in the minor axis direction, moment capacity of the minor axis connection can still be enhanced by welding a stiffener plate in the major axis direction. But this conclusion did not apply to the equivalent concrete-filled connections. Similarly to major axis connections, the capacity of Joint-DC without stiffeners was slightly higher than the stiffened counterpart Joint-EC.

3.2. Failure modes

The failures of all the specimens are illustrated in Figs. 7–11. After the tests, a portion of the steel tube was removed from the concrete-filled columns, in order to inspect the condition of the concrete core (Figs. 7(e), 8(c), 9(c), 11(e)). For hollow specimens, it was found that local buckling failure (see Fig. 7(c)) occurred on the column surface near the joint portion with perpendicular compression for connections without concrete. Although Joint-A, -C, and -E had stiffeners in either the minor or major axis direction, inwards local buckling still occurred near the top section of the connection owing to the direct compression from the top flange of the beam (see Figs. 7(a), 9(a) and 11(a)). This phenomenon disappeared in the corresponding concrete-filled connections. The core concrete mitigated the severe deformations that occurred in the hollow columns (Fig. 7(b)), while instead, one or more bolts failed in the final stage of the experiments for connections with concrete infill. Shear failure of one bolt is shown in Fig. 7(d).

An approximately square cross-sectional shape was obtained eventually in the Joint-A column, caused by compressive load transferred from the beam, as depicted in Fig. 7(c). Tearing failure on the tube wall near the left fin plate was found in the later stage

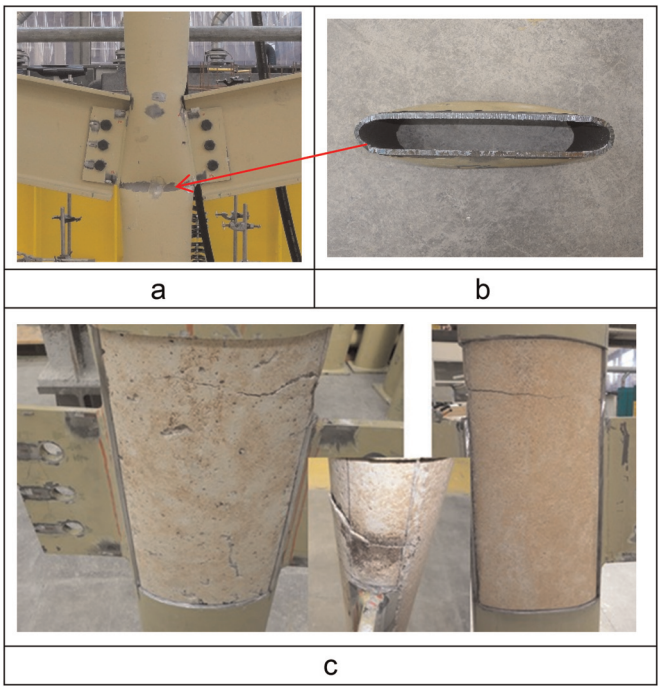

Fig. 8. Failure of Type-B connections: (a) Joint-B; (b) bottom cross-section of Joint-B column and (c) core concrete of Joint-BC.

of the test for Joint-A. In contrast, there was no obvious local failure and no cracks in the core concrete (see Fig. 7(e)) which means that the stiffener, core concrete and steel tube worked really well in this case.

Similar deformation was observed at the upper portion of the Joint-B column, but an elliptical cross-sectional shape with a higher aspect ratio was obtained near the bottom of the connection owing to the direct tension force and the absence of a stiffening plate. In contrast to Joint-AC, cracks occurred on the core concrete of Joint-BC around the upper worst section initiating at the right hand side of the ellipse, as shown in Fig. 8(c). Both of the bottom bolts of Joint-BC failed in shear.

Inward local failure of Joint-C and the most severely deformed section are shown in Fig. 9(a) and (b), respectively. With the

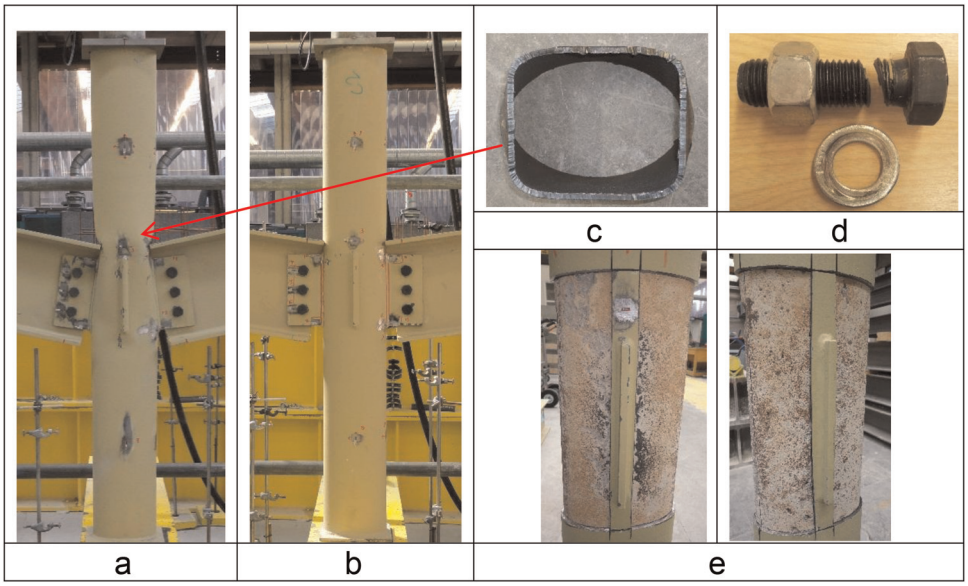

Fig. 7. Failure of Type-A connections: (a) Joint-A; (b) Joint-AC; (c) worst section of Joint-A; (d) bolt failure of Joint-AC; and (e) core concrete of Joint-AC.

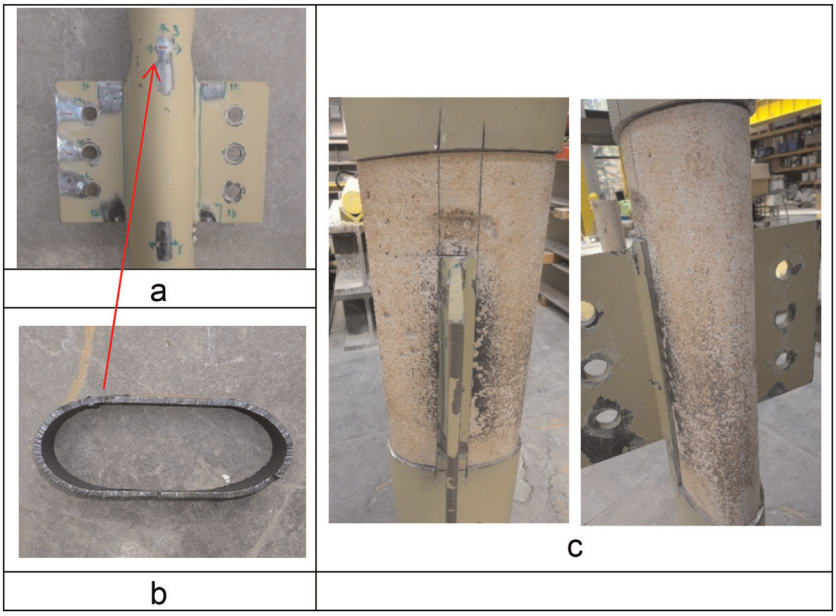

Fig. 9. Failure of Type-C connections: (a) Joint-C; (b) top cross-section of Joint-C column and (c) core concrete of Joint-CC.

exception of these locations, there is no obvious deformation in the Joint-C column and no cracks in the core concrete of Joint-CC (Fig. 9 (c)). The reason is that together with the bolts, the through plate in the minor axis direction, which combined the stiffener and fin plates, endured almost the whole shear force and moment transferred from the beam before beam end touched the column face. The load was transferred from the beam to the bolts and then to the through plate. Owing to the external fillet welds between the "fin plate" and the column face, the EHS tube wall was subjected to compressive force near the upper section and tensile force near the bottom part. However, the "stiffener plate" helped to endure most of the compressive or tensile load, thus large concave or convex deformations occurred in the EHS column around the connection and cracks in core concrete were prevented. Shear force increased with the increasing of joint rotation, and thus leaded to failure of bolts. In particular, two bottom bolts of Joint-C failed while those in Joint-A and -B did not, which verified the above explanation.

Comparison of failure modes of Type-D connections can be seen in Fig. 10. Inward local buckling was observed in the Joint-D column, in contrast, no deformation occurred in the steel tube but cracking occurred throughout the core concrete at the same position. The concrete failure of Joint-DC was more severe than that of Joint-BC because it was subjected to bending in the weaker axis direction. Moreover, for Joint-DC, the bottom and middle bolts at the left side failed in sequence eventually, along with the tear failure of the column wall on the right side.

Failures of Type-E connections are illustrated in Fig. 11. Gr. 8.8 bolts were used firstly in this joint assembly. For the unfilled connection Joint-E, inward local buckling occurred on the elliptical column tube (see Fig. 11(a) and (b)), while the bottom bolts at both sides of Joint-EC failed and small cracks initiated in the column surface near the bottom of the fin plates. Expecting better bending capacity, Gr. 10.9 bolts were then adopted to repeat the experiment of Joint-EC. However, the bottom and middle bolts at the left side failed in sequence eventually, accompanied with extension of the cracks on the right hand side (see Fig. 11(d)). Similar to Joint-AC and Joint-CC with stiffeners in the columns, no severe cracks were observed in the core concrete of Joint-EC as shown in Fig. 11(e).

4. Conclusions

A number of experiments were conducted to investigate the rotation behavior of simple bolted beam to elliptical column

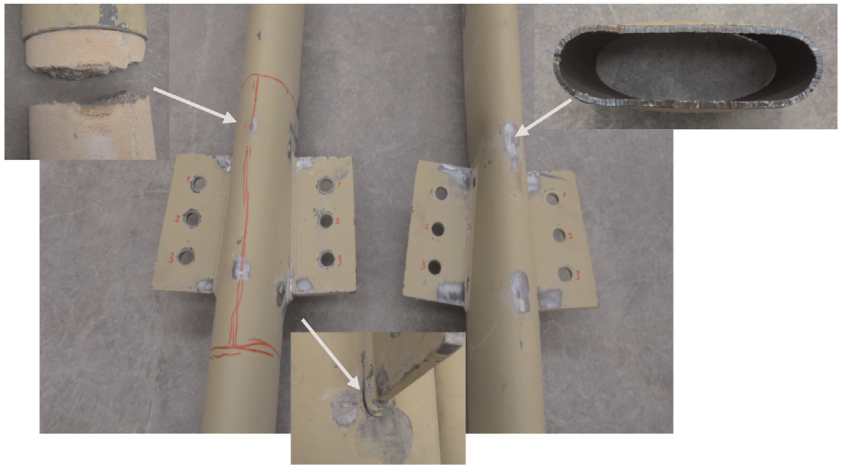

Fig. 10. Failure of Type-D connections.

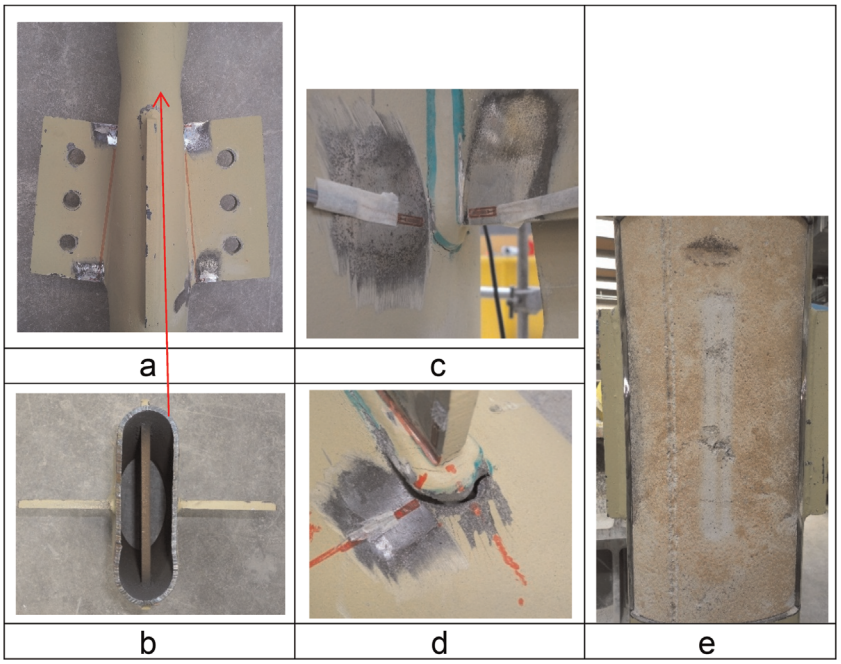

Fig. 11. Failure of Type-E connections: (a) Joint-E; (b) top section of Joint-E column; (c) initial cracks of Joint-EC; (d) fracture failure of Joint-EC and (e) core concrete of Joint-EC.

connections. Based on the experimental results, the typical failure mode of the connections with hollow columns was found to be inward local buckling of the column surface near the upper portion of the joints, though stiffeners were arranged in either the major or minor axis direction in some cases. However, the inward deformation was eliminated by the core concrete. Instead, shear failure of the bolts governed the ultimate rotation capacity of the joints with concrete infill.

According to the moment versus rotation responses of beam to elliptical column connections, friction was in control in the initial stage with the friction force existing between fin plates, beams and bolts. In this section, the rotation of the connection was quite low but the slope of the moment–rotation curves was nearly constant, with the column, beam and bolts working well together. Then, slippage occurred when the load applied was bigger than the friction force, and the moment climbed slowly with the increase of rotation. Afterwards, the bolts, the bolt holes in the fin plates and the beam webs acted together in resisting the load until the joints failed in one of the modes described previously.

For all of the joint assemblies, connections with concrete-filled columns had much higher moment capacity than their unfilled counterparts. The enhancement in moment ranged from 1.91 to 5.19. Additionally, a minor axis through plate connection was found to have higher stiffness and better moment capacity, hence this joint type was recommended for minor axis beam to elliptical column connections.

References

[1] CEN, Hot Finished Structural Hollow Sections of Non-alloy and Fine Grain Steels – Part 2: Tolerances, Dimensions and Sectional Properties, EN 10210-2:2006(E), European Committee for Standardization, Brussels, Belgium, 2006.
[2] J.A. Packer, Going Elliptical. Modern Steel Construction, American Institute of Steel Construction, 2008.
[3] T.M. Chan, L. Gardner, Bending strength of hot-rolled elliptical hollow sections, J. Constr. Steel Res. 64 (9) (2008) 971–986.
[4] F. Nowzartash, M. Mohareb, Plastic interaction relations for elliptical hollow sections, Thin-Walled Struct. 47 (6–7) (2009) 681–691.
[5] A.M. Ruiz-Teran, L. Gardner, Elastic buckling of elliptical tubes, Thin-Walled Struct. 46 (11) (2008) 1304–1318.
[6] T.M. Chan, L. Gardner, Compressive resistance of hot-rolled elliptical hollow sections, Eng. Struct. 30 (2) (2008) 522–532.
[7] H. Yang, D. Lam, L. Gardner, Testing and analysis of concrete-filled elliptical hollow sections, Eng. Struct. 30 (12) (2008) 3771–3781.
[8] T. Sheehan, X.H. Dai, T.M. Chan, D. Lam, Structural response of concrete-filled elliptical steel hollow sections under eccentric compression, Eng. Struct. 45 (2012) 314–323.
[9] X. Dai, D. Lam, Numerical modelling of the axial compressive behaviour of short concrete-filled elliptical steel columns, J. Constr. Steel Res. 66 (7) (2010) 931–942.
[10] N. Jamaluddin, D. Lam, X.H. Dai, J. Ye, An experimental study on elliptical concrete filled columns under axial compression, J. Constr. Steel Res. 87 (2013) 6–16.
[11] E. Bortolotti, J.-P. Jaspart, C. Pietrapertosa, G. Nicaud, P.D. Petitjean, J.P. Grimault, Testing and modelling of welded joints between elliptical hollow sections, in: Proceedings of the 10th International Symposium on Tubular Structures, Madrid, Taylor & Francis, London, 2003, pp. 259–266.
[12] C. Pietrapertosa, J.P. Jaspart, Study of the behaviour of welded joints composed of elliptical hollow sections, in: Proceedings of the 10th International Symposium on Tubular Structures, Madrid, Taylor & Francis, London, 2003, pp. 601–608.
[13] Y.S. Choo, J.X. Liang, L.V. Lim, Static strength of elliptical hollow section X-joint under brace compression, in: Proceedings of the 10th International Symposium on Tubular Structures, Madrid, 2003, pp. 253–258.
[14] S. Willibald, J.A. Packer, A.P. Voth, X. Zhao, Through-plate joints to elliptical and circular hollow sections, in: Proceedings of the Tubular Structures Conference, 2006.
[15] A. Elremaily, A. Azizinamini, Experimental behavior of steel beam to CFT column connections, J. Constr. Steel Res. 57 (2001) 1099–1119.
[16] J.-F. Wang, L.-H. Han, B. Uy, Behaviour of flush end plate joints to concrete-filled steel tubular columns, J. Constr. Steel Res. 65 (4) (2009) 925–939.
[17] J.-F. Wang, L.-H. Han, B. Uy, Hysteretic behaviour of flush end plate joints to concrete-filled steel tubular columns, J. Constr. Steel Res. 65 (8–9) (2009) 1644–1663.
[18] C.-T. Cheng, C.-F. Chan, L.-L. Chung, Seismic behavior of steel beams and CFT column moment-resisting connections with floor slabs, J. Constr. Steel Res. 63 (11) (2007) 1479–1493.
[19] L.-H. Han, W. Li, Seismic performance of CFST column to steel beam joint with RC slab: experiments, J. Constr. Steel Res. 66 (11) (2010) 1374–1386.
[20] T.-Y. Song, L.-H. Han, Post-fire behaviour of concrete-filled steel tubular column to axially and rotationally restrained steel beam joint, Fire Saf. J. 69 (2014) 147–163.
[21] D. Lam, X. Dai, Finite element modelling of beam to concrete filled elliptical steel column connections, in: Gardner (Ed.), Tubular Structures XIV, Taylor and Francis Group, London, 2012, pp. 289–296, ISBN: 978-0-415-62137-3.

Structures xxx (2016) xxx–xxx

Contents lists available at ScienceDirect

Structures

journal homepage: www.elsevier.com/locate/structures

Structural Behaviour of Beam to Concrete-filled Elliptical Steel Tubular Column Connections

J. Yang *, T. Sheehan, X. Dai, D. Lam

School of Engineering, University of Bradford, Bradford, UK

ARTICLE INFO

Article history:
Received 3 June 2016
Received in revised form 25 August 2016
Accepted 7 September 2016
Available online xxxx

Keywords:
Concrete-filled columns
Elliptical hollow section
Beam to column connections
Finite element modeling

ABSTRACT

Elliptical hollow sections (EHSs) have been utilized in construction recently because of their visual appearance as well as the potential structural efficiency owing to the presence of the two principle axes. However, little information currently exists for the design of beam to elliptical column connections, which is an essential part of a building structure. Thus, to ensure the safe and economic application of EHSs, a new research project has been initiated. Rotation behaviour of simply bolted beam to concrete-filled elliptical steel column connections was investigated experimentally. Various joint types were considered and the benefits of adopting core concrete and stiffeners were highlighted. This paper covers the experimental studies and simulation of the connections using the ABAQUS standard solver. Comparisons of failure modes and moment vs. rotation relationships of the connections between numerical and experimental results were given. Good agreement has been obtained and the developed finite element model was therefore adopted to conduct a preliminary parametric study to explore the effect of critical parameters on the structural behaviour of beam to concrete-filled elliptical column connections.

1. Introduction

Concrete-Filled Steel Tubular (CFST) columns are well-known for their superior structural properties due to the mutual complementation of the steel tube and the concrete core. The most common cross-sectional shapes of CFST columns are circular, square and rectangular. A new range of elliptical hollow sections (EHSs) has been made available recently by the manufacturing industry, which adds diversity to the sectional shape and fulfils the aesthetics demand by designers. However, limited information exists to enable safe and economic design of EHS components/connections in structures, which might limit its widespread application. Efforts have been made on investigating the structural behaviour of elliptical columns [1,2], beams [3], welded truss EHS connections [4,5]. Zhao and Packer [1] experimentally investigated both unfilled and concrete-filled EHS stub columns filled with normal concrete and self-consolidating concrete. According to the obtained results, they derived the yield slenderness limit which is used to identify occurrence of local buckling of steel hollow sections subjected to axial compressive force for carbon steel EHS based on the equivalent rectangular hollow sections (RHS). They also extended the above concept and method to predict the load carrying capacity of concrete-filled EHS stub columns and good prediction was generated by using procedures in Eurocode 4. Dai and Lam [2] investigated the axial compressive behaviour of short concrete-filled EHS columns by using ABAQUS finite element analyzing (FEA) software and an improved confined concrete stress-strain model was proposed for concrete-filled EHS stub columns. Typical failure modes, static bearing capacities and load versus end shortening relationships of the composite stub columns obtained by the finite element analysis were verified against experimental observations. The comparison and analysis indicated the FEA method was reliable in prediction the basic structural behaviour of concrete-filled EHS stub columns under compression. Static strength of axially loaded EHS X-joints with brace members welded to the narrow sides of the EHSs has been studied experimentally and numerically by Shen

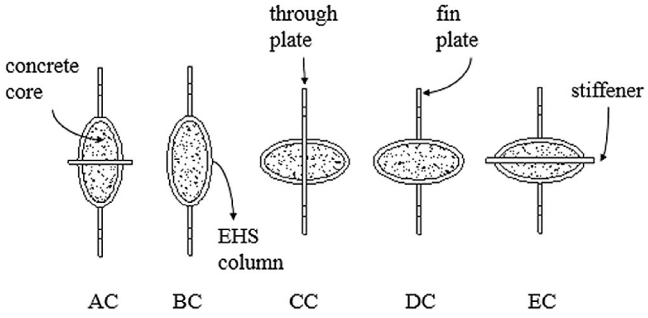

Fig. 1. Joint types.

* Corresponding author.
E-mail addresses: j.yang17@bradford.ac.uk (J. Yang), t.sheehan@bradford.ac.uk (T. Sheehan), x.dai@bradford.ac.uk (X. Dai), d.lam1@bradford.ac.uk (D. Lam).

http://dx.doi.org/10.1016/j.istruc.2016.09.005
2352-0124/

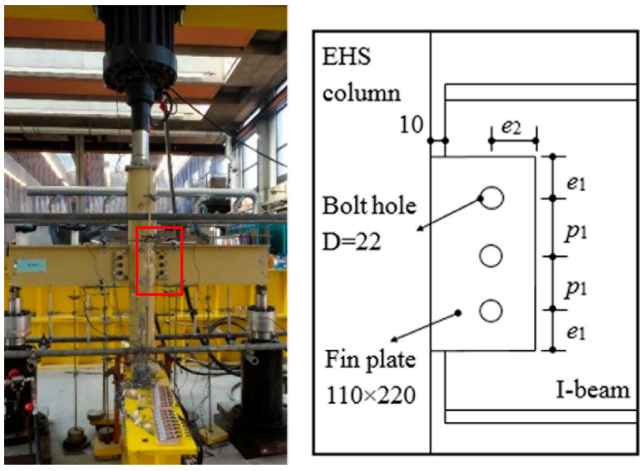

Fig. 2. Test arrangements & Planed connection dimensions ($e_1 = 50$, $e_2 = 50$, $p_1 = 60$; mm).

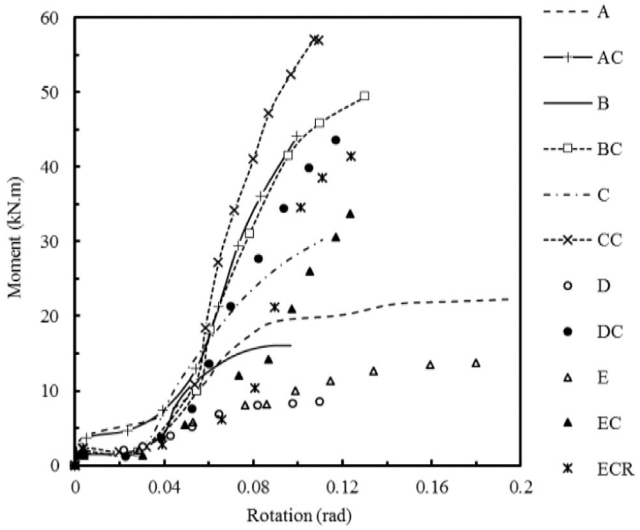

Fig. 3. Summarized moment vs. rotation relationships.

et al. [4]. In their study, both brace member compression tests and tension tests were performed. They found that this type of EHS X-joint could be related to relevant circular hollow section X-joints. Despite the above mentioned attempts of investigation on EHS and those not specified provided herein, large gaps still exist in research. Beam to concrete-filled elliptical column connections, which are essential in framed structures, remain unfamiliar to designers. The fabrication of such connections could be complicated and cumbersome owing to the curved face of the column. Fin plate connections have been widely adopted owing to the merits of easier erection, rapid construction and lower cost. Jones [6] studied the behaviour of single-sided fin plate to steel tubular columns loaded by tensile and shear force. Parameters including column cross-section shape (CHS and RHS), column and fin plate thickness, concrete infill, elevated temperatures and lever arm were considered. In this study, failure modes including fracture of the fin plate and tearing out of the tube around the welds were observed, deformation limit of 3% of the tube width for hollow tubes in CIDECT Guide was re-evaluated and proved to be inadequate to extract the ultimate strength of the connections. In addition, concrete infill was observed to significantly increase the capacity of connections over empty ones and specimens with CHS were found to have greater strength than similarly proportioned RHS ones. However, this study only focus on isolated fin plate with column connections regardless of bolts that linking beams to the connections and also the moment behaviour of the connections was not explored especially when large beam rotation occurred. A series of double-sided fin plate beam-column connections considering different joint assemblies was investigated by Lam & Dai [7] through a numerical modeling technique, aiming to investigate their moment-rotation behaviour. Connections with and without concrete core and stiffener plates were studied. The studied joint types are illustrated in Fig. 1, from type-AC to DC. An experimental study [8] was carried out to verify the obtained preliminary findings and also to provide better understanding of the structural behaviour of these joints, including an additional joint type-EC (Fig. 1, EC) which considered an embedded stiffener plate in the major axis direction of the EHS column. Corresponding connections with EHS columns, i.e. without concrete infill, were also tested to highlight the benefit of using the concrete infill. This paper herein presents the experimental program and details of a finite element (FE) model for the simulation of the experiments on concrete-filled joints. Preliminary parametric numerical results based on the verified FE model are given to highlight the effect of critical parameters on the structural behaviour of beam to concrete-filled elliptical column connections.

2. Description of experimental program

2.1. Test arrangements

Details of the experiments can be found in the previous paper [8], so only a brief summary is given in this section. A total of ten specimens (of which five are connections with a concrete core in the column and the other five are corresponding to hollow connections) were tested to failure with the column under a constant downward compressive force and the beams subjected to upward concentrated forces at the beam ends, replacing the slab-floor load that would occur in a real structure. Three hydraulic actuators were employed to exert these forces. Test arrangement and a typical beam to elliptical column specimen is shown in Fig. 2 in which some dimensions of the connection are also illustrated.

Table 1
Mean measured dimensions of EHS columns (mm).

Specimen ID	$2a \times 2b \times t$ mm × mm × mm	L mm
Joint-A	198.43 × 99.52 × 5.05	1500
Joint-AC	198.60 × 101.89 × 4.97	1499
Joint-B	200.01 × 101.51 × 4.92	1487
Joint-BC	198.47 × 101.57 × 5.01	1498
Joint-C	198.50 × 100.50 × 4.88	1498
Joint-CC	198.21 × 101.42 × 5.02	1498
Joint-D	197.78 × 102.03 × 4.54	1497
Joint-DC	198.50 × 101.62 × 5.05	1500
Joint-E	197.82 × 102.10 × 4.75	1495
Joint-EC	198.11 × 101.58 × 5.17	1495

Table 2
Failure moment and corresponding rotation.

Specimen ID	Failure moment kN·m	Rotation rad	M_{filled}/M_{hollow}
Joint-A	22.3	0.20	/
Joint-AC	43.8	0.11	1.96
Joint-B	16.0	0.10	/
Joint-BC	49.6	0.12	3.10
Joint-C	30.0	0.11	/
Joint-CC	57.2	0.11	1.91
Joint-D	8.4	0.12	/
Joint-DC	43.6	0.11	5.19
Joint-E	13.3	0.18	/
Joint-EC	33.8	0.13	2.54
Joint-ECR	41.4	0.13	3.11

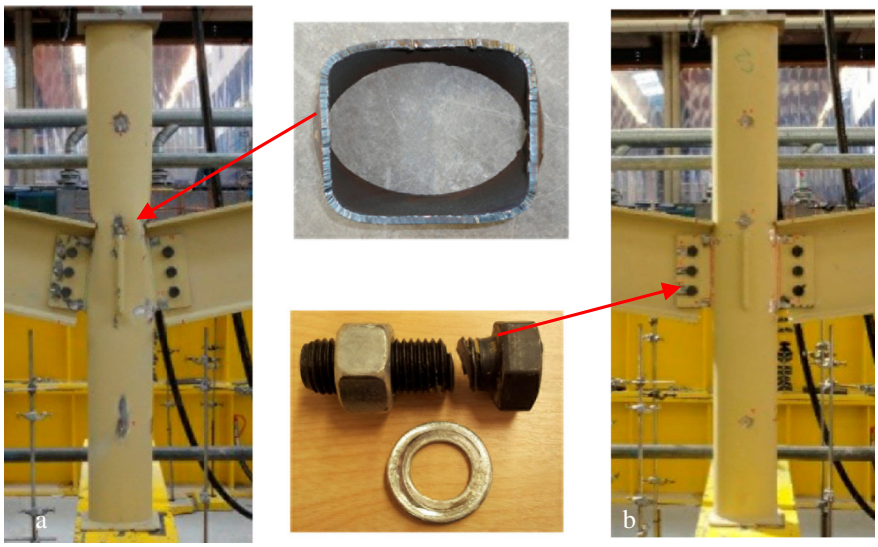

Fig. 4. Typical failure modes: (a) hollow connection (Joint-A); (b) concrete-filled connection (Joint-AC).

All EHS columns (200 × 100 × 5 mm, 1500 mm in length, mean measured dimensions are listed in Table 1) were made of S355 steel with a tested average yield strength of 355.3 MPa and an ultimate strength of 522.1 MPa, respectively; fin plates and stiffener plates were made of S275 steel with tested yield strength and ultimate strength of 333.1 MPa and 444.5 MPa, respectively; elastic modulus was 205 GPa. Steel coupon tests were conducted in accordance with BS EN 6892-1 [9]. The unconfined average cube strengths of the infilled concrete (C30) were 37 MPa on 28 days and 42 MPa on the test dates. M20 Gr. 8.8 bolts (for type-D, DC, E, EC connections, where "type-D", for example, means type-DC connection without infilled concrete) or Gr. 10.9 bolts (for type-A, AC, B, BC, C, CC connections) were used to connect the beams (305 × 127 × 48 UB, 900 mm in length) to the fin plates (220 × 110 × 10 mm), while the fin plates were welded to the external faces of the EHS columns using 6 mm fillet welds. Bolt holes in both fin plates and through plate had a diameter of 22 mm. Stiffener plates/through plates (10 mm in thickness) ran through either the minor or major axes of the EHS columns with an extended length of 20 mm on each side. Vertical deflections of the beams and lateral deflections at the positions of the top and bottom bolts were measured by LVDTs during tests, to calculate rotations of each connection.

2.2. Test results

Summarized moment vs. rotation curves were illustrated in Fig. 3, where the moment of each fin-plate connection is equal to the force at the beam end (recorded automatically by a data logger) multiplied by the functional distance (0.8 m) from the loading point to the rotation center. Curve "ECR" represents the result of a repeat test of concrete-filled type-EC connection, replacing M20 Gr. 8.8 bolts by M20 Gr. 10.9 bolts after the bolts fractured in the initial test. To improve the clarity of the comparison between the curves, only the phases before the failure points were plotted in this figure. The initial stage of the curves was found to be linear, and the slope was determined by the friction force that existed between the fin plates, beam webs and bolts. Slippage occurred in all cases before the bolt shanks touched the edges of bolt

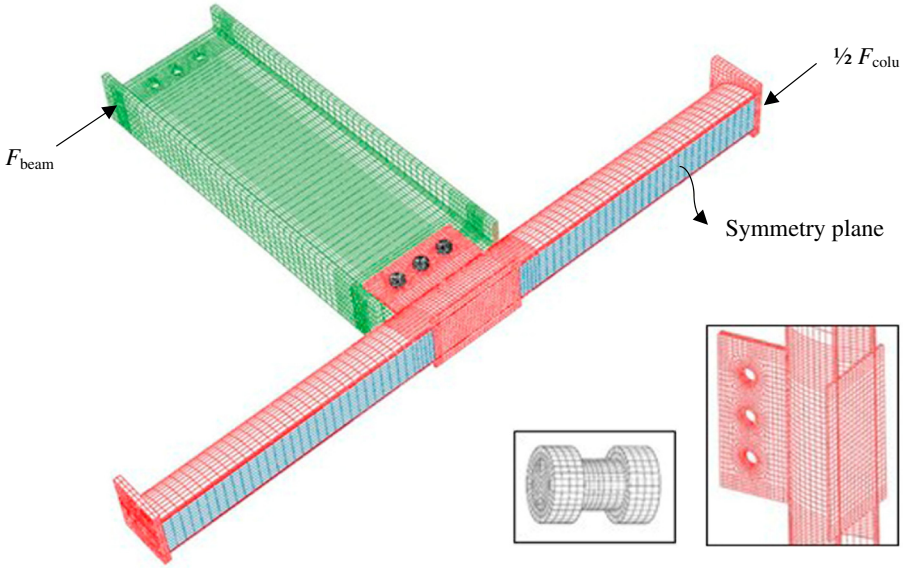

Fig. 5. Finite element model with mesh (1/2 model).

holes. The duration of this phase varied owing to the 2 mm clearance between the bolt shanks and holes. With the increase of rotation, slopes of the curves increased especially for concrete-filled column connections. The reason is that the top flange of each beam touched the EHS column face at some stage during the tests, while the transverse stiffness of the EHS was significantly enhanced by the core concrete. Summarized failure moment and the corresponding rotations are listed in Table 2. The main findings in regards to the moment capacity are: 1) the moment resistance of simply bolted fin plate connections can be improved considerably by infilling concrete to the EHS column, enhancing moment resistance by a factor ranging from 1.91 to 5.19; 2) the minor axis through plate connection, type-CC, had much higher stiffness and better moment capacity and is thus to be recommended for minor axis beam to EHS column connections.

Typical failure modes of connections with hollow columns and concrete-filled columns are illustrated in Fig. 4 (a) and (b), respectively. For all joint assemblies, connections with hollow EHS columns failed by inward local buckling although stiffeners were used in some cases. However, this phenomenon was eliminated by using core concrete. Large concave (in the upper portion of the connection, caused by direct compression of beam flange) or convex (in the lower portion, caused by tensile force transferred from fin plates) deformations that had occurred in the hollow columns were prevented when concrete infill was employed. Consequently, bolts fractured (shear failure) at the final stage of the tests. In contrast to the other hollow column specimens, the through plate connection, type-C, failed by bolt shear failure owing to the contribution of the through plate to the transverse stiffness of the connection.

3. Finite element modeling method

3.1. Geometric model

To achieve computational efficiency, only half of each specimen was modelled by defining appropriate symmetry in the boundary conditions. The geometric model with mesh is shown in Fig. 5, including the symmetry plane and the applied loads. Mean measured dimensions of EHS columns illustrated in Table 1 were used. Bolt hole positions of both beam web and fin plates are shown in Fig. 2. Note that the actual gap between end of the beam flange and the EHS column face was not exactly equal to the design value of 10 mm after assembling the connection, owing to the imperfections of the bolt hole positions and the 2 mm clearance between the bolts and the holes. Therefore, the actual gap was considered in the FE Model accordingly. The bolts were positioned in accordance to the test setup, in order to provide a more accurate simulation to the test; adopted positions were illustrated in Fig. 6 as an example. Hexagonal bolt heads and nuts were simplified as cylinders in the models. This simplification was also adopted by other researchers [10,11]. A pre-tightening load of 20 kN was applied to each bolt of the BC, CC, DC and EC connections. Note that fillet weld and washers were not included in the FE models.

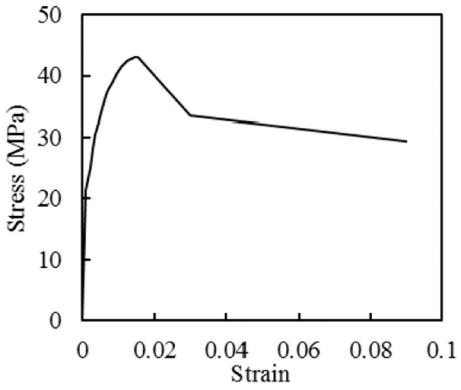

Fig. 7. Stress-strain curves of EHS confined concrete [2].

3.2. Material properties

A four part stress-strain model described by Dai & Lam [2] was adopted for the EHS confined concrete, and the calculated compressive stress-strain curve is shown in Fig. 7; key parameters are listed below: maximum unconfined compressive cylinder strength was 33.2 MPa; initial elastic modulus was 30,826 MPa; maximum confined compressive strength was 43 MPa. A fracture energy based option was selected to define the tensile behaviour of the concrete, with the failure stress approximately equals to 0.1 times the corresponding compressive stress and a fracture energy of 0.08 N/mm which was obtained through linear interpolation between 0.04 N/mm for C20 concrete and 0.12 N/mm for C40 concrete [12].

The stress-strain model of steel is illustrated in Fig. 8 where the vertical and horizontal axes represent the true stress and strain converted

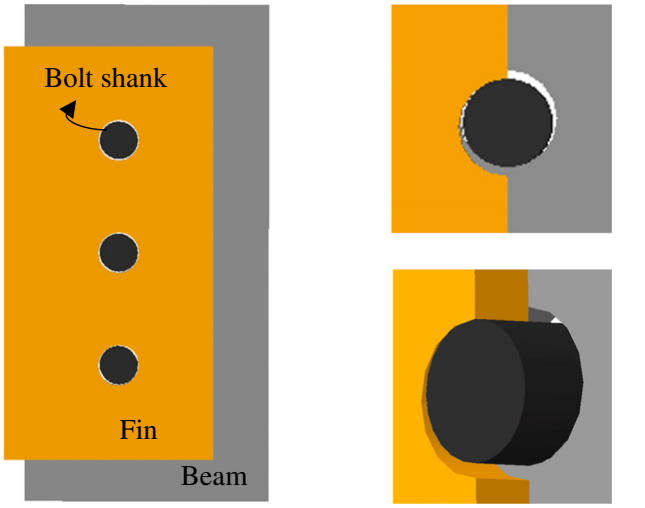

(a) Central position (b) Off center (Joint-AC)

Fig. 6. Bolt positions in FE models.

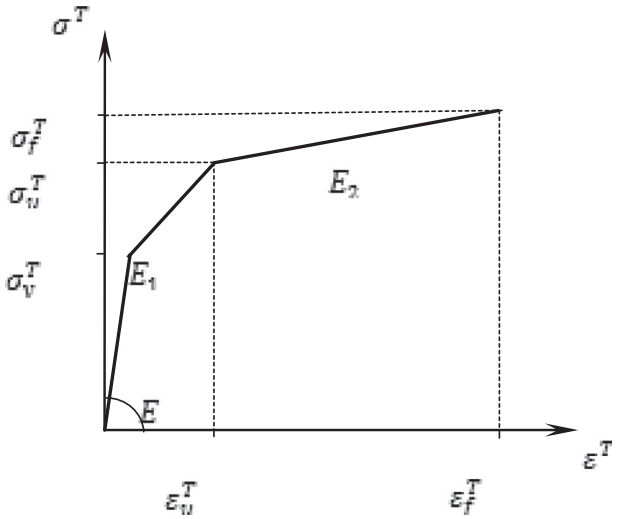

Fig. 8. Stress-strain model of steel [21].

from the tested nominal values via the following recognized expressions based on the principle of constant-volume:

$$\sigma^t = \sigma^n(1+\varepsilon^n) \quad \text{(a)}$$

$$\varepsilon^t = \ln(1+\varepsilon^n) \quad \text{(b)}$$

where σ^t and ε^t denote the true stress and true strain, respectively; σ^n and ε^n refer to the nominal stress and strain. The true stress and strain at fracture are obtained by using the following equations:

$$\sigma_f = \frac{F_{frac}}{A_{frac}} \times 100\% \quad \text{(c)}$$

$$\varepsilon_f = \ln\left(\frac{A_0}{A_f}\right) \quad \text{(d)}$$

where F_{frac} and A_{frac} are the load and smallest cross-sectional area when the coupon is fully fractured; A_f is the smallest cross-sectional area after fracture. Tested σ_f and ε_f are 940.5 MPa and 96.4% for S355 steel; 943.7 MPa and 102.9% for S275 steel. As material tests for bolts were not conducted, the minimum nominal yield and ultimate strength were used in this paper.

3.3. Mesh type and size

C3D8, an 8-node linear brick element, was adopted for the FE model. Incompatible mode was selected for steel component elements to avoid possible hourglass phenomena while 'reduced integration' was used for the concrete core elements to reduce computational cost.

For the tested specimens, failure normally occurred around the connection, thus a finer mesh was used to obtain accurate simulation while a coarser mesh was adopted further away from the connection area to save computational time. No global buckling of the EHS column was observed during the tests, therefore the following mesh size recommendations for elliptical stub concrete-filled columns could be followed: 5–10 mm for EHS and 10–20 mm for concrete; the concrete element size could be set as twice the element size of the EHS column where applicable [2]. Also, a mesh size of 20 mm was employed for both steel and column of the through-plate concrete-filled connection [13], which gave sufficiently accurate results with quick convergence and reasonable computational time. Taking the above findings into consideration, global mesh sizes of 20 mm were adopted for both the EHS and concrete core while mesh sizes of 10 mm and 5 mm were used in the connection area for concrete and EHS, respectively. The hoop direction of the EHS column was meshed using a single bias meshing method with a minimum mesh size of 10 mm (curved side of EHS) and maximum of 20 mm (flat side, this value may be reduced accordingly); the same technique was used in the longitudinal direction of the EHS column. The steel components had two layers of mesh in their thickness directions. A bolt mesh size of 3 mm was recommended by Yu et al. [14] and was thus adopted as the global size for the bolts in this paper. In particular, mesh size was minimized to 2 mm along part of the bolt shank longitudinal edges where the surface was defined as 'slave surface' in one of the contact pairs. In the circumferential direction of the bolts/bolt holes, 32 elements were adopted. Mesh sensitivity analysis was conducted in terms of this element quantity by increasing the number to 48 and 60. As shown in Fig. 9(a), the moment-rotation curves obtained are nearly identical and this proves that the FE model could adopt the 32 elements as the optimum option regarding computational efficiency and result convergence. Further evidence is given in Fig. 9(b) where the

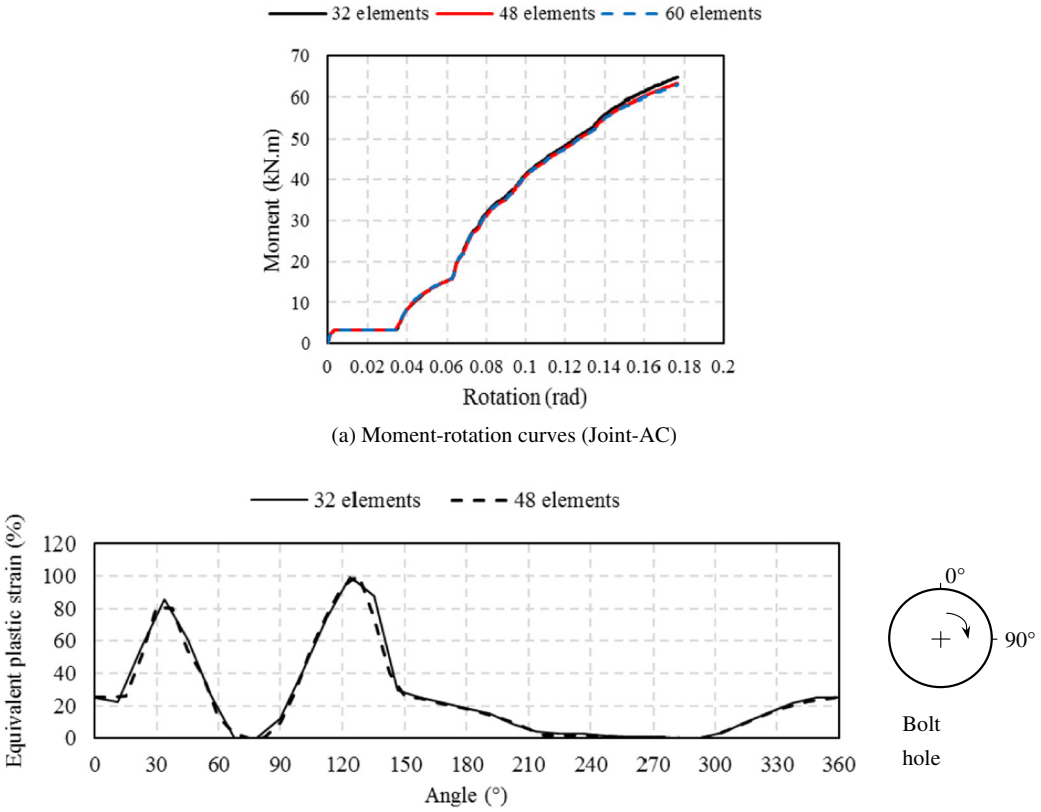

(a) Moment-rotation curves (Joint-AC)

(b) Equivalent plastic strain distribution (Joint AC-4mm-Fin)

Fig. 9. Mesh sensitivity analysis. (a) Moment-rotation curves (Joint-AC). (b) Equivalent plastic strain distribution (Joint AC-4 mm-Fin).

equivalent plastic strain distribution along the critical bolt hole in fin plate (Joint AC-4 mm-Fin, model details can be found in the following parametric study) was illustrated. The x-axis represents the angle initiating from 0° to 360°.

3.4. Contact

Contact interaction is complicated when conducting the nonlinear analysis of concrete-filled bolted connections by using the ABAQUS standard solver. Proper definitions of master and slave surfaces in contact pairs (in accordance with the below two criteria: 1) stiffer material is normally set as the master surfaces; 2) a surface should not be used as slave surface in two or more different interactions and contact properties were essential to avoid possible convergence problems and to successfully capture the moment-rotation behaviour of the connections. Surface-to-surface contact with a finite sliding option was used in this paper for the following contact pairs: beam-fin plate, beam/fin plate-bolt, stiffener plate/through plate-concrete, rigid plate/roller (described in the next section) -concrete, EHS-concrete. 'Hard contact' in the normal direction was defined to fully transfer the load from beam to column through fins and bolts; a friction coefficient of 0.3 was assumed for all of the contact surfaces in the tangential direction.

3.5. Failure criteria

The strain based failure criterion for bolted connections adopted by Salih et al. [15] were employed to define the bolt shear and plate failure in the numerical studies. In this paper, bolt failure is deemed to occur when the equivalent plastic strain over the full critical cross-section of the bolt exceeds 1%. The plates bearing failure and net section failure are adopted with the criterion that the localized equivalent plastic strain reaches the true fracture strain [15] to identify the failure modes and the failure moment of the bolted connections regardless of the deformation limit of bolt holes. For the true fracture strain, experiments have been carried out by Khoo et al. [16], Dowling [17], Huns et al. [18] and Nip et al. [19] and an average value of 100% was obtained for structural carbon steels [15]. Based on the uniaxial tension test results of 96.4% for S355 steel and 102.9% for S275 steel obtained by authors, this value 100% is reasonable and therefore was used in the parametric studies conducted in this paper.

4. Verification of developed FE model

Based on the above described FE simulating method, moment vs. rotation relationships of concrete-filled connections were obtained and compared with the corresponding test results, see Fig. 10(a)–(e), where dotted lines with hollow circles represent the test results while solid lines denote the corresponding FE results; the dotted line with filled circular data points and the thicker dashed line in Fig. 10(e) refer to test result and FE result of the repeat experiment of Joint-EC (replacing Gr. 8.8 bolts by Gr. 10.9 bolts), respectively.

In general, the whole experimental moment vs. rotation curves before the maximum point (caused by bolt shear failure) can be well captured by the FE modeling with the exception of Joint-EC. The EC connection underwent yielding, along the intersection between the fin plate and the EHS column during the initial testing (see Fig. 11), however this is not considered in the FE modeling. The friction and slippage between beam and fin plate can be predicted reasonably in all specimens based on the initial stages of these moments vs. rotation curves from the FE simulation and experimental result. Nevertheless, there was a gentle transition phase in the experimental curve before the bolt shanks fully contacted the surface of the bolt holes, which was governed by bolt positions. The positions of bolts in the holes could not always locate in the center and thus real positions were used, e.g. Joint-AC (see Fig. 6). Good agreement of the transition phase could be obtained for Joint-AC which means the actual bolt positions were correctly assumed. However, the bolt positions could have a number of combinations and thus leads to the differences on the moment-rotation curves at around 0.04 rad to 0.06 rad for the rest of connections. But this phenomenon will not affect the subsequent stage of the moment behaviour of the connections nor the ultimate moment capacities after beam end touching the column sides. The gap between beam end and column face affected the slope of the curve in the later stage: a smaller gap caused the slope to change at an earlier stage. The gaps used in the FE models are listed as follows: AC, 9.1 mm; BC, 9 mm; CC, 8.5 mm; DC, 7 mm; EC, 12 mm, ECR, 11 mm.

Fig. 12 shows the equivalent plastic strain distribution along the critical bolt hole in both the fin plate and the beam web of Joint-AC when bolt failure occurred. The data points were extracted in a clockwise

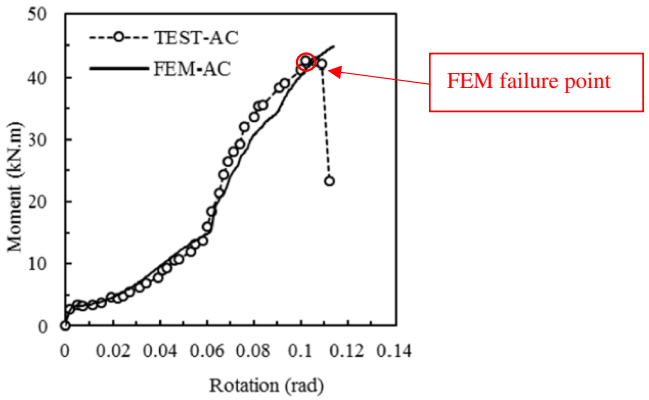

(a) Joint-AC

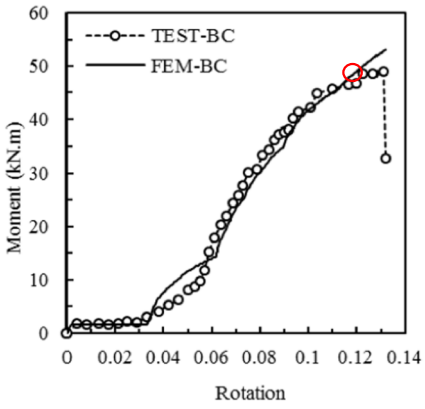

(b) Joint-BC

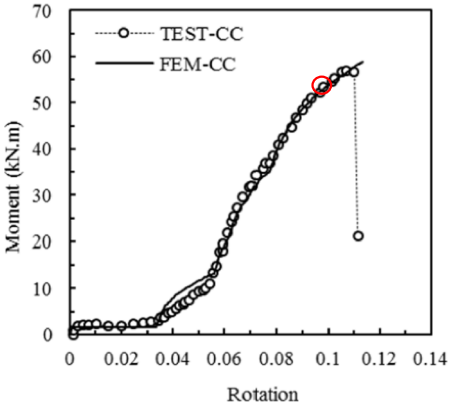

(c) Joint-CC

Fig. 10. Comparisons of moment vs rotation relationships. (a) Joint-AC. (b) Joint-BC. (c) Joint-CC. (d) Joint-DC. |(e) Joint-EC & ECR.

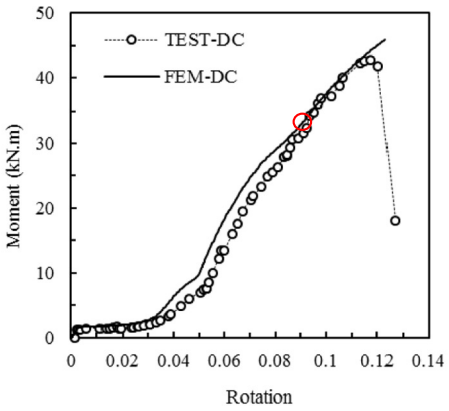

(d) Joint-DC

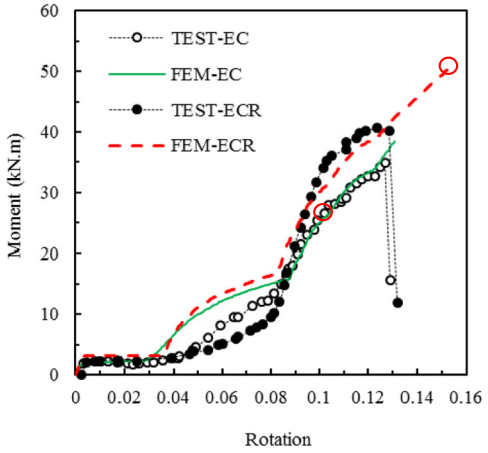

(e) Joint-EC & ECR

Fig. 10 (*continued*).

direction with the angle initiating from 0° to 360°. It indicates that the connection did not fail by plate failure since the maximum equivalent plastic strain (around 40%) is below the limit of 100%.

Fig. 13 (a)–(c) shows the comparisons of typical failure modes of concrete-filled connections between experimental result and FE result, e.g. Joint-BC. As can be seen from these comparisons, the obtained FE models could reasonably replicate the failure of the connections which proves the validity of the described FE modeling method.

Table 3 shows a comparison of ultimate moment between those extracted from experiments and FE simulation, where M_{TEST} represents the ultimate moment obtained from the experiments and M_{FEM} refers to the failure moment provided by FE simulation based on the bolt failure criteria. The failure point in the FE result was illustrated in Fig. 10 with a red circle. Good agreement within a satisfied accuracy of 7% has been obtained for Joint-AC, BC and CC which utilized the Gr. 10.9 bolts which means that the developed FE model, adopted material properties and failure criteria could reasonably determine the moment capacities of the concrete-filled connections adopting Gr. 10.9 bolts. For the cases of Joint-DC and EC in which Gr. 8.8 bolts were utilized, the simulation results are in the safe side which means the adopted bolt nominal properties and the equivalent plastic strain limit of 1% underestimated the connection capacities based on the comparison in Table 3.

5. Parametric studies

5.1. Key parameters

Parametric studies were performed based on the joint types-AC (major axis fin plate connection with stiffener), BC (major axis fin plate connection without stiffener) and CC (minor axis through plate connection). The key parameters selected are: end distance e_1 (1.5d, 2.0d, 2.5d, 3.0d, 3.5d), end distance e_2 (1.5d, 2.0d, 2.5d, 3.0d, 3.5d), bolt spacing p_1 (2.0d, 2.5d, 3.0d, 3.5d, 4.0d), fin plate thickness t_p (4 mm, 6 mm, 8 mm); d is the diameter of the bolt which equals to 20 mm. Symbols are illustrated in Fig. 2. Dimensions of the beams, EHS column are

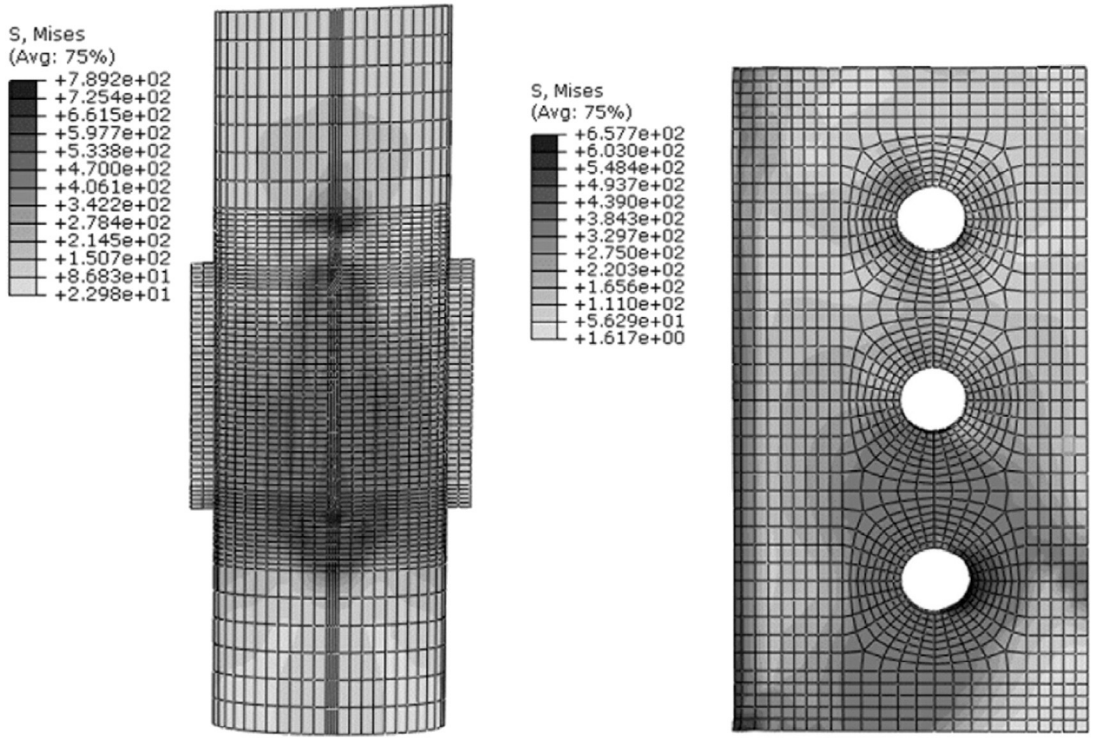

Fig. 11. Von Mises contour around connection after bolt failure (Joint-EC).

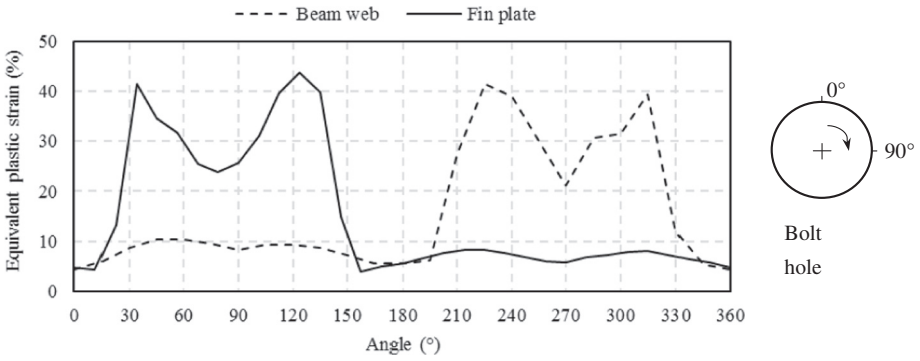

Fig. 12. Equivalent plastic strain distribution at bolt failure (Joint-AC).

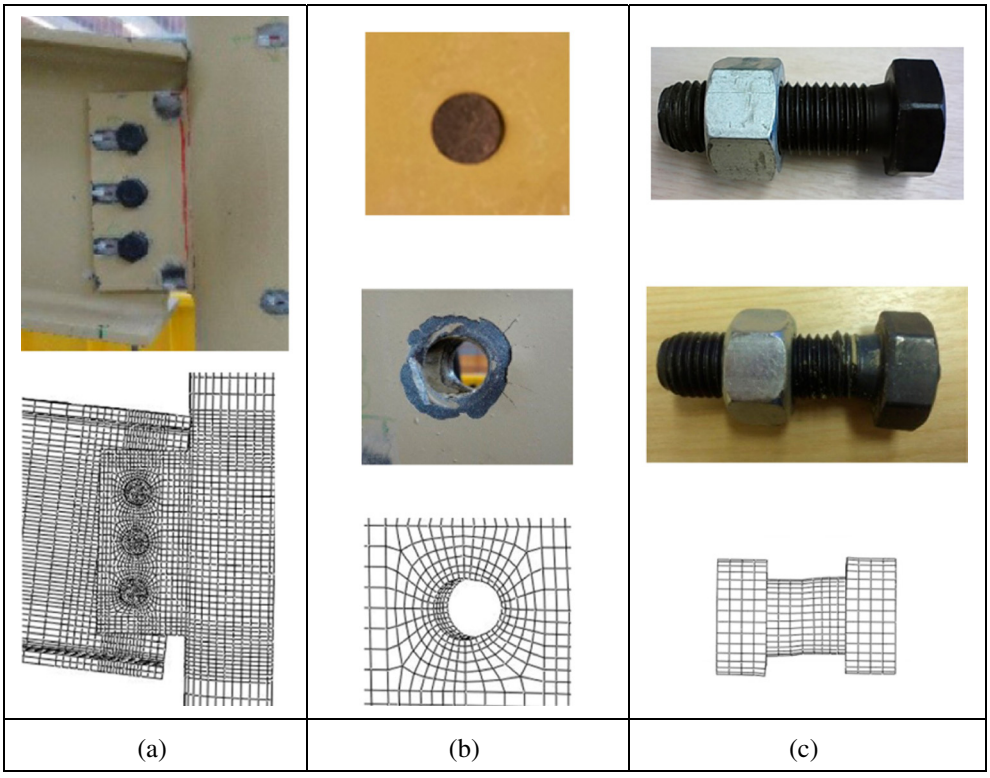

Fig. 13. Comparison of failures (Joint-BC): (a) connection rotation; (b) bolt hole bearing failure in fin plate; (c) bolt shear failure (bolt deformation scale: 1.5).

identical with those adopted in the experiments. The column end was fixed on the bottom while only axial shortening was allowed at the top end. Three Gr. 10.9 bolts were adopted with a constant diameter of 20 mm. The beam flange and fin plate/through plate was tightened with bolt load of 20 kN. No weld and washers are included in the FE models.

Table 3
Comparison of ultimate moments from experiments and FE simulations.

Specimen ID	M_{TEST} kN·m	M_{FEM} kN·m	M_{TEST}/M_{FEM}
Joint-AC	43.8	44.5	0.98
Joint-BC	49.6	48.5	1.02
Joint-CC	57.2	53.3	1.07
Joint-DC	43.6	32.8	1.33
Joint-EC	33.8	27.6	1.23
Joint-ECR	41.4	50.6	0.82

S355 steel was adopted for the EHS columns and beams with a nominal yield strength of 355 MPa and a nominal minimum ultimate strength of 470 MPa [20] while S275 steel was selected for the fin plates which has a nominal yield strength of 275 MPa and nominal minimum

Table 4
List of beam to elliptical connections analyzed in Section 5.2.

Connection ID	n_l mm	t_p mm	Failure moment kN·m	Rotation at failure rad	Failure mode
AC-4 mm-Fin	0.4	4	26.08	0.120	PF
AC-6 mm-Fin	0.4	6	39.63	0.148	PF
AC-8 mm-Fin	0.4	8	47.66	0.150	BF
BC-4 mm-Fin	0.4	4	26.11	0.118	PF
BC-6 mm-Fin	0.4	6	39.95	0.146	PF
BC-8 mm-Fin	0.4	8	48.58	0.151	BF
CC-4 mm-Fin	0.4	4	26.72	0.114	PF
CC-6 mm-Fin	0.4	6	41.70	0.134	PF
CC-8 mm-Fin	0.4	8	50.78	0.131	BF

Note: Connection ID, e.g. AC-4 mm-Fin denotes type-AC connection with a 4 mm fin plate; BF - bolt failure and PF - fin/through plate failure.

ultimate strength of 410 MPa. True stress-strain relationships were converted using the equations where $E_2 = \sigma_u$ was assumed [21]. The three-part linear stress-strain curve was adopted for steel. C30 concrete was used in the EHS columns.

5.2. Effect of fin plate thickness

To evaluate the influence of fin plate thickness on the moment-rotation behaviour and failure modes of the beam to concrete-filled elliptical column connections, a set of thickness values of 4 mm, 6 mm and 8 mm was selected for Joint types-AC, BC and CC. Bolt arrangement and fin plate profile can be found in Fig. 2. The maximum moment with corresponding joint rotation at failure were extracted from the numerical results and are listed in Table 4. Fig. 14 shows the equivalent plastic strain distribution along the critical bolt hole in both fin plate and beam web where the x-axis represents the angle initiating from 0° to 360°. This figure indicates that the critical position along bolt hole in the beam web and fin plate is around 120°-135°. Note that the connections with fin plate thickness of 4 mm and 6 mm failed in fin plate failure since the equivalent plastic strain at the critical position reached the limit of 100% (highlighted with a red dash line in the graph) while the bolts did not fail as the shear resistance of M20 Grade 10.9 bolts was larger than the fin plate bearing resistance. In contrast, bolt shear failure occurred prior to the fin plate failure in the connection with 8 mm fin plate and evidence was shown in the Fig. 14 that the critical equivalent plastic strain is lower that the strain limit of 100%. An equivalent plastic strain contour was illustrated in Fig. 15, showing that local failure in the fin plate occurred in this case and thus the stiffener plate inserted into

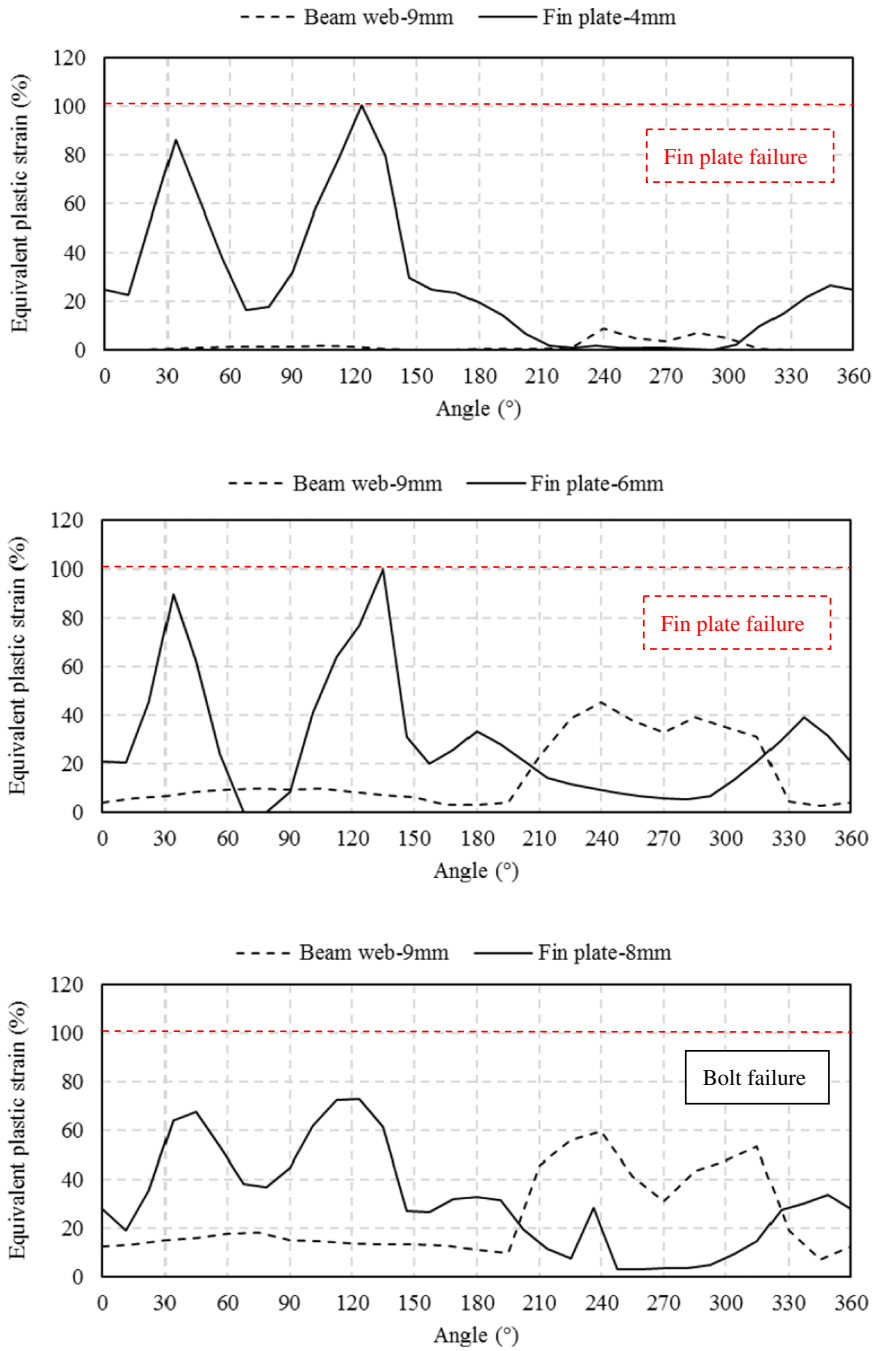

Fig. 14. Equivalent plastic strain distribution along the side bolt hole at failure (AC).

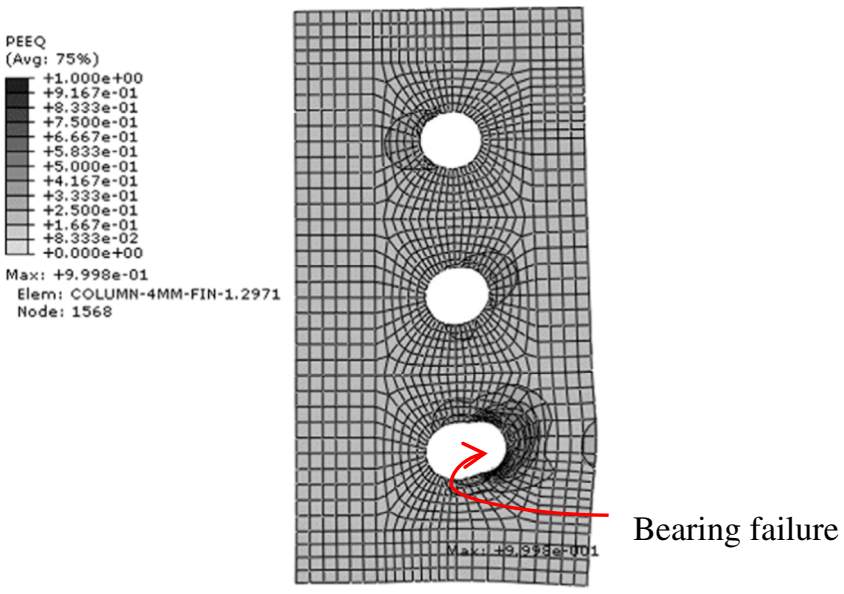

Fig. 15. Equivalent plastic strain contour in fin plate (AC-4 mm-Fin).

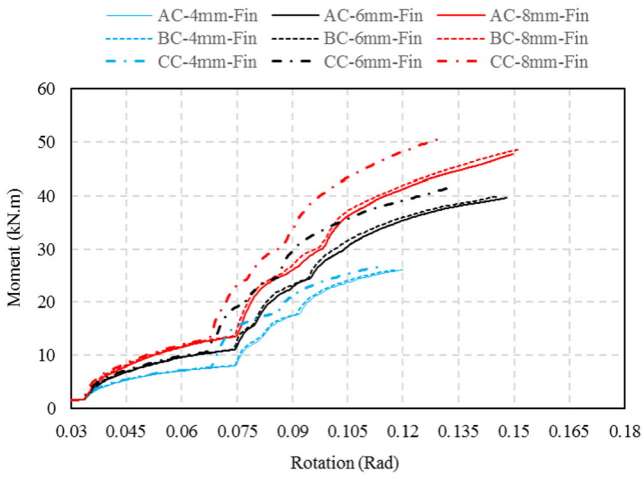

Fig. 16. Moment vs. rotation relationships.

the concrete-filled column of type-AC connection could not provide obvious enhancement to the resistance on the connection level. Thus there would be no significant difference in the moment response between the stiffened type-AC connections and type-BC connections. The moment vs. rotation curves of the connections considered in this section are illustrated in Fig. 16 where the curves were cut at the failure points to clarify the comparisons within the graph. Obviously, the fin plate thickness plays important role in the structural performance of these types of connections. The stiffness and ultimate moment of the connections increase with the increasing of fin plate thickness even through failure mode might change. The connections analyzed in this section was summarized in Table 4 with the failure moment, corresponding rotation and failure mode; failure points are given in Fig. 16 with circles for type-CC connections and triangles for both AC and BC connections.

5.3. Effect of end distance-e_1 and bolt spacing-p_1

Optimum arrangement of the bolts in the fin plate (110 mm in width and 220 mm in length) was investigated by changing the end distance e_1 and vertical bolt spacing p_1. Considered combinations of e_1 and p_1 are given as follows: 1.5d & 4.0d; 2.0d & 3.5d; 2.5d & 3.0d; 3.0d & 2.5d; 3.5d & 2.0d. Ultimate moment capacities obtained from type-BC and

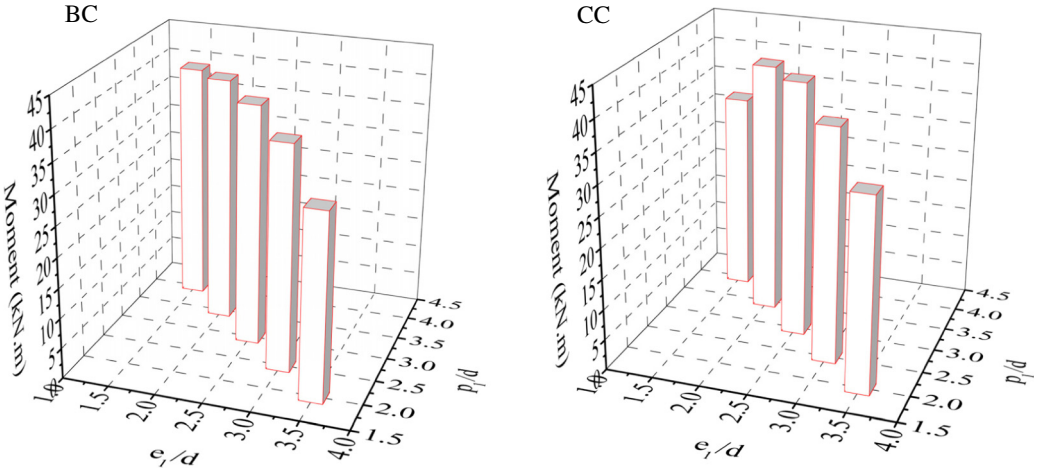

Fig. 17. Effect of end distance e_1 and bolt spacing p_1 (type-BC and CC).

Table 5
List of beam to elliptical connections analyzed in Section 5.3 ($e_2 = 2.5d$).

Connection ID	n_l mm	t_p mm	Failure moment kN·m	Rotation at failure rad	Failure mode
BC-6-E1-15-P1-40	0.4	6	39.63	0.125	PF
BC-6-E1-20-P1-35	0.4	6	40.81	0.135	PF
BC-6-E1-25-P1-30	0.4	6	39.95	0.146	PF
BC-6-E1-30-P1-25	0.4	6	37.36	0.146	PF
BC-6-E1-35-P1-20	0.4	6	30.85	0.130	PF
CC-6-E1-15-P1-40	0.4	6	32.67	0.111	PF
CC-6-E1-20-P1-35	0.4	6	41.32	0.116	PF
CC-6-E1-25-P1-30	0.4	6	41.84	0.134	PF
CC-6-E1-30-P1-25	0.4	6	38.31	0.134	PF
CC-6-E1-35-P1-20	0.4	6	31.79	0.124	PF

Table 6
List of beam to elliptical connections analyzed in Section 5.4 ($e_1 = 2.5d$; $p_1 = 3d$).

Connection ID	n_l mm	t_p mm	Failure moment kN·m	Rotation at failure rad	Failure mode
BC-6-E2-15	0.4	6	30.30	0.119	PF
BC-6-E2-20	0.4	6	36.75	0.135	PF
BC-6-E2-25	0.4	6	39.95	0.146	PF
BC-6-E2-30	0.4	6	41.33	0.148	PF
BC-6-E2-35	0.4	6	42.03	0.147	PF
CC-6-E2-15	0.4	6	31.13	0.111	PF
CC-6-E2-20	0.4	6	37.6	0.122	PF
CC-6-E2-25	0.4	6	41.84	0.134	PF
CC-6-E2-30	0.4	6	42.96	0.134	PF
CC-6-E2-35	0.4	6	43.55	0.132	PF

CC FE models are presented in Fig. 17 and are also summarized in Table 5. It is shown that bolt spacing p_1 is more influential than the end distance e_1 on the moment capacities of the connections. Based on the comparison within and between graphs, vertical bolt spacing is suggested to be at least 2.5d; the minimum e_1 could be 1.5d in type-BC connection but this value should be increased to 2.0d in type-CC connection; and the combination of $e_1 = 2.0d$ and $p_1 = 3.5d$ may be the optimum option for the bolts' arrangement in the cases studied.

5.4. Effect of edge distance-e_2

Fig. 18 presents the moment capacities of analyzed BC and CC connections in terms of edge distance e_2. The studied e_2 values were equal to 1.5d, 2.0d, 2.5d, 3.0d and 3.5d, respectively, and the corresponding fin plate width was $(60 + e_2)$ mm while the length is kept as 220 mm. Table 6 lists the corresponding FE results the connections. As shown from the results, the moment capacities increased with the increasing of the edge distance e_2 while the increment was not obvious after e_2 reaching 3d; the difference between the ultimate moments between connection types BC and CC is not significant but the capacity of the CC connection is always slightly bigger than that of the BC connection. The minimum value of e_2 is suggested to be at least 2.5d in both cases.

6. Conclusions

To enable better understanding of the moment-rotation behaviour and failure mechanism of fin plate connections to elliptical column, limited experimental work has been conducted by authors. Due to experiment is costly and time consuming, a finite element modeling method was developed via ABAQUS and was adopted to conduct further investigation. After the developed numerical model was validated against the experimental results, a preliminary parametric study is then performed to evaluate the influence of several main parameters to the behaviour of the prescribed connections. The following conclusions are made based on the research work presented in the paper.

- The concrete core increased the moment capacity significantly due to it restrained the column wall buckling at the vicinity of the joint. The moment enhancement ratio ranging from 1.91 to 5.19 (compared with corresponding hollow connections).
- Typical failure of the concrete-filled connections was observed as bolt shear failure while that of the hollow connections was inwards local buckling, which occurred in compression zone of the EHS column face near the connection area.
- Based on the comparisons between experimental result and FE analysis prediction, the described simulation method/FE model could predict the ultimate moment capacity of concrete-filled connections adopting M20 Gr. 10.9 bolts within a satisfactory error value of 7% and could also capture the typical failure mode of these connections.
- The numerical results obtained from the parametric studies indicates that the fin plate thickness affects the moment capacity of the connections significantly. Normally, the ultimate moment increases with the increasing of the fin plate thickness although the failure mode may change when the thickness reaches a certain value, e.g. 8 mm.
- Vertical bolt spacing is suggested to be at least 2.5d for both type-BC and CC connections; the minimum e_1 could be 1.5d in type-BC connection and 2.0d in type-CC connection. The minimum value of e_2 is suggested to be at least 2.5d in both cases.

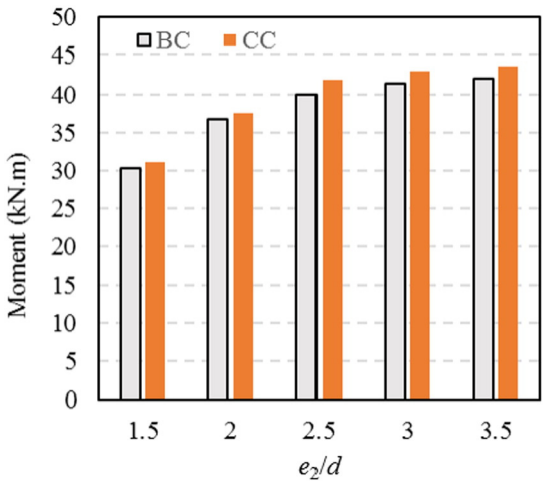

Fig. 18. Effect of end distance e_2.

References

[1] Zhao XL, Packer JA. Tests and design of concrete-filled elliptical hollow section stub columns. Thin-Walled Struct 2009;47:617–28.
[2] Dai X, Lam D. Numerical modelling of the axial compressive behaviour of short concrete-filled elliptical steel columns. J Constr Steel Res 2010;66:931–42.
[3] Law KH, Gardner L. Lateral instability of elliptical hollow section beams. Eng Struct 2012; 37:152–66.
[4] Shen W, Choo YS, Wardenier J, Packer JA, van der Vegte GJ. Static strength of axially loaded EHS X-joints with braces welded to the narrow sides of the chord. J Constr Steel Res 2013; 88:181–90.
[5] Shen W, Choo YS, Wardenier J, Packer JA, van der Vegte GJ. Static strength of axially loaded elliptical hollow section X joints with braces welded to wide sides of chord I: numerical investigations based on experimental tests. J Struct Eng 2014;140:04013035.
[6] Jones MH. Tensile and shear behaviour of fin-plate connections to hollow and concrete-filled steel tubular columns at ambient and elevated temperatures. (PhD Thesis) University of Manchester; 2008.
[7] Lam D, Dai X, Gardner. Finite element modelling of beam to concrete filled elliptical steel column connections. Tubular structures XIV. London: Taylor and Francis Group; 2012 (ISBN 978-0-415-62137-3:289-96).
[8] Yang J, Sheehan T, Dai XH, Lam D. Experimental study of beam to concrete-filled elliptical steel tubular column connections. Thin-Walled Struct 2015;95:16–23.
[9] CEN. Metallic materials-tensile testing-part1: method of test at ambient temperature. EN ISO 6892-1: 2009; 2009.
[10] Sarraj M, Burgess IW, Davison JB, Plank RJ. Finite element modelling of steel fin plate connections in fire. Fire Saf J 2007;42:408–15.

[11] Wang J, Spencer BF. Experimental and analytical behavior of blind bolted moment connections. J Constr Steel Res 2013;82:33–47.
[12] Han LH. Concrete-filled steel tubular structures-theory and practice. 2nd ed. Beijing: China Science Press; 2007(in Chinese).
[13] Mollazadeh MH, Wang YC. New insights into the mechanism of load introduction into concrete-filled steel tubular column through shear connection. Eng Struct 2014;75:139–51.
[14] Yu H, Burgess IW, Davison JB, Plank RJ. Numerical simulation of bolted steel connections in fire using explicit dynamic analysis. J Constr Steel Res 2008;64:515–25.
[15] Salih EL, Gardner L, Nethercot DA. Numerical investigation of net section failure in stainless steel bolted connections. J Constr Steel Res 2010;66:1455–66.
[16] Khoo HA, Cheng RJJ, Hrudey TM. Ductile fracture of steel. Structural engineering report no. 233. Canada: Department of Civil & Environmental Engineering, University of Alberta; 2000.
[17] Dowling NE. Mechanical behaviour of materials. New Jersey: Prentice Hall; 1999.
[18] Huns BB, Grondin GY, Driver RG. Block shear behaviour of bolted gusset plates. Structural engineering report no. 248 Canada. Department of Civil & Environmental Engineering, University of Alberta; 2002.
[19] Nip KH, Gardner L, Davies CM, Elghazouli AY. Extremely low cycle fatigue tests on structural carbon steel and stainless steel. J Constr Steel Res 2010;66:96–110.
[20] CEN. Hot finished structural hollow sections of non-alloy and fine grain steels-part 1: technical delivery conditions. EN 10210-1:2006(E). Brussels, Belgium: European Committee for Standardization; 2006.
[21] Fernandez-Ceniceros J, Sanz-Garcia A, Antoñanzas-Torres F, Martinez-de-Pison FJ. A numerical-informational approach for characterising the ductile behaviour of the T-stub component. Part 1: refined finite element model and test validation. Eng Struct 2015;82:236–48.